ҚАЗАҚСТАН РЕСПУБЛИКАСЫ
ҒЫЛЫМ ЖӘНЕ ЖОҒАРЫ БІЛІМ МИНИСТРЛІГІ

SATBAYEV UNIVERSITY
МЕТАЛЛУРГИЯ ЖӘНЕ КЕН БАЙЫТУ ИНСТИТУТЫ

ISSN 2616-6445 (Online)
ISSN 2224-5243 (Print)
DOI 10.31643/2018/166445

Минералдық шикізаттарды кешенді пайдалану

3(342)

Комплексное Использование Минерального Сырья

Complex Use of Mineral Resources

ШІЛДЕ-ҚЫРКҮЙЕК 2027
JULY-SEPTEMBER 2027
ИЮЛЬ-СЕНТЯБРЬ 2027

ЖЫЛЫНА 4 РЕТ ШЫҒАДЫ
QUARTERLY JOURNAL
ВЫХОДИТ 4 РАЗА В ГОД

ЖУРНАЛ 1978 ЖЫЛДАН БАСТАП ШЫҒАДЫ
JOURNAL HAS BEEN PUBLISHING SINCE 1978
ЖУРНАЛ ИЗДАЕТСЯ С 1978 ГОДА

АЛМАТЫ - 2027

Редакция мекен жайы:
«Металлургия және кен байыту институты» АҚ
050010, Қазақстан Республикасы, Алматы қ., Шевченко к-сі, Уәлиханов к-нің қиылысы, 29/133,
Fax. +7 (727) 298-45-03, Tel. +7-(727) 298-45-02, +7 (727) 298-45-19
E mail: journal@kims-imio.kz, product-service@kims-imio.kz
http://kims-imio.com/index.php/main

«Минералдық шикізаттарды кешенді пайдалану» журналы ғылыми жұмыстардың негізгі нәтижелерін жариялау үшін Қазақстан Республикасы Білім және ғылым министірлігінің Білім және ғылым сапасын қамтамасыз ету комитеті ұсынған ғылыми басылымдар тізіміне енгізілген.
Меншік иесі: «Металлургия және кен байыту институты» АҚ

Журнал Қазақстан Республикасының Ақпарат және коммуникация министрлігінің Байланыс, ақпараттандыру және бұқаралық ақпарат құралдары саласындағы мемлекеттік бақылау комитетінде қайта тіркелген

2016 ж. 18 қазандағы № 16180-Ж Куәлігі

Address:
"Institute of Metallurgy and Ore Beneficiation" JSC
29/133 Shevchenko Street, corner of Ch. Valikhanov Street, Almaty, 050010, Kazakhstan
Fax. +7 (727) 298-45-03, Tel. +7-(727) 298-45-02, +7 (727) 298-45-19
E mail: journal@kims-imio.kz, product-service@kims-imio.kz
http://kims-imio.com/index.php/main

The Journal "Complex Use of Mineral Resources" is included in the List of publications recommended by the Committee for Control in the Sphere of Education and Science of the Ministry of Education and Science of the Republic of Kazakhstan for the publication of the main results of scientific activities.
Owner: "Institute of Metallurgy and Ore Beneficiation" JSC

The Journal was re-registered by the Committee for State Control in the Sphere of Communication, Information and Mass Media of the Ministry of Information and Communication of the Republic of Kazakhstan.

Certificate № 16180-Ж since October 18, 2016

Адрес редакции:
АО «Институт металлургии и обогащения»
050010, Республика Казахстан, г. Алматы, ул. Шевченко, уг. ул. Валиханова, 29/133,
Fax. +7 (727) 298-45-03, Tel. +7 (727) 298-45-02, +7 (727) 298-45-19
E mail: journal@kims-imio.kz, product-service@kims-imio.kz
http://kims-imio.com/index.php/main

Журнал «Комплексное использование минерального сырья» включен в Перечень изданий, рекомендуемых Комитетом по контролю в сфере образования и науки Министерства образования и науки Республики Казахстан для публикации основных результатов научной деятельности.
Собственник: АО «Институт металлургии и обогащения»

Журнал перерегистрирован в Комитете государственного контроля в области связи, информатизации и средств массовой информации
Министерства информации и коммуникации Республики Казахстан
Свидетельство № 16180-Ж от 18 октября 2016 г.

Crossref
DOI: 10.31643/2027/6445.25
Metallurgy and Metallurgical Engineering

Effect of Chromium on Phase Formation of Intermetallic Aluminum Alloys in the Al-Fe-Si System

Andreyachshenko V.A., *Toleuova A.R.

Abylkas Saginov Karaganda Technical University, Karaganda, Kazakhstan

**Corresponding author email: rymkul.ainagul@mail.ru*

Received: *September 16, 2025*
Peer-reviewed: *November 11, 2025*
Accepted: *December 11, 2025*

ABSTRACT

The article explores the prospects for the development of Kazakhstan's aluminum industry, with a focus on the application of additive manufacturing technologies for the synthesis of chromium-alloyed composite aluminum alloys in the Al-Fe-Si system. A comprehensive metallographic and thermodynamic analysis of the phase composition of alloys synthesized by consumable electrode surfacing was carried out. The use of Thermo-Calc software enabled the construction of polythermal sections and the assessment of the influence of alloying element concentrations on the formation of intermetallic phases, including $Al_{13}Fe_4$ (θ-phase) and Al_8Fe_2Si. The optimal chromium alloying conditions were substantiated, ensuring reduced brittleness and improved mechanical properties through the formation of a fine-grained structure, stabilization of the phase composition, and removal of large primary dendrites. The obtained results confirm the potential of chromium alloying as an effective approach in developing intermetallic aluminum alloys with the desired properties. The study's results contribute to the advancement of technologies for producing aluminum alloys with enhanced performance characteristics, thereby expanding the potential for industrial applications of additive manufacturing methods.

Keywords: AlFeSi, intermetallic phases, simulation and modelling, diagrams phase transformation, microstructure.

Information about authors:

Andreyachshenko Violetta Alexandrovna — *PhD, associate professor, Head of the Testing Laboratory, Engineering Profile, Comprehensive Development of Mineral Resources. Abylkas Saginov Karaganda Technical University, N. Nazarbayev Ave., 56, Karaganda, Kazakhstan. E-mail: v.andreyachshenko@ktu.edu.kz; ORCID ID: https://orcid.org/0000-0001-6933-8163*

Toleuova Ainagul Rymkulovna — *PhD, associate professor, docent of the department of Nanotechnology and Metallurgy. Abylkas Saginov Karaganda Technical University, N. Nazarbayev Ave., 56, Karaganda, Kazakhstan. Email: rymkul.ainagul@mail.ru; ORCID ID: https://orcid.org/0000-0002-3216-1824*

Introduction

Currently, the prospects for the development of the aluminum industry in the Republic of Kazakhstan appear highly promising, driven by a number of key factors. First, the modernization of production facilities is actively ongoing, which undoubtedly contributes to increased technological efficiency, reduced energy consumption, and enhanced competitiveness of domestic products on the international market.

Second, the implementation of innovative technologies, including additive manufacturing methods for synthesizing composite materials, opens up new opportunities for the creation of high-performance aluminum alloys with improved operational characteristics [1].

In addition, government support and the attraction of investments into the sector create favorable conditions for expanding production capacities and entering new markets. Collectively, these factors ensure the sustainable development of Kazakhstan’s aluminum industry, strengthening its position both regionally and globally.

Modern processing technologies for metallic materials have a significant impact on improving their properties [[2], [3], [4], [5], [6], [7], [8], [9]]. At the same time, layer-by-layer material deposition (additive manufacturing) offers a unique opportunity for precise and fine-tuned control over the structure and composition of alloys [[10], [11], [12], [13], [14]]. Unlike conventional casting and machining methods, additive techniques allow the production of complex composite materials with tailored properties, enhancing the strength,

ductility, corrosion resistance, and electrical conductivity of aluminum alloys [[15], [16]].

Particularly promising is the alloying and microalloying of aluminum alloys with various elements to achieve the desired levels of mechanical and service properties [[17], [18], [19], [20], [21]]. Similar improvements can also be achieved by altering the equilibrium conditions of phase transformations in alloys. Of growing interest is the Al–Fe–Si–X system, where intermetallics are used as strengthening phases.

For example, in [22], the authors investigated the influence of cooling rate and subsequent hot strengthening on the microstructure and mechanical properties of an Al–20Si–5Fe–2X alloy (X = Cu, Ni, and Cr). The samples were produced via gas atomization with cooling rates of 1×10^5 K/s and 5×10^7 K/s. The results showed a significant effect of cooling rate and the presence of transition metals on the microstructure and mechanical strength of Al–20Si–5Fe alloys. The beneficial effect of transition metals on the thermal stability of Al–20Si–5Fe, particularly for Ni-containing alloys, was noted.

In studies of the Al–Fe–Si system, iron is generally considered to have a detrimental effect on Al–Si alloys, as it promotes the formation of needle-like intermetallic phases, which considerably reduce the operational properties of the final product. The adverse effects of iron are mitigated through alloying with elements such as chromium, manganese, and rare earth metals. On the other hand, [23] proposed using Fe to counteract the negative influence of Si. The authors studied the effect of Fe content and subsequent homogenization on a dilute Al–Si alloy. An increase in electrical conductivity was observed with the specific addition of Fe. Moreover, the tensile strength and electrical conductivity of the Al–Fe–Si alloy could be further improved after homogenization. It was suggested that the favorable performance characteristics of the Al–Fe–Si alloy may be attributed to the formation and evolution of the ternary eutectic phase α-Al_8Fe_2Si. It was also found that elevated homogenization temperatures and grain refinement promote the precipitation of the α-phase.

In [24], rapidly solidified Al–20Si–5Fe–2X alloys (X = Cr, Zr, or Ni), produced via gas atomization, were degassed under varying vacuum conditions before hot extrusion. The study demonstrated that the addition of a fourth element leads to the formation of dispersed particles that contribute to improved mechanical properties, particularly at elevated temperatures.

It is well known that the addition of alloying elements such as manganese and chromium suppresses the formation of the θ-phase ($Al_{13}Fe_4$) in favor of the less detrimental α-Al_{15}(Fe, Mn, Cr)$_4Si_2$ phase, which is less brittle and less prone to cracking. Silicon is added to promote the precipitation of the Al_8Fe_2Si phase in the alloy [[25], [26]].

The objective of this study was a fundamental investigation of the Al–Fe–Si system. The work focused on identifying optimal concentrations and temperatures for the formation of the high-symmetry Al_8Fe_2Si phase when chromium is used as an alloying element.

Experimental part

An Al-Fe-Si system alloy of the base modification (a system in which impurity atoms are present as a result of processing the original charge components) was produced using additive technology through synthesis by surfacing with a horizontally oriented consumable electrode. Commercial-grade materials were used as the charge. The electrode was made of St3-grade steel, with dimensions of 2×20×150 mm. Aluminum was introduced into the alloy by melting aluminum sheets of AD31 grade, sized 2×30×100 mm. Silicon was introduced using KR00-grade silicon, crushed to a -63 μm fraction.

Before synthesis, a layered package was prepared from aluminum and silicon, consisting of four aluminum sheets with silicon applied between the layers using a wet method. After application, the package was assembled and dried at room temperature for no less than 24 hours. The package was then placed on a steel substrate made of St3-grade steel, which did not participate in the synthesis process. The top of the package was covered with a pumice-like flux of AN-348 grade to prevent additional alloying of the melt with flux components. The target composition of the alloy was Al–30Fe–10Si (at.%).

After synthesis, semi-elliptical ingots were obtained, which were then sectioned into templates for metallographic analysis. Microsections were prepared using standard techniques, including coolant-assisted cutting, grinding, and polishing with lubricants. Metallographic investigations were carried out using an Altami optical microscope. The resulting microstructure is shown in Figure 1.

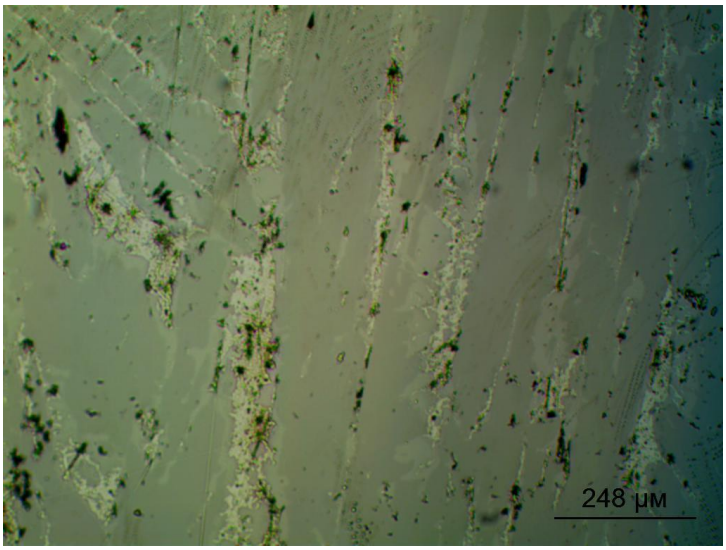

Figure 1 - Microstructure of the Al-Fe-Si alloy of the basic modification after synthesis, x200

As seen, the microstructure exhibits a distinct directional pattern of structural constituents. It is composed of alternating intermetallic dendrites and aluminum layers with minimal dissolution of both base and alloying components. This type of morphology tends to degrade mechanical performance, particularly ductility. As demonstrated in [27], one effective way to mitigate this issue is alloying, including microalloying, with elements that promote dissolution of the primary binary θ-phase during alloy cooling.

Considering the composition under study, the θ-phase is expected to be present at room temperature, but conditions must be created for the formation of a secondary θ-phase – i.e., one that precipitates as a result of solid-solid phase interactions. Accordingly, this study explores the potential of alloying the base-modified Al-Fe-Si alloy with chromium and investigates the fundamental aspects of such alloying.

Results and Discussion

For a more substantiated selection of alloying element concentrations and optimization of heat treatment regimes, a comprehensive analysis focusing on the phase composition of the alloy is required. The analysis was performed excluding impurities and trace elements introduced during synthesis, in order to concentrate solely on the influence of chromium additions. This analysis was conducted using Thermo-Calc software, version 2024a, with the aluminum-based thermodynamic database TCAL8.2.

Thermo-Calc is a computational tool for the calculation of phase equilibria, based on the global minimization of the Gibbs free energy in multicomponent systems. The software also enables the calculation of thermodynamic properties of phases (such as Gibbs energy, enthalpy, and others), including metastable equilibria. A key feature of Thermo-Calc is its modular and extensible architecture, along with a continually expanding database of elements for various systems, including metallic, salt, oxide, and aqueous solution systems.

The program allows for the calculation of phase diagrams of multicomponent systems, including the construction of polythermal and isothermal sections, phase composition predictions, and cooling curve simulations – all of which were employed in this study.

Using Thermo-Calc (version TCW8 with database TCAL8.2), Al-based systems were analyzed to determine the concentration boundaries for the formation of primary crystals of Fe-containing phases.

Figure 2 shows a polythermal section of the Al–30Fe–9Si–1Cr system with variable aluminum and iron content. Chromium alloying was introduced by reducing the aluminum fraction.

According to Table 1, under equilibrium conditions, aluminum and iron form solid solutions, intermetallic compounds, and eutectic mixtures. As shown in the section diagram, during solidification of an aluminum–iron alloy, the $Al_{13}Fe_4$ phase (~59.41 at.% Al) appears in the structure, forming via a peritectic reaction at 997 °C. At approximately 18 at.% Fe and a temperature of 622 °C, a eutectic transformation occurs, resulting in the formation of an aluminum solid solution (Al).

Further increases in iron content in the alloy lead to the formation of the following chemical

compounds: $Al_{15}Si_2Cr_4$ (~61.43 at.% Al), AlFeSi (~51.44 at.% Al), Al_8Fe_2Si (~58.17 at.% Al), and $Al_9Fe_2Si_2$ (~60.1 at.% Al).

Table 1 - Distribution of phase regions depending on temperature

Designation	Phase domain
1	Liquid
2	Liquid + $Al_{13}Fe_4$
3	Liquid + $Al_{13}Fe_4$+ $Al_{15}Si_2Cr_4$
4	Liquid + $Al_{13}Fe_4$+ $Al_{15}Si_2Cr_4$+ AlFeSi
5	Liquid + $Al_{15}Si_2Cr_4$
6	Liquid + $Al_{13}Fe_4$+ $Al_{15}Si_2Cr_4$ + Al_8Fe_2Si
7	Liquid + $Al_{15}Si_2Cr_4$+ Al_8Fe_2Si
8	Liquid + $Al_{15}Si_2Cr_4$+ Al_8Fe_2Si + $Al_9Fe_2Si_2$
9	$Al_{15}Si_2Cr_4$+ Al_8Fe_2Si + $Al_9Fe_2Si_2$+ (Al)
10	$Al_{15}Si_2Cr_4$+ Al_8Fe_2Si + $Al_9Fe_2Si_2$
11	$Al_{15}Si_2Cr_4$+ Al_8Fe_2Si
12	$Al_{13}Fe_4$+ $Al_{15}Si_2Cr_4$+ Al_8Fe_2Si
13	$Al_{13}Fe_4$+ $Al_{15}Si_2Cr_4$+ Al_8Fe_2Si + AlFeSi
14	$Al_{13}Fe_4$+ $Al_{15}Si_2Cr_4$+ AlFeSi

The $Al_{13}Fe_4$ phase, also known as the θ-phase, is one of the most structurally complex intermetallic compounds, possessing a monoclinic unit cell. It is important to note that the formation of this phase in the form of needle-like particles or large, highly oriented intermetallic dendrites significantly reduces the technological ductility of aluminum alloys. The θ-phase ($Al_{13}Fe_4$) can have a detrimental effect on the mechanical properties of the alloy due to its inherently low ductility and impact toughness.

When this phase forms as large inclusions, it may act as a crack initiation site under mechanical loading and also degrades the overall quality of the cast metal structure. Therefore, the presence of this phase requires particular attention, especially in the development of alloys produced using additive manufacturing technologies.

Table 2 presents the calculated parameters of primary crystallization for the Fe-containing phase in the Al–30Fe–9Si–1Cr system.

Table 2 - Calculated parameters of primary crystallization of the Fe-containing phase in the Al–30Fe–9Si–1Cr alloy system

Phase	Content of components, %			
	Al	***Fe***	***Si***	***Cr***
t = 1083 °C (1 area)				
Liquid	73.58	16.41	9.00	1.00
t = 997 °C (2 area)				
Liquid	59.61	28.07	11.06	12.49
$Al_{13}Fe_4$	59.41	39.85	0.72	0.00
t = 878 °C (3 area)				
Liquid	73.08	15.9	10.8	0.21
$Al_{13}Fe_4$	59.55	39.49	0.95	0.00
$Al_{15}Si_2Cr_4$	63.18	21.79	08.05	06.96
t = 820 °C (4 area)				
Liquid	73.00	13.84	13.12	0.03
$Al_{13}Fe_4$	59.22	39.37	14.03	0.00
$Al_{15}Si_2Cr_4$	61.92	23.91	8.13	6.02
AlFeSi	51.21	33.9	14.88	0.00
t = 799 °C (5 area)				
Liquid	84.16	9.18	6.51	0.14
$Al_{15}Si_2Cr_4$	63.05	20.27	9.5	7.16
t = 742 °C (6 area)				
Liquid	83.03	9.52	7.44	0.0004
$Al_{13}Fe_4$	59.54	39.23	12.2	0.00
$Al_{15}Si_2Cr_4$	61.75	25.64	8.22	4.38
Al_8Fe_2Si	56.91	32.54	10.54	0.00
t = 686 °C (7 area)				
Liquid	86.98	4.36	8.65	0.000
$Al_{15}Si_2Cr_4$	61.25	26.27	8.69	3.77
Al_8Fe_2Si	57.38	32.55	10.05	0.00
t = 622 °C (8 area)				
Liquid	89.76	2.09	8.13	0.000
$Al_{15}Si_2Cr_4$	60.56	27.03	9.35	3.04
Al_8Fe_2Si	57.94	32.56	9.49	0.00
$Al_9Fe_2Si_2$	58.03	26.9	15.06	0.00
t = 569 °C (9 area)				
$Al_{15}Si_2Cr_4$	61.00	26.63	8.93	3.42
Al_8Fe_2Si	59.67	32.58	7.74	0.00
$Al_9Fe_2Si_2$	60.9	26.93	12.1	0.00
(Al)	99.55	0.13	0.42	0.000
t = 530 °C (10 area)				
$Al_{15}Si_2Cr_4$	60.49	25.86	9.48	4.15
Al_8Fe_2Si	59.85	32.58	7.5	0.00
$Al_9Fe_2Si_2$	61.39	26.93	11.6	0.00
t = 603 °C (11 area)				
$Al_{15}Si_2Cr_4$	60.79	26.18	9.16	3.85
Al_8Fe_2Si	58.49	32.56	8.94	0.00
t = 671 °C (12 area)				
$Al_{13}Fe_4$	59.53	39.17	1.29	0.00
$Al_{15}Si_2Cr_4$	61.34	25.78	8.62	4.24
Al_8Fe_2Si	57.66	32.55	9.77	0.00
t = 665 °C (13 area)				
$Al_{13}Fe_4$	59.36	39.18	1.45	0.00
$Al_{15}Si_2Cr_4$	61.12	25.5	8.86	4.50
Al_8Fe_2Si	57.48	32.55	9.96	0.00
AlFeSi	52.38	33.91	13.69	0.00
t = 646 °C (14 area)				
$Al_{13}Fe_4$	58.6	39.27	2.11	0.00
$Al_{15}Si_2Cr_4$	60.72	22.61	9.41	7.24
AlFeSi	50.73	33.89	15.37	0.00

A slightly different phase transformation pathway is observed when chromium is introduced by reducing the amount of iron.

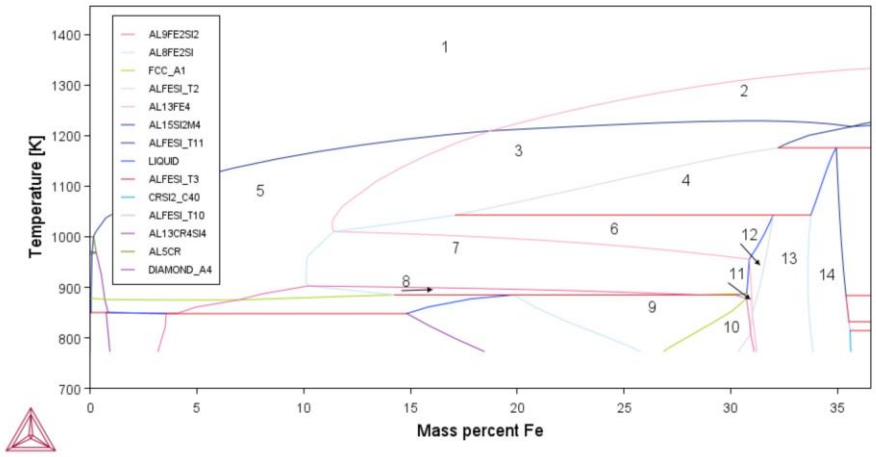

Figure 2 - Polythermal section of the Al-30Fe-9Si-1Cr system with variable aluminum and iron content, with constant silicon and chromium content

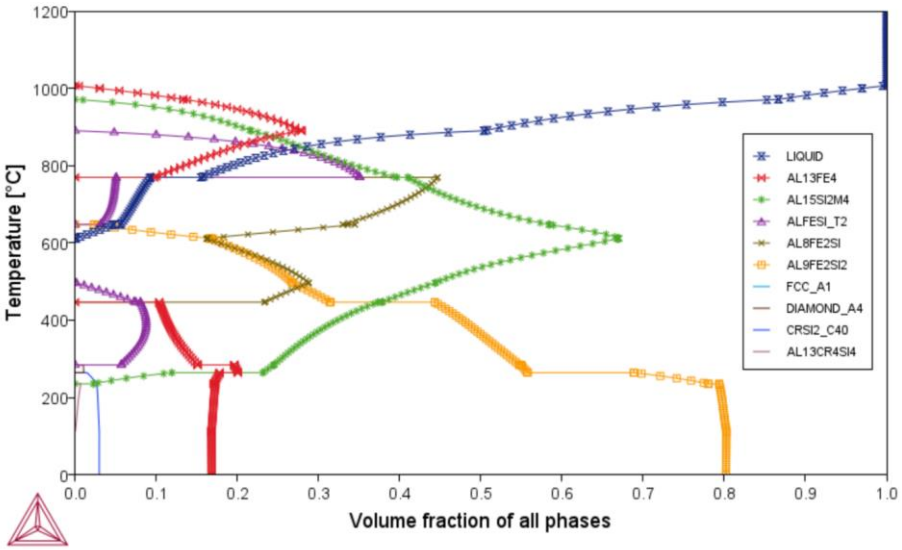

Figure 3 - Volume fraction of all phases depending on temperature in the Al-28Fe-10Si-2Cr alloy

To provide a more detailed analysis of this alloying approach, a polythermal section was constructed (Figure 3), highlighting three regions most favorable for the formation of the primary strengthening phases.

In the first region (3% Cr, 27% Fe), below 980 °C, the θ-phase ($Al_{13}Fe_4$) forms via a eutectic reaction. The temperature range of 980–780 °C corresponds to the stability region of the primary θ-phase. As the temperature further decreases, this phase completely dissolves, accompanied by the formation of the α-phase (Al_8Fe_2Si) in the 770–680 °C range. A subsequent solid-state transformation leads to the re-precipitation of the θ-phase (Region 22) down to room temperature.

At high temperatures, based on the characteristic transformation path, the first phases to precipitate from the melt are hexagonal α (α_h) and cubic α (α_c). Later, αh is fully replaced by the cubic α-phase, stabilized by the chromium addition. Subsequently, the hexagonal α-phase reappears and coexists with the cubic α-phase. The hexagonal α-phase is a high-temperature phase with a narrower stability range (up to 450 °C) compared to its cubic counterpart (stable up to ~240 °C).

In the second region (15% Cr, 15% Fe), the most notable phase formation zones are Regions 2, 8, 24, and 37. In Region 2, a eutectic reaction results in the formation of $CrSi_2$ and α-Cr from the aluminum melt. This transformation concludes in Region 8, where both phases coexist. Chromium disilicide ($CrSi_2$) is an intermetallic compound with a hexagonal structure consisting of alternating layers of chromium and silicon atoms, which defines its mechanical behavior [28]. It exhibits high hardness and brittleness – typical for intermetallics – as well as wear and scratch resistance.

The α_c phase is a hard and brittle intermetallic constituent, which can either enhance or impair the properties of aluminum alloys depending on its morphology and distribution. It is a cubic modification of the α-phase, formed by partially substituting iron atoms with chromium. When uniformly distributed, α_c can inhibit grain growth and stabilize the microstructure. In heat-resistant aluminum alloys, it improves thermal stability. However, in wrought and cast aluminum alloys, this phase can have several detrimental effects, such as increased cracking tendency at elevated temperatures and the creation of internal stress concentrators, reducing ductility and fatigue strength. To minimize these effects, careful control of chromium and silicon content is required, and the use of modifying elements such as Zr, Ti, or Sc may be beneficial for microstructural control.

Region 24 is characterized by the presence of the θ-phase ($Al_{13}Fe_4$), α_c, and the τ_{1Cr} phase within the temperature range of 420–275 °C. This is followed by the formation of the β-phase through a eutectoid transformation (Region 37).

The intermetallic τ_{1Cr} phase ($Al_{13}Cr_4Si_4$ or $Al_{13}Cr_2$) reduces the alloy's tendency to crack and contributes to microstructural stabilization. In this case, chromium acts as a grain growth inhibitor, promoting the formation of a fine-grained, homogeneous structure, which improves the mechanical performance of the alloy. In systems with excess chromium and reduced iron content, conditions are created that favor the formation of this phase instead of the iron-containing θ-phase.

The β-phase ($Al_9Fe_2Si_2$) is one of the most commonly encountered intermetallic compounds in the Al–Si–Fe system. In conventional alloys, it is generally considered undesirable, as it significantly reduces mechanical properties [29]. It commonly forms at grain boundaries as long, needle-like precipitates, sharply decreasing ductility and impact toughness. In intermetallic-rich compositions, the β-phase may also appear as coarse dendrites or flake-like compact particles, typically located along the previously formed θ-phase boundaries.

The third region (27% Cr, 3% Fe) is characterized by a high chromium content, leading to the formation of the Al_4Cr phase, which appears in the structure as a granulated, rounded morphology. Overall, Al_4Cr is considered a favorable phase, as it improves high-temperature strength without significantly compromising corrosion resistance or impact toughness [30].

To quantitatively assess the phase constituents, temperature-dependent volume fraction curves were constructed for all phases along the characteristic transformation paths considered.

As shown in Figure 3, the primary θ-phase ($Al_{13}Fe_4$) crystallizes first at approximately 1000 °C, then dissolves and reprecipitates at around 448 °C. At room temperature, the volume fraction of this phase accounts for approximately 18% of the total alloy volume.

The volume fraction of the α-phase ($Al_{15}(Fe, Cr)_3Si_2$) reaches approximately 68% at 600 °C and is formed over a relatively wide temperature range. The β-phase ($Al_9Fe_2Si_2$) begins to form at 648 °C and continues to exist down to room temperature, comprising about 80% of the total alloy volume in this temperature range.

The α-phase (Al_8Fe_2Si) forms within a relatively narrow and discrete temperature range of 800–445 °C, with a volume fraction of approximately 45%.

Subsequently, a temperature-dependent phase volume fraction diagram was constructed for the Al–27Fe–10Si–3Cr alloy system (Figure 4).

Even a slight increase in chromium content by 1% leads to a significant change in the phase composition. In this case, the α-phase (Al_8Fe_2Si) exhibits a very limited solubility range, constituting only about 18% of the total alloy volume. The volume fraction of the cubic α-phase ($Al_{15}(Fe,Cr)_3Si_2$) reaches 89% at 610 °C, while the amount of β-phase ($Al_9Fe_2Si_2$) decreases to 77% at room temperature. The increase in the cubic α-phase fraction is compensated by the hexagonal α_h phase.

With an increase in chromium content up to 15% (Figure 5), the cubic modification completely replaces the α-phase (Al_8Fe_2Si), with its volume fraction reaching 98% in the temperature range of 980–430 °C. Below 220 °C, a gradual transformation into the β-phase begins, accompanied by the precipitation of θ and $Al_{13}Cr_4Si_4$ phases. Notably, the αCr phase persists down to room temperature.

At the same time, the near-complete substitution of iron with chromium does not promote an increase in the volume fraction of the cubic α-phase ($Al_{15}(Fe, Cr)_3Si_2$) (Figure 6).

On the contrary, the τ_1-Cr phase ($Al_{13}Cr_4Si_4$) begins to dominate in terms of volume fraction, while the hexagonal α-phase is also not formed. It should be noted that in the Al–15Fe–10Si–15Cr composition, increasing the silicon content leads to a reduction in the ($Al_{15}(Fe, Cr)_3Si_2$) phase and the precipitation of free (unbound) silicon.

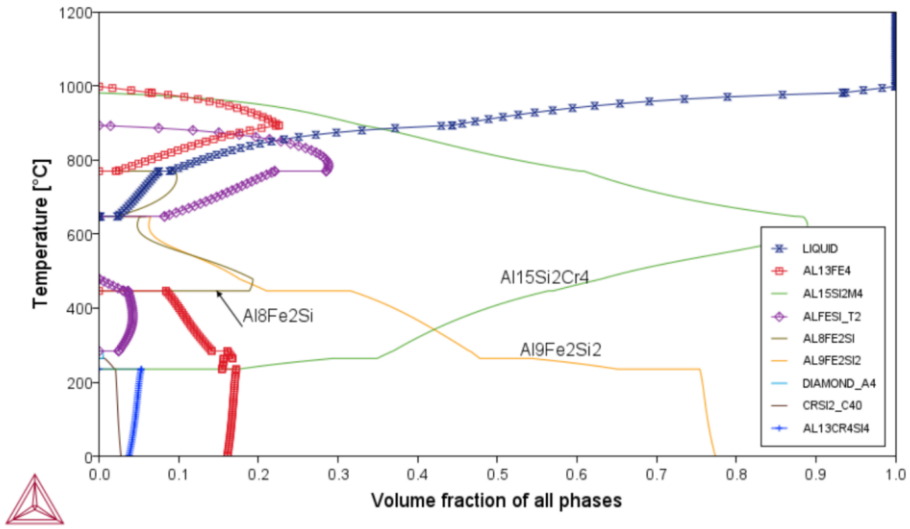

Figure 4 - Volume fraction of all phases depending on temperature in the Al-27Fe-10Si-3Cr alloy

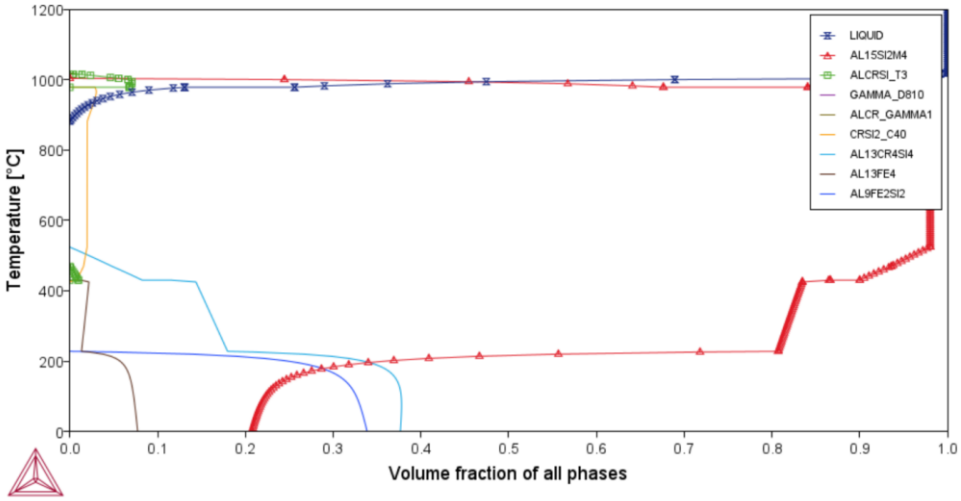

Figure 5 - Volume fraction of all phases depending on temperature in the Al-15Fe-10Si-15Cr alloy

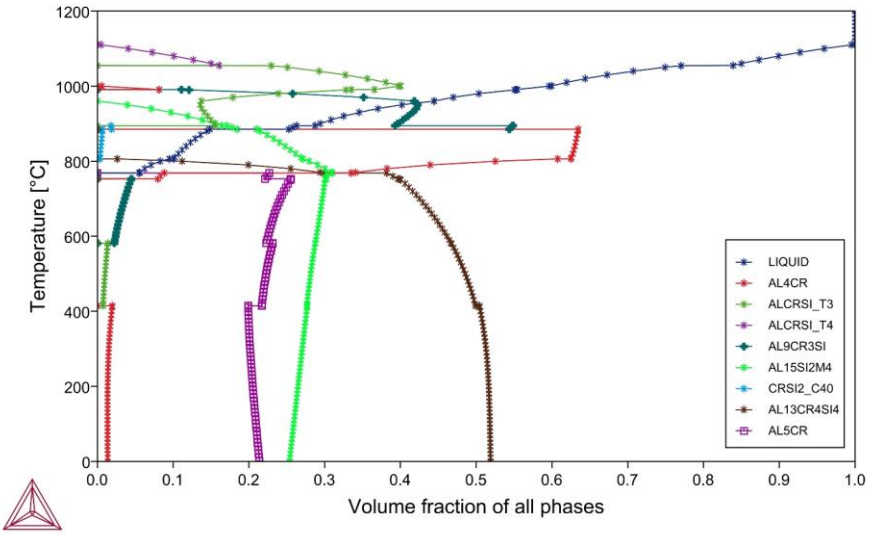

Figure 6 - Volume fraction of all phases depending on temperature in the Al-3Fe-10Si-27Cr alloy

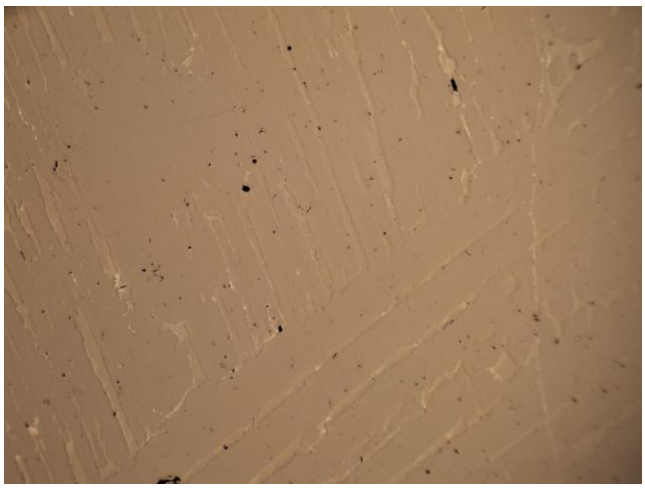

Figure 7 - Microstructure of the Al-Fe-Cr-Si alloy after synthesis, x200

Thus, it has been established that the addition of 2–3% chromium promotes an increase in the fraction of the high-temperature cubic modification of the α-phase, while simultaneously suppressing the growth of the binary θ-phase.

In the Al–15Fe–10Si–3Cr composition, within the temperature range of 980–430 °C, the alloy consists of up to 98% cubic α-phase (αc), with the θ-phase formation significantly suppressed. From our perspective, this phase composition is the most favorable for an intermetallic aluminum alloy.

To validate the obtained modeling results, an additional study was conducted by introducing 3% chromium into the base composition. Figure 7 shows the microstructure of the alloy after chromium addition. As predicted by the modeling results, chromium does not form independent inclusions at room temperature; however, it contributes to the stabilization of the microstructure. After synthesis, the microstructure is predominantly composed of β-phase dendrites, a small fraction of θ-phase distributed between the β-phase dendrites, and a minor amount of chromium-containing phases. The intermetallic compounds exhibit no segregation or cracking.

The primary effect of chromium alloying is manifested in improved stability at elevated temperatures and enhanced plasticity due to the formation of the cubic αc phase.

This study examined the effect of chromium on the properties of aluminum alloys. As an alloying element, chromium plays a crucial role: it enhances structural stability, reduces the risk of defect formation, and improves the mechanical performance of aluminum-based components. Its application may expand the use of aluminum alloys in high-tech industries such as electrical engineering, nuclear power, and aerospace engineering.

Conclusions

A fundamental investigation of the Al–Fe–Si alloy system was conducted with the aim of optimizing its composition. It was found that the use of the base configuration leads to the formation of undesirable morphologies of intermetallic phases. Chromium alloying significantly alters the phase composition, reduces the content of the detrimental θ-phase ($Al_{13}Fe_4$), and promotes the formation of more stable strengthening phases and Cr-containing intermetallics. The introduction of as little as 2% chromium yields notable changes. The obtained results confirm the potential of alloying as an effective approach for developing intermetallic aluminum alloys with tailored properties. This opens new opportunities for advancing the aluminum industry in Kazakhstan and enhancing the global competitiveness of its products. These results hold practical value for the development of new composite materials and for interpreting the microstructure of industrial aluminum alloys.

Conflict of interest. On behalf of all authors, the corresponding author declares that there is no conflict of interest.

CRediT author statement: **V. Andreyachshenko**: Conceptualization, Methodology, Investigation, Reviewing and Editing; **A. Toleuova:** Software. Visualization, Writing draft preparation.

Acknowledgements. This research is funded by the Science Committee of the Ministry of Science and Higher Education of the Republic of Kazakhstan. Grant No. AP19675471 Development of technology for the synthesis of composite ceramic materials of the AlxFeySi system using the additive method**.**

Cite this article as: Andreyachshenko VA, Toleuova AR. Effect of Chromium on Phase Formation of Intermetallic Aluminum Alloys in the Al-Fe-Si System. Kompleksnoe Ispolzovanie Mineralnogo Syra = Complex Use of Mineral Resources. 2027; 342(3):5-15. https://doi.org/10.31643/2027/6445.25

Al-Fe-Si жүйесінің металаралық алюминий қорытпаларының фазалық түзілуіне және микроқұрылымына хромның әсері

Андреященко В.А., Толеуова А.Р.

Әбілқас Сағынов атындағы Қарағанды техникалық университеті, Қарағанды, Қазақстан

Мақала келді: *16 қыркүйек 2025*
Сараптамадан өтті: *11 қараша 2025*
Қабылданды: *11 желтоқсан 2025*

ТҮЙІНДЕМЕ

Мақалада хром қорытпасымен Al-Fe-Si жүйесінің композиттік алюминий қорытпаларын синтездеу үшін аддитивті технологияларды қолдануға баса назар аудара отырып, Қазақстандағы алюминий өнеркәсібінің даму перспективалары қарастырылады. Балқитын электродпен қаптау әдісімен синтезделген қорытпалардың фазалық құрамына кешенді металлографиялық және термодинамикалық талдау жүргізілді. Thermo-Calc бағдарламалық құралын пайдалану политермиялық қималарды салуға және легірлеуші элементтер концентрациясының металаралық фазалардың, соның ішінде Al13Fe4 (θ-фаза) және Al8Fe2Si түзілуіне әсерін анықтауға мүмкіндік берді. Хроммен оңтайлы легрлеу шарттары негізделді, бұл ұсақ түйіршікті құрылымның пайда болуына, фазалық құрамның тұрақтануына және ірі бастапқы дендриттердің жойылуына байланысты сынғыштықтың төмендеуін және механикалық қасиеттердің жоғарылауын қамтамасыз етеді. Алынған нәтижелер хром қорытпаларының қажетті қасиеттері бар интерметалдық алюминий қорытпаларын әзірлеудегі тиімді тәсіл ретіндегі әлеуетін растайды. Зерттеу нәтижелері жақсартылған өнімділік сипаттамалары бар алюминий қорытпаларын алу технологияларын әзірлеуге ықпал етеді және өнеркәсіпте аддитивті әдістерді қолдану мүмкіндіктерін кеңейтеді.

Түйін сөздер: Al-Fe-Si, интерметалдық фазалар, модельдеу, фазалық түрлендіру диаграммасы, микроқұрылым.

Андреященко Виолетта Александровна

Автор туралы ақпарат:
PhD, қауымдастырылған профессор, Минералдық шикізат қазбаларды кешенді игеру инженерлік бейіндегі сынақ зертханасының басшысы, Әбілқас Сағынов атындағы Қарағанды техникалық университеті, Н. Назарбаев даңғылы, 56, Қарағанды, Қазақстан. E-mail: v.andreyachshenko@ktu.edu.kz; ORCID ID: https://orcid.org/0000-0001-6933-8163

Толеуова Айнагуль Рымкуловна

PhD, қауымдастырылған профессор, Нанотехнология және металлургия кафедрасының доценті, Әбілқас Сағынов атындағы Қарағанды техникалық университеті, Н.Назарбаев даңғылы, 56, Қарағанды, Қазақстан. Email: rymkul.ainagul@mail.ru; ORCID ID: https://orcid.org/0000-0002-3216-1824

Влияние хрома на фазообразование и микроструктуру интерметаллидных алюминиевых сплавов системы Al-Fe-Si

Андреященко В.А., Толеуова А.Р.

Карагандинский технический университет имени Абылкаса Сагинова, Караганда, Казахстан

Поступила: *16 сентября 2025*
Рецензирование: *11 ноября 2025*
Принята в печать: *11 декабря 2025*

АННОТАЦИЯ

В статье рассмотрены перспективы развития алюминиевой промышленности Казахстана с акцентом на применение аддитивных технологий для синтеза композиционных алюминиевых сплавов системы Al-Fe-Si с легированием хромом. Проведен комплексный металлографический и термодинамический анализ фазового состава сплавов, синтезированных методом наплавки плавящимся электродом. Использование программного обеспечения Thermo-Calc позволило построить политермические разрезы и определить влияние концентрации легирующих элементов на формирование интерметаллических фаз, включая Al13Fe4 (θ-фазу) и Al8Fe2Si. Обоснованы условия оптимального легирования хромом, обеспечивающие снижение хрупкости и повышение механических свойств за счет формирования мелкозернистой структуры, стабилизации фазового состава и устранение крупных первичных дендритов. Полученные результаты подтверждают потенциал легирования хромом как эффективного подхода в разработке интерметаллидных алюминиевых сплавов с заданными свойствами. Результаты исследования способствуют развитию технологий получения алюминиевых сплавов с улучшенными эксплуатационными характеристиками и расширяют возможности применения аддитивных методов в промышленности.

Ключевые слова: Al-Fe-Si, интерметаллидные фазы, моделирование, диаграмма фазовой трансформации, микроструктура.

Андреященко Виолетта Александровна	***Информация об авторах:*** *PhD, ассоциированный профессор, руководитель испытательной лаборатории инженерного профиля Комплексное освоение ресурсов минерального сырья, Карагандинский технический университет имени Абылкаса Сагинова, пр. Н. Назарбаева, 56, Караганда, Казахстан. E-mail: v.andreyachshenko@ktu.edu.kz; ORCID ID: https://orcid.org/0000-0001-6933-8163*
Толеуова Айнагуль Рымкуловна	*PhD, ассоциированный профессор, доцент каф. нанотехнологии и металлургии, Карагандинский технический университет имени Абылкаса Сагинова, пр. Н. Назарбаева, 56, Караганда, Казахстан. Email: rymkul.ainagul@mail.ru; ORCID ID: https://orcid.org/0000-0002-3216-1824*

References

[1] Zhang X, Wang D, Li X, Zhang H, Nagaumi H. Understanding crystal structure and morphology evolution of Fe, Mn, Cr-containing phases in Al-Si cast alloy. Intermetallics. 2021; 131:107103. https://doi.org/10.1016/j.intermet.2021.1071034

[2] Kocich R. Effects of Twist Channel Angular Pressing on Structure and Properties of Bimetallic Al/Cu Clad Composites. Mater. Des. 2020; 196:109255. https://doi.org/10.1016/j.matdes.2020.109255

[3] Xia X, Chen M, Lu Y-J, Fan F, Zhu C, Huang J, Deng T, Zhu S. Microstructure and Mechanical Properties of Isothermal Multi-Axial Forging Formed AZ61 Mg Alloy. Trans. Nonferrous Met. Soc. China. 2013; 23:3186–3192. https://doi.org/10.1016/S1003-6326(13)62851-4

[4] Que Z, Fang C, Mendis CL, Wang Y, Fan Z. Effects of Si solution in θ-Al13Fe4 on phase transformation between Fe-containing intermetallic compounds in Al alloys. Journal of Alloys and Compounds. 2023; 932:167587. https://doi.org/10.1016/j.jallcom.2022.167587

[5] Andreyachshenko VA. Finite element simulation (FES) of the fullering in device with movable elements. Metalurgija. 2016; 55(4):829-831.

[6] Naizabekov AB, Andreyachshenko VA, Kliber J, Kocich R. Tool for realization several plastic deformation. In: Proceedings of the 22nd International Conference on Metallurgy and Materials METAL; Brno, Czech Republic. 2013, 317-321.

[7] Andreyachshenko V, et al. ECAP-treated aluminium alloy AA2030: microstructure and mechanical properties. Materials & Technologies. Materiali in Tehnologije. 2019; 53(6):805-810. https://doi.org/10.17222/mit.2018.250

[8] Kunčická L, Kocich R. Effect of Activated Slip Systems on Dynamic Recrystallization during Rotary Swaging of Electroconductive Al-Cu Composites. Materials Letters. 2022; 321:10-13.

[9] Lukáč P, Kocich R, Greger M, Padalka O, Szaraz Z. Microstructure of AZ31 and AZ61 Mg Alloys Prepared by Rolling and ECAP. Kovove Materialy. Metallic Materials. 2007; 45:115-120.

[10] Andreyachshenko VA, Ibatov MK. Optimization of the three-component Al-Fe-Si system composition. Metallurgical Research and Technology. 2024; 121(3):315. https://doi.org/10.1051/metal/2024035

[11] Arbeiter J, Vončina M, Volšak D, Medved J. Evolution of Fe-based intermetallic phases during homogenization of Al–Fe hypoeutectic alloy. Journal of Thermal Analysis and Calorimetry. 2020; 142(5):1693-1699. https://doi.org/10.1007/s10973-020-10161-8

[12] Kocich R, Kunčická L. Optimizing Structure and Properties of Al/Cu Laminated Conductors via Severe Shear Strain. J. Alloys Compd. 2023; 953:170124. https://doi.org/10.1016/j.jallcom.2023.170124

[13] Belov NA, Alabin AN, Matveeva IA, Eskin DG. Effect of Zr additions and annealing temperature on electrical conductivity and hardness of hot rolled Al sheets. Trans. Nonferrous Met. Soc. China. 2015; 25:2817-2826. https://doi.org/10.1016/S1003-6326(15)63907-3

[14] Hemachandra M, Mamedipaka R, Kumar A, Thapliyal S. Investigating the Microstructure and Mechanical Behavior of Optimized Eutectic Al-Si Alloy Developed by Direct Energy Deposition. Journal of Manufacturing Processes. 2024; 110:398-411.

[15] Fang X, Li K, Ma M, Shang J, Feng X, Hou Y, Zhu Y, Huang K. Microstructure and Properties of a Novel High-Performance Al-Si-Mg Alloy Fabricated by Wire-Arc Directed Energy Deposition. Materials Letters. 2024; 360:136010.

[16] Mikolajczak P. Distribution and Morphology of α-Al, Si and Fe-Rich Phases in Al–Si–Fe Alloys under an Electromagnetic Field. Materials. 2023; 16:3304.

[17] Becker H, Thum A, Distl B, Kriegel MJ, Leineweber A. Effect of melt conditioning on removal of Fe from secondary Al-Si alloys containing Mg, Mn, and Cr. Metallurgical and Materials Transactions A. 2018; 49:6375-6389. https://doi.org/10.1007/s11661-018-4930-7

[18] Jiang H, Li S, Zhang L, He J, Zheng Q, Song Y, et al. The influence of rare earth element lanthanum on the microstructures and properties of as-cast 8176 (Al-0.5 Fe) aluminum alloy. Journal of Alloys and Compounds. 2021; 859:157804. https://doi.org/10.1016/j.jallcom.2020.157804

[19] Chen Y, Xiao C, Zhu S, Li Z, Yang W, Zhao F, et al. Microstructure characterization and mechanical properties of crack-free Al-Cu-Mg-Y alloy fabricated by laser powder bed fusion. Additive Manufacturing. 2022; 58:103006. https://doi.org/10.1016/j.addma.2022.103006

[20] Sersour Z, Amirouche L. Effect of Alloying Additions and High Temperature T5-Treatment on the Microstructural Behavior of Al-Si-Based Eutectic and Hypo-Eutectic Alloys. International Journal of Metals. 2022; 16:1276-1291.

[21] Jin D, Li H, Yang C, Han Y, Zhu Z, Miao Y, Xu C, Chen B. The Effects of Mg and Si Contents on the Microstructure and Solidification Behavior of Dilute Al-Mg-Si-Fe Alloys. JOM. 2023; 75:4845-4857.

[22] Rajabi M, Vahidi M, Simchi A, Davami P. Effect of rapid solidification on the microstructure and mechanical properties of hot-pressed Al–20Si–5Fe alloys. Materials Characterization. 2009; 60(11):1370-1381. https://doi.org/10.1016/j.matchar.2009.06.014

[23] Zhao Q, Qian Z, Cui X, Wu Y, Liu X. Optimizing microstructures of dilute Al–Fe–Si alloys designed with enhanced electrical conductivity and tensile strength. Journal of Alloys and Compounds. 2015; 650:768-776. https://doi.org/10.1016/j.jallcom.2015.08.052

[24] Kim TS, Suryanarayana C, Chun BS. Effect of alloying elements and degassing pressure on the structure and mechanical properties of rapidly solidified Al–20Si–5Fe–2X (X = Cr, Zr, or Ni) alloys. Materials Science and Engineering A. 2000; 278(1-2):113-120. https://doi.org/10.1016/S0921-5093(99)00589-4

[25] Aranda VA, Figueroa IA, González G, García-Hinojosa JA, Alfonso I. Study of the microstructure and mechanical properties of Al-Si-Fe with additions of chromium by suction casting. Journal of Alloys and Compounds. 2021; 853:157155. https://doi.org/10.1016/j.jallcom.2020.157155

[26] Aranda VA, Figueroa IA, González G, García-Hinojosa JA, Alfonso I. Study of the Microstructure and Mechanical Properties of Al-Si-Fe with Additions of Chromium by Suction Casting. Journal of Alloys and Compounds. 2021; 853:157155.

[27] Pang N, Shi Z, Wang C, Li N, Lin Y. Influence of Cr, Mn, Co and Ni Addition on Crystallization Behavior of Al13Fe4 Phase in Al-5Fe Alloys Based on ThermoDynamic Calculations. Materials. 2021; 14(4):768. https://doi.org/10.3390/ma14040768

[28] Kakitani R, et al. The roles of solidification cooling rate and (Mn, Cr) alloying elements in the modification of β-AlFeSi and hardness evolvements in near-eutectic Al-Si alloys. Journal of Alloys and Metallurgical Systems. 2023; 1:100005. https://doi.org/10.1016/j.jalmes.2023.100005

[29] Kumar PSSR, et al. The Influence of Shock Wave Surface Treatment on Vibration Behavior of Semi-Solid State Cast Aluminum—Al2SiO5 Composite Crystals. [Open Source Preview] 2022; 12(11):1587-1594.

[30] Tsaknopoulos K, Walde C, Tsaknopoulos D, Cote DL. Evolution of Fe-Rich Phases in Thermally Processed Aluminum 6061 Powders for AM Applications. Materials. 2022; 15(17):5853. https://doi.org/10.3390/ma15175853

Crossref
DOI: 10.31643/2027/6445.26
Metallurgy and Metallurgical Engineering

Mineralogical features and optimization of combined beneficiation flowsheets for refractory gold-bearing ores of the Pakrut deposit (Central Tajikistan)

[1,2*]Kholov Kh.I., [3]Juraqulov Sh.R., [1]Samihzoda Sh.R., [4]Mahmudov H.A.

[1]V.I. Nikitin Institute of Chemistry NAST, Dushanbe, Tajikistan
[2]TSPU named after S. Aini, Dushanbe, Tajikistan
[3]Institute of Geology, Earthquake-Resistant Construction and Seismology of the NAST, Dushanbe, Tajikistan
[4]Mining Metallurgical Institute of Tajikistan, Buston, Tajikistan

**Corresponding author email: Kholmahmad90@mail.ru*

Received: *October 8, 2025*
Peer-reviewed: *November 1, 2025*
Accepted: *January 5, 2025*

ABSTRACT

Against the backdrop of depleted rich deposits and the increasing proportion of refractory gold-bearing ores, improving their processing methods has become an urgent task. This work presents the results of a comprehensive study of gold-bearing ores from the Pakrut deposit, located in Central Tajikistan's Zeravshan–Gissar zone. Mineralogical analysis established that the principal gold carriers are pyrite and arsenopyrite, with the metal predominantly localized as fine inclusions and fracture-related accumulations. A notable fraction of gold occurs as free particles (17.03%); however, the dominant share is fracture-bound (62.41%) and is predominantly associated with arsenopyrite. This distribution explains the limited efficiency of single-stage treatment and substantiates the need for combined unlocking and recovery routes. Physicochemical studies confirmed the ores' refractory nature, attributed to the fine dissemination of gold within the sulfide matrix, combined with high hardness and abrasiveness. At the laboratory scale, various beneficiation flowsheets were tested, including direct cyanidation; flotation combined with additional leaching of tailings; and variants incorporating gravity separation. A comparative analysis showed that the highest gold recovery rate (92.23%) was achieved by the flowsheet involving cyanidation, followed by tailings leaching and flotation. Although direct cyanidation also demonstrated a high recovery rate (90.05%), it was less effective. The flotation–cyanidation and gravity–flotation schemes yielded comparatively lower performance. The obtained data confirm the effectiveness of an integrated approach to processing the refractory ores from the Pakrut deposit. Optimizing the beneficiation flowsheet enables a significant increase in precious metal recovery, reduces technological losses, and minimizes environmental risks associated with the accumulation of arsenic-bearing waste.

Keywords: Pakrut deposit, refractory ores, gold, pyrite, arsenopyrite, cyanidation, flotation, gravity separation, mineralogy, beneficiation.

Information about authors:

Kholov Kh.I. — *Cand. Sc. (Tech.), Senior Researcher at the Laboratory of Ore Processing, V.I. Nikitin Institute of Chemistry, National Academy of Sciences of Tajikistan; Senior Lecturer of the Department of Chemical Technology and Ecology at the Tajik State Pedagogical University named after S. Aini, 734063, Dushanbe, Aini St., 299/2, Republic of Tajikistan. E-mail: Kholmahmad90@mail.ru; ORCID ID: https://orcid.org/0000-0002-8202-5919*

Juraqulov Sh.R. — *Senior Researcher, Institute of Geology, Earthquake-Resistant Construction and Seismology, National Academy of Sciences of Tajikistan; 734063, Republic of Tajikistan, Dushanbe, Ayni St., 299/2. E-mail: shaih8888@mail.ru; ORCID ID: https://orcid.org/0009-0001-1255-8541*

Samikhov Sh.R. — *Dr. Sc. (Tech.), Chief Researcher at the Laboratory of Ore Processing, V.I. Nikitin Institute of Chemistry, National Academy of Sciences of Tajikistan, 734063, Dushanbe, Aini St., 299/2, Republic of Tajikistan. E-mail: samikhov72@mail.ru; ORCID ID: https://orcid.org/0009-0002-7454-7343*

Mahmudov H.A. — *Cand. Sc. (Tech.), Dean of the Faculty of Mining, Mining and Metallurgical Institute of Tajikistan, 735730, Buston, Mayakovski St. 6, Republic of Tajikistan. E-mail: obogatitel_0903@mail.ru; ORCID ID: https://orcid.org/0009-0005-8428-5334*

Introduction

In the current context of depleting rich gold deposits, the importance of beneficiating low-grade and “refractory” ores is growing [[1], [2]]. In Tajikistan and worldwide, the quality of mined gold-bearing feedstock is declining: an increasing share of extracted ores are minerals with low gold contents and complex composition [[3], [4]]. According to expert estimates, more than one-third of gold reserves are classed as difficult-to-beneficiate (refractory) ores [5]. A similar trend is

observed globally: roughly 24% of the world's gold reserves are contained in refractory ores [[6], [7]]. Most such deposits are concentrated in traditional gold-mining regions, including CIS countries [8]. Mining forecasts indicate that production from refractory ores will grow at a faster rate (about 1.4% per year) than from conventional ores (≈0.3% per year) [9]. At the same time, conventional processing technologies for these ores remain insufficiently effective: analyses of Russian operations show that, as mining shifts toward poorer and more complex ores, precious-metal losses to tailings have reached 60–85% [10]. All this underscores the urgency of developing modern, more efficient, and environmentally safer beneficiation and leaching approaches for refractory gold-bearing ores [11].

The Pakrut deposit (Central Tajikistan) is an important prospective gold-mining target within the Zeravshan–Gissar zone. Hydrogeologically and structurally, it lies on the southern slopes of the Gissar Range in the Sardoi-Miyona River basin [[12], [13]]. Genetically, Pakrut ores belong to the quartz–gold–low-sulfide formation. Primary ore bodies are represented by lens-like and vein-disseminated zones of metasomatites of carbonate–quartz–albite and quartz–sericite composition, occurring within strongly altered chlorite–sericite–quartz schists of the Upper Ordovician [14]. Mineralization is chiefly confined to subvertical fracture zones, with networks of quartz veins and faults developed there. The key controlling structures are the Pakrut anticline and the cross-cutting Graphite Fault. The principal ore minerals in the mineralized zone are pyrite and arsenopyrite, which dominate the gold-bearing veins. In other words, the richest gold areas are associated with vein-disseminated ores saturated with pyrite and arsenopyrite inclusions.

Native gold in Pakrut ores is extremely fine [15], occurring as dusty or granular inclusions and irregular clod-, droplet-, or platy aggregates, typically along quartz–carbonate boundaries, in sulfide intergranular fissures, and in microcracks; emulsion-like inclusions within pyrite and arsenopyrite are common [16]. This fine, inclusion-bound distribution hampers gravity recovery and prevents direct cyanidation without prior matrix breakdown, explaining the ores' pronounced refractoriness [17].

The main challenge is the low gold recovery caused by the metal being "locked" in sulfides, which leads to losses of 60–85% during direct cyanidation. The solution is to apply ore-unlocking methods—fine grinding, bio-oxidation, or thermal oxidation [18]. The best results are achieved with combined technologies (e.g., flotation + bio-oxidation + cyanidation) [19]. For deposits such as Pakrut, process optimization is key to substantially increasing gold recovery, improving economic efficiency, and reducing environmental impact. Moreover, more complete extraction of gold from refractory ores reduces the volume of toxic waste (e.g., arsenic-bearing sludges) and the environmental burden. From a scientific standpoint, devising an optimal beneficiation scheme requires a deep understanding of how gold is distributed within the complex ore matrix and of the mechanisms governing its transfer into concentrate and solution – knowledge that is important for advancing the entire field.

The aggregate features of Pakrut ores – the fine size of native gold, its association with robust sulfides (pyrite, arsenopyrite), and a complex mineralogical environment – define the core problem addressed here. Traditional single-stage beneficiation schemes do not ensure complete gold recovery from such ores, as evidenced by substantial metal losses [20]. The scientific objective of this study is to develop an optimal combined flowsheet for processing Pakrut's gold-bearing ores that accounts for their geological and mineralogical characteristics. This entails characterizing the ore's mineralogy and gold occurrence, evaluating liberation and beneficiation stages, and selecting a cost-effective, environmentally sound process configuration to maximize recovery.

Materials and Methods

Representative run-of-mine ore from the Pakrut deposit was homogenized, riffle split, and characterized by particle-size distribution and head assays. Mineralogical characterization combined reflected-light microscopy, X-ray diffraction, and diagnostic leaching (chemical phase analysis) to quantify the principal gold carriers (pyrite, arsenopyrite), the modes of occurrence (free, fracture-related, intergranular/enclosed), and the size–morphology spectrum of native gold. At bench scale, we evaluated four processing routes: (a) direct cyanidation of ore ground to −0.074 mm (90% passing) at pH 11.5 with 1.5 kg/t NaCN, 40% solids, 24 h; (b) cyanidation with subsequent leaching of tailings and flotation; (c) flotation followed by cyanidation of a reground concentrate (−0.038 mm, 95% passing; CIP/CIL with up to 14 kg/t NaCN, 48 h); (d) gravity preconcentration + flotation

+ cyanidation, with the bulk mixture cyanidized at up to 18 kg/t NaCN. Flotation tests employed sodium butyl xanthate (collector), copper sulfate (activator), sodium carbonate and sodium hexametaphosphate (modifiers), and pine oil (frother); grind sizes and reagent dosages were optimized in closed-circuit experiments. Flotation experiments were carried out using a laboratory flotation machine (Model 237 FL-A, Mechanobr, Russia) equipped with a 0.75-L cell. The pulp solids content was maintained at 25–40 wt.% solids, and more than 50% of the particles were finer than 0.074 mm. Prior to flotation, flotation reagents were added to the cell and the pulp was conditioned under agitation for several minutes to ensure a homogeneous suspension. Flotation tests were performed in a closed-circuit configuration comprising rougher flotation, two cleaning stages, and two scavenging stages. The pulp pH was monitored and controlled using sodium carbonate (Na2CO3). The number of stages and operating parameters were kept constant across all reported tests to ensure comparability of recoveries and product grades. Gold grade and recovery were determined by fire assay and mass balance; the concentrate composition (Au, Ag, S, As, and major elements) was analyzed to assess downstream processing constraints and compare flowsheet performance.

Results and Discussion

The Pakrut ores are multimineralic: the framework is formed by pyrite and arsenopyrite, with a substantial contribution from quartz – the principal hosts of gold. Feldspars, carbonates, chlorite, and sericite are also present in notable amounts; average contents are listed in Table 1. Variations in composition and texture affect liberation and the choice of beneficiation regimes.

Table 1 – Mineral composition of Pakrut gold-bearing ores

Minerals	Content, %
Pyrite	0.98
Arsenopyrite	0.70
Magnetite	0.67
Ilmenite	
Rutile	
Feldspar	38.20
Quartz	36.28
Dolomite and carbonates	8.07
Chlorite	8.61
Sericite, kaolinite	5.72
Others	0.77

Diagnostic (chemical phase) analysis indicates a predominance of free (native) gold and fine to submicroscopic inclusions within sulfides. Hard-to-access forms account for only 2–3%, which implies the potential for high recoveries with fine grinding and a rational combination of processing stages.

Additional investigation of mineral composition was carried out by X-ray phase analysis. On the X-ray pattern of the initial ore (Fig. 1), the main phases are clearly registered. Quantitative analysis showed: quartz 39.28–92.38%; talc 14.97%; alumina 1.49–23.06%; iron(III) and iron(II) oxides 0.93–10.58%; manganese 0.01–0.38%; magnesium 0.10–6.12%; calcium 0.84–12.33%; potassium 0.20–7.54%; sodium 0.19–8.45%; phosphorus(V) 0.01–0.73%; sulfur 0.00–0.05%; carbon dioxide 0.20–7.92%; water 0.02–0.48%; other components 0.38–14.79%.

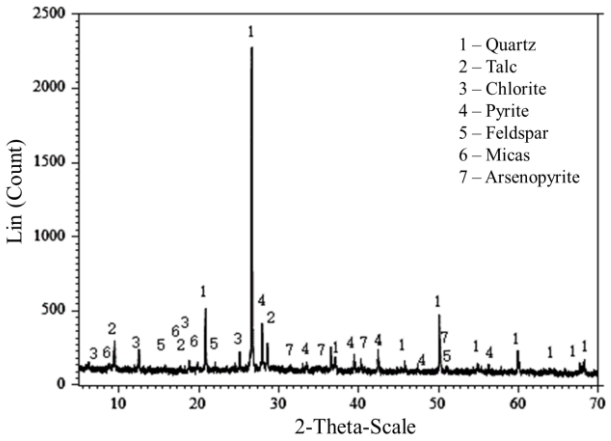

Figure 1 - X-ray of the initial ore

Study of the size distribution of native-gold particles showed a predominance of medium and fine fractions (Table 2). Over 99% of visible gold is concentrated in the size range from −0.3 to +0.01 mm, which requires careful control of ore grinding before beneficiation (Table 3).

Table 2 – Distribution of gold by phases

Phase	Native gold	Gold enclosed in sulfides	Gold bound to other minerals	Total
Grade, g/t	5.01	0.39	0.12	5.52
Percent, %	90.76	7.07	2.17	100

Gold is present mainly as native gold. As the silver content in gold increases, its microscopic color changes from golden-yellow to bright yellow. Gold occurs primarily as included gold, crack-

contained gold, and intergranular gold in pyrite, arsenopyrite, sphalerite, jamesonite, and gangue.

Table 3 – Size distribution of native-gold particles

Class	Particle size, mm	Percent, %	Cumulative, %
Coarse	-0.3+0.074	36.43	36.43
Medium	-0.074+0.030	32.24	68.67
Fine	-0.030+0.010	31.19	99.86
Microfine	-0.010+0.001	0.14	100.00

The shape of native gold is also an important factor governing its technological behavior. As seen from Table 4, granular and irregular particles predominate and together account for more than half of all gold.

Table 4 – Morphologies of native gold in Pakrut ores

Particle shape	Percent, %
Granular	31.51
Irregular	24.66
Dendritic, veined	17.81
Platy, triangular	9.59
Rounded	12.33
Ellipsoidal	4.11
Total	100

Analysis of the distribution of native-gold morphologies is important for understanding the geological conditions of its formation and for selecting optimal recovery methods. At this deposit, the morphology of native gold is quite diverse.

From the table it is evident that the most common are granular gold particles (31.51%) and irregular forms (24.66%). Dendritic and veined forms account for 17.81%, while platy and triangular forms make up 9.59%. Rounded particles and ellipsoidal forms are less frequent, amounting to 12.33% and 4.11%, respectively.

Overall, rounded or ellipsoidal gold is less prone to grinding, which can hinder leaching and flotation. In contrast, native gold of irregular morphologies – such as dendritic, veined, or platy particles – is more readily milled. This has a favorable effect on the efficiency of gold flotation and leaching.

Occurrence of Gold

The study of the morphology and distribution of gold in the gold-bearing ores of the Pakrut deposit showed that it occurs both in free and in bound form. The most common are crack-related segregations of gold associated with arsenopyrite, pyrite, quartz, and sericite (Table 5).

Table 5 – Forms of gold occurrence and associated minerals

Form	Associated minerals	Share, %	Cumulative, %
Wrapped gold	Arsenopyrite	0.05	1.97
	Pyrite	0.20	
	Sericite	1.72	
Intercrystalline gold	Arsenopyrite, quartz	1.24	18.58
	Arsenopyrite, sericite	1.93	
	Arsenopyrite, pyrite	0.06	
	Quartz, sericite	1.68	
	Pyrite, quartz	13.73	
Crack-type gold	Arsenopyrite	58.66	62.41
	Quartz	1.12	
	Sericite	0.97	
	Pyrite	1.29	
	Siderite	0.37	
Free gold	–	17.03	17.03
Total	–	100.00	100.00

A smaller but technologically important fraction of the metal occurs in the free state (17%), which favors its recovery by conventional processing methods. At the same time, the presence of gold wrapped in sulfide minerals, as well as intercrystalline gold, imparts technological refractoriness to the ores and requires the use of combined unlocking methods.

The analysis of the data indicates that more than half of the gold is concentrated as crack-related segregations in arsenopyrite, which confirms the leading role of this mineral as the main carrier of the precious metal. A significant portion of gold (about 17%) is present in the free form, which ensures the possibility of its effective recovery by cyanidation and gravity concentration. At the same time, the presence of intercrystalline and wrapped gold (about 20%) requires fine grinding of the ore and the application of flotation or alternative unlocking methods capable of releasing gold from the sulfide matrix.

Characteristics of the Distribution of Other Metal-Bearing Minerals

Mineralogical study of the gold-bearing ores of the Pakrut deposit showed that, along with native gold and its inclusions in sulfides, pyrite, arsenopyrite, and several subordinate minerals play a significant role in the formation of the ore mass, exerting a direct influence on the conditions of beneficiation and recovery of the precious metal.

Pyrite (FeS_2) is one of the most widespread sulfide minerals in the Pakrut ores and at the same time an important gold carrier. It occurs both as independent grains of varying size and as intergrowths with vein and other ore minerals. The distribution of pyrite across size fractions is uneven: large grains up to 0.8 mm are found alongside much smaller particles down to 0.002 mm. Particularly inaccessible are gold inclusions within microfine pyrite, since their liberation requires ultrafine grinding, which increases the energy costs of processing. Pyrite is often associated with arsenopyrite, limonite, and quartz, forming complex aggregates that determine the refractory nature of the ore and cause elevated gold losses in flotation and cyanidation tails.

Arsenopyrite (FeAsS) plays a key role in ore formation and is the main carrier of finely dispersed gold. Its grains range in size from 0.005 to 0.050 mm and occur both in free form and as intergrowths with vein minerals. Characteristic features include arsenopyrite–quartz and arsenopyrite–sericite aggregates, as well as fine and microfine inclusions that are difficult to liberate during conventional grinding. It is these arsenopyrite associations that account for the predominance of crack-related gold in Pakrut ores, making it necessary to use combined unlocking methods, including flotation and oxidative processes.

Limonite ($2Fe_2O_3 \cdot 3H_2O$). Although present only in small amounts, limonite commonly infills fractures and grain boundaries in pyrite, modifying sulfide surfaces, lowering hydrophobicity, and complicating flotation; accordingly, the reagent scheme must be adjusted to maintain selectivity. Overall, the spatial association of pyrite, arsenopyrite, and limonite indicates that gold is closely tied to these phases. The main processing challenges are gold microinclusions in pyrite and arsenopyrite and the difficulty of liberating the precious metal from stable intergrowths. These features confirm the refractory nature of the ore and necessitate the application of fine and ultrafine grinding, flotation, and additional oxidative unlocking stages to improve gold recovery.

Physical Properties of the Ore

Pakrut gold ore has an average density of about 2.62 t/m³ (medium density) and a Mohs hardness of 6–8, indicating a moderately hard material. The presence of abrasive minerals such as quartz, pyrite, and arsenopyrite means the ore can cause significant equipment wear, necessitating heavy-duty crushing and grinding to effectively liberate the fine gold particles. The ore's crushability index of around 1.6 further suggests it is a medium-strength rock, consistent with its density and hardness. Additionally, with an angle of repose of roughly 40°, the ore forms stable piles — an important factor for safe stockpiling and tailings management.

Beneficiation Experiment

A series of laboratory experiments on processing the gold-bearing ores of the Pakrut deposit was carried out at several research laboratories, including the chemical laboratory of JV "Pakrut", the ore beneficiation laboratory of the V.I. Nikitin Institute of Chemistry of the NAST, the Central Chemical Laboratory of the Main Geological Directorate under the Government of the Republic of Tajikistan and the Beijing Research Institute of Mining and Metallurgy (Kryso Resources plc). During these experiments, various technological approaches were investigated, including direct cyanidation, flotation, gravity separation, and combined variants thereof. The experiments aimed to determine the optimal flowsheet that would ensure the maximum possible gold recovery under acceptable processing conditions.

Direct Cyanidation

Direct cyanidation was performed on ore ground to 90% −0.074 mm using 1.5 kg/t NaCN at pH = 11.5 (maintained with 1.5 kg/t lime), with 40% solids for 24 h. The test yielded 90.05% Au recovery, 0.55 g/t Au in tails, and 1.5 kg/t cyanide consumption. The experimental results are presented in Table 6.

Table 6 – Results of direct cyanidation

Gold in tails, g/t	Gold recovery, %	NaCN consumption, kg/t
0.55	90.05	1.5

The obtained data showed a fairly high level of gold recovery (90.05%), confirming the

effectiveness of cyanidation for finely ground ore. However, part of the metal remained in the cyanidation tailings, which necessitated the evaluation of more advanced flowsheets. The next stage was the study of a combined process that included cyanidation, subsequent leaching of the cyanidation tailings, and flotation. The results obtained are given in Table 7.

Table 7 – Results of flotation of cyanidation tailings

Product	Yield, %	Au grade, g/t	Au recovery, %
Flotation concentrate	1.58	23.43	64.12
Flotation tails	98.42	0.21	35.88
Cyanidation tailings (feed)	100.0	0.55	100.00

Cyanidation + Tailings Leaching and Flotation

To increase gold recovery, a combined flowsheet was tested that included flotation and additional leaching of the cyanidation tailings. This scheme made it possible to achieve a more complete recovery of gold (overall above 92%), confirming its advantages over direct cyanidation.

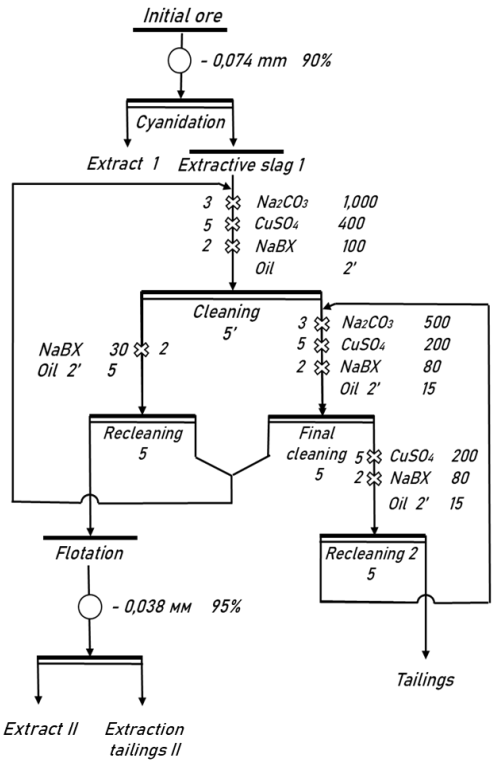

Figure 2 - Process flowsheet: cyanidation + tailings leaching + flotation

The efficiency of a flotation–cyanidation scheme was also tested. The ore was floated, after which the concentrate was treated by cyanidation at a higher reagent dosage (NaCN – 4 kg/t; grind size −0.038 mm with 95% of the fine class). The results are given in Table 8.

Table 8 – Results of cyanidation of flotation concentrate

Concentrate grade, g/t	Gold in tails, g/t	Recovery, %	NaCN, kg/t
23.43	15.42	34.19	4.0

In this case, the total gold recovery was 85.24%, which is lower than for the combined scheme Fig. 2. Closed-circuit flotation tests nevertheless showed the possibility of obtaining concentrates with high gold contents.

Flotation + Cyanidation

Within this beneficiation option, the initial ore was ground to −0.074 mm with 81% of the fine fraction, while the flotation concentrate was ground to −0.038 mm (95%). At the flotation stage, a concentrate with a high gold grade of 127 g/t was obtained, with a yield of 3.85% and a recovery of 91.87% (Table 9). However, significant metal losses (8.13%) were recorded in the flotation tails, which ultimately harmed the overall efficiency of the scheme.

Table 9 – Flotation results (closed circuit)

Product	Yield, %	Au grade, g/t	Au recovery, %
Concentrate	3.85	127	91.87
Tails	96.15	0.45	8.13
Ore	100.0	5.32	100.0

The obtained flotation concentrate was subjected to cyanidation under both CIL and CIP schemes. With a NaCN dosage of 14 kg/t, pH = 11.5, and a leaching duration of 48 hours, gold recovery reached 92.79% (CIL) and 92.12% (CIP), while the gold content in the tails remained as high as 9.16–10.01 g/t (Table 10). Thus, despite the high degree of concentrate enrichment, a significant portion of the precious metal remained in the solid phase.

The “flotation + cyanidation” scheme, presented in Figure 3, demonstrated a total gold recovery of 85.24%. This result was lower compared with other combined options, particularly “cyanidation + tailings leaching + flotation” (92.23%) and “gravity + flotation + cyanidation” (86.62%). The reason lies in the fact that during

flotation, part of the finely disseminated gold, closely associated with pyrite and arsenopyrite, remains in the tails, and subsequent cyanidation of the concentrate does not compensate for these losses.

Table 10 – Results of cyanidation of the flotation concentrate

Product	Au, g/t	Au in tails, g/t	Recovery, %	NaCN, kg/t
Concentrate (CIL)	127	9.16	92.79	14
Concentrate (CIP)	127	10.01	92.12	14
Flotation tails	0.45	0.38	15.56	1

Therefore, the flotation–cyanidation scheme is characterized by a high degree of gold concentration in the beneficiation product but a relatively low overall process efficiency. For practical application, it may be advisable in cases where the priority is obtaining concentrates with high gold grades. However, to achieve maximum overall gold recovery, it should be combined with additional stages (e.g., tailings leaching or finer grinding).

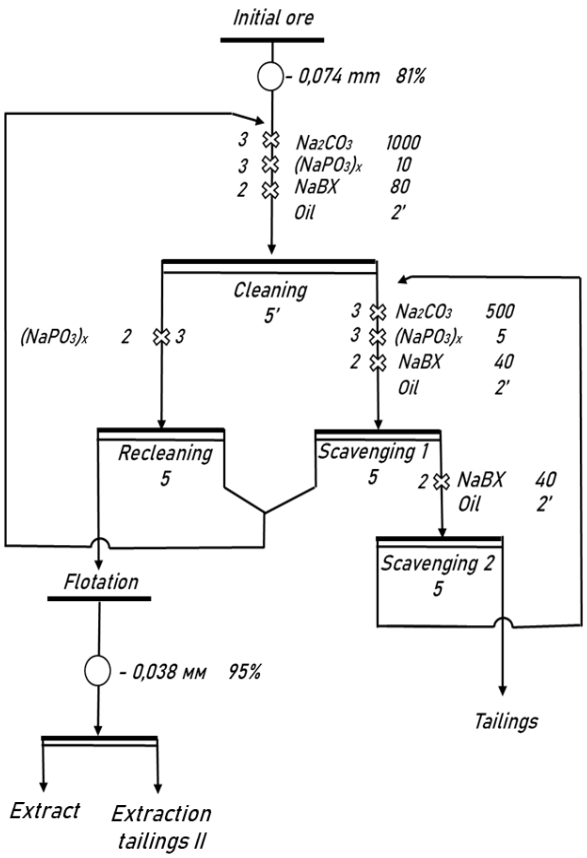

Figure 3 - Flotation + cyanidation flowsheet

3.4.4. Gravity + Flotation + Cyanidation

To improve the selectivity of gold recovery, a combined flowsheet was tested in which gravity separation was applied prior to flotation. The gravity stage allowed the isolation of a high-grade concentrate (471 g/t Au) with a recovery of 31.46%, although its yield was relatively low at only 0.37%. The subsequent flotation step produced an additional concentrate containing 120.1 g/t Au with 61.84% recovery. When the gravity and flotation concentrates were combined, the resulting mixture reached an average gold grade of 160.4 g/t and an overall recovery of 93.30% (Table 11).

Table 11 – Results of gravity and flotation beneficiation

Product	Yield, %	Au grade, g/t	Au recovery, %
Concentrate 1 (gravity)	0.37	471.00	31.46
Concentrate 2 (flotation)	2.83	120.10	61.84
Mixture of concentrates	3.19	160.40	93.30
Tails	96.81	0.38	6.70
Ore	100.0	5.49	100.0

The combined concentrate was then subjected to cyanidation at a NaCN dosage of 18 kg/t. Under these conditions, the recovery reached 92.84%, with residual gold content in the leaching tails of 11.48 g/t (Table 12).

Table 12 – Cyanidation of the concentrate mixture

Product	Au, g/t	Au in tails, g/t	Recovery, %	NaCN, kg/t
Mixture of concentrates	160.4	11.48	92.84	18

As illustrated in Figure 4, the gravity–flotation–cyanidation scheme ensured a total recovery of 86.62%. Although this result was higher than for the flotation–cyanidation option (85.24%), it remained lower compared with the cyanidation + tailings leaching + flotation scheme (92.23%). The main limitation of this approach is the extremely low yield of the gravity concentrate, which, despite its exceptionally high gold grade, contributes only marginally to the overall metal balance.

Thus, the gravity–flotation–cyanidation scheme demonstrates the potential to enhance concentrate quality and recovery efficiency. However, its industrial application is constrained by the low productivity of the gravity stage, which reduces its attractiveness compared with other combined processing options.

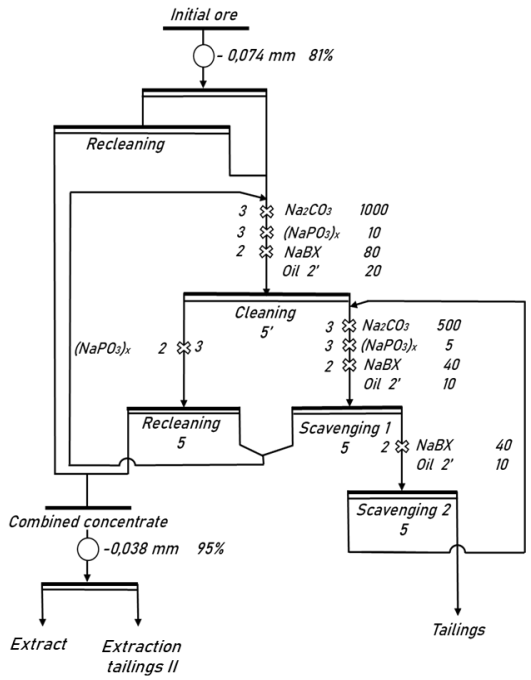

Figure 4 - Gravity + flotation + cyanidation flowsheet

Comparative Analysis

The experimental studies demonstrated that the efficiency of different processing flowsheets for the Pakrut gold-bearing ores varies significantly (Table 13). The highest performance was achieved with the combined flowsheet "cyanidation + tailings leaching + flotation," which ensured total gold recovery of 92.23%. This option allows for a more complete release of finely disseminated gold and minimizes metal losses in the tails, making it the most promising for practical implementation.

Table 13 – Comparison of beneficiation scheme effectiveness

№	Technology	Au recovery, %
1	Cyanidation	90.05
2	Cyanidation + tailings leaching + flotation	92.23
3	Flotation + cyanidation	85.24
4	Gravity + flotation + cyanidation	86.62

Direct cyanidation also showed a high result (90.05%); however, part of the gold remained in the solid phase due to its association with pyrite and arsenopyrite. This limits the method's effectiveness and indicates its applicability mainly for ores that are relatively easy to unlock.

The "flotation + cyanidation" scheme provided a lower recovery rate of 85.24%. Despite the high gold grade in the flotation concentrate (127 g/t), substantial metal losses in the flotation tails led to reduced overall efficiency. Similar limitations were observed in the "gravity + flotation + cyanidation" scheme, where the total recovery was 86.62%. Although the gravity concentrate showed very high gold grades, its yield was extremely low, which reduces the industrial value of this option.

Thus, the comparative analysis confirms that the most rational approach for processing refractory gold-bearing ores of the Pakrut deposit is the flowsheet combining cyanidation with subsequent tailings leaching and flotation. This scheme ensures the best balance between gold recovery, concentrate quality, and minimization of technological losses.

Chemical Composition of Products

To refine the quality of the obtained concentrates, a chemical analysis of their composition was carried out (Tables 14, 15). The results showed that, along with a high gold content, the concentrates contained significant amounts of associated components, primarily sulfur and arsenic.

The gold content in the concentrate after the cyanidation and flotation stage ranged from 23 to 43 g/t, while silver was 14.24 g/t. At the same time, the sulfur content reached 34.13%, and arsenic 9.86% (Table 14). These values indicate strong sulfide mineralization of the ore, which explains its refractory nature and the necessity of additional stages to break down the sulfide matrix during metallurgical processing.

Table 14 – Composition of the concentrate after cyanidation and flotation

Element	Au, g/t	Ag, g/t	S, %	As, %
Values	23 – 43	14.24	34.13	9.86

Analysis of the flotation concentrate showed an even higher gold grade of 127 g/t, with a silver content of 20.92 g/t. The sulfur content was 17.29%, and arsenic 7.78%. Calcium (0.75%), magnesium (0.78%), and manganese (0.041%) were also present (Table 15). These elements may influence subsequent hydrometallurgical processes by altering leaching kinetics and solution properties.

Table 15 – Composition of the flotation concentrate

Element	Au, г/т	Ag, г/т	S, %	Ca, %	Mg, %	Mn, %	As, %
Values	127	20.92	17.29	0.75	0.78	0.041	7.78

Thus, chemical analysis confirmed that the concentrates from the Pakrut deposit have a complex composition with high levels of harmful impurities, primarily sulfur and arsenic. This requires a specific approach to subsequent metallurgical processing, including the application of oxidative pretreatment technologies aimed at reducing the content of these elements and improving the recovery of precious metals.

Conclusion

The conducted studies confirmed that the gold-bearing ores of the Pakrut deposit are characterized by complex mineralogy and a refractory nature, which significantly complicates the extraction of the precious metal by traditional methods. It has been established that native gold occurs predominantly in a finely dispersed form, closely associated with pyrite and arsenopyrite, which necessitates the use of combined technologies. Comparative analysis of the flowsheets showed that the maximum gold recovery (over 92%) is achieved by combining cyanidation with tailings leaching and flotation. This scheme not only improves metallurgical performance but also reduces metal losses and lowers the volume of toxic waste. The results of the work confirm the need for an integrated approach to processing refractory ores of Central Tajikistan and provide a foundation for developing industrial technologies capable of ensuring efficient and environmentally safe gold recovery.

Conflict of interest. There are no competing interests for all authors.

CRediT author statement: **Kh. Kholov:** development of the research idea; analysis of the topic development, development of the technological scheme, formulation of conclusions, selection of bibliography, writing the text; **Sh. Juraqulov:** processing of research results using program Microsoft Excel; **Sh. Samihzoda** – is a performer of experimental works, direct management of experimental research; **H. Mahmudov** – analysis of the results obtained in geology and mineralogy.

Cite this article as: Kholov KhI, Juraqulov ShR, Samihzoda ShR, Mahmudov HA. Mineralogical features and optimization of combined beneficiation flowsheets for refractory gold-bearing ores of the Pakrut deposit (Central Tajikistan). Kompleksnoe Ispolzovanie Mineralnogo Syra = Complex Use of Mineral Resources. 2027; 342(3):16-26. https://doi.org/10.31643/2027/6445.26

Пакрут кенорнының (Орталық Тәжікстан) қиын өңделетін алтынқұрамды кендерінің минералогиялық ерекшеліктері және оларды байытудың құрамдастырылған технологиялық сұлбаларын оңтайландыру

[1,2*]Холов Х.И., [3]Жұрақұлов Ш.Р., [1]Самихзода Ш.Р., [4]Махмудов Х.А.

[1]В.И. Никитин атындағы химия институты Тәжікстан ҰҒА, Душанбе, Тәжікстан
[2]С. Айни атындағы Тәжік мемлекеттік педагогикалық университеті, Душанбе, Тәжікстан
[3]Геология, жер сілкінісіне төзімді құрылыс және сейсмология институты Тәжікстан ҰҒА, Душанбе, Тәжікстан
[4]Тәжікстан тау-кен металлургия институты, Бустон, Тәжікстан

Мақала келді: *8 қазан2025*
Сараптамадан өтті: *1 қараша 2025*
Қабылданды: *5 қаңтар 2025*

ТҮЙІНДЕМЕ

Бай кен орындарының сарқылуы және қиын өңделетін алтын құрамды кендер үлесінің артуына байланысты оларды өңдеу әдістерін жетілдіру өзекті міндетке айналды. Бұл мақалада Орталық Тәжікстанның Зеравшан-Гиссар аймағында орналасқан Пакрут кен орнындағы алтын құрамды кендерді кешенді зерттеу нәтижелері ұсынылған. Минералогиялық талдау алтынның негізгі тасымалдаушылары пирит пен арсенопирит екенін көрсетті, металл негізінен ұсақ қосындылар мен жарықшақты байланысқан шоғырланулар түрінде орналасқан. Алтынның айтарлықтай бөлігі бос күйінде (17,03%) кездеседі; дегенмен, басым бөлігі жарықшақты байланысқан (62,41%) және негізінен арсенопиритпен қауымдастырылған түрде болады. Мұндай бөлінү бір сатылы өңдеудің тиімділігі шектеулі болатынын және ашу мен бөліп алудың құрамдастырылған әдістерінің қажеттілігін түсіндіреді. Кендердің физика-химиялық зерттеулері сульфид матрицасында алтынның ұсақ сеппелі болатынын, сондай-ақ жоғары қаттылығы мен абразивтілігіне байланысты қиын өңделетін сипатын анықтады. Зертханалық жағдайларда әртүрлі байыту процесінің сұлбалары сыналды: олар, тікелей цианидтеу; флотациямен қалдықтарды қосымша шаймалауды үйлестіру; және гравитациялық байытуды қамтитын нұсқалар. Салыстырмалы талдау ең жоғары тиімділікке (Au экстракциясы 92,23%) «цианидтеу + қалдықтарды шаймалау + флотация» сұлбасын қолдану арқылы қол жеткізілетінін көрсетті. Тікелей

	цианидтеу жоғары көрсеткіш көрсетті (90,05%), бірақ тиімділігі төмен болды. Флотация-цианидтеу және гравитация-флотация сұлбалары салыстырмалы түрде төмен нәтижелер көрсетті. Алынған деректер Пакрут кен орнының қиын өңделетін кендерін өңдеуге арналған кешенді тәсілдің келешегі бар екендігін растайды. Байыту сұлбаларын оңтайландыру бағалы металдарды өндіруді айтарлықтай арттыруға, технологиялық шығындарды азайтуға және мышьяк бар қалдықтардың жиналуымен байланысты экологиялық тәуекелдерді азайтуға мүмкіндік береді.
	Түйін сөздер: Пакрут кенорны, қиын өңделетін кендер, алтын, пирит, арсенопирит, циандау, флотация, гравитациялық байыту, минералогия, кендерді байыту.
Холов Х.И.	***Авторлар туралы ақпарат:*** *Техника ғылымдарының кандидаты, Тәжікстан Ұлттық Ғылым Академиясы В.И. Никитин атындағы Химия институтының Кенді байыту зертханасының аға ғылыми қызметкері; С. Әйни атындағы Тәжікстан Мемлекеттік Педагогикалық Университетінің Химиялық технология және экология кафедрасының аға оқытушысы, 734063, Әйни көш., 299/2, Душанбе, Тәжікстан. E-mail: Kholmahmad90@mail.ru; ORCID ID: https://orcid.org/0000-0002-8202-5919*
Жұрақұлов Ш.Р.	*Аға ғылыми қызметкер, Тәжікстан Ұлттық ғылым академиясының Геология, жер сілкінісіне төзімді құрылыс және сейсмология институты, 734063, Айни к-сі, 299/2, Душанбе, Тәжікстан. E-mail: shaih8888@mail.ru; ORCID ID: https://orcid.org/0009-0001-1255-8541*
Самихзода Ш.Р.	*Техника ғылымдарының докторы, Тәжікстан Ұлттық ғылым академиясының В.И. Никитин атындағы Химия институтының кендерді байыту зертханасының бас ғылыми қызметкері, 734063, Айни к-сі, 299/2, Душанбе, Тәжікстан. E-mail: samikhov72@mail.ru; ORCID ID: https://orcid.org/0009-0002-7454-7343*
Махмудов Х.А.	*Техника ғылымдарының кандидаты, Тәжікстан тау-кен металлургия институтының Тау-кен ісі факультетінің деканы, 735730, Маяковский к-сі, 6, Бустон, Тәжікста. E-mail: obogatitel_0903@mail.ru; ORCID ID: https://orcid.org/0009-0005-8428-5334*

Минералогические особенности и оптимизация комбинированных схем обогащения упорных золотосодержащих руд месторождения Пакрут (Центральный Таджикистан)

[1,2*]Холов Х.И., [3]Джуракулов Ш.Р., [1]Самихзода Ш.Р., [4]Махмудов Х.А.

[1]Институт химии им. В.И. Никитина НАН Таджикистана, Душанбе, Таджикистан
[2]Таджикский государственный педагогический университет им. С. Айни, Душанбе, Таджикистан
[3]Институт геологии, сейсмостойкого строительства и сейсмологии НАНТ, Душанбе, Таджикистан
[4]Горно-металлургический институт Таджикистана, Бустон, Таджикистан

Получена: *8 октября 2025*
Рецензирована: *1 ноября 2025*
Принята: *5 января 2025*

АННОТАЦИЯ

На фоне истощения богатых месторождений и роста доли упорных золотосодержащих руд совершенствование методов их переработки стало актуальной задачей. В данной работе представлены результаты комплексного исследования золотосодержащих руд месторождения Пакрут, расположенного в Зеравшан-Гиссарской зоне Центрального Таджикистана. Минералогический анализ показал, что основными носителями золота являются пирит и арсенопирит, при этом металл преимущественно локализован в виде тонких включений и трещинно-связанных скоплений. Заметная доля золота присутствует в свободном состоянии (17,03%); однако преобладающая часть является трещинно-связанной (62,41%) и главным образом ассоциирована с арсенопиритом. Такое распределение объясняет ограниченную эффективность одностадийной переработки и обосновывает необходимость комбинированных методов вскрытия и извлечения. Физико-химические исследования руд выявили их упорный характер, обусловленный тонким вкраплением золота в сульфидной матрице, а также высокой твердостью и абразивностью. В лабораторных условиях были опробованы различные технологические схемы обогащения: прямая цианидация; комбинации с флотацией и дополнительным выщелачиванием хвостов; а также варианты с включением гравитационного обогащения. Сравнительный анализ показал, что наибольшая эффективность (извлечение Au 92,23%) достигается по схеме «цианидация + выщелачивание хвостов + флотация». Прямая цианидация показала высокий показатель (90,05%), но оказалась менее эффективной. Схемы «флотация-цианирование» и «гравитация-флотация» показали сравнительно более низкие результаты. Полученные данные подтверждают перспективность комплексного подхода для переработки упорных руд Пакрута. Оптимизация схем обогащения позволяет существенно повысить извлечение драгоценного металла, сократить технологические потери и минимизировать экологические риски, связанные с накоплением мышьяксодержащих отходов.

Ключевые слова: месторождение Пакрут, упорные руды, золото, пирит, арсенопирит, цианирование, флотация, гравитационное обогащение, минералогия, обогащение руд.

Холов Х.И.	***Информация об авторах:*** *Кандидат технических наук, старший научный сотрудник лаборатории обогащения руд Института химии им. В.И. Никитина Национальной академии наук Таджикистана; старший преподаватель кафедры химической технологии и экологии Таджикского государственного педагогического университета им. С. Айни, 734063, ул. Айни, 299/2, Душанбе, Таджикистан. E-mail: Kholmahmad90@mail.ru; ORCID ID: https://orcid.org/0000-0002-8202-5919*
Джуракулов Ш.Р.	*Старший научный сотрудник, Институт геологии, сейсмостойкого строительства и сейсмологии Национальной академии наук Таджикистана, 734063, ул. Айни, 299/2, Душанбе, Таджикистан. E-mail: shaih8888@mail.ru; ORCID ID: https://orcid.org/0009-0001-1255-8541*
Самихзода Ш.Р.	*Доктор технических наук, главный научный сотрудник лаборатории обогащения руд Института химии им. В.И. Никитина Национальной академии наук Таджикистана, 734063, ул. Айни, 299/2, Душанбе, Таджикистан. E-mail: samikhov72@mail.ru; ORCID ID: https://orcid.org/0009-0002-7454-7343*
Махмудов Х.А.	*Кандидат технических наук, декан факультета Горное дело Горно-металлургического института Таджикистана, 735730, ул. Маяковского, 6, Бустон, Таджикистан. E-mail: obogatitel_0903@mail.ru; ORCID ID: https://orcid.org/0009-0005-8428-5334*

References

[1] Barbouchi A, et al. Advancements in improving gold recovery from refractory gold ores/concentrates: a review. Canadian Metallurgical Quarterly. 2024; 1-18. https://doi.org/10.1080/00084433.2024.2441548

[2] Surimbayev B, et al. Processing of refractory gold-bearing sulfide concentrates: A review. Mineral Processing and Extractive Metallurgy Review. 2024; 45(6):573-591. https://doi.org/10.1080/08827508.2023.2230344

[3] Vikentyev IV, Bortnikov NS. Gold deposits of Central and North. Geology of Ore Deposits. 2024; 66(5):477-483. DOI:10.1134/S1075701524700326

[4] Dosmukhamedov N, et al. Chlorination treatment for gold extraction from refractory gold-copper-arsenic-bearing concentrates. Sustainability. 2022; 14(17):11019. https://doi.org/10.3390/su141711019

[5] Anderson CW, Behum PT, Miller FW. Environmental and Occupational Health Regulations in the US Lead Industry. 1986.

[6] Mudd GM. Global trends in gold mining: Towards quantifying environmental and resource sustainability. Resources Policy. 2007; 32(1-2):42-56. https://doi.org/10.1016/j.resourpol.2007.05.002

[7] Foster RP. Gold in the year 2000: A global overview. Australian Journal of Earth Sciences. 1996; 43(1):1-14. https://doi.org/10.1080/08120099608728231

[8] Goldfarb RJ, et al. Phanerozoic continental growth and gold metallogeny of Asia. Gondwana Research. 2014; 25(1):48-102. https://doi.org/10.1016/j.gr.2013.03.002

[9] Wilson R, Mercier PHJ, Navarra A. Integrated artificial neural network and discrete event simulation framework for regional development of refractory gold systems. Mining. 2022; 2(1):123-154. https://doi.org/10.3390/mining2010008

[10] Sagers MJ. Regional trends in Russian gold production. Post-Soviet geography and economics. 1997; 38(6):315-356. https://doi.org/10.1080/10889388.1997.10641052

[11] Kholov KI, et al. Gold leaching by various solutions, alternative of cyanide and their prospects in the future //Journal of Siberian Federal University. Engineering & Technologies. 2021; 14(4):433-447. http://dx.doi.org/10.17516/1999-494X-0324

[12] Rahimov FK, Mamadjonov YM. Mineral resource potential of Tajikistan: As an important component of sustainable development of the silk road economic belt. Journal of Resources and Ecology. 2015; 6(2):125-128. https://doi.org/10.5814/j.issn.1674-764x.2015.02.012

[13] Kholov KhI, Niyozov AS, Juraqulov ShR, Samikhov ShR. Mineralogical and geochemical features of the gold-containing ores of the Pakrut deposit (Central Tajikistan) as the basis of gravity enrichment. Transbaikal State University Journal. 2024; 30(2):82-92. https://doi.org/10.21209/2227-9245-2024-30-2-82-92

[14] Kholov KI, et al. Geological study of gold deposits in the Republic of Tajikistan. Conference'X IV Numanov's readings' Proceedings. 2017; INIS-TJ(017):25-27.

[15] Rozhdestvina VI, Sorokin AP. First finds of native palladium, platinum, gold, and silver in brown coals of the Erkovets field (upper Amur region). Russian Journal of Pacific Geology. 2010; 4(6):483-494. https://doi.org/10.1134/S1819714010060035

[16] Shen L, et al. Atacamite discolouration under the influence of arsenates in wall paintings in the Kizil Grottoes, Xinjiang, China. Heritage Science. 2024; 12(1):292. https://doi.org/10.1186/s40494-024-01406-y

[17] Clarke J. A simplified gravity-recoverable-gold test. 2005.

[18] Gill CB. Gravity concentration. Materials beneficiation. New York, NY: Springer New York. 1991, 148-175. https://doi.org/10.1007/978-1-4612-3020-5_9

[19] Guner MK, et al. Automated mineralogy and diagnostic leaching studies on bulk sulfide flotation concentrate of a refractory gold Ore. Minerals. 2023; 13(10):1243. https://doi.org/10.3390/min13101243

[20] Vikentyev IV. Invisible and microscopic gold in pyrite: Methods and new data for massive sulfide ores of the Urals. Geology of ore deposits. 2015; 57(4):237-265. https://doi.org/10.1134/S1075701515040054

Crossref

DOI: 10.31643/2027/6445.27
Earth and Planetary Sciences: Earth-Surface Processes

Mathematical Model of the Dynamics of the Armament of the Tricone Drill Bit

[1] Toshov J.B., [2] Sherov K.T., [3] Baratov B.N., [4*] Rabatuly M., [1] Erkinov D.I.

[1] Islam Karim Tashkent State Technical University, Tashkent, Uzbekistan
[2] S. Seifullin KazakhAgro Technical University, Astana, Kazakhstan
[3] Almalyk branch of NUST MISIS, Almalyk, Uzbekistan
[4]NPJSC Abylkas Saginov Karaganda Technical University, Karaganda, Kazakhstan

**Corresponding author email: mukhammedrakhym@mail.ru*

Received: *September 1, 2025*
Peer-reviewed: *November 1, 2025*
Accepted: *January 8, 2025*

ABSTRACT

This study presents a mathematical model of the dynamics of tricone drill bits, which remain widely used in open-pit mining due to their reliability and versatility. Despite their extensive application, improving their efficiency and durability remains a relevant issue. The main operational challenges are identified, including insufficient knowledge of the stress–strain state of rocks in the contact zone and the effect of tooth geometry on kinematics and rock-breaking efficiency. Analytical dependencies are proposed to account for bit geometry, trajectory motion, transmission ratios, and tooth–rock interaction. Based on the principles of theoretical mechanics, performance criteria are formulated through specific contact and volumetric work of rock destruction, enabling an objective assessment of energy consumption. The model demonstrates the potential of analytical methods for optimizing drill bit design and kinematics, reducing energy consumption, increasing productivity, and extending tool life. The results can be applied in the design of next-generation drill bits and in engineering software for selecting rational drilling parameters under specific geological conditions. The proposed approach provides a foundation for further studies in mathematical modeling of rock destruction dynamics and the advancement of open-pit mining technologies.

Keywords: rock, drilling, drill bit, kinematics, work, design, model, equation.

Information about authors:

Toshov Javokhir Buriewicz — *Doctor of Technical Sciences, Professor of Islam Karim Tashkent State Technical University, 100095, Almazar district, Universitetskaya street, Tashkent, Republic of Uzbekistan. E-mail: j.toshov@tdtu.uz; ORCID ID: https://orcid.org/0000-0003-4278-1557*

Sherov Karibek Tagayevich — *Doctor of Engineering Sciences, Professor, S. Seifullin KazakhAgro Technical University, 010000, Ave. Zhenis, 62, Astana, Republic of Kazakhstan. E-mail: shkt1965@mail.ru; ORCID ID: https://orcid.org/0000-0003-0209-180X*

Baratov Bakhtiyor Nusratovich — *Ph.D., Associate Professor of Almalyk branch of NUST MISIS, 110104, Amir Temur Street, 56, Almalyk, Republic of Uzbekistan. E-mail: bakhtiyor.baratov@yandex.ru; ORCID ID: https://orcid.org/0000-0002-6621-5974*

Rabatuly Mukhammedrakhym — *Ph.D., Acting Associate Professor, Department of Development of Mineral Deposits of NPJSC Abylkas Saginov Karaganda Technical University, 100027, Ave. Nursultan Nazarbayev, 56, Karaganda, Republic of Kazakhstan. E-mail: mukhammedrakhym@mail.ru; ORCID ID: https://orcid.org/0000- 0002-7558-128X*

Erkinov Dilshodbek Ilhomjonovich — *Ph.D. student of Islam Karim Tashkent State Technical University, 100095, Almazar district, Universitetskaya street 2, Tashkent, Republic of Uzbekistan. E-mail: dilshodbek.ilhomovich@gmail.com; ORCID ID: https://orcid.org/0009-0006-5970-416X*

Indroduction

In global open-pit mining practice, well drilling is mainly performed using roller bits, which are the key tools in this production process. This type of work is characterized by high labor intensity and high costs. At the same time, about 80-85% of all drilling operations are carried out using three-cone bits. Drilling accounts for 25-40% of the total cost of production, therefore, the tasks of increasing the service life of bits and reducing the costs of their use are of paramount importance [1].

Despite the accumulated experience in the field of design and operation of roller bits, many aspects of their operation have not been fully studied. In particular, questions remain open regarding the stress-strain state of the rock in the contact zone with the teeth, an accurate description of the dynamics of the interaction of the rollers with the rock, as well as taking into account the forces of penetration of the rock-destroying tool when determining the kinematic parameters. Existing approaches are often empirical in nature and do not allow for a full consideration of the influence of the

geometric parameters of the teeth on the efficiency of rock destruction [2].

The modern development of drilling theory and tool design requires a transition to mathematical models that allow the real dynamics of the interaction between the drill bit structure and the rock to be described. This approach provides not only a fundamental understanding of the destruction process, but also the ability to optimize the design of drill bits for specific operating conditions.

In the conditions of the mining industry of Uzbekistan, where large-scale open-pit mining is carried out, the issues of improving the design and increasing the durability of drill bits are of particular importance. The use of mathematical modeling allows solving the problems of optimizing the structure of roller cutters, choosing rational drilling modes and developing new tools that can reduce costs and increase the reliability of the production process.

However, to date, the stress–strain state of rocks in contact with the working parts of drill bits, as well as the dynamics of roller drilling tools and the modeling of their interaction, have not been fully investigated. There are unresolved problems due to the failure to take into account the forces of penetration of the teeth of the rock-cutting tool into the rock when determining the kinematic parameters of the drill bits [3].

The purpose of this work is to develop and analyze a mathematical model of the dynamics of three-cone drill bits, taking into account the geometric parameters of their weapons, gear ratios, and features of the trajectories of the teeth. Based on the model, criteria for the tool's performance are formed, allowing not only to evaluate its effectiveness, but also to use the obtained results in the design and implementation of new designs of drill bits [4].

Materials

The main objective of the studies described in this and the following chapters is to establish the relationship between the obtained criteria for assessing the performance of the roller cutter structure and the classical criterion for the cost of drilling per linear meter, known as the Bingham criterion [5]. It should be noted that the kinematic criteria in the form of relatively specific contact work and volumetric destruction work were obtained on a deterministic basis. We need to determine the possibilities of efficient manufacturing of such structures in the conditions of Uzbekistan.

Today, the goal of increasing the efficiency of three-cone bits is viewed through optimization of the process of rock destruction during drilling. This requires a corresponding mathematical model that describes the mechanism of interaction of the cutting tool adequately to their real dynamics in the well bottom [6].

Rock destruction by drilling bits can be assessed by determining two parameters, such as specific contact and specific volumetric work of destruction, and are presented as follows [7]:

$$A_S = \frac{A_{gen}}{S}, \quad (1)$$

where: A_s - specific contact work of destruction, kgs.mm/mm^2;

A_{gen} - total work expended on deformation and destruction of rock when pressing the stamp, kgs.mm;

S - area of the flat base of a cylindrical stamp, mm^2;

$$A_v = \frac{A_{gen}}{V}, \quad (2)$$

where: A_v - specific volumetric work of destruction, kgs.mm/mm^3;

V - volume of deformed rock, mm^3.

Next, it is necessary to show that the criteria for specific contact work and volumetric destruction work are functions of the geometric parameters of drill bits, by varying which it is possible to solve optimization problems to improve the dynamics of tricone bit armament [8].

How the criteria for specific contact work and volumetric destruction work depend on the geometric parameters of the bit is easiest to trace in the process of constructing their analytical structures. All this is based on the method for calculating the main parameter of these criteria - the contact path of the teeth of the roller cutters at a given depth of their immersion in the rock [9].

To calculate the technological criteria for the performance of three-cone bits, it is necessary to construct two-parameter equations of the trajectories of the movement of the tooth tip of the roller cutter in the form [10]:

$$\left.\begin{aligned} x &= x(G,\varphi,\psi) \\ y &= y(G,\varphi,\psi) \\ z &= z(G,\varphi,\psi) \end{aligned}\right\}, \quad (3)$$

or

$$\left.\begin{aligned} x &= R\sin\varphi - r\sin\psi\cos\varphi - r\left(1-\cos\psi\right)\sin\varphi\cos\alpha, \\ y &= R\cos\varphi + r\sin\psi\sin\varphi - r\left(1-\cos\psi\right)\cos\varphi\cos\alpha, \\ z &= r\left(1 \quad \cos\psi\right)\sin\alpha; \end{aligned}\right\}, \tag{4}$$

where Γ is a set of geometric parameters, and ϕ and ψ are the angles of rotation of the bit and roller around their axes.

R is the radius of the circle at the bottom of the well along which the crown rolls, mm;

r is the radius of the crown, mm;

α is the angle of inclination of the plane of the crown to the plane of the cross section of the well, deg.;

Next, we consider the transformations of two-parameter equations (3) to one-parameter ones

$$\left.\begin{aligned} x &= x(G,i,\psi) \\ y &= y(G,i,\psi) \\ z &= z(G,i,\psi) \end{aligned}\right\} \tag{5}$$

The gear ratio of the roller cutter i, which determines how many revolutions the roller cutter will make around its axis in one revolution of the bit, can be calculated using a special method [11].

The transformation of two-parameter equations of motion trajectories in the form (5) to one-parameter equations is carried out by substituting [12]:

$$\varphi = \frac{\psi}{i}, \tag{6}$$

where *i* - gear ratio of the bit. Then we have:

$$\left.\begin{aligned} x_j &= R_j \sin\frac{}{i} - r_j \sin\psi\cos\left(\frac{\psi}{i} - \quad_j\right), \\ y_j &= R_j \cos\frac{\psi}{i} + r_j \sin\psi\sin\left(\frac{\psi}{i} - \quad_j\right), \\ z_j &= r_j\left(1 \quad \cos\psi\right). \end{aligned}\right\}, \tag{7}$$

where R_j, r_j, *and* i - constant parameters that determine the external appearance (geometry) of a tricone drill bit;

ψ – variable parameter.

On the basis of theoretical mechanics, it is possible to construct analytical structures of dynamic criteria for assessing the performance of three-cone bits [13].

The speed of movement of the teeth of the drill bit rollers must be integrated and have the form of a function of the parameter ψ.

Let's find it using the well-known formula of theoretical mechanics [14]

$$V\left(\psi\right) = \sqrt{\left(\frac{dx}{\psi}\right)^2 + \left(\frac{dy}{d\psi}\right)^2 + \left(\frac{dz}{d\psi}\right)^2} \tag{8}$$

Further

$$V(\psi) = \sqrt{A_j + B_j\,cos\,\psi + C_j\,sin\,\psi + D\,cos^2\,\psi}, \tag{9}$$

Where:

$$A_j = \frac{R_j^2 + r_j^2}{i^2} + r_j^2,$$
$$B_j = -\frac{2R_j r_j}{i} cos\,\gamma\,,$$
$$C_j = \frac{2R_j r_j}{i} sin\,\gamma\,,$$
$$D_j = -\frac{r_j^2}{i^2},$$
$$\gamma_j = arcsin\left(\frac{k}{R_j}\right). .$$

Here, it should be noted that the offset angle γ_j refers to the *j*-th crown, and is determined through the magnitude of the offset of the roller cutter axis in the plan *k* and through the radius of the circle at the well bottom R_j, along which this crown rolls.

Expressions for calculating the path of contact of a roller cutter tooth with displaced axes of rotation in the plan are found using the well-known formula of theoretical mechanics:

$$S = \int_{\psi_0}^{\psi_1} V\left(\psi\right) d\psi, \tag{10}$$

where: ψ_0 and ψ_1, respectively, the lower and upper limits of integration, depending on a given or certain depth of immersion of the contact paths into the rock.

The expression we are looking for is:

$$S_j = \int_0^{\psi_j} V_j\left(\psi\right) d\psi + \int_{2\pi-\psi_j}^{2\pi} V_j\left(\psi\right) d\psi \tag{11}$$

Where is $\psi_j = \arccos\left(1 \quad \frac{H_j}{r_j \sin\alpha}\right)$;

$H_j = h_j$ - calculated height on the toroid belt if the crown is in contact with the rock on the periphery, mm;

$H_j = \delta_j$ - Specified height of the trajectory on the toroid belt, if the crown contacts the face not on the periphery, mm.

Here it is necessary to consider two cases of assigning the limits of integration:

1. If the *j-th* crown is not rolled on the periphery of the face, then

2.
$$S_j = \int_0^{\psi_{j(\delta)}} V_j(\psi)\,d\psi + \int_{2\pi-\psi_j(\delta)}^{2\pi} V_j(\psi)\,d\psi \qquad (12)$$

3. If the crown is peripheral (first, calibrating), then

4.
$$S_j = \int_0^{\psi_{j(\delta)}} V_j(\psi)\,d\psi + \int_{2\pi-\psi_j(h)}^{2\pi} V_j(\psi)\,d\psi . \qquad (13)$$

In general, the integration of the contact paths of the teeth of the cutters with the offset axes of rotation in the plan is since the contact and contact paths are not equal to the contact paths of the exit from the contact, even with equal values of their immersion in the rock.

Results

Next, let's look at the calculation of the cutter ratio of a tricone drill bit *i*, which is the main parameter for calculating contact paths when embedded in rock. The gear ratio of the cutters can be determined by the ratio of the radius of the net rolling ring r_0 and the radius of the circle at the bottom of the hole along which it rolls R_0 in the form:

$$\frac{R_0}{r_0} = i = \frac{\psi}{\varphi} \qquad (14)$$

To determine the performance assessment of tricone drill bits, the following criteria should be considered:

- analytical structure of the criteria;
- The physical meaning of the criteria;
- Possibilities of Criteria for Evaluating the Performance of Tricone Bits in Solving Optimization Problems.

Criteria (1) and (2) are objective energy criteria for the static destruction of rock under a stamp in the study of the physical and mechanical properties of rocks [[16], [17]].

Energy criteria for the physical and mechanical properties of rocks during their static fracture are the criteria for assessing the performance of drill bits in the form of relative specific contact and volumetric fracture work, the analytical structure of which is presented below in the formulas.

It is proposed to take the following functional dependencies as criteria for assessing the performance of drilling tricone bits:

$$A'_{q,j} = \frac{F_{q,j}\,i}{3\cdot\Delta S} T_{q,j} I_{q,j} \sin 2\psi + \frac{I_{q\,j}}{2} \sin 4\psi , \qquad (15)$$

$$A''_{q,j} = \sum_{q=1}^{3} \frac{\left(\frac{h}{d}\left(\cos\left(\frac{\theta}{2}-\beta\right)\frac{a}{b}\right)\right)\left(Fz_{q,j}\,i_q\right)}{3\left(2\pi R_{q,j} D_{q,j}\left(r_t - \sqrt{r_t^2 - \frac{Pax}{\pi p_h (1+tg\varsigma)}}\right)\right)} T_{q,j} I_{q,j} \sin 2\psi + \frac{I_{q,j}}{2} \sin 4\psi, \qquad (16)$$

Where is

$$T_{q,j} = 4\cdot\left\lfloor \frac{1}{i_q^2}\left\{\left(R_{q,j} - 2r_{q,j}\cos\gamma_{q,j}\cos\alpha\right) + r_{q,j}^2\left[\cos\alpha\left(\cos\alpha - 2i_q\right) + \left(1+j\right)\right]\right\}\right\rfloor +$$

$$+2\cdot\left\lfloor \frac{2r_{q,j}}{i_q^2}\left(r_{q,j}\cos\alpha - R_{q,j}\cos\gamma_{q,j}\right)\left(i_q - \cos\alpha\right)\right\rfloor +$$

$$+2\cdot\left\lfloor \frac{2R_{q,j}r_{q,j}}{q}\left(r_{q,j}\cos\alpha - R_{q,j}\cos\gamma_{q,j}\right)\left(i_q - \cos\alpha\right)\right\rfloor - \left(\frac{r_{q,j}^2}{i_q^2}\sin^2\alpha\right);$$

$$I_{q,j} = \frac{1}{2}\left|\begin{array}{l} 8\cdot\left\lfloor \frac{1}{i_q^2}\left\{\left(R_{q,j} - 2r_{q,j}\cos\gamma_{q,j}\cos\alpha\right) + r_{q,j}^2\left[\cos\alpha\left(\cos\alpha - 2i_q\right) + \left(1+j\right)\right]\right\}\right\rfloor - \\ -8\cdot\left[\frac{2R_{q,j}r_{q,j}}{2}\left(r_{q,j}\cos\alpha - R_{q,j}\cos\gamma_{q,j}\right)\left(i_q - \cos\alpha\right)\right] - 3\cdot\left(\frac{r_{q,j}^2}{i_q}\sin^2\alpha\right) \end{array}\right|;$$

q, j – The index that determines the number of the cutter and the number of the crown;

R – Crown rolling radius at the bottom of the well, mm;

r –radius of crown, mm;

i – drill bit gear ratio;

α – Corner of the Axis of cone bits, deg;

$\gamma = \arcsin\left(\frac{K}{R}\right)$ – offset angle, deg;

ψ – variable parameter of the cone bit, deg;

β – Tooth sharpening angle, deg;

ϑ – Angle of inclination of the axis of the crown, deg;

a – Tooth cross-section length, mm;

b – Tooth cross-section width, mm;

F – Tooth movement resistance force, N;

z – Number of teeth, pcs;

P_{ax} – Axial load on the tooth, kN;

P_h – Rock hardness, Pa;

ς - Angle of internal friction, deg;

r_t – radius of the cutting part of the tooth, mm.

The assessment of the performance of drill bits is the kinematic parameters, for the kinematic passport of the tricone bit, tabular and graphic forms are presented [18,19,20].

Without the use of computer technology, calculations and analysis of the dynamics of tricone bit armament based on these formulas are ineffective [21].

Discussion

As can be seen, formulas (15) and (16) show the set of geometric parameters of drill bits.

The implicit dependence of these criteria lies in the specified value of insertion (immersion) of the teeth of the cutters into the rock. This dependence is associated with the geometric parameters of the drill bits, on the shape of the teeth, on the energy parameters transmitted to the teeth, on the physical and mechanical properties of rocks in certain conditions (constrained, lightweight) at the bottom of the well, i.e.:

$$\delta = \delta(D, P, E). \quad (17)$$

To date, this function has not been built in an explicit form. But this fact is not an obstacle for studying the performance of tricone bits under other equal conditions, i.e., at a given value of tooth insertion. At the same time, we also know the limits of change in this value

$$0 \le \delta \le h_t, \quad (18)$$

where: h_t - the height of the tooth departure from the body of the ball, mm.

Thus, it can be argued that the criteria for assessing the performance of tricone bits in the form (15) and (16) are functions of the triad: bit – rock – energy.

The physical essence of kinematic criteria and their obvious dependence on the geometric parameters of drill bits serve as an objective basis for the development of a methodology for improving the dynamics of new structures and their modifications.

Conclusion

The conducted research has resulted in the development of a mathematical model describing the dynamics of the armament of tricone drill bits, taking into account their geometric parameters, gear ratios, and the kinematics of tooth movement in the rock contact zone. Analytical dependencies have been obtained that make it possible to quantitatively assess the specific contact and volumetric work of rock destruction, which serve as objective criteria for evaluating drilling efficiency.

The proposed model provides a theoretical framework for determining the relationship between the structural parameters of drill bits and their operational performance, thereby enabling optimization of bit geometry and operating modes under various geological conditions. The results demonstrate that improving the dynamic characteristics of tricone bits through mathematical modeling can significantly reduce energy consumption, increase drilling productivity, and extend tool life.

The formulated energy and kinematic criteria can be effectively used in the design of next-generation drill bits and in computer-aided engineering systems for simulating drilling processes. Further research should focus on experimental verification of the developed model and on the integration of the obtained results into practical design and optimization methodologies for rock-destroying tools in open-pit and deep drilling operations.

Conflict of interest. On behalf of all the authors, the corresponding author declares that there is no conflict of interest.

***CRediT author statement*: J. Toshov, M. Rabatuly:** Conceptualization, Methodology, Software; **D. Erkinov, B. Baratov**: Data curation, Writing-Original draft preparation; **K. Sherov:** Visualization, Investigation; **D. Erkinov, J. Toshov:** Software, Validation.

Cite this article as: Toshov JB, Sherov KT, Baratov BN, Rabatuly M, Erkinov DI. Mathematical Model of the Dynamics of the Armament of the Tricone Drill Bit. Kompleksnoe Ispolzovanie Mineralnogo Syra = Complex Use of Mineral Resources. 2027; 342(3):27-34. https://doi.org/10.31643/2027/6445.27

Үш қашау тісті бұрғыларды жабдықтау динамикасының математикалық моделі

[1] Тошов Ж.Б., [2] Шеров К.Т., [3] Баратов Б.Н., [4*]Рабатулы М., [1] Эркинов Д.И.

[1] Ислам Каримов атындағы Ташкент Мемлекеттік Техникалық Университеті, Өзбекстан
[2] С. Сейфуллин Атындағы Қазақ Агротехникалық Университеті, Астана, Қазақстан
[3] ҰЗТУ МИСиС Алмалық филиалы, Алмалық, Өзбекстан
[4] КЕАҚ Ә. Сағынов атындағы Қарағанды техникалық университеті, Қарағанды, Қазақстан

Мақала келді: *1 қыркүйек 2025*
Сараптамадан өтті: *1 қараша 2025*
Қабылданды: *8 қаңтар 2025*

ТҮЙІНДЕМЕ

Мақалада сенімділігі мен әмбебаптылығына байланысты ашық карьерлік тау-кен жұмыстарында кеңінен қолданылатын үш қашау тісті бұрғыларды жабдықтау динамикасының математикалық моделі ұсынылған. Ұзақ мерзімді пайдалану тәжірибесіне қарамастан, олардың тиімділігі мен беріктігін арттыру мәселелері өзекті болып қала береді. Негізгі пайдалану мәселелері, соның ішінде жанасу аймағындағы тау жыныстарының кернеу-деформация күйі және бұрғылау қашауының тістері геометриясының кинематика мен қирату тиімділігіне әсері туралы білімнің жеткіліксіздігі анықталды. Жасалған аналитикалық тәуелділіктер қашаудың геометриясын, қозғалыс траекториясын, беріліс қатынастарын және тістердің жыныспен өзара әрекеттесуін ескеруге мүмкіндік береді. Теориялық механикаға сүйене отырып, энергия шығындарын объективті бағалауды қамтамасыз ететін меншікті жанасу және көлемдік бұзу жұмыстары арқылы өнімділік критерийлері тұжырымдалды. Ұсынылған модель қашаулардың құрылымын және кинематикасын оңтайландыруға, энергия шығынын азайтуға, өнімділікті арттыруға және қызмет ету мерзімін ұзартуға мүмкіндік береді. Алынған нәтижелерді жаңа буын қашауларды жобалауда және нақты тау-кен және геологиялық жағдайларда ұтымды бұрғылау параметрлерін таңдауға арналған инженерлік бағдарламалық жасақтаманы жасауда пайдалануға болады. Ұсынылған тәсіл тау жыныстарының бұзылуы динамикасын модельдеу және ашық карьерлік өндіру технологияларын жетілдіру саласындағы одан әрі зерттеулердің негізін құрайды.

	Түйін сөздер: тау жынысы, бұрғылау, бұрғы қашауы, кинематика, жұмыс, жобалау, модель, теңдеу.
Тошов Жавохир Буриевич	***Авторлар туралы ақпарат:*** *Техника ғылымдарының докторы, Ислам Карим атындағы Ташкент мемлекеттік техникалық университетінің профессоры, 100095, Алмазар ауданы, Университетская көшесі 2, Ташкент, Өзбекстан. E-mail: j.toshov@tdtu.uz; ORCID ID: https://orcid.org/0000-0003-4278-1557*
Шеров Карибек Тагаевич	*Техника ғылымдарының докторы, профессор, С.Сейфуллин Атындағы Қазақ Агротехникалық Университеті, 010000, Жеңіс даңғ., 62, Астана, Қазақстан. E-mail: shkt1965@mail.ru; ORCID ID: https://orcid.org/0000-0003-0209-180X*
Баратов Бахтиер Нусратович	*Phd., ҰЗТУ МИСиС, Алмалық филиалының доценті, 110104, Әмір Темір көшесі, 56, Алмалық, Өзбекстан. E-mail: bakhtiyor.baratov@yandex.ru; ORCID ID: https://orcid.org/0000-0002-6621-5974*
Рабатұлы Мұхаммедрахым	*PhD докторы, КЕАҚ Әбілқас Сағынов атындағы Қарағанды техникалық университетінің Пайдалы қазбалар кенорындарын өндіру кафедрасының доцент м.а., 100027, Нұрсұлтан Назарбаев даңғ. 56, Қарағанды, Қазақстан. E-mail: mukhammedrakhym@mail.ru; ORCID ID: https://orcid.org/0000-0002-7558-128X*
Эркинов Дилшодбек Илхомджонович	*Ислам Карим атындағы Ташкент Мемлекеттік Техникалық Университетінің PhD докторанты, 100095, Алмазар ауданы, Университетская көшесі, 2, Ташкент Өзбекстан. E-mail: dilshodbek.ilhomovich@gmail.com; ORCID ID: https://orcid.org/0009-0006-5970-416X*

Математическая модель динамики вооружения трехшариковых долот

[1] Тошов Ж.Б., [2] Шеров К.Т., [3] Баратов Б.Н., [4*]Рабатұлы М., [1] Эркинов Д.И.

[1] Ташкентский государственный технический университет имени Ислама Каримова, Узбекистан
[2] Казахский аграрный технический университет им. С. Сейфуллина, Астана, Казахстан
[3] Алмалыкский филиал НИТУ МИСиС, Алмалык, Узбекистан
[4]НАО Карагандинский технический университет имени А. Сагинова, Караганда, Казахстан

Поступила: *1 сентября 2025*
Рецензирование: *1 ноября 2025*
Принята в печать: *8 января 2025*

АННОТАЦИЯ

В работе представлена математическая модель динамики трёхшарошечных буровых долот, которые сохраняют широкое применение в условиях открытых горных работ благодаря своей надёжности и универсальности. Несмотря на длительный опыт использования, вопросы повышения их эффективности и долговечности остаются актуальными. Уточнены ключевые эксплуатационные проблемы, включая недостаточную изученность напряжённо-деформированного состояния пород в зоне контакта и влияние геометрии зубьев на кинематику и эффективность разрушения. Предложены аналитические зависимости, учитывающие геометрию вооружения, траекторию движения, передаточные отношения и взаимодействие зубьев с породой. На основе теоретической механики сформулированы критерии работоспособности через удельные контактные и объёмные работы разрушения, что обеспечивает объективную оценку энергетических затрат. Модель демонстрирует возможности аналитических методов для оптимизации конструкции и кинематики долот, снижения энергопотребления, повышения производительности и увеличения срока службы. Полученные результаты могут быть использованы при проектировании долот нового поколения и создании инженерного программного обеспечения для выбора рациональных параметров бурения в конкретных горно-геологических условиях. Предложенный подход формирует основу для дальнейших исследований в области моделирования динамики разрушения пород и совершенствования технологий открытых горных работ.

Ключевые слова: порода, бурение, буровое долото, кинематика, работа, проектирование, модель, уравнение.

Тошов Жавохир Буриевич	***Информация об авторах:*** *Доктор технических наук, профессор Ташкентского государственного технического университета имени Ислама Карима, 100095, Алмазарский район, улица Университетская 2, Ташкент, Узбекистан. E-mail: j.toshov@tdtu.uz; ORCID ID: https://orcid.org/0000-0003-4278-1557*
Шеров Карибек Тагаевич	*Доктор технических наук, профессор Казахского агропромышленного технического университета им. С. Сейфуллина, 010000, Астана, пр. Женис, 62, Астана, Казахстан. E-mail: shkt1965@mail.ru; ORCID ID: https://orcid.org/0000-0003-0209-180X*
Баратов Бахтиер Нусратович	*Ph.D., доцент Алмалыкского филиала НИТУ МИСиС, 110104, ул. Амира Темура, 56, Алмалык, Узбекистан. E-mail: bakhtiyor.baratov@yandex.ru; ORCID ID: https://orcid.org/0000-0002-6621-5974*
Рабатулы Мухаммедрахым	*PhD, и.о. доцента кафедры Разработки месторождений полезных ископаемых НАО Карагандинского технического университета имени Абылкаса Сагинова, 100027, пр. Нурсултана Назарбаева, 56, Караганда, Казахстан. E-mail: mukhammedrakhym@mail.ru; ORCID ID: https://orcid.org/0000-0002-7558-128X*

Эркинов Дилшодбек Илхомджонович	*PhD докторант Ташкентского государственного технического университета имени Ислама Карима, 100095, Алмазарский район, ул. Университетская, 2, Ташкент, Узбекистан. E-mail: dilshodbek.ilhomovich@gmail.com; ORCID ID: https://orcid.org/0009-0006-5970-416X*

References

[1] Toshov JB, Rabatuly M, Bogzhanova ZhK, Zheldikbayeva AT, Malikov ShR, Toshov BR, Ergashev OS. Influence of Radiation and Magnetic Pulse Treatment on The Wear Resistance of Carbide Tools. Kompleksnoe Ispolzovanie Mineralnogo Syra = Complex Use of Mineral Resources. 2026; 337(2):47-54. https://doi.org/10.31643/2026/6445.16

[2] Alikulov Sh, Toshov J, Mussin R, Rabatuly M, Tolovkhan B, Bogzhanova Zh, Gabitova A. Study of rational solution parameters during in-situ uranium leaching. Mining of Mineral Deposits. 2025; 19(1):37-46. https://doi.org/10.33271/mining19.01.037

[3] Burievich TJ. The questions of the dynamics of drilling bit on the surface of well bottom. Arch. Min. Sci. 2016; 61(2):275–283. https://doi.org/10.1515/amsc-2016-0020

[4] Yunin EK. Dynamics of oil and gas well drilling. Moscow. Geobook. 1984, 256.

[5] Falaleev AP. Modeling the interaction of spherical chisels with rock. Modern problems of science and education. 2016; 1:2-7.

[6] Zhuravlev AN. Improvement of the methodology for optimizing the parameters of the drilling regime with three-ball chisels: dis. ... Candidate of Technical Sciences. Moscow 2005, 150.

[7] Kamenskikh SV. Razvitiye metodiki optimizatsii rezhimov bureniya sharoshechnymi dolotami [Development of a methodology for optimizing drilling modes with roller bits] Neft' i gaz [Oil and Gas]. 2006; 4:115-120. (In Russ).

[8] Ayushiev OV. Mathematical modeling of the operation process of a ball chisel: bachelor's thesis. Krasnoyarsk: Siberian Federal University. 2018, 68.

[9] Gerbaud L, Menand S, Sellami H. Drilling signals analysis for tricone bit condition monitoring. International Journal of Rock Mechanics and Mining Sciences. 2006; 43:1230–1242.

[10] Ma D, Azar JJ. Dynamics of roller cone bits. Journal of Energy Resources Technology. 1995; 117:209–217.

[11] Rashidi B, Hareland G, Nygaard R. A New Drilling Rate Model for Tricone Bits and Its Application to Predict Rock Compressive Strength. ARMA. 2010, 10.

[12] Rabatuly M, Demin VF, Kenetaeva AA, Steflyuk YuYu, Toshov JB. Evaluation of modern methods and techniques for calculating parameters during coal bed degassing. Kompleksnoe Ispolzovanie Mineralnogo Syra = Complex Use of Mineral Resources. 2025; 334(3):110-120. https://doi.org/10.31643/2025/6445.33

[13] Liu Y, Wang J. Research on kinematics analysis of spherical single-cone PDC compound bit. Oil & Gas Science and Technology. 2021; 76:105.

[14] Wang X, Li Z. A novel method for estimating the real-time dullness of tri-cone oil drill bits. Engineering Failure Analysis. 2020; 109:104–112.

[15] Feng J, Li X, Zhang Y. Nonlinear Dynamics of Tricone Bit-Drillstring Coupling System in Deviated Wellhole with Air Circulating. Journal of Vibration Engineering & Technologies. 2025; 13:21-35.

[16] Chaib A, Bouabdallah S, Ferfar M, Dovbash N, Bellucci S. Investigation Of Physicochemical Characterization And Magnetic Enrichment Of Iron Ore From Sidi Maarouf Deposit. Technology Audit and Production Reserves. 2024; 1(3(75)):37-42. https://doi.org/10.15587/2706-5448.2024.297846

[17] Mannanov U, Toshov J, Toshniyozov L. Perspective Solutions for the Design of Drilling Tools. E3S Web of Conferences. IVth International Innovative Mining Symposium. 2019; 105. https://doi.org/10.1051/e3sconf/201910503027

[18] Yurov VM, Portnov VS, Rabatuly M, Khamze A, Yessendossova A, Abdrasheva Z, Kerimbayeva N, Kaiyrbek A. Mechanism of fracto- and triboluminescence of quartz. Conference Secretary of ICAMEM 2024.

[19] Zhengbing Hu, Viktor Legeza, Ivan Dychka, Dmytro Legeza. Mathematical Model of the Damping Process in a One System with a Ball Vibration Absorber. International Journal of Intelligent Systems and Applications (IJISA). 2018; 10(1):24–33. https://doi.org/10.5815/ijisa.2018.01.04

[20] Stelian Alaci, Florina-Carmen. Mathematical Model of the Evolution of a Simple Dynamic System with Dry Friction. Axioms. 2024; 13:372. https://doi.org/10.3390/axioms13060372

Crossref

DOI: 10.31643/2027/6445.28

Earth and Planetary Sciences: Earth-Surface Processes

Prospects for Industrial Extraction of Methane from Coal Seams in the Karaganda Basin: Results of Experimental-Industrial Studies at the Taldykuduk Site

***Mussin R.A., Akhmatnurov D.R., Zamaliyev N.M., Issina N.E.**

NPJSC Abylkas Saginov Karaganda Technical University, Karaganda, Kazakhstan

** Corresponding author email: r.a.mussin@mail.ru*

Received: *November 7, 2025*
Peer-reviewed: *December 10, 2025*
Accepted: *January 8, 2025*

ABSTRACT

The study focuses on assessing the industrial potential of coalbed methane production in the Karaganda Basin based on drilling and testing data from wells T7 and T8 at the Taldykuduk site. The goal is to develop and verify engineering solutions, ensuring efficient methane extraction from unstressed seams under real geological and technical conditions. The research object is the coal seams of the Karaganda suite, characterized by high gas content, developed fracturing, and heterogeneous reservoir structure. Vertical wells were drilled with local enlargement of productive intervals, zone isolation using packers, and controlled hydraulic stimulation. A set of geophysical surveys was conducted, including gamma, density, and neutron logs, caliper logging, inclinometry, gas-geochemical monitoring, and flow tests, to determine reservoir pressure and permeability. Laboratory analyses of core and coal samples examined adsorption–desorption properties, elemental composition, and formation water characteristics, enabling the selection of optimal reagents and gas treatment schemes. Stable methane inflows up to 30 m³/day were obtained under steady depression without water inflow, confirming readiness for pilot-industrial operation. After hydraulic stimulation and optimization of well regimes, an increase in gas flow rate was recorded, confirming the efficiency of reservoir stimulation. Based on pressure and flow curves, technological parameters were defined — perforation intervals, hydraulic treatment conditions, and requirements for gas collection, dehydration, and compression systems. The practical significance of the study lies in substantiating a technological scheme for industrial methane extraction and reducing methane hazards during mining. Implementation of the proposed approach will enable integration of extracted gas into the regional energy balance and reduce uncontrolled methane emissions, providing environmental and economic benefits.

Keywords: methane, degasification, drilling, hydraulic fracturing, industrial production, gas permeability.

Information about authors:

Mussin Ravil Altavovich — *PhD, Acting Associate Professor, NPJSC Abylkas Saginov Karaganda Technical University, Karaganda, Kazakhstan. Email: R.A.Mussin@mail.ru; ORCID ID: https://orcid.org/0000-0002-1206-6889*

Akhmatnurov Denis Ramilievich — *PhD, Head of Laboratory, NPJSC Abylkas Saginov Karaganda Technical University, Karaganda, Kazakhstan. Email: d.akhmatnurov@gmail.com; ORCID ID: https://orcid.org/0000-0001-9485-3669*

Zamaliyev Nail Mansurovich — *PhD, Associate Professor, NPJSC Abylkas Saginov Karaganda Technical University, Karaganda, Kazakhstan. Email: nailzamaliev@mail.ru; ORCID ID: https://orcid.org/0000-0003-0628-2654*

Issina Nazym Erbolatovna — *Master's student, NPJSC Abylkas Saginov Karaganda Technical University, Karaganda, Kazakhstan. Email: nazym.issina@gmail.com; ORCID ID: https://orcid.org/0009-0006-5914-6671*

Introduction

Over recent decades, coalbed methane has evolved from a source of heightened mining hazard into an independent type of hydrocarbon feedstock actively incorporated into the energy balances of many countries. The experience of the United States, China, and Australia confirms that coalbed methane production volumes can reach tens of billions of cubic meters per year, comparable to conventional natural gas production [[1], [2], [3], [4]]. The technologies for its extraction are based on the use of specialized drilling and inflow-stimulation methods—horizontal and directional wells, hydraulic fracturing, mechanical enlargement of productive zones, and optimization of drawdown. These processes are accompanied by geophysical and gas-geochemical monitoring, filtration and desorption modeling, and a system for conditioning the gas for transportation.

In Kazakhstan, interest in industrial coalbed methane production has intensified thanks to the large resources of the Karaganda Basin, whose total potential is estimated at up to 2 trillion m³ [5]. For a

long time, degasification activities were carried out mainly to improve the safety of underground operations. Under current conditions of growing gas demand and the transition to low-carbon energy, the key task is to shift from degasification as a safety measure to industrial development of coalbed methane and its integration into the gas-transport infrastructure. The main technological obstacle is the low permeability and pronounced anisotropy of coal reservoirs, which require multistage stimulation methods and precise selection of drainage regimes to prevent water loading and stabilize inflow.

Particular attention is given to the Taldykuduk area of the Karaganda Basin, where pilot-industrial work has been carried out on the construction and testing of vertical wells using technologies for enlarging productive intervals and hydraulic fracturing [6]. Commissioning of well T7 demonstrated a stable methane inflow of about 30 m^3 per day, which is comparable to the initial stages of industrial development of analogous fields abroad. The results obtained and the interpretation of pressure and rate curves made it possible to formulate initial technological regulations for selecting exposure intervals, injection parameters, and drawdown management, as well as to determine requirements for gas dehydration, compression, and utilization systems.

The scientific novelty of the study lies in the comprehensive validation of various inflow-stimulation technologies—from mechanical enlargement to hydraulic impact—applied to the geological and technical conditions of the Karaganda Basin. An essential element is the implementation of proprietary solutions protected by patents: a method for advance reduction of natural gas content [7], a method for advanced degasification of a coal seam by an inclined-directed well with branches [8], and a method of degasification using an injection well [9]. These technologies form a unified system—from preliminary reduction of reservoir pressure and redistribution of flows to the formation of high-conductivity channels.

The relevance of the topic is determined by the combination of the Karaganda Basin's substantial resource base, the insufficient maturity of domestic industrial production technologies, and the need to adapt global experience to local conditions. The expected results include an increase in recoverable methane reserves, enhanced energy security, and a reduction in uncontrolled emissions through managed extraction and utilization of gas. Going forward, plans include expanding the network of pilot wells, implementing multistage hydraulic-stimulation technologies, refining geomechanical and flow models, and conducting a techno-economic assessment for the transition to the industrial stage of coalbed methane development in Kazakhstan.

Experimental part

The methodology applied at the Taldykuduk site was designed to evaluate the industrial potential of methane extraction from coal seams. The work was carried out in stages: preparation and drilling of reference wells, geophysical surveys to identify promising zones, local operations to increase near-wellbore permeability, stepwise inflow tests with pressure-recovery monitoring, and laboratory studies of core and formation water. The approach focuses on result reproducibility and safe technology scaling under conditions of low natural permeability of coal reservoirs.

Field tests were conducted on wells T7 and T8. During drilling, mechanical penetration rate, torque, axial load, drilling fluid flow rate, and density were controlled; productive intervals were selectively exposed for subsequent studies. The suite of geophysical measurements included gamma-ray, density, and neutron logs, acoustic profiling, caliper logging, and inclinometry. Joint interpretation made it possible to determine lithological associations, identify zones of increased fracturing, and assess gas saturation of the rocks.

Figure 1 – General view of the U/Reamer MOT 7-1/2 in × 22 in

Mechanical enlargement was used as a gentle method for increasing permeability without applying proppant. A U Reamer 7-1/2 × 22-inch reamer provided uniform enlargement of the borehole diameter within the productive layer under controlled axial load and rotation frequency. The effectiveness of the operation was confirmed by

changes in caliper profiles without excessive ovality. To prevent clogging of the fracture–pore space, circulation flushing with low-salinity water and an inhibitor additive was used to reduce coal fines dispersion. This ensured preservation of the filtration properties of the rock mass and stability of the obtained results (Figure 1).

Hydraulic fracturing was performed in well T8 within a specially isolated coal interval. Injection parameters were selected based on calculations of the minimum horizontal stress derived from acoustic and density measurements, using empirical relationships characteristic of coal rocks. The operations were carried out in stages: interval sealing with packers, initiation of the injection stage, main stage of fracture opening and formation of a conductive channel, followed by controlled closure. Pressure and flow rate were recorded with high temporal resolution, which allowed, through interpretation of the closure curves, to estimate the conductivity of the created channel and the expected productivity increase. The layout and sequence of operations are shown in Figure 2.

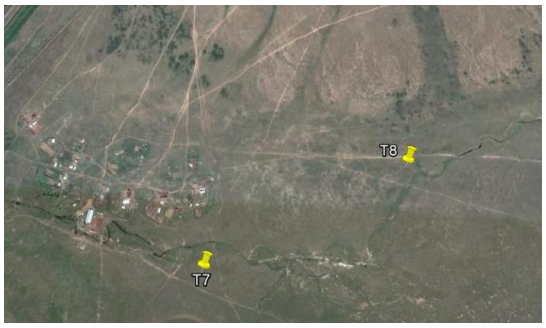

Figure 2 – Location of wells T7 and T8

Inflow tests were performed using a stepwise scheme with sequential increases in drawdown followed by stabilization of the flow rate. Reservoir pressure was determined using buildup periods, which made it possible to calculate the permeability–thickness product (kh), skin factor, and drainage radius from logarithmic and derivative diagnostics. After hydraulic fracturing, the linear-flow component was additionally analyzed using square-root-of-time analysis, allowing estimation of the fracture half-length and effective conductivity.

Laboratory studies included determination of bulk and grain density, porosity by helium pycnometry, gas content from desorption canisters, and methane adsorption characteristics from Langmuir isotherms—capacity and saturation pressure. Gas permeability was measured under steady-state and quasi-steady-state conditions while varying effective stress and orientation relative to bedding [10]. Mechanical tests were carried out on dry and wetted specimens under uniaxial compression and Brazilian tension; the resulting static moduli were compared with dynamic values calculated from acoustic data [11]. The ranges of the obtained parameters are summarized in Table 1 for subsequent calibration of flow models.

Table 1 – Results of laboratory studies and test intervals of coal seams in well T7

№	Seam No.	Roof, m	Floor, m	Total thickness, m	Purpose
1	8	186.6	210.3	23.7	For methane gas inflow
	9	212.0	216.3	4.3	For methane gas inflow
2	5	154.2	165.1	10.9	For methane gas inflow
	6	165.1	176.6	11.5	For methane gas inflow
	7	176.6	182.1	5.5	For methane gas inflow
3	3	119.2	121.1	1.9	For methane gas inflow

The chemical composition of formation waters was determined using certified methods, including analysis of ionic composition, total mineralization, and assessment of the medium's tendency to form scale and corrosion. The data obtained were used in selecting inhibitor programs, gas dehydration schemes—adsorption or glycol—and in choosing compression parameters, which made it possible to avoid technological flow-rate limitations at the early stage of development.

Interpretation of hydrodynamic data was performed taking into account gas supercompressibility by transforming to pseudopressure, as well as the two-component structure of the coal seam, represented by the matrix and a fracture system with active desorption–diffusion exchange. Exchange parameters were determined from the character of the early and late segments of the pressure-buildup curves and from the behavior of the derivative function. Matching of calculated and actual data was carried out iteratively on the basis of the set of rate–pressure relationships, with laboratory results used as a priori

constraints. To assess parameter uncertainty, bootstrap analysis and Bayesian regularization were applied.

Quality control included preliminary calibration of pressure, temperature, and flow sensors, as well as inter-operational checks. Geophysical instruments were verified on control intervals, and calipers on standard calibration rings. Operational logs contained detailed entries on depth, regimes, and the tools used, which ensured accurate tracing of operations and made it possible to promptly identify the causes of possible discrepancies.

The efficiency criteria were stable gas inflow at moderate drawdown, a decrease in skin factor after stimulating treatments, absence of early water breakthrough, and reproducibility of results in repeated test cycles. The flow rates obtained at well T7, on the order of several tens of cubic meters of gas per day under a stable regime, make it possible to consider this approach as a basis for expanding the pilot network with the use of multistage stimulation technologies.

Results and Discussion

Well T7: drilling, enlargement, and completion.

In June 2016, drilling began on the vertical pilot-production well T7 at the Taldykuduk site (Figure 2). The wellbore design included a direction with a diameter of 340 mm, a 244.5 mm conductor, and a 140 mm production casing with full cementing to the surface. This scheme ensured borehole stability within the section of argillites and siltstones, as well as the possibility of selective exposure of coal interbeds. Low-mineralized water with an inhibitor preventing the dispersion of coal fines was used as the drilling fluid. Drilling regimes were selected with limits on axial load and torque, with continuous control of mechanical penetration rate and fluid flow rate, which made it possible to minimize near-wellbore damage.

To increase the contact area between the borehole walls and the coal seam, as well as to open microfracturing, a U Reamer MOT 7-1/2 × 22-inch (559 mm) reamer was used. The increase in effective filtration area was confirmed by caliper logging results (Figure 2).

The suite of geophysical surveys conducted before and after mechanical enlargement made it possible to identify, within the 154–216 m interval, coal interbeds with reduced apparent density (1.59–2.21 g/cm³) and increased specific electrical resistivity (15.3–118.4 Ω·m). In combination with acoustic characteristics, these data indicate high gas saturation and low wettability of the rocks. Joint interpretation of gamma-ray, density, and neutron logs with the caliper results was used to refine test boundaries and select sections for mechanical enlargement (Tables 2–3). Caliper profiles confirmed uniform diameter increase within the target intervals without signs of ovality or loss of borehole wall stability.

Table 2 – Main physical parameters of the rock skeleton and fluids in the section of well T7.

Rock skeleton	σ, g/cm³	ΔT, μs/m
Sandstone	2.65	165
Clay	2.40-2.55	275-325
Limestone	2.71	155
Fresh water	1.00	610
Saline water	1.05	590

The technological sequence of operations included borehole cleaning, enlargement of productive zones, repeat geophysical surveys, isolation of seams using packers, and a series of stepwise inflow tests. During mechanical enlargement, axial load and tool rotation frequency were controlled, and continuous circulation of low-mineralized water ensured efficient removal of cuttings and coal dust. To prevent secondary clogging of the fracture–pore space, a specially selected inhibitor was used that accounted for the ionic composition of formation waters; the parameters of its selection are provided in the summary materials. According to control caliper logging, a uniform diameter increase of 20–60 mm was recorded within the target intervals while maintaining the proper cylindrical shape of the borehole.

Well cleanup and commissioning were carried out according to the standard scheme: initial cleaning, gradual reduction of bottomhole pressure, stabilization of flow rate, and a final pressure-buildup stage. During the cleaning stage, a short-term removal of drilling fluid and fine coal was observed, after which gas inflow became stable. The series of stepwise tests showed a regular increase in flow rate with growing drawdown; at the control step, a stable methane inflow of about 30 m³ per day was obtained under a moderate pressure differential and with no signs of water breakthrough [12]. Analysis of pressure-buildup data made it possible to determine integral permeability, skin

factor, and drainage radius. A decrease in the skin parameter relative to the initial values confirmed the positive effect of mechanical enlargement of the productive interval, which is consistent with the results presented in Table 3.

Table 3 - Results of interpretation of open-hole well-logging data for well T7 in the Taldykuduk area.

a – Geophysical and geometric parameters of coal seams.

№	Top, m	Base, m	H, m	ΔS, mm	GZ3, Ω·m	GZ3B, Ω·m	GR, μR/h
1	112.9	113.9	1.0	242	75.3	38.7	6.5
2	114.8	117.0	2.2	289	54.4	34.2	6.3
3	119.2	121.1	1.9	286	27.7	29.0	5.1
4	144.2	145.1	0.9	254	44.1	34.7	7.5
5	154.2	165.1	10.9	289	118.4	113.4	2.5
6	165.1	176.6	11.5	359	45.9	41.7	1.9
7	176.6	182.1	5.5	324	75.2	50.7	1.5
8	186.6	210.3	23.7	381	36.2	33.7	3.7
9	212.0	216.3	4.3	312	26.4	36.0	4.7
10	248.5	251.7	3.2	314	30.6	21.0	7.8
11	266.8	268.6	1.8	311	25.6	30.1	8.1
12	280.5	282.4	1.9	298	27.3	27.6	8.5
13	284.5	286.4	1.9	235	31.9	35.0	7.9
14	299.3	308.5	9.2	436	15.7	15.3	7.0
15	309.9	316.3	6.4	444	16.1	20.0	6.4

b - Physical and petrophysical parameters of coal seams

№	ρ, g/cm³	Kclay, %	Kp, %	Lithology
1	2.17	45.8	6.5	Carbonaceous argillite
2	2.09	44.3	6.3	Carbonaceous argillite
3	1.64	32.0	2.6	Coal
4	2.18	60.1	6.5	Carbonaceous argillite
5	1.63	9.1	1.2	Coal
6	1.59	5.4	0.8	Coal
7	1.59	3.1	0.4	Coal
8	1.66	17.9	2.4	Coal
9	1.73	27.0	3.8	Coal
10	1.93	64.9	9.2	Carbonaceous argillite
11	1.79	69.4	9.9	Carbonaceous argillite
12	2.21	76.6	10.9	Carbonaceous argillite
13	2.05	65.3	9.3	Carbonaceous argillite
14	1.68	54.3	7.7	Carbonaceous argillite
15	1.62	45.4	6.2	Carbonaceous argillite

Laboratory studies for T7 included porosity (helium pycnometry), gas content (desorption canisters), adsorption parameters from Langmuir isotherms, and gas permeability under steady-state/quasi-steady-state conditions with control of effective stress. The obtained ranges were used as a priori inputs for calibration of flow models and were compared with well-logging density and acoustic indicators; the consistency of field and laboratory estimates confirms the correctness of interval selection. Formation-water analysis (ionic composition, mineralization) was applied to select inhibitor programs and gas dehydration schemes at the compression-preparation stage, which removed technological flow-rate limitations during the commissioning period [13].

The following operational recommendations were formulated for well T7: maintain stable, moderate drawdowns without abrupt changes in wellhead pressure; in case of increasing hydraulic resistance, perform preventive flushing of the near-wellbore zone; provide for gas dehydration using glycol or adsorption systems, taking into account moisture-content fluctuations; upon the appearance of local signs of water breakthrough, adjust offtake regimes and, if necessary, perform targeted isolation of water inflow. Overall, the combination of mechanical enlargement with a gentle operating regime ensured stable gas inflow at an early stage without increasing geomechanical risks and can be considered a baseline scheme for analogous coal seams at the pilot-industrial development stage.

During T7 operation, a stable methane inflow of about 30 m³ per day was recorded, which, under moderate drawdown, confirms the industrial potential of the site. The liquid rate was in the range of 0.9–5.6 m³ per day, which is associated with the removal of residual drilling fluid and partial inflow of formation waters from adjacent interbeds [14]. Chemical analysis revealed elevated mineralization—about 12.5 g/L of dry residue with chloride concentration up to 7.5 g/L. Such an ionic signature is characteristic of the participation of formation waters and indicates well-developed natural fracturing that provides hydraulic communication of coal interbeds with water-bearing intervals (Tables 2, 3). Taking into account the chloride–sodium type of water, the use of corrosion-resistant materials and inhibitor programs with control of pH and hardness is recommended; for gas conditioning—glycol dehydration with control of salt

deposition in heat-exchange units. According to pressure-buildup analysis, a decrease in the skin parameter relative to the initial values was noted, which confirms the effect of mechanical enlargement. The “soft” operating regime was recognized as optimal: gradual increase in drawdown, maintenance of balance between the gas and liquid phases at the wellhead, preventive flushing with low-mineralized water with an inhibitor additive preventing dispersion of coal fines (Figure 2; Tables 2, 3).

Well T8: drilling and preparation for hydraulic fracturing.

In August 2016, a vertical pilot-production well T8 was drilled at the Taldykuduk site (Figure 2). The design included a direction with a diameter of 340 mm, a 244.5 mm conductor, and a 140 mm production casing run to a depth of about 550 m with cementing to the surface, which ensured borehole stability and reliable isolation of non-productive intervals at the stage of subsequent stimulation. The suite of geophysical studies identified priority coal interbeds with low apparent density (1.75–1.89 g/cm³), elevated specific resistivity (25.4–197.1 Ω·m), and increased P-wave transit time (428–627 μs/m)—Tables 4–7. These indicators correspond to slightly wetted, highly gas-saturated reservoirs with low natural permeability, where formation of an artificial conductive system is required to ensure stable inflow.

Taking into account geophysics, caliper logging, and geomechanical constraints, hydraulic fracturing was planned in T8 within the priority intervals (Tables 6, 7). The preparatory stage included refinement of the minimum horizontal stress from acoustic and density data, determination of a safe pressure range, a diagnostic injection to evaluate breakdown pressure, leakoff coefficient, and closure character, as well as verification of cement quality and tightness of the packered zone. In addition, the working fluid was selected with regard to the ionic composition of formation waters to minimize the risks of swelling and plugging [15]. Based on the diagnostic injection, volumes and injection rate were refined, as were the parameters of the selected proppant—preferably a lightweight fine fraction with good transportability and moderate requirements for pressure and rate.

The technological sequence of hydraulic fracturing provided for interval isolation with packers, initiation of the injection stage, the main stage of conductive fracture formation with control of bottomhole pressure and rate, and controlled closure with recording of the pressure-falloff curve. From sections of linear and radial flow on time and logarithmic plots, effective conductivity and fracture half-length were determined. Comparison with pressure-buildup results after the operation made it possible to assess the decrease in skin parameter and the increase in integral permeability.

The success criteria were the formation of stable gas inflow at moderate drawdown, absence of increased water inflow at an early stage, and reproducibility of flow rate in repeated tests. To manage risks, online monitoring of pressure and rate with high temporal resolution was used, adjustment of injection rate in the presence of signs of unstable opening, and post-operation analysis of closure mechanics with evaluation of the leakoff-to-storage ratio [16].

Post-fracturing startup was carried out according to a gentle scheme: minimal drawdowns during the first day, control of gas humidity and composition of produced fluid, gradual increase in offtake under stable dynamics. At the initial stage, a predominance of linear inflow with a gradual transition to a quasi-radial regime is expected as the fracture is cleaned and the filtration properties of the near-wellbore zone stabilize (Tables 4–7). If signs of water breakthrough appear, regrouping of intervals, reduction of drawdown, selective isolation of water inflow, or adjustment of the working-fluid composition during repeated treatments is envisaged. Overall, the strategy implemented at T8 logically complements the results obtained for T7: mechanical enlargement made it possible to ensure rapid inflow startup, while hydraulic fracturing creates conditions for long-term conductivity and a stable gas regime while maintaining controlled geomechanical risks (Figure 2; Tables 4–7).

Table 4 - Suite of open-hole geophysical studies for well T8 in the Taldykuduk area.

a – Electrical methods

Parameter	**1**	**2**	**3**
Method	KS (N0.5M2A; A2M05N)	SP	BK
Mnemonic	GZ3B, GZ3	SP	LL3
Depth scale	1:500	1:500	1:500
Logging interval, m	146.3–506.0	146.3–502.0	146.3–508.5
Instrument	EK-73	EK-73	EK-73
Data quality	Good	Good	Good

b – Radioactive methods

Parameter	4	5	6
Method	GR	NK	GGK-p
Mnemonic	GR	RFTN, RNTN, TRNP	RHOB
Depth scale	1:500	1:500	1:200
Logging interval, m	146.3–509.5	146.3–511.0	146.3–511.0
Instrument	2NNK-73	2NNK-73	PK-73
Data quality	Good	Good	Good

c – Other methods

Parameter	7	8	9	10
Method	Caliper, Profilometry	Inclinometry	Acoustic logging (AK)	Cement-bond log (AKC)
Mnemonic	CALI, C1, C2	AZIM, DEVI	DTP, DTS	CBL
Depth scale	1:500	1:500	1:200	1:500
Logging interval, m	146.3–511.0	0.0–510.0	146.3–509.5	0.0–146.3
Instrument	4PM-73	IN-73	2AK	2AK
Data quality	Good	Good	Good	Good

The presented suite of geophysical studies made it possible to obtain a complete understanding of the lithological structure, fracturing, and gas saturation of the coal seams. The use of a combination of electrical, radioactive, and acoustic methods ensured high interpretation accuracy of the section and identification of priority intervals for stimulation operations. Data from gamma, density, and neutron logs were used in constructing correlation models and determining the dynamic properties of the reservoirs.

Table 5 - Main physical parameters of the rock skeleton and fluids in the section of well T8.

Rock skeleton	ρ, g/cm³	ΔT, μs/m
Sandstone	2.65	165
Clay	2.40–2.55	275–325
Limestone	2.71	155
Fresh water	1.00	610
Saline water	1.05	590

The data in the table illustrate the ranges of density and acoustic parameters used in the interpretation of geophysical survey results. Comparison of these values with field measurements made it possible to refine rock types, assess gas and water saturation of the coal seams, and adjust reservoir boundaries.

Table 6 - Testing recommendations.

№	Seam №	Roof, m	Floor, m	Total thickness, m	Purpose
1	7	314.1	324.9	10.8	For methane gas inflow
	8	325.9	326.8	0.9	For methane gas inflow
	9	328.2	330.5	2.3	For methane gas inflow
2	1	150.2	158.7	8.5	For methane gas inflow

Table 7 - Results of interpretation of open-hole geophysical logging data for well T8 at the Taldykuduk area

a - Coal intervals (well T8, open hole)

Parameter	1	7	8	9
Seam №	1	7	8	9
Roof, m	150.2	314.1	325.9	328.2
Bottom, m	158.7	324.9	326.8	330.5
Total, m	8.5	10.8	0.9	2.3
DS, mm	477	295	256	249
BK, Ω·m	59.5	159.5	197.1	158.2
GK, μR/h	2.7	2.7	3.3	3.0
W, %	58.6	54.0	50.3	52.3
GGKp, g/cm³	1.77	1.76	1.89	1.75
AK, μs/m	627.32	445.17	429.72	428.39
Kgl, %	8.6	9.1	13.0	10.8
Kp GGKp, %	2.7	2.6	4.2	3.4
Kp NK, %	1.2	1.2	1.7	1.4
Kp AK, %	1.6	1.4	2.4	1.8
Lithology	Coal			

b - Carbonaceous argillite (shallower)

Parameter	**2**	**3**	**4**	**5**	**6**
Seam №	2	3	4	5	6
Roof, m	177.5	181.2	183.8	199.6	201.7
Bottom, m	178.5	182.3	185.2	200.4	202.9
Total, m	1.0	1.1	1.4	0.8	1.2
DS, mm	467	460	329	465	425
BK, Ω·m	19.6	19.3	23.7	10.6	25.4
GK, µR/h	5.0	5.5	5.2	6.7	4.3
W, %	57.0	48.5	45.6	53.1	46.8
GGKp, g/cm³	1.75	1.76	1.99	1.76	1.75
AK, µs/m	612.03	440.46	297.77	500.75	596.56
Kgl, %	26.6	30.9	28.3	44.7	20.4
Kp GGKp, %	8.5	9.9	9.0	14.3	6.5
Kp NK, %	3.8	4.4	4.0	5.7	2.9
Kp AK, %	5.0	5.7	5.3	8.3	3.8
Lithology	Carbonaceous argillite				

c - Carbonaceous argillite (deeper)

Parameter	**10**	**11**	**12**
Seam №	10	11	12
Roof, m	334.5	384.6	389.5
Bottom, m	336.8	388.2	390.6
Total, m	2.3	3.6	1.1
DS, mm	293	399	245
BK, Ω·m	107.2	21.2	21.5
GK, µR/h	5.5	7.9	8.5
W, %	47.7	51.8	41.8
GGKp, g/cm³	1.81	1.76	1.91
AK, µs/m	445.01	380.95	299.11
Kgl, %	31.4	59.0	69.0
Kp GGKp, %	10.0	18.9	22.1
Kp NK, %	4.5	8.3	9.8
Kp AK, %	5.5	10.8	12.8
Lithology	Carbonaceous argillite		
Parameter	**13**	**14**	**15**
Seam №	13	14	15
Roof, m	412.2	434.0	497.4
Bottom, m	416.8	438.4	499.3
Total, m	4.6	4.4	1.9
DS, mm	307	277	276
BK, Ω·m	28.8	25.9	45.4
GK, µR/h	7.8	8.6	8.4
W, %	41.5	49.7	41.7
GGKp, g/cm³	1.77	1.86	1.81
AK, µs/m	288.82	283.13	289.79
Kgl, %	58.0	69.7	66.5
Kp GGKp, %	18.6	22.3	21.3
Kp NK, %	8.0	9.9	9.4
Kp AK, %	10.8	13.0	12.4
Lithology	Carbonaceous argillite		

Comparison of the data for wells T7 and T8 makes it possible to identify two different approaches to the opening and development of the coal seams of the Karaganda Basin. At well T7, mechanical enlargement of the productive intervals was used, which ensured a rapid transition to a gas regime and a stable methane inflow of about 30 m³ per day. At the same time, the inflow of mineralized waters with a high chloride content was recorded, indicating the presence of natural fractures and a hydraulic connection between the coal and aquifer interbeds. This feature increases drainage efficiency but requires the use of corrosion-resistant materials and inhibitor programs to prevent salt deposition and equipment degradation.

In contrast, at well T8, a strategy of hydraulic fracturing aimed at creating an artificial filtration system under conditions of low natural permeability was implemented. The method requires precise geomechanical calculations, diagnosis of the formation state, and selection of the composition of working fluids and proppants. Despite greater technological complexity and costs, hydraulic stimulation ensures expansion of the drainage radius and the formation of a stable conductive system, which in the future increases the stability of gas deliverability and reduces the skin factor.

The mechanical enlargement applied at T7 is effective for the rapid initiation of flow and confirmation of seam productivity, whereas the hydraulic treatment at T8 provides long-term conductivity and a more uniform drainage of the formation. A comprehensive analysis of the results of both wells demonstrates the possibility of adapting different stimulation methods depending on geological conditions and the technological objectives, and lays the groundwork for transitioning to an industrial level of methane production from the coal seams of the Karaganda Basin.

The results of commissioning well T7 and drilling well T8 at the Taldykuduk site of the Karaganda Basin make it possible to perform a comparative analysis of the effectiveness of the applied technologies against international practice. In the United States—in the San Juan and Powder River basins—industrial methane production from coal seams is based on drilling horizontal and inclined-directional wells with multistage hydraulic fracturing. This approach provides stable gas rates on the order of 30–80 thousand m³ per day and higher [[17], [18], [19], [20]]. In China, vertical and horizontal hydraulic stimulation methods, as well as directional drilling technologies, are developing rapidly, which has made it possible to raise annual

methane production to more than 10 billion m³ [21], [22]. The Australian experience shows that combining vertical and horizontal wells with hydraulic fracturing forms the most stable drainage system, especially in low-permeability coals [[23], [24], [25]].

Against this backdrop, research in Kazakhstan is still at the stage of pilot-industrial testing; however, the methane inflow of about 30 m³ per day at well T7 can be regarded as a significant achievement for the initial stage of development. Similar figures were recorded in the early stages of coal seam development in the United States and China. The application of mechanical enlargement at T7 confirmed its effectiveness in increasing the filtration surface, but also revealed an accompanying issue—the inflow of mineralized waters that partially reduces the net gas rate. Meanwhile, the hydraulic fracturing implemented at well T8 is aimed at forming a long-term network of drainage channels capable of ensuring a more stable and higher level of performance [26].

For the geological conditions of the Karaganda Basin, the most rational option appears to be a combined approach that includes preliminary mechanical enlargement of productive zones followed by multistage hydraulic fracturing. Such a combination makes it possible to unite the advantages of both technologies: rapid engagement of coal interbeds in gas release and the subsequent stable development of the drainage system. These solutions logically continue the results of the pilot-industrial works and provide a basis for scaling up production while controlling risks associated with rate nonuniformity and water inflow.

Overall, a comparison of global and domestic experience confirms that the Karaganda Basin has high potential for industrial development of coal seam methane. Further progress requires improving inclined-directional drilling technologies, introducing multistage hydraulic fracturing, and integrating domestic patented solutions into a unified technological complex, which will enable a transition from the experimental level to industrial-scale production.

Conclusions

Field work carried out at the Taldykuduk site in the Karaganda Coal Basin has convincingly confirmed the possibility of shifting from traditional degasification measures—aimed mainly at ensuring the safety of underground mining—to industrial production of methane from coal seams. Testing of the T7 pilot-production well showed a stable gas inflow of about 30 m³ per day already at the initial stage of commissioning. This result indicates the high gas content of the Karaganda Suite seams and confirms the site's prospects for scaling industrial methane production technologies.

Analysis of the effectiveness of various opening and stimulation methods showed differences in the mechanisms of formation impact and in operational outcomes. The mechanical enlargement applied at well T7 significantly increased the filtration surface and enabled a rapid transition to a gas regime. This approach is distinguished by implementation simplicity and high reproducibility of results while minimizing risks to the geomechanical stability of the borehole. At the same time, an inflow of mineralized waters with a high chloride content was recorded, indicating the involvement of formation horizons in the drainage process. The water factor—especially during long-term operation—requires the introduction of specialized inhibitor programs, the use of corrosion-resistant materials, and monitoring systems that ensure control of the near-wellbore zone condition and the stability of the hydrodynamic regime.

Hydraulic fracturing of the seam, prepared for implementation at well T8, is a more expensive and technologically complex operation, but it provides different operational advantages. By creating an artificial network of fractures, a stable filtration system is formed in a coal mass with low natural permeability, capable of maintaining a steady gas inflow. An increase in the drainage radius and a reduction in the skin parameter contribute to the long-term stability of the flow rate and to bringing low-permeability seams into production. Global practice—primarily the experience of China, the United States, and Australia—confirms that this method is key in moving from the experimental level to industrial-scale methane production.

Of particular importance is the possibility of integrating mechanical enlargement and hydraulic fracturing with domestic engineering solutions protected by patents No. 8188, No. 10961, and No. 10923. The combined use of these technologies creates a technologically flexible system that makes it possible to adapt impact methods to specific geological and technical conditions. Comprehensive application of the methods ensures effective reduction of reservoir pressure, redistribution of flows, and formation of high-conductivity zones, thereby increasing the system's overall energy return.

The practical value of the results obtained lies in creating the prerequisites for organizing, on the basis of the Karaganda Basin, a pilot-industrial test site for methane production from coal seams. Implementation of such a complex will not only diversify Kazakhstan's fuel and energy balance and reduce dependence on imported natural gas, but also raise the level of industrial safety of coal enterprises through controlled reduction of gas hazard and prevention of sudden outbursts.

Overall, the results of studies on wells T7 and T8 confirm the technological and economic feasibility of industrial development of coal seam methane in the Karaganda Basin. Combining stimulation methods, applying innovative engineering solutions, and adapting best international practices form the basis for establishing a new coalbed methane industry in Kazakhstan. This industry can not only strengthen the country's energy independence, but also ensure sustainable regional development through more environmentally friendly and rational use of hydrocarbon resources.

Conflicts of interest. On behalf of all authors, the corresponding author states that there is no conflict of interest.

CRediT author statement: **R. Mussin**: Conceptualization, Methodology; **D. Akhmatnurov**: Data curation, Writing draft preparation, Visualization; **N. Zamaliyev:** Validation, Reviewing and Editing; **N. Issina:** Investigation, Supervision, Software.

Acknowledgements. The research was funded by the Science Committee of the Ministry of Science and Higher Education of the Republic of Kazakhstan as part of program-targeted funding for the implementation of the scientific and scientific-technical program IRN №BR24993009.

Cite this article as: Mussin RA, Akhmatnurov DR, Zamaliyev NM, Issina NE. Prospects for Industrial Extraction of Methane from Coal Seams in the Karaganda Basin: Results of Experimental-Industrial Studies at the Taldykuduk Site. Kompleksnoe Ispolzovanie Mineralnogo Syra = Complex Use of Mineral Resources. 2027; 342(3):35-46. https://doi.org/10.31643/2027/6445.28

Қарағанды көмір бассейнінің көмір қабаттарынан метанды өнеркәсіптік өндірудің перспективалары: Талдықұдық учаскесіндегі тәжірибелік-өндірістік зерттеулер нәтижелері

***Мусин Р.А., Ахматнуров Д.Р., Замалиев Н.М., Исина Н.Е.**

КЕАҚ Әбілқас Сағынов атындағы Қарағанды техникалық университеті, Қарағанды, Қазақстан

Мақала келді: *7 қараша 2025*
Сараптамадан өтті: *10 желтоқсан 2025*
Қабылданды: *8 қаңтар 2025*

ТҮЙІНДЕМЕ

Зерттеу Қарағанды көмір бассейніндегі Талдықұдық учаскесіндегі Т7 және Т8 ұңғымалары бойынша бұрғылау және сынақ деректері негізінде көмір қабаттық метанын өнеркәсіптік өндіру әлеуетін бағалауға арналған. Жұмыстың мақсаты — нақты геологиялық-техникалық жағдайларда жүктемесі түсірілмеген қабаттардан метанды тиімді өндіруді қамтамасыз ететін инженерлік шешімдерді әзірлеу және тексеру. Зерттеу нысаны — жоғары газдалған, біртекті емес фильтрация-сыйымдылық құрылымымен, өте жарықшақтылықпен сипатталатын Қарағанды свитасының көмір қабаттары. Өнімді интервалдарды жергілікті кеңейте отырып, пакерлерді пайдалану арқылы аймақтық оқшаулау және бақыланатын гидравликалық стимуляция қолданылған тік ұңғымалар бұрғыланды. Гамма-, тығыздық және нейтрондық каротаж, каверонометрия, инклинометрия, газ-геохимиялық мониторинг және қабат қысымы мен өтімділігін анықтау үшін ағындық сынақтардан тұратын геофизикалық зерттеулер кешені орындалды. Керн мен көмір үлгілерінің зертханалық талдаулары адсорбция–десорбция қасиеттерін, элементтік құрамын және пласт суларының сипаттамаларын қамтыды, бұл оңтайлы реагенттер мен газды дайындау схемаларын таңдауға мүмкіндік берді. Тұрақты депрессия жағдайында тәулігіне 30 м³-ге дейін ағымды метан сусыз алынды, бұл тәжірибелік-өндіріске пайдалануға дайын екенін растады. Гидравликалық стимуляция және ұңғымалар жұмыс режимдерін оңтайландырудан кейін газ дебитінің артуы тіркелді, бұл қабатқа әсер етуді және тиімді екенін дәлелдеді. Дебит және қысым қисықтары бойынша перфорация аралықары , гидроөндеу шарттары, сондай-ақ газды сығымдау, сусыздандыру жинақтау жүйелеріне қойылатын технологиялық параметрлер айқындалды. Жұмыстың практикалық маңыздылығы өнеркәсіптік метан өндірудің технологиялық схемасын негіздеуде және тау-кен жұмыстары кезінде метан қаупін азайтуда Ұсынылған тәсілді іске асыру өндірілген газды аймақтық энергетикалық балансқа және бақыланбайтын метан шығарындыларын азайтуға мүмкіндік береді, экологиялық әрі экономикалық пайда әкеледі.

Түйін сөздер: метан, дегазация, бұрғылау, қабатты гидроажырату, өнеркәсіптік өндіру, газ өткізгіштік.

Авторлар туралы ақпарат:

Мусин Равиль Альтавович — *PhD докторы, қауымдастырылған профессор, КЕАҚ Әбілқас Сағынов атындағы Қарағанды техникалық университеті, Қарағанды, Қазақстан. Email: R.A.Mussin@mail.ru; ORCID ID: https://orcid.org/0000-0002-1206-6889*

Ахматнуров Денис Рамильевич — *PhD докторы, зертхана жетекшісі, КЕАҚ Әбілқас Сағынов атындағы Қарағанды техникалық университеті, Қарағанды, Қазақстан. Email: d.akhmatnurov@gmail.com; ORCID ID: https://orcid.org/0000-0001-9485-3669*

Замалиев Наиль Мансурович — *PhD докторы, қауымдастырылған профессор, КЕАҚ Әбілқас Сағынов атындағы Қарағанды техникалық университеті, Қарағанды, Қазақстан. Email: nailzamaliev@mail.ru; ORCID ID: https://orcid.org/0000-0003-0628-2654*

Исина Назым Ерболатовна — *Магистрант, КЕАҚ Әбілқас Сағынов атындағы Қарағанды техникалық университеті, Қарағанды, Қазақстан. Email: nazym.issina@gmail.com; ORCID ID: https://orcid.org/0009-0006-5914-6671*

Перспективы промышленной добычи метана из угольных пластов Карагандинского бассейна: результаты экспериментально-промышленных исследований на Талдыкудукском участке

***Мусин Р.А., Ахматнуров Д.Р., Замалиев Н.М., Исина Н.Е.**

НАО Карагандинский технический университет имени Абылкаса Сагинова, Караганда, Казахстан

Поступила: *7 ноября 2025*
Рецензирование: *10 декабря 2025*
Принята в печать: *8 января 2025*

АННОТАЦИЯ

Исследование посвящено оценке промышленного потенциала добычи метана из угольных пластов Карагандинского бассейна на основе данных бурения и испытаний скважин Т7 и Т8 на Талдыкудукском участке. Цель работы — разработать и верифицировать инженерные решения, обеспечивающие эффективное извлечение метана из неразгруженных пластов в реальных геолого-технических условиях. Объект исследования — угольные пласты карагандинской свиты, характеризующиеся высокой газоносностью, развитой трещиноватостью и неоднородной фильтрационно-ёмкостной структурой. Пробурены вертикальные скважины с локальным расширением продуктивных интервалов, зональной изоляцией с применением пакеров и контролируемой гидравлической стимуляцией. Выполнен комплекс геофизических исследований, включающий гамма-, плотностной и нейтронный каротаж, кавернометрию, инклинометрию, газогеохимический мониторинг и приточные испытания для определения пластового давления и проницаемости. Лабораторные анализы керна и угля охватывали адсорбционно-десорбционные свойства, элементный состав и характеристики пластовых вод, что позволило выбрать оптимальные реагенты и схемы подготовки газа. Получены устойчивые притоки метана до 30 м³/сут при стабильной депрессии и отсутствии притока воды, что подтверждает готовность к опытно-промышленной эксплуатации. После гидростимуляции и оптимизации режимов работы скважин зафиксировано увеличение дебита газа, подтверждающее эффективность воздействия на пласт. По кривым давления и дебита определены технологические параметры — интервалы перфорации, условия гидрообработки и требования к системам сбора, осушки и компримирования газа. Практическая значимость работы заключается в обосновании технологической схемы промышленной добычи метана и снижении метаноопасности при ведении горных работ. Реализация предложенного подхода позволит интегрировать добытый газ в региональный энергобаланс и уменьшить неконтролируемые выбросы метана, обеспечивая экологические и экономические преимущества.

Ключевые слова: метан, дегазация, бурение, гидроразрыв пласта, промышленная добыча, газопроницаемость.

Информация об авторах:

Мусин Равиль Альтавович — *PhD, Ассоциированный профессор, НАО Карагандинский технический университет имени Абылкаса Сагинова, Казахстан, Караганда. Email: R.A.Mussin@mail.ru; ORCID ID: https://orcid.org/0000-0002-1206-6889*

Ахматнуров Денис Рамильевич — *PhD, руководитель лаборатории, НАО Карагандинский технический университет имени Абылкаса Сагинова, Казахстан, Караганда. Email: d.akhmatnurov@gmail.com; ORCID ID: https://orcid.org/0000-0001-9485-3669*

Замалиев Наиль Мансурович — *PhD, Ассоциированный профессор, НАО Карагандинский технический университет имени Абылкаса Сагинова, Казахстан, Караганда. Email: nailzamaliev@mail.ru; ORCID ID: https://orcid.org/0000-0003-0628-2654*

Исина Назым Ерболатовна — *Магистрант, НАО Карагандинский технический университет имени Абылкаса Сагинова, Казахстан, Караганда. Email: nazym.issina@gmail.com; ORCID ID: https://orcid.org/0009-0006-5914-6671*

References

[1] Sunkyo Kim, Pyeong-Ik Hwang, Jaewan Suh. Automatic Generation Control Ancillary Service Cost-Allocation Methods Based on Causer-Pays Principle in Electricity Market. Energies. 2024; 17(1):11. https://doi.org/10.3390/en17010011

[2] Liu Zh, et al. Research on Fracturing Optimization of Coalbed Methane Wells Aiming at Economic Benefit—A Case Study of Liulin Block. Energies. 2024; 17(8):1829. https://doi.org/10.3390/en17081829

[3] Drizhd NA, Kamarov RK, Akhmatnurov DR, Zamaliev NM, Shmidt-Fedotova IM. Ugol'nyi metan Karagandinskogo basseina v gazovom balanse Respubliki Kazakhstan: sostoyanie i perspektivy [Coalbed methane of the Karaganda Basin in the gas balance of the Republic of Kazakhstan: Status and prospects]. Naukovyi Visnyk Natsionalnoho Hirnychoho Universytetu = Scientific Bulletin of the National Mining University. 2017; 1(12):20–26. (in Russ.).

[4] Mussin RA, Asanova ZhM, Khalikova ER, Dzhusupov ND, Golik AV. Razrabotka tekhnologicheskikh kriteriev otsenki dlya vybora perspektivnykh uchastkov dobychi ugol'nogo metana [Development of technological evaluation criteria for selecting promising coalbed methane production sites]. Ugol = Coal Journal. 2024; 4:102–108. (in Russ.). https://doi.org/10.18796/0041-5790-2024-4-102-108

[5] Pat. 8188 KZ. Sposob zablagovremennogo snizheniya prirodnoi gazonosnosti s zemnoi poverkhnosti [Method for preliminary reduction of natural gas content from the earth's surface]. Mussin RA, Khusan B, Zamaliev NM, Bogazhanova ZhK, Murtazina FE, Fain AV, Rybalov AS, Tileukarim IB. Publ. 2023. (in Russ.).

[6] Pat. 10961 KZ. Sposob zablagovremennoi degazatsii ugol'nogo plasta naklonno-napravlennoi skvazhinoi s otvetvleniyami [Early degasification of a coal seam using an inclined directional borehole with branches]. Mussin RA, Zamaliev NM, Akhmatnurov DR, Khasen BP, Gogol DB. Publ. 2025. (in Russ.).

[7] Pat. 10923 KZ. Sposob zablagovremennoi degazatsii pri pomoshchi nagnetatel'noi skvazhiny [Early degasification using an injection borehole]. Mussin RA, Zamaliev NM, Akhmatnurov DR, Khasen BP, Gogol DB. Publ. 2025. (in Russ.).

[8] Xiao H, et al. Numerical Study on Hydraulic Fracture Propagation in Coalbed Methane Considering Coal Seam Cleats. Processes. 2025; 13(4):1036. https://doi.org/10.3390/pr13041036

[9] Wu Zh, et al. Research on Damage Characteristics of Clean Fracturing Fluid in Deep Coal Seam. Processes. 2025; 13(9):2669. https://doi.org/10.3390/pr13092669

[10] Ahmed AJ. Coalbed Methane: Clean Energy for the World. US Geological Survey Professional Paper 1625-F. Washington: USGS. 2009. https://pubs.usgs.gov/publication/70034970

[11] Altovilib A, et al. Reserves Estimation for Coalbed Methane Reservoirs: A Review. Sustainability. 2020; 12(24):10621. https://doi.org/10.3390/su122410621

[12] Li J, et al. High quality of Jurassic Coals in the Southern and Eastern Junggar Coalfields, Xinjiang, NW China: Geochemical and mineralogical characteristics. International Journal of Coal Geology. 2012; 101:36-81. https://doi.org/10.1016/j.coal.2012.05.003

[13] Chen W, et al. The Influence of Fracturing Fluid Volume on the Productivity of Coalbed Methane Wells in the Southern Qinshui Basin. Energies. 2022; 15(20):7673. https://doi.org/10.3390/en15207673

[14] Wang F, Huang F, Guan Y, Xu C. Mitigation of Fracturing Fluid Leak-Off and Subsequent Formation Damage Caused by Coal Fine Invasion in Fractures: An Experimental Study. Processes. 2024; 12(8):1711. https://doi.org/10.3390/pr12081711

[15] Zhang B, et al. Mitigation of Fracturing Fluid Leak-Off and Subsequent Formation Damage Caused by Coal Fine Invasion in Fractures: An Experimental Study. Processes. 2023; 11(12):3269. https://doi.org/10.3390/pr11123269

[16] Kao B. A novel implicit method of characteristics using pressure-referenced correction for transient flow in natural gas pipelines. Journal of Natural Gas Science and Engineering. 2022; 104:104665. https://doi.org/10.1016/j.jngse.2022.104665

[17] Li Y, et al. Impact of Coal Orthotropic and Hydraulic Fracture on Pressure Distribution in Coalbed Methane Reservoirs. 2022; 2(3):6. https://doi.org/10.3390/gases2030006

[18] Qiao L, et al. Numerical Investigation of Vertical Hydraulic Fracture Propagation and Fracturing Parameter Optimization in Deep Coalbed Methane Reservoirs. Processes. 2025; 13(3):909. https://doi.org/10.3390/pr13030909

[19] Avan F, Keshavarz A, Akhonzade H, Al-Ansari S, Al-Yaseri A, Nosrati A, Ali M, Iglauer S. Stable Dispersion of Coal Fines during Hydraulic Fracturing Flowback in Coal Seam Gas Reservoirs—An Experimental Study. Energy & Fuels. 2020; 34(12):16018-16029. https://doi.org/10.1021/acs.energyfuels.0c00045

[20] Xu Y, Lin B, Zhai C, Zhu C, Regenauer-Lieb K, Chen S. Enhanced Coalbed Methane Extraction by Geothermal Stimulation in Deep Coal Mines: An Appraisal. Energy. 2021; 228:120595. https://doi.org/10.48550/arXiv.2102.02348

[21] Guseva IP. Reduction of greenhouse gas emission through processing of coal mine methane using energy-conversion technology. Energy Policy. 2023; 2:113-116. https://doi.org/10.17580/em.2023.02.25

[22] Sadavarte P, Pandey S, Maasakkers JD, Lorente A, Borsdorff T, Denier van der Gon H, Houweling S, Aaben I. Methane Emissions from Super-emitting Coal Mines in Australia quantified using TROPOMI Satellite Observations. Environmental Science & Technology. 2021; 55(24):16573-16580. https://doi.org/10.48550/arXiv.2106.10457

[23] Sadavarte P, Pandey S, Maasakkers JD, Denier van der Gon H, Houweling S, Aaben I. A high-resolution gridded inventory of coal mine methane emissions for India and Australia. Elementa: Science of the Anthropocene. 2021; 10(1):00056. https://doi.org/10.1525/elementa.2021.00056

[24] Pashin JC. Coalbed Methane of the Black Warrior Basin, Alabama: Resource Guide. Alabama Geological Survey Bulletin. 2010; 180:80.

[25] Karacan CO, Diamond WP, Schatzel SJ. Swelling-induced volumetric strains internal to a stressed coal associated with CO2 sorption. International Journal of Coal Geology. 2007; 72(1-2):15-32. https://doi.org/10.1016/j.coal.2007.01.003

[26] Zamaliev NM, Mussin RA, Akhmatnurov DR, Rabatuly MR, Ganyukov NYu. Perspektivy i problemy zablagovremennogo izvlecheniya metana iz ugol'nykh plastov Karagandinskogo ugol'nogo basseina [Prospects and challenges of early methane extraction from coal seams of the Karaganda Coal Basin]. Ugol = Coal Journal. 2025; 9:100-105. (in Russ.). https://doi.org/10.18796/0041-5790-2025-9-100-105

Crossref
DOI: 10.31643/2027/6445.29
Earth and Planetary Sciences: Earth-Surface Processes

Technological and operational properties of composite magnesia binders

[1*] Miryuk O.A., [2]Gorshkova L.V.

[1] Rudny Industrial University, Rudny, Kazakhstan
[2] Toraigyrov University, Pavlodar, Kazakhstan

** Corresponding author email: psm58@mail.ru*

Received: *October 28, 2025*
Peer-reviewed: *December 8, 2025*
Accepted: *January 9, 2025*

ABSTRACT

The article presents the results of studies of magnesia binders of various material compositions. The purpose of the work is to study the technological and operational properties of composite magnesia binders containing metallurgical slag and magnetite ore. Solutions of magnesium chloride and magnesium sulfate, as well as a mixture of them, were used to seal magnesia binders. The technological properties of magnesia binders were evaluated by the consumption of saline solution, consistency, and viscosity changes of the suspensions. To determine the operational quality of composite binders, indicators of density, strength, water absorption and water resistance were used. The dependences of the rheological properties of suspensions on the composition of the dispersed phase and the type of saline solution are revealed. The operational advantages of composite magnesia binders have been established and substantiated: increased density, lower water absorption, increased water resistance and comparable strength compared with caustic magnesite. The directions of using the developed magnesia-slag and magnesia-magnetite binders are proposed. The research results are aimed at developing resource-saving technologies for magnesia binders and concretes.

Keywords: caustic magnesite, metallurgical slag, magnetite ore, composite binders, viscosity of suspensions, stone structure.

Information about authors:

Miryuk Olga Aleksanrovna — *Doctor of Technical Sciences, Professor, Rudny Industrial University, 50 let Oktyabrya str., 38, 111500, Rudny, Kazakhstan. Email: psm58@mail.ru, ORCID ID: https://orcid.org/0000-0001-6892-2763*

Gorshkova Larisa Vladimirovna — *Candidate of technical sciences, Associate professor, Toraigyrov University, Lomova str., 64, 140008, Pavlodar, Kazakhstan. Email: gorshkova_larisa@mail.ru, ORCID ID: https://orcid.org/0009-0000-3173-753X*

Introduction

Modern trends in the development of construction materials science are aimed at developing resource-saving technologies using man-made waste from various industries [[1], [2], [3]].

Cement production consumes significant volumes of carbonate raw materials and fuel resources, and is also accompanied by harmful emissions into the environment [[4], [5]]. An alternative to energy-intensive Portland cement are composite binders containing active mineral additives (granulated metallurgical slag, waste from thermal power plants, etc.). Composite cements are characterized by a reduced clinker content and improved technical properties. However, cements with a high content of mineral additives often harden slowly early and fail to achieve high design strength values. To address these issues, technological approaches (increasing the fineness of the binder grinding, introducing water-reducing additives) are used, which complicate the process and require additional costs [[1], [3]].

The development of modern construction technologies is facilitated by the use of effective materials. Magnesia binders, primarily caustic magnesite, are characterized by high activating properties for materials of various origins.

The hydration properties of latent substances are activated by the combined action of caustic magnesite (MgO) and a salt binder ($MgCl_2$ or $MgSO_4$ solutions). Composite binders combined with magnesium chloride exhibit increased hydraulic activity due to the participation of chloride ions in the formation of bridging polymer structures that strengthen the magnesite rock [[6], [7], [8], [9]].

Consequently, the activating capacity of magnesite binders is determined not only by the

caustic magnesite but also by the composition of the salt solution. This advantage of magnesite-chloride activation underlies the production of composite magnesite binders, which are comparable in strength to caustic magnesite. Moreover, composite binders differ from caustic magnesite in their increased resistance to water and aggressive environments [[10], [11], [12]].

The properties of composite magnesite binders depend on the composition of the mineral component. Several studies have confirmed the effectiveness of combining caustic magnesite with fuel combustion ash, metallurgical slag, and other man-made materials [[13], [14], [15], [16]].

A positive effect of iron additives on the physical and mechanical properties and durability of magnesite binders has been revealed [[17], [18], [19]]. It is believed that the reduction in the hygroscopicity of magnesite oxychloride binders containing trivalent iron cations occurs through the neutralization of the negative charge of magnesium hydroxyl chlorides by the positive charge of trivalent ions, as well as by reducing the electrostatic attraction of water dipoles [[20], [21]].

To expand the scope of magnesite concrete applications, research is needed into the properties of composite binders, which determine the nature of the technological process and the intended use of the materials.

The aim of this study is to investigate the technological and operational properties of composite magnesite binders.

Experimental part

The object of the study was composite magnesite binders based on caustic magnesite, aluminosilicate, and iron components.

To produce the composite binders, caustic magnesite grade 75 powder, containing 75–85% MgO and characterized by a specific surface area of 290 m^2/kg, was used.

Metallurgical slag containing the following (wt.%) was used as the aluminosilicate component of magnesite composites: SiO_2 44.1; Al_2O_3 13.2; Fe_2O_3 0.9; CaO 31.3; MgO 5.2; SO_3 2.1; other 3.2. The main phases of the metallurgical slag were åkermanite, anorthite, and gehlenite. Magnetite ore with a magnetite iron content of 89.6% was used as the ferrous component. Non-metallic minerals accompanying magnetite included pyroxene, garnet, scapolite, actinolite, and epidote.

Composite binders were obtained by combined milling of the components to a specific surface area of 300–320 m^2/kg. The dispersion of the binders was assessed using a PSKh-10M device (manufacturer: Own Technologies (Sobstvennyye Tekhnologii) from Russia).

Magnesia binders are mixed with salt solutions. The combination of caustic magnesite and magnesium chloride solution ensures intensive hardening and high strength. When caustic magnesite is mixed with magnesium sulfate solution, the hardened stone is more stable in an aqueous environment [9]. For mixing the studied composite magnesia binders, a magnesium chloride solution with a density of 1250 kg/m^3, a magnesium sulfate solution with a density of 1220 kg/m^3, and a mixture of these solutions with a magnesium chloride content of 70% were used. The density of the salt solutions was determined with a hydrometer at a liquid temperature of 20–22 °C.

An important technological parameter determining the performance characteristics of composite materials is the rheological properties of molding suspensions. Molding binders are non-Newtonian fluids. During the preparation and compaction of molding mixtures, internal friction occurs between the layers of the suspensions, which is characterized by viscosity. Suspensions exhibit thixotropy if their viscosity decreases over time and under mechanical stress. Suspensions are rheopexic if their viscosity increases over time [22].

Suspensions were prepared using the binders studied, and their state was assessed using a standard instrument — a Suttard viscometer — based on the diameter of the suspension's flow. The amount of salt solution was adjusted to produce a suspension with a flow diameter of 250–270 mm.

This state of magnesite suspensions is necessary for viscosity measurements using an M3600 automatic rotational viscometer, which operates on the "cylinder-in-cylinder" principle (manufacturer: Grace Instrument, USA). The viscometer's cylindrical measuring vessel was filled with the suspension, and then the cylindrical rotor sleeve was immersed in the suspension. The study algorithm involved rotating the rotor at 10 revolutions per minute (rpm) for 60 seconds, followed by 200 rpm for the next 3600 seconds. Selecting the rotational viscometer mode allowed us to observe changes in the viscosity of the

suspensions during the period of active technological impact on the molding mixtures.

The performance characteristics of magnesite binders were measured using physical and mechanical properties such as density, strength, water absorption, and water resistance of the hardened stone.

To evaluate the properties of the hardened binders, 20 x 20 x 20 mm samples were molded from suspensions tested in a rotational viscometer. The samples were allowed to harden in air.

Strength testing of the samples was performed using a 100MG4A compact hydraulic test press (manufactured by Special Design Bureau Stroypribor, Russia).

Water absorption of the hardened stone was determined based on the change in sample weight after 24 hours of exposure to water.

The water resistance of the binders was assessed using the softening coefficient, which was calculated as the ratio of the strength of the material exposed to water for two days to the strength of the material hardening in air. Physical and mechanical tests of the binders were conducted on six samples from each series. The range of test results was 4.5-6.7%.

Discussion of results

Preliminary studies demonstrated the preference for composite binders containing 50% mineral component (Table 1).

The liquid component content influences the consistency of molding sands, the curing behavior, and strength properties. The combination of caustic magnesite with mineral components reduces the need for a salt solution to form a slurry of a given consistency. The use of magnesium sulfate solution increases the liquid-to-solid ratio for the studied slurries.

The graphical dependencies (Figure 1) reflect the nature of the change in suspension viscosity when the rotor is running at 200 rpm. In the first 500 seconds, a decrease in viscosity is observed in all suspensions due to the increased mixing speed in the viscometer. Subsequent changes in viscosity characterize the structure formation processes in the suspensions. Initial viscosity values depend on the composition of the binders. The use of magnesium sulfate solution is accompanied by a decrease in initial viscosity (Figure 1).

The viscosity of the MX suspension increases starting from 1000 s and reaches 420 Cp (centipoise) by the end of the tests. The MS suspension, containing a magnesium sulfate solution, increases its viscosity to 580 Cp in the period from 500 to 2400 s; subsequently, the suspension remains unchanged. The MC suspension, containing a mixed salt solution, increases its viscosity in the period from 700 to 2500 s. After reaching a viscosity of 580 cP, the suspension remains unchanged until the end of the tests.

Unlike caustic magnesite suspensions, the viscosity of magnesite-slag suspensions begins to increase later and exhibits increased sensitivity to the composition of the brine. The viscosity of the FX suspension increases in the range of 1200–2500 cP, reaching 580 cP, and subsequently remains stable.

Table 1 – Composition of magnesite binder suspensions

Composition code	Composition of the binder, %			Composition of the mixing fluid, %		Liquid to binder ratio
	caustic magnesite	*metallurgical slag*	*magnetite ore*	*magnesium chloride*	*magnesium sulfate*	
MX	100	–	–	100	–	0.65
MS	100	–	–	–	100	0.73
MC	100	–	–	70	30	0.75
FX	50	50	–	100	–	0.51
FS	50	50	–	–	100	0.53
FC	50	50	–	70	30	0.54
KX	50	–	50	100	–	0.43
KS	50	–	50	–	100	0.48
KC	50	–	50	70	30	0.50

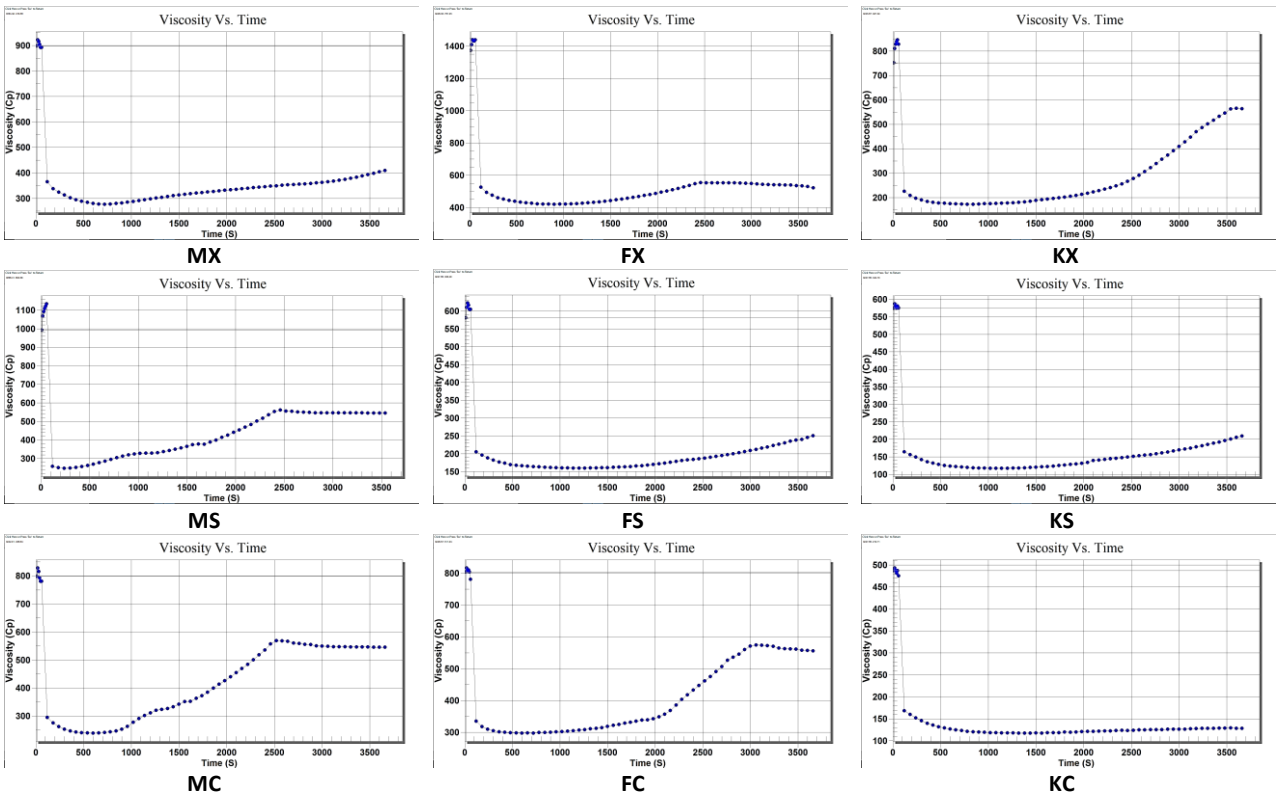

Figure 1 – The influence of the composition of binder suspensions on the change in viscosity in a rotational viscometer (binders' designations as in Table 1)

The viscosity of the FS suspension increases starting from 1600 cP and by the end of the tests it is 250 cP.

Magnesia-slag suspension FC, containing a mixed salt solution, increases its viscosity in the range of 1100–3000 s to 580 cP, and then remains unchanged. Magnesia-magnetite suspensions, compared to similar magnesia and magnesia-slag suspensions, are characterized by a lower initial viscosity. The viscosity of the KX suspension increases in the range of 1500–3600 s and reaches 580 cP. The viscosity of the KS suspension increases in the period from 1500 to 3600 s and reaches 210 cP. Magnesia-magnetite suspension containing a mixed salt solution increases its viscosity from 110 to 130 cP in the range of 1600–3600 s. Iron, being an acceptor metal, is capable of liquefying binder suspensions [21].

The revealed patterns of influence of the material composition of magnesite binders on the rheological properties of suspensions will allow to regulate the technological parameters of processing molding mixtures in the manufacture of products.

The density of hardened binders reflects the structural properties of the stone and depends on the material composition (Figure 2). The binders tested, hardened with magnesium sulfate solution, are characterized by a stone density 16-19% lower than similar oxychloride-cured binders. The reduced density of oxysulfate-cured binders is due to the lower density of the magnesium sulfate solution, the increased amount of liquid used to obtain the suspensions, and the amount and morphology of hydrates.

The density of hardened magnesite composite binders exceeds that of caustic magnesite due to the chemical and mineral composition of metallurgical slag and magnetite ore and the formation of hydrates with their participation. The density of hardened magnesite-slag binders is 3–14% higher than that of caustic magnesite. The density of magnesite-magnetite binders is 26–32% higher than that of hardened caustic magnesite.

The water absorption of binder stone characterizes the porosity of the structure and affects the strength and durability of the material (Figure 3). Open porosity of the stone, accessible to water penetration, is formed due to unbound liquid and also depends on the structure of hydrate formations.

There is no direct correlation between stone water absorption and the liquid-to-solid ratio. The type of salt solution and the presence of aluminosilicate and ferrous components have a significant impact on stone water absorption (Figure 3).

The loose structure of binders produced using magnesium sulfate solutions exhibits increased water absorption. For example, the water absorption of MS, FS, and KS stones exceeds that of MX, FX, and KX stones by 1.8, 2.8, and 3.1 times, respectively. However, the differences in water absorption between MS, FS, and KS are insignificant. KX, a magnesia-magnetite binder of oxychloride hardening, exhibits the lowest water absorption. The amount of water absorbed by KX is 2.3 times less than that of MX and 1.5 times less than that of FX.

The strength of hardened stone at 28 days demonstrates the superiority of oxychloride-cured binders (Figure 4). The strength of MX, FX, and KX binders exceeds that of MS, FS, and KS binders by 2.0, 2.3, and 1.9 times, respectively. Binders tempered with a mixed salt solution are comparable in strength to oxychloride-cured binders.

The strength of magnesia-slag and magnesia-magnetite binders is 87-102% and 85-95% of the strength of caustic magnesite, respectively.

This proves that the strength of composite binders is formed not only by magnesium hydroxychlorides and hydroxysulphates, but also by hydrates based on metallurgical slag and magnetite ore [[11], [15], [16]].

The widespread use of magnesite binders is hampered by their low resistance to water. It is known that the combination of caustic magnesite with mineral components increases the binder's water resistance [[10], [12], [19]]. The results of the study confirm the operational advantages of composite magnesite binders (Figure 5). The softening coefficient of oxychloride-cured composite binders is 1.5-1.6 times higher than that of caustic magnesite mixed with magnesium chloride solution.

Binders obtained using magnesium sulfate solutions are generally characterized by increased water resistance due to the stability of magnesium hydroxy sulfates [[9], [17], [18]]. The low softening coefficient values of the studied hydroxy sulfate-hardening binders are due to the loose structure of the stone obtained from suspensions with a low content of the dispersed phase. The reason for the low strength of MS, FS, and KS in water is the erosion of contacts between hydrates, which is facilitated by the high-water absorption of the stone.

Increased water resistance of composite binders is ensured by the helicrystalline structure of the stone, which, along with magnesium hydrochlorides and hydroxysulfates, is formed by weakly crystallized hydroaluminosilicates, hydrosilicates, magnesium hydroferrites, hydrogarnets and iron hydroxides [[12], [16]].

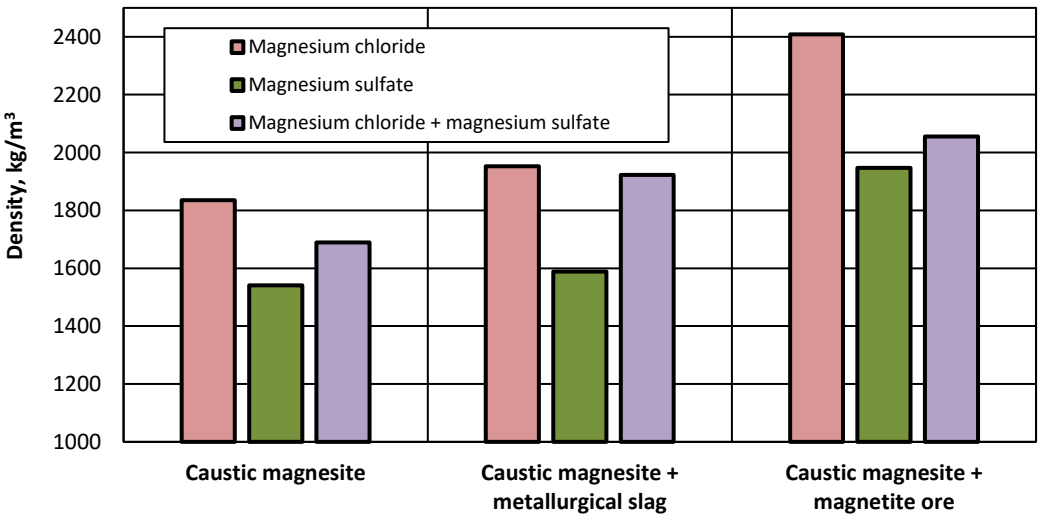

Figure 2 – The influence of the composition of magnesite binders mixed with various salts on the density of hardened stone

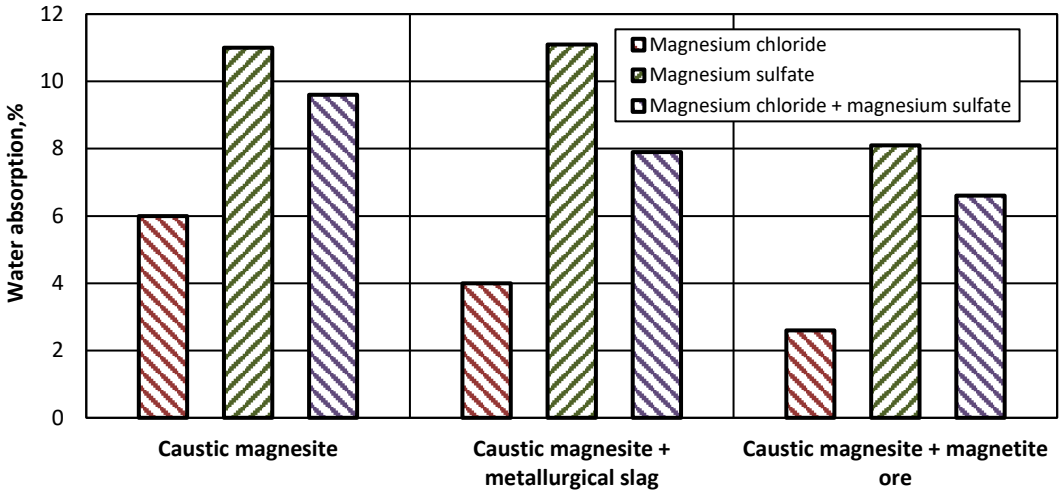

Figure 3 – The influence of the composition of magnesite binders mixed with various salts on the water absorption of hardened stone

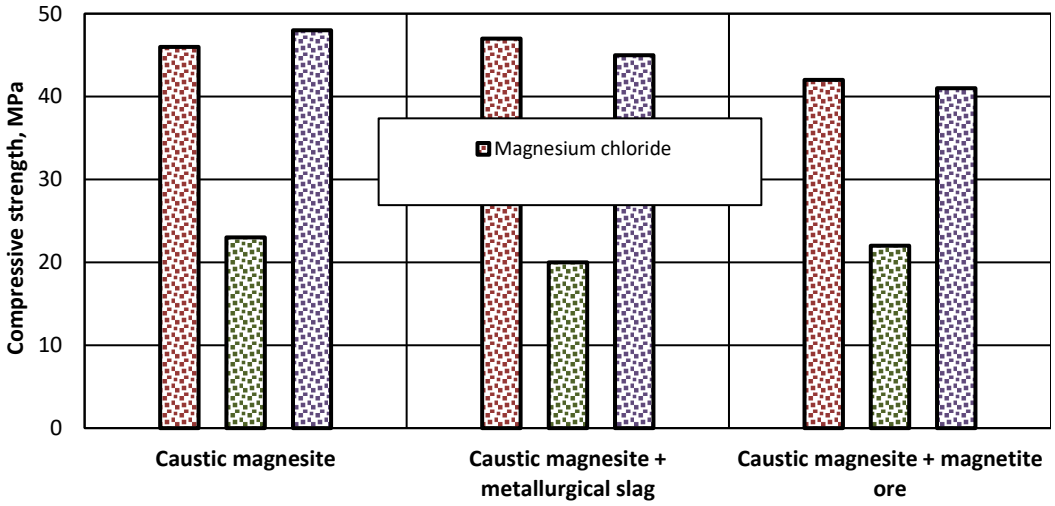

Figure 4 – The influence of the composition of magnesite binders mixed with various salts on the strength of hardened stone

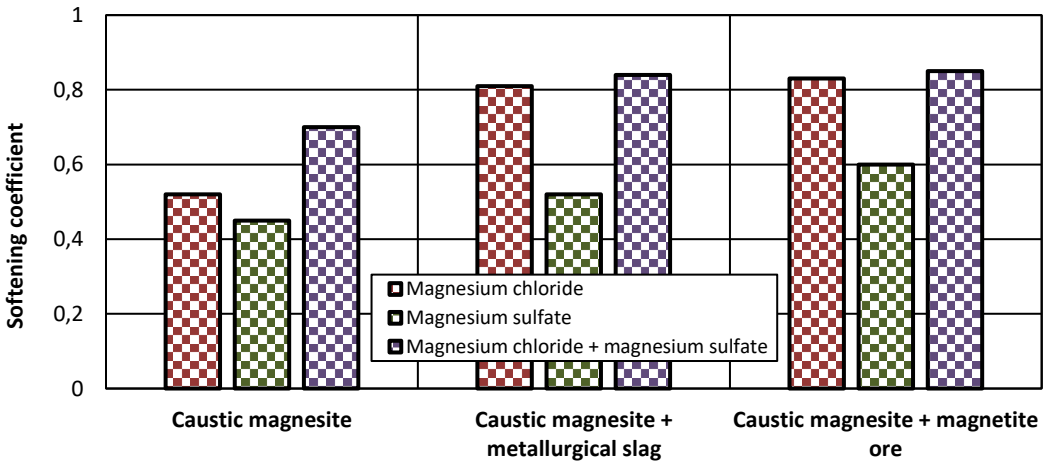

Figure 5 – The influence of the composition of magnesite binders mixed with various salts on the water resistance of hardened stone

Hardened binder is the component of concrete structure that determines the strength and performance properties of construction projects. Magnesia binders offer a wide range of compositional possibilities due to the combination of caustic magnesite with mineral components and salt solutions of varying compositions.

The ability to influence the physical and mechanical properties of composite magnesite binders through targeted selection of mineral components and the composition of the salt solution makes it possible to obtain building materials with a wide range of changes in structural characteristics.

The high density of magnesia-magnetite rock makes it suitable for use in radiation-protection concrete.

Magnesia-slag binders of oxychloride hardening, comparable in strength and other technical characteristics to caustic magnesite, contain up to 50% man-made components and contribute to the development of resource-saving concrete technologies with a low carbon footprint.

The diversity of composite magnesite binders is the basis for targeted modification of the processes of structure formation and regulation of the properties of concrete for general construction and special purposes.

Conclusions

The possibility of regulating the technological and operational properties of magnesia binders of oxychloride and oxysulfate hardening by using metallurgical slag and magnetite ore in their composition has been proven.

Composite magnesia-slag and magnesia-magnetite suspensions differ from magnesia suspension of equal consistency by a decrease in the content of salt solution by 1.2-1.5 times.

Composite magnesite suspensions are characterized by long-lasting thixotropy. This will expand the processing capabilities of molding mixtures containing magnesite composites.

Hardened composite binders form a stone of increased density, which reaches 1950-2400 kg/m^3, and it can be used to produce particularly heavy concrete.

Composite binders are characterized by slow structure formation, while they are not inferior in design strength to caustic magnesite.

The reduced water absorption of composite binders is predetermined by the denser structure of the stone. Magnesia-slag and magnesia-magnetite binders exhibit increased water resistance due to the helicrystalline structure of the stone. Weakly crystallized hydrates formed with the participation of metallurgical slag and magnetite concentrate are compacted by undissolved particles of the original phases, clogging the voids of the composite binders, promoting compaction and increasing the stability of the crystalline framework of magnesium hydroxychlorides and hydroxysulfates.

The use of a mixed solution of magnesium chloride and magnesium sulfate does not impair the technological properties of magnesite suspensions and allows for the regulation of the formation and properties of the stone structure.

The developed composite binders ensure resource conservation by reducing the proportion of caustic magnesite by up to 50% and decreasing the consumption of salt solution, expanding the possibilities of using magnesite concrete for various construction areas.

Composite magnesite binders are an alternative to Portland cement. The excellent physical and mechanical properties of magnesite binders, coupled with their pronounced adhesive properties, allow for the production of effective concretes based on various aggregates. A promising application for magnesite binders is multilayer concrete with variable structure for enclosing structures of buildings with various operating conditions.

Conflicts of interest. On behalf of all co-authors, the corresponding author states, that no conflict of interest exists.

CRediT author statement: **O. Miryuk**: Conceptualization, Methodology, Writing draft preparation, Reviewing and Editing; **L. Gorshkova:** Data curation, Visualization, Investigation.

Gratitude: This research has been funded by the Science Committee of the Ministry of Science and Higher Education of the Republic of Kazakhstan (Grant No. AP26199493).

Cite this article as: Miryuk OA, Gorshkova LV. Technological and operational properties of composite magnesia binders. Kompleksnoe Ispolzovanie Mineralnogo Syra = Complex Use of Mineral Resources. 2027; 342(3):47-55. https://doi.org/10.31643/2027/6445.29

Композициялық магнезиялық тұтқыр заттардың технологиялық және пайдалану қасиеттері

[1*] Мирюк О.А., [2] Горшкова Л.В.

[1] Рудный Индустриялық Университеті, Рудный, Қазақстан
[2] Торайғыров Университеті, Павлодар, Қазақстан

Мақала келді: *28 қазан 2025*
Сараптамадан өтті: *8 желтоқсан 2025*
Қабылданды: *9 қаңтар 2025*

ТҮЙІНДЕМЕ

Мақалада әртүрлі заттық құрамдағы магнезиялық байланыстырғыштарды зерттеу нәтижелері келтірілген. Жұмыстың мақсаты – құрамында металлургиялық қож және магнетит кені бар композициялық магнезиялық тұтқыр заттардың технологиялық және пайдалану қасиеттерін зерттеу. Магний тұтқырларын араластыру үшін магний хлориді мен магний сульфатының ерітінділері, сондай-ақ олардың қоспасы қолданылды. Магнезиялық тұтқыр заттардың технологиялық қасиеттері тұз ерітіндісінің шығынына, консистенциясына және суспензиялардың тұтқырлығының өзгеруіне негізделіп бағаланды. Композициялық тұтқырлардың пайдалану сапасын анықтау үшін тығыздық, беріктік, суды сіңіру және суға төзімділік көрсеткіштері қолданылды. Суспензиялардың реологиялық қасиеттерінің дисперсті фазаның құрамына және тұзды ерітіндінің түріне тәуелділігі анықталды. Тығыздығының жоғарылауы, су сіңірілуінің төмендеуі, суға төзімділіктің жоғарылауы және каустикалық магнезитпен салыстырғанда салыстырмалы беріктігі сияқты композициялық магнезиялық тұтқыр заттардың пайдалану артықшылықтары анықталды. Әзірленген магнезиялық-қожды және магнезиялық-магнетиттік тұтқыр заттарды пайдалану бағыттары ұсынылды. Зерттеу нәтижелері магнезит байланыстырғыштары мен бетон үшін ресурстарды үнемдейтін технологияларды әзірлеуге бағытталған.

Түйін сөздер: каустикалық магнезит, металлургиялық қож, магнетит кені, композициялық тұтқыр, суспензияның тұтқырлығы, тастың құрылымы.

Мирюк Ольга Александровна

Авторлар туралы ақпарат:
Техника ғылымдарының докторы, профессор, Рудный Индустриялық Университеті, Октябрге 50 жыл көшесі, 38, 111500, Рудный, Қазақстан. E-mail: psm58@mail.ru; ORCID ID: https://orcid.org/0000-0001-6892-2763

Горшкова Лариса Владимировна

Техника ғылымдарының кандидаты, доцент, Торайғыров Университеті, Ломов көшесі, *64, 140008, Павлодар, Казахстан. Email: gorshkova_larisa@mail.ru; ORCID ID: https://orcid.org/0009-0000-3173-753X*

Технологические и эксплуатационные свойства композиционных магнезиальных вяжущих

[1*] Мирюк О.А., [2] Горшкова Л.В.

[1]Рудненский Индустриальный Университет, Рудный, Казахстан
[2] Торайгыров Университет, Павлодар, Казахстан

Поступила: *28 октября 2025*
Рецензирование: *8 декабря 2025*
Принята в печать: *9 января 2025*

АННОТАЦИЯ

В статье приведены результаты исследований магнезиальных вяжущих различного вещественного состава. Цель работы – исследование технологических и эксплуатационных свойств композиционных магнезиальных вяжущих, содержащих металлургический шлак и магнетитовую руду. Для затворения магнезиальных вяжущих использовали растворы хлорида магния и сульфата магния, а также их смесь. Технологические свойства магнезиальных вяжущих оценивали по расходу солевого раствора, консистенции и изменению вязкости суспензий. Для определения эксплуатационного качества композиционных вяжущих использовали показатели плотности, прочности, водопоглощения и водостойкости. Выявлены зависимости реологических свойств суспензий от состава дисперсной фазы и вида солевого раствора. Установлены и обоснованы эксплуатационные преимущества композиционных магнезиальных вяжущих: повышенная плотность, меньшее водопоглощение, повышенная водостойкость и сопоставимая прочность по сравнению с каустическим магнезитом. Предложены направления использования разработанных магнезиально-шлаковых и магнезиально-магнетитовых вяжущих. Результаты исследований направлены на развитие ресурсосберегающих технологий магнезиальных вяжущих и бетонов.

Ключевые слова: каустический магнезит, металлургический шлак, магнетитовая руда, композиционные вяжущие, вязкость суспензий, структура камня.

Мирюк Ольга Александровна	***Информация об авторах:*** *Доктор технических наук, профессор, Рудненский Индустриальный Университет, улица 50 лет Октября, 38, 111500, Рудный, Казахстан. E-mail: psm58@mail.ru; ORCID ID: https://orcid.org/0000-0001-6892-2763*
Горшкова Лариса Владимировна	*Кандидат технических наук, доцент, Торайгыров Университет, улица Ломова, 64, 140008, Павлодар, Казахстан. Email: gorshkova_larisa@mail.ru; ORCID ID: https://orcid.org/0009-0000-3173-753X*

References

[1] Khabiyev AT, Yulussov SB, Abduraimov AE, Kamal AN, Kumarbek NE, Makhmet SB, Merkibayev YS. Use of Industrial By-products from Metallurgical Production for the Development of Heat-Resistant Building Mixes and their Molding in an Improved Device. Kompleksnoe Ispolzovanie Mineralnogo Syra=Complex Use of Mineral Resources. 2027; 341(2):16-26. https://doi.org/10.31643/2027/6445.14

[2] Juenger MCG, Siddique R. Recent advances in understanding the role of supplementary cementitious materials in concrete. Cement and Concrete Research. 2015; 78:71-80. https://doi.org/10.1016/j.cemconres.2015.03.018

[3] Atabaev FB, Aripova MKh, Khadzhiev ASh, Tursunova GR, Tursunov ZR. Effect of multicomponent mineral additives on the microstructure and strength of composite cement. Kompleksnoe Ispolzovanie Mineralnogo Syra = Complex Use of Mineral Resources. 2027; 340(1):45-57. https://doi.org/10.31643/2027/6445.05

[4] Benhelal E, Shamsaei E, Rashid MI. Challenges against CO_2 abatement strategies in cement industry: A review. Journal of Environmental Sciences. 2021; 104: 84-101. https://doi.org/10.1016/j.jes.2020.11.020

[5] Tang Y, Qiu J. CO_2-sequestering ability of lightweight concrete based on reactive magnesia cement and high-dosage biochar aggregate. Journal of Cleaner Production. 2024; 451:141922. https://doi.org/10.1016/j.jclepro.2024.141922

[6] Tan Y, Wu C, Yu H, Li Y, Wen J. Review of reactive magnesia-based cementitious materials: Current developments and potential applicability. Journal of Building Engineering. 2021; 40: 102342. https://doi.org/10.1016/j.jobe.2021.102342

[7] Hu C, Xu B, Ma H, Chen B, Li Z. Micromechanical investigation of magnesium oxychloride cement paste. Construction and Building Materials. 2016; 105: 496-502. https://doi.org/10.1016/j.conbuildmat.2015.12.182

[8] Huang Q, Zheng W, Dong J. Influences of different bischofite on the properties of magnesium oxychloride cement. Journal of Building Engineering. 2022; 57:104923. https://doi.org/10.1016/j.jobe.2022.104923

[9] Du H, Li J, Ni W, Hou C, Liu W. The hydration mechanism of magnesium oxysulfate cement prepared by magnesium desulfurization byproducts. Journal of materials research and technology 2022; 17:1211-1220. https://doi.org/10.1016/ j.jmrt.2022.01.070

[10] He P, Poon CS, Tsang DCW. Comparison of glass powder and pulverized fuel ash for improving the water resistance of magnesium oxychloride cement. Cement and Concrete Composites. 2018; 86:98-109. https://doi.org/10.1016/j.cem concomp.2017.11.010

[11] Miryuk OA. Study of Magnesite Binders' Resistance in Liquid Aggressive Environments. Material and Mechanical Engineering Technology. 2025; 11(3):22-30. https://doi.org/10.52209/2706-977X_2025_3_22 IRSTI 81.09.03

[12] Nie Y, Lu J, Liu Z, Meng D, He Z, Shi J. Mechanical, water resistance and environmental benefits of magnesium oxychloride cement incorporating rice husk ash. Science of The Total Environment. 2022; 849:157871. https://doi.org/ 10. 1016/ j.scitotenv.2022.157871

[13] Lauermannova AM, Lojka M, Jankovsky O, Faltysova I, Pavlıkova M, Pivak A, Zaleska M, Antoncık F, Pavlık Z. High-performance magnesium oxychloride composites with silica sand and diatomite. Journal of materials research and technology. 2021; 11: 957-969. https://doi.org/10.1016/j.jmrt.2021.01.028

[14] Miryuk OA. Magnesia composite materials for layered products. Kompleksnoe Ispolzovanie Mineralnogo Syra = Complex Use of Mineral Resources. 2024; 328(1):5 -12. https://doi.org/10.31643/2024/6445.01

[15] Zhang N, Yu H, Gong W, Liu T, Wang N, Tan Y, Wu C. Effects of low- and high-calcium fly ash on the water resistance of magnesium oxysulfate cement. Construction and Building Materials. 2020; 230:116951. https://doi.org/10.1016/j.conbuil dmat.2019.116951

[16] Erdman SV, Gapparova KM, Khudyakova TM, Tomshina AV. Magnesia binder preparation from local natural and technogenic raw materials. Procedia Chemistry. 2014; 10: 310-313. http://creativecommons.org/licenses/by-nc-nd/3.0/

[17] Li Y, Li Z, Pei H, Yu H. The influence of $FeSO_4$ and KH_2PO_4 on the performance of magnesium oxychloride cement. Construction and Building Materials. 2016; 102: 233-238. https://doi.org/10.1016/j.conbuildmat.2015.10.186

[18] Sheng G, Zheng L, Li P, Sun B, Li X, Zuo Y. The water resistance and mechanism of $FeSO_4$ enhancing bamboo scraps/magnesium oxychloride cement composite. Construction and Building Materials. 2022; 317:125942. https://doi.org/ 10.1016/j.conbuildmat.2021.125942

[19] Miryuk O, Liseitsev Y, Fediuk R. Influence of Iron-Containing Components on the Curing and Hardening Properties of Magnesium Oxychloride Binders. Journal of Materials in Civil Engineering. 2024; 36(12):04024413. https://doi.org/ 10.1061/MCEE7.MTENG-17856

[20] Zimich V. Effect of Ferrous Additives on Magnesia Stone Hydration. IOP Conf. Series: Materials Science and Engineering. 2017; 262:012001. https://doi.org/10.1088/1757-899X/262/1/012001

[21] Klimenko V, Volodchenko A, Sidelnikov R. Modification of Magnesia Binder with Iron Ore Concentrate. Proceedings of the International Conference Industrial and Civil Construction. 2021; 974:113-118. https://doi.org/ 10.1007/978-3-030-68984-1_30

[22] Peng Y, Unluer C. Magnesium-silicate-hydrate cement pastes: Rheological behavior and strength development. Case Studies in Construction Materials. 2024; 20:e03400. https://doi.org/10.1016/j.cscm.2024.e03400

Crossref

DOI: 10.31643/2027/6445.30

Earth and Planetary Sciences: Earth-Surface Processes

Development of technology for obtaining high-purity sodium chloride with induced impurity removal and process modeling

Urazkeldiyeva D.A., *Kadirbayeva A.A.

M.Auezov South Kazakhstan Research University, Shymkent, Kazakhstan

** Corresponding author email: diac_2003@mail.ru*

Received: *November 7, 2025*
Peer-reviewed: *November 19, 2025*
Accepted: *January 12, 2026*

ABSTRACT

High-purity NaCl is required for chemical processes. Halite from the South Kazakhstan Bakhyt Tany deposit contains $CaSO_4$ and Ca^{2+}/Mg^{2+} that degrade quality and operability. The article presents statistical processing and modeling of impurity deposition with phosphate ions using an automated calculation process. A stoichiometric amount of Na_3PO_4 was added to the NaCl 315 mol/dm^3 brine, stirred for 25-30 minutes, precipitated for 30 minutes, and filtered. Sulfate was quantified by barium-sulfate turbidimetry; residual Ca^{2+}/Mg^{2+} in the filtrate was measured titrimetrically. The Excel 2000 workbook performs coefficient estimation, significance testing, model adequacy testing, and error analysis. Response optimisation is also carried out through protected input fields. The resulting second-order models are adequate within the studied range of factors, reflect significant main effects and interactions, and predict optimal process modes, which have been confirmed experimentally. Under optimized conditions, removal reached 99.9% for Ca^{2+} and 99.8% for Mg^{2+}. Sulfate ions remained at trace levels in the NaCl product. The framework enables reproducible parameter selection and provides a basis for integrating near-zero-waste handling of co-products in subsequent process design.

Keywords: phosphate-induced precipitation, high-purity sodium chloride, modeling & statistical analysis, near-zero-waste flowsheet, Ca/Mg ions removal.

Dilbar Urazkeldiyeva Abdikhmidovna

Information about authors:
PhD doctoral student, The Higher School of Chemical Engineering and Biotechnology, M.Auezov South Kazakhstan University, Shymkent, Kazakhstan. Email: urazkeldieva.97@list.ru; ORCID ID: https://orcid.org/0000-0001-7825-6995

Kadirbayeva Almagul Akkopeykyzy

Candidate of technical sciences. Assistant Professor, The higher School of chemical engineering and biotechnology, M.Auezov South Kazakhstan University, Shymkent, Kazakhstan. Email: diac_2003@mail.ru; ORCID ID: https://orcid.org/0000-0003-0702-1114

Introduction

Sodium chloride is one of the most important reagents in the chemical industry and one of the most common mineral salts. Of all the Asian countries, Kazakhstan has the largest number of salt lakes [1]. The salt deposits in southern Kazakhstan have a high sodium chloride concentration and also contain sodium sulphate, as well as calcium and magnesium salts in the form of chlorides and sulphates. In deposits closer to the west, such as Inder, Chelkar, and Satimola, the mineral also contains potassium chloride [[2],[3]].

The price of sodium chloride is directly dependent on its purity [4]. Sodium chloride is found in a solid mineral state in nature. In most cases, insoluble residue and calcite magnesium ions crystallise into the mineral along with sodium chloride [[5], [6]]. Consequently, it is imperative to dissolve the mineral and subsequently precipitate the residual ions [7]. The conventional methodologies employed for the purification of sodium chloride encompass the utilisation of sodium bicarbonate and limestone. However, to obtain high-purity sodium chloride by these methods, the process must be multi-stage [[8],[9]].

After precipitation, any solid particles that are insoluble in the solution are removed by filtration. The crystallisation of sodium chloride allows pure salt to be separated from impurities; this process is also subject to the kinetic laws related to solubility and temperature [10]. The technological processes of natural salt raw materials are determined by the final equilibrium states of the processed raw materials' components and the introduced reagents, as well as by kinetic factors. The latter either hinders or facilitates the implementation of technical solutions. The kinetics of dissolution processes

depend on various factors, including the nature and composition of solids, the composition and temperature of solutions, the size and shape of crystals, and the instrumental conditions of dissolution [11].

Understanding the kinetics of the process of purifying sodium chloride from calcium and magnesium ions is key to developing effective technologies for producing a high-purity product. Understanding the reaction rate, mechanism, and factors affecting the process enables the purification conditions to be optimised and salt of the required purity to be obtained [[12], [13]]. Using mathematical modelling and experiments helps control the process more accurately and achieve the desired results. The precipitation rate depends on the concentration of the reagent, the temperature, and the reaction time [14]. The purification of saturated brines containing sodium chloride from calcium and magnesium is of great importance for a number of industrial processes. These include the production of chlorine and alkali, as well as food and pharmaceutical salts.

As demonstrated in the studies conducted by Mi et al. [15], Bouaziz et al. [16], and Pérez-González et al. [17], elevated ion concentrations, in conjunction with the presence of competing anions such as sulfate, have been shown to impede the process of calcium and magnesium precipitation. A variety of purification methods are employed in industrial settings, including the lime-soda method and selective precipitation using phosphates or carbonates. However, magnesium precipitates to a greater extent than calcium and requires stricter pH control. Despite the incorporation of a sufficient quantity of reagent, magnesium may persist in solution. Consequently, a combination of reagents and multi-stage treatment is frequently employed in practice. Presently, the potential for the utilisation of impurities as valuable resources is a subject that is being subjected to actively studied. Precipitation of magnesium from brines is a promising area of research. As research has shown, [[15], [16]]. The brine purification process can be integrated with the production of magnesium salts and magnesium hydroxide. Magnesium salts have a wide range of applications, including in the production of materials or fertilizers. Studies have shown that the effectiveness of purification from impurities depends not only on the choice of reagent, but also on consideration of kinetic factors such as time, temperature, and mixing speed.

The objective of the present study is to develop and validate mathematical models of the purification of sodium chloride solutions from calcium and magnesium ions by sodium phosphate and to perform statistical analysis of the resulting datasets. To enable optimization toward a high-purity NaCl product, we further identify and quantify the factors controlling the rate and efficiency of impurity precipitation. In parallel, we design and assess a near-zero-waste flowsheet that converts phosphate-bearing by-streams into fertilizer co-products. The combined modeling, statistical treatment, and flowsheet evaluation provide a basis for comparative benchmarking against conventional purification routes.

Experimental part

The salt of the South Kazakhstan region of the Bakhyt Tany deposit was selected for the study. The quantification of sulfate ions was achieved through the implementation of barium sulfate turbidimetry. The content of calcium and magnesium ions was measured using EDTA titration. Microstructure of the samples and elemental analysis were performed using a JSM 6610 LV scanning electron microscope manufactured by the Japanese company JEOL, using the INCA Energy 450 energy dispersive microanalysis system. The measurement accuracy was within 0.01%.

In the process of cleaning the brine from impurities, phosphate ions were used as a precipitator. A saturated salt solution of halite with a concentration of 315 mol/dm^3 was prepared for the experiment. A stoichiometric amount of sodium phosphate was added to the concentrated solution to precipitate calcium and magnesium salts. The resulting mixture was continuously stirred in a thermostat for 25-30 minutes, then the particles were allowed to settle for 20-25 minutes and filtered. The filth was rinsed with clean water. The remains of insoluble salt and insoluble calcium and magnesium compounds settled on the filter in the form of sediment. The amount of calcium and magnesium ions present in the filtered brine was determined by titration with EDTA. The NaCl solution thus obtained is then employed in the treatment and drying of the target product.

The objective of the present study is to automate the processing of research results. To this end, a program for a personal computer has been developed. The program is based on MS Excel 2000 running on Windows. This development allows you to quickly obtain all the necessary calculation results online. This, in turn, made it possible to accurately determine the optimal conditions for the ion deposition reaction. The programme has been developed in the form of an Excel workbook. It is

evident that within the confines of the book, on a specific page, ancillary materials are present. These materials encompass matrices of intermediate values, formulae for calculating parameter b, and statistical processing, among others. It is important to note that all fields on this page, with the exception of input fields, are protected from random changes. The following elements are designated as input fields: a column for entering output Y values; a row for entering input parameters X on a natural scale, utilised in the search for the optimal mode; and a field for entering the experimental output value obtained after laboratory testing of optimisation results. In addition to the current input values, the main sheet displays: coefficient estimates b; significant coefficients according to the Student's criterion; the result of the Fischer criterion adequacy test; for each experiment, there are absolute and relative approximation errors when using all b and only significant b; average total relative error in the sample; the result of the search for the optimal mode; absolute and relative error for computational and experimental verification.

The discussion of the results

The mineral halite from the Bakhyt-Tany deposit in the Sozak district of the South Kazakhstan region was selected for detailed study. The sodium mineral present in the selected deposit is distinguished by its low impurity content, its superficial location, and its high sodium chloride concentration. Preliminary research by the authors [18] indicates that the moisture content of the samples ranges from 0.6 to 3%. It was possible to calculate the approximate salt composition of the halite mineral based on the results obtained. The composition of the solution is as follows: calcium sulfate ($CaSO_4$) at 2.5%, magnesium sulfate ($MgSO_4$) at 0.18%, magnesium chloride ($MgCl_2$) at 0.37%, and sodium chloride (NaCl) at 88.4%. The mineral has been found to contain up to 2-3% by mass of insoluble residue.

In a previously published paper [[17], [18]], we presented experimental results on the purification of NaCl solutions from Ca^{2+} and Mg^{2+} ions using sodium phosphate. The present article is devoted to the statistical processing of the aforesaid experimental data and the mathematical modelling of the process, with a view to identifying significant factors, constructing predictive regression models, and optimising the conditions for obtaining a high-purity product. Consequently, the present study extends the findings of [18] from the level of a laboratory experiment to that of a quantitatively verified model and computational optimisation, whilst also addressing integration into a near-zero-waste scheme.

A study was conducted to ascertain the most effective method of purifying the natural mineral of the Bakhyt Tany ore – halite. The study incorporated various factors into its mathematical planning, including the chemical composition of the raw materials, the degree of purification, the temperature, and the time of purification. The study aimed to determine the dependence of the degree of purification Y on such factors as: a) temperature X_1 (K), b) time X_2 (min), and c) degree of purification X_3 (%). In order to establish the dependency sought, it was necessary to ascertain the value parameters in the mathematical model that adequately described the cleaning process. These were given in the form of the regression equation below:

$$У=B_0+B_1X_1+B_2X_2+B_3X_3+B_{11}X_1^2+ B_{22}X_2^2+ B_{33}X_3^2+ B_{12}X_1X_2+ B_{13}X_1 X_3+ B_{23}X_2 X_3 \quad (1)$$

The determination of the value parameters b was achieved by utilising the method of planning a second-order rotatable experiment. Following a comprehensive analysis of the system in question, the range of possible changes to the factors was determined and is presented in Table 1 and Figure 1. Based on the results of the experiments, the optimal parameters of the technological regime were determined, and they are shown in Table 2. The processing of the experimental results was conducted in accordance with the prevailing methodology.

The following table presents the results of studies undertaken to ascertain the levels of factors and their ranges of variation.

Table 1 - Results of studies to determine the level of factors and their ranges of variation

Factors	X_1	X_2	X_3
Lower level (-1)	10	20	90
High Level (+1)	45	25	105
Zero level (0)	27.5	22.5	97.5
Variation interval (ΔX)	17.5	2.5	7.5
Shoulder+α	56.935	26.705	110.115
Shoulder-α	-1.935	18.295	84.885

Table 2 - Calculated optimal parameters of the technological regime

№	X_1 , ^0C	X_2 , min	X_3 , %	Y, degree of purification
1	25	30	95	99.9

Coefficients of the model			
	At:	all coefficients	significant
B0		97.88290	97.88290
B1	X1	-0.02928	0.00000
B2	X2	-1.22742	-1.22742
B3	X3	-0.32341	-0.32341
B11	X1*X1	0.53413	0.53413
B22	X2*X2	-1.28667	-1.28667
B33	X3*X3	0.07451	0.07451
B12	X1*X2	0.47500	0.47500
B13	X1*X3	-0.92500	-0.92500
B23	X2*X3	-0.32500	-0.32500
The number is significant.coefficient.			9
The calculated F-criterion			4.1
Tabular F-criteria			5.1

The equation is adequate**!**

(**a**)

Coefficients of the model			
	At:	all coefficients	significant
B0		99.07944	99.07944
B1	X1	0.75263	0.75263
B2	X2	-0.27084	0.00000
B3	X3	-0.42955	-0.42955
B11	X1*X1	-1.40842	-1.40842
B22	X2*X2	-1.12557	-1.12557
B33	X3*X3	-0.78970	-0.78970
B12	X1*X2	-0.13750	0.00000
B13	X1*X3	0.11250	0.00000
B23	X2*X3	-1.73750	-1.73750
The number is significant.coefficient.			7
The calculated F-criterion			4.5
Tabular F-criteria			5.1

The equation is adequate**!**

(**b**)

Figure 1 – Coefficients of the quadratic regression model and the experimental plan in coded variables (X1–X3); the values of all significant coefficients, a matrix of dimensionless inputs, as well as the result of the adequacy test by the F-criterion are shown: (**a**)Mg; (**b**) Ca

During the mathematical processing of the fractional factor experiment data, the coefficients of the regression equations were estimated, and the following second-order models were obtained in encoded coordinates:

$$У=97{,}88290-0{,}02928X_1-1{,}22742X_2-0{,}32341X_3+0{,}53413X_1^2-1{,}28667X_2^2+0{,}7451X_3^2+0{,}47500X_1X_2-0{,}92500X_1X_3-0{,}32500X_2X_3 \quad (2)$$

$$У=99{,}07944+0{,}75263X_1-0{,}27084X_2-0{,}42955X_3-1{,}40842X_1^2-1{,}12557X_2^2-0{,}78970X_3^2-0{,}13750X_1X_2+0{,}11250X_1X_3-1{,}73750X_2X_3 \quad (3)$$

The obtained regression equations (2) and (3) adequately describe the behavior of the system in the studied range of factors (verification by the Fisher criterion: $F_{calculation}<F_{table}$ The signs and relative values of the coefficients are consistent with chemical expectations: the linear contribution of X_2 and negative quadratic terms for X_1-X_3 indicate the existence of internal limitations on "supersaturation" and optimal dose/time windows beyond which precipitation efficiency decreases. The presence of statistically significant interactions confirms that process management requires balancing factors rather than independently adjusting them. The mean relative approximation errors are negligible, and the discrepancy between the calculated and verified (laboratory) Y output is within the stated margin of error. This renders models a viable engineering tool for operational forecasting of the degree of purification and the selection of modes. To assess the reproducibility of the results, the variation in the degree of purification of the solution from magnesium and calcium ions was analysed. The measurements were performed in three parallel repetitions (n = 3), and the obtained values are presented as fluctuation intervals. The degree of purification from magnesium ions after optimisation was 98.5–99.8%, which corresponds to a relative error of approximately ±0.6%. Similarly, the degree of purification from calcium ions was in the range of 98.2–99.8%, which corresponds to an error of approximately ±0.8%. Such small fluctuations in the results indicate high stability and reproducibility of the process.

Flow chart and its comparison with analogues

The conventional protocol for the purification of salt rocks and brines involves a series of operations, including rock crushing, dissolution, removal of insoluble residue, precipitation of impurities, and filtration. In patent KG 1428 (C01D 3/08, 03/30/2012) [19], it is proposed that barium hydroxide be introduced into a heated (50-70 °C) solution at a sulfate-ion ratio of 1.37-1.50:1. The method's primary benefits are twofold: firstly, it accelerates the process by eliminating multi-stage

deposition; secondly, it reduces consumption of reagents and energy.

The principal disadvantage of the barium approach is the use of toxic $Ba(OH)_2$ (hazard class 2), which complicates the achievement of a reagently pure salt and increases safety and waste management requirements. Furthermore, in the presence of $Ba(OH)_2$ and subsequent neutralisation of HCl, soluble $CaCl_2$ and $MgCl_2$ are formed; thus, calcium and magnesium pass into solution and are not removed from the sodium chloride matrix.

An evaporative method for producing commercial salt is also widely known [20] [RU 2075440, C01D 3/06, 1997], which provides "Extra" quality for the food industry (Ca ≈ 0.02 wt.%, Mg ≈ 0.01 wt.%, K ≈ 0.02 wt.%, SO_4^{2-} ≈ 0.16% by weight). Nevertheless, this level of purity is inadequate for the tasks of fine organic synthesis, electrochemistry, and microelectronics, where lower levels of impurities and the absence of corrosive acid residues are required.

The closest method to ours is the RU 2495825 method (C01B 3/14, 10/20/2013) [21], which involves the purification of a saturated NaCl solution at 25 °C from mechanical impurities. This is achieved through a series of processes including evaporation, crystallisation, centrifugation, subsequent washing and drying. Before the process of evaporation, the solution is subjected to treatment with HCl at a concentration of 1.0–1.5 wt. %. This is followed by the process of boiling and the washing of the crystals with high-purity water. The process is characterised by multifarious disadvantages, including but not limited to:

- Multi-stage operation, which is both inefficient and costly.
- The use of concentrated hydrochloric acid, which is liable to cause corrosion of equipment and necessitates additional flushing with expensive water, thus increasing capital and operating costs. Existing solutions are characterised by the utilisation of toxic reagents ($Ba(OH)_2$), the provision of food but not chemical purity, or the requirement of acid treatment and energy-intensive steaming. It is imperative that a technologically simple, safe, and economical scheme is implemented for the selective removal of Ca^{2+} and Mg^{2+} ions, without the introduction of corrosive components.

The proposed method is based on the selective precipitation of calcium and magnesium in the form of insoluble phosphates during the treatment of brine with sodium phosphate. The technology combines mechanical desalination, dissolution, and circulation of saturated NaCl fluxes with single-stage stoichiometric phosphate injection and subsequent gravity filtration phase separation. $CaSO_4$ is an undesirable impurity in the composition of salt and insoluble residue. In the production of soda, it increases the formation of scale in evaporators and reduces the efficiency of the process. There are special purity requirements for food salt.

Calcium sulfate is a valuable raw material. Recent studies [[22], [23]] have shown that it is widely used in various fields, including the production of building materials, ceramics, soil improvement products, and asphalt concrete composites. Thus, the removal of $CaSO_4$ from halite has two main advantages. The first is to improve the quality of salt. Secondly, the creation of opportunities for processing and reuse of this by-product in other industries.

Based on the results of the study, a technological scheme was developed, shown in Figure 2. The production process of table salt begins with loading salt into a mixer (1). Then, mechanical impurities are removed using a circulating saturated solution, which is heated to a temperature of 20-25 ° C and remains for 30 minutes.

Throughout the entire process, a constant ratio of solution and salt is maintained — 3:1 by weight. The resulting suspension is separated by sieving on a sieve (2). The solution containing mechanical impurities passes through a walnut filter (3), where it is cleaned. This solution is returned to wash the sodium chloride salt.

The ore that has been washed is dissolved in water, and the resulting solution is passed through a filter press to remove any remaining water. Then the solution reaches a saturation state in the reactor at a temperature of 25 °C. At this point, sodium phosphate is added to the solution in an amount equal to 95% of the stoichiometric norm. This is necessary for the precipitation of calcium and magnesium impurities. The resulting suspension is then settled in a sump (5), where it is divided into two layers. The top layer containing impurities is a condensed pulp, which is filtered in a filter (6). The filtered sludge is removed, and the filtrate and washing water are returned to the reactor (4) for reuse.

The clarified part of the solution is drained from the sump and enters the spray dryer (7), where it is dried using flue gases at a temperature of 100-110 ° C. As a result of this process, sodium chloride crystallizes. The dried crystalline product is transferred from the dryer to the screw feeder (9), where it undergoes a cooling period, and then packed.

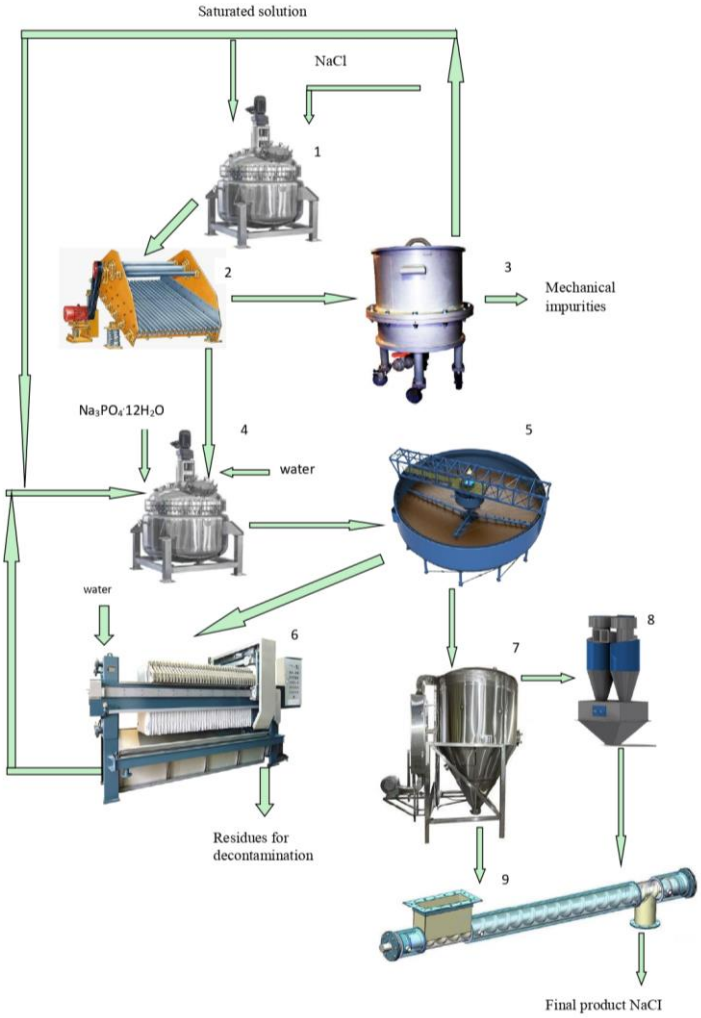

Figure 2 - Technological scheme

The proposed method has several advantages over the existing method. Firstly, it does not require the use of concentrated hydrochloric acid in the cleaning process, which avoids corrosion of the equipment and eliminates the need for thorough washing of sodium chloride crystals with high-purity water. Secondly, this method significantly simplifies the technological process and reduces energy costs.

This scheme provides three valuable products:

1. Pure NaCl
2. Building composite $CaSO_4$
3. Phosphorites, which can be used as raw materials for fertilizers

In addition, solutions are recycled during the processing process, which helps to reduce costs and minimize toxic by-products. This technological approach is characterized by almost zero waste, which is an important aspect of sustainable production. During the processing process, impurities are converted into resources, which effectively eliminates their waste status.

As illustrated in Figure 3, the spectrogram of the resulting product is evident. As demonstrated in Table 3, the analysis of the elements has been shown to confirm the high degree of purity of the sodium chloride obtained.

Table 3 - Elemental composition of the obtained sodium chloride

Element	Mass %	Atom, %
Na	36.87	47.39
Cl	63.13	52.61

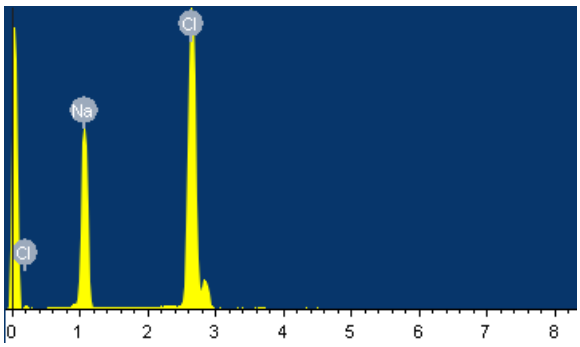

Figure 3 - Spectrogram of the obtained sodium chloride

Cost analysis showed that the main costs of obtaining one ton of purified sodium chloride are related to the price of the feedstock and reagent, sodium phosphate. Under optimal conditions, the cumulative variable costs amount to KZT 25,782 per ton, and the permanent costs amount to KZT 5,000 per ton. This results in a total cost of about 30,782 tenge per ton. Taking into account the trade margin of 15%, the selling price of the product is 35,399 tenge per ton. Thus, the expected profit from the sale of one ton of purified sodium chloride is approximately 4,600 tenge. Calculations confirm that the use of sodium phosphate as the main reagent significantly affects the cost of the process. However, the optimized technology remains economically beneficial. The absence of significant energy costs and a small amount of waste make this method more preferable from an environmental and economic point of view compared to alternative cleaning methods.

Conclusions

A statistical and mathematical model of phosphate-induced purification of NaCl brines from Ca^{2+} and Mg^{2+} has been developed and verified; second-order models (2)-(3) are adequate according to the Fisher criterion and technologically interpretable.

The identification of dominant factors and significant interactions has been achieved, thereby excluding independent parameter setting and requiring coordinated mode management.

The calculation of optimisation, based on the models, provides the target removal rates: The concentrations of Ca^{2+} and Mg^{2+} were found to be 99.9% and 99.8%, respectively, within the specified factor windows.

It has been demonstrated that $SO4^{2-}$ does not integrate into the halite lattice and is concentrated in the mother cell; only trace amounts of sulfates remain in solid NaCl, which confirms the consistency of the model with product analysis.

A scheme for the reduction of waste, with three distinct streams, has been established. The target product is pure NaCl, $CaSO_4$, with mechanical impurities, has been identified as a suitable building material/filler. Phosphates of calcium and magnesium are considered suitable as co-products for use as fertiliser.

In comparison with conventional acid-evaporation and barium methods, the proposed scheme eliminates the use of toxic reagents and corrosive media, reduces the number of stages, water capacity and OPEX, while maintaining or exceeding the purity level.

The implementation of an application tool in the form of an Excel workbook has been undertaken for the purpose of facilitating instant calculations, optimising search functions and expediting the verification of modes. This development serves to streamline the transfer of results to the production site.

The dependencies obtained provide direct engineering regulations, including factor operating windows, sensitivity gradients, stopping criteria, and quality control metrics.

The original experimental arrays from the previously published work have been rethought, and through statistical processing and modelling they have been transformed into a predictive optimisation tool ready for scaling.

The environmental impact of the process is evident in the transformation of "impurities" into resource flows, as well as the closure of brine circulation. These factors serve as indicators of a practical, waste-free process. This section is not mandatory but can be added to the manuscript if the discussion is unusually long or complex.

The proposed model and scheme ensure industrially significant purity of NaCl with a minimum of stages and waste, as well as create economically useful co-products ($CaSO_4$ and Ca/Mg phosphates). This makes the technology competitive and sustainable for implementation in modern chemical technology chains.

CRediT author statement: **Urazkeldiyeva D.A**.: Methodology, formal analysis, investigation, Data writing, Original draft preparation, writing– review and editing. **Kadirbayeva A.A.:** Data curation, Reviewing, and Editing.

Conflicts of Interest. On behalf of all authors, the corresponding author declares that there is no conflict of interest.

Funding: This research was funded by the intramural grant “Zhas Galym” of M. Auezov South Kazakhstan Research University, Grant No. ЮКУ2024-005.

Cite this article as**:** Urazkeldiyeva DA, Kadirbayeva AA. Development of technology for obtaining high-purity sodium chloride with induced impurity removal and process modeling. Kompleksnoe Ispolzovanie Mineralnogo Syra = Complex Use of Mineral Resources. 2027; 342(3):56-64. https://doi.org/10.31643/2027/6445.30

Қоспаларды кетіруді индукциялау арқылы жоғары тазалықтағы натрий хлоридін алу технологиясын әзірлеу және процесті модельдеу

Уразкелдиева Д.А., *Кадирбаева А.А.

М. Әуезов атындағы Оңтүстік Қазақстан Зерттеу Университеті, Шымкент, Қазақстан

Мақала келді: *7 қараша 2025*
Сараптамадан өтті: *19 қараша 2025*
Қабылданды: *12 қаңтар 2026*

ТҮЙІНДЕМЕ

Химиялық процестерге жоғары тазалықтағы NaCl қажет. Дегенмен Оңтүстік Қазақстандағы Бақыт таңы кен орнынан алынған галиттің құрамында $CaSO_4$ және Ca^{2+}/Mg^{2+} бар, олар өнім сапасын төмендетеді. Бұл мақалада фосфат иондары арқылы қоспалардың тұнуын автоматтандырылған есептеу процесінің көмегімен статистикалық өңдеу және модельдеу ұсынылады. 315 моль/дм³ NaCl тұзды ерітіндісіне стехиометриялық мөлшерде Na_3PO_4 қосылды, қоспа 25–30 минут араластырылды, 30 минут тұндырылды және кейін сүзілді. Сульфаттың мөлшері барий сульфатын қолданатын турбидиметриялық әдіспен анықталды; фильтраттағы қалдық Ca^{2+}/Mg^{2+} титриметриялық әдіспен өлшенді. Excel-2000 жұмыс кітабында қорғалған енгізу өрістері арқылы коэффициенттерді бағалау, Стьюденттің t-сынағына негізделген мәнділікті тексеру, Фишердің сәйкестік критерийі, қателерді диагностикалау және қорғалған енгізу өрістерін пайдаланып жауап бетін оңтайландыру жүзеге асырылды. Нәтижесінде алынған екінші ретті модельдер зерттелген факторлық кеңістікте адекватты болып шықты, маңызды негізгі және өзара әрекеттесу әсерлерін ашып көрсетті және тәжірибе жүзінде расталған жұмыс аймақтарын болжады. Оңтайландырылған жағдайларда Ca^{2+} үшін жою тиімділігі 99,9%-ға, Mg^{2+} үшін 99,8%-ға жетті, ал NaCl өніміндегі сульфат мөлшері болмашы деңгейде қалды. Ұсынылып отырған әдіс оптималды параметрлерді таңдауға мүмкіндік береді және процесті кейін жобалау кезеңінде қалдықсыз технологиялық үрдісті құрастыруға негіз болады.

Түйін сөздер: фосфаттармен тұндыру, жоғары тазалықтағы натрий хлориді, модельдеу және статистикалық талдау, қалдықтардың нөлге жақын деңгейі, Ca/Mg иондарын жою.

Уразкелдиева Дилбар Абдихамидовна

Авторлар туралы ақпарат:
PhD докторант, Химиялық инженерия және биотехнология жоғарғы мектебі, М. Әуезов атындағы Оңтүстік Қазақстан зерттеу университеті, Шымкент, Қазақстан. E-mail: urazkeldieva.97@list.ru; ORCID ID: https://orcid.org/0000-0001-7825-6995

Қадірбаева Алмагүл Ақкөпейқызы

Техника ғылымдарының кандидаты, қауымдастырылған профессор. Химиялық инженерия және биотехнология жоғарғы мектебі, М. Әуезов атындағы Оңтүстік Қазақстан зерттеу университеті, Шымкент, Қазақстан. E-mail: diac_2003@mail.ru; ORCID ID: https://orcid.org/0000-0003-0702-1114

Разработка технологии получения хлорида натрия высокой чистоты с индуцированием удаления примесей и моделирование процесса

Уразкелдиева Д.А., *Кадирбаева А.А.

Южно-Казахстанский Исследовательский Университет имени М. Ауезова, Шымкент, Казахстан

Поступила: *7 ноября 2025*
Рецензирование: *19 ноября 2025*
Принята в печать: *12 января 2026*

АННОТАЦИЯ

Для химических процессов требуется высокочистый NaCl, однако галит с южно-казахстанского месторождения Бахыттаны содержит $CaSO_4$ и Ca^{2+} /Mg^{2+}, которые ухудшают качество и работоспособность. В этом исследовании представлена статистическая обработка и моделирование очистки, вызванной использованием фосфатов, с использованием автоматизированного процесса расчетов. В статье представлена статистическая обработка и моделирование осаждение примесей с фосфат ионами, с использованием автоматизированного процесса расчетов. В рассол NaCl 315 моль/дм³, добавляли стехиометрическое колличество Na_3PO_4, перемешивали в течение 25-30 мин, осаждали в течение 30 мин и фильтровали. Количественное определение сульфата проводили с помощью турбидиметрии сульфатом бария; остаточное содержание Ca^{2+} /Mg^{2+} в фильтрате определяли титриметрически. Рабочая тетрадь Excel-2000 реализует оценку коэффициентов, проверку значимости на основе t-критерия Стьюдента, критерий адекватности Фишера, диагностику ошибок и оптимизацию поверхности отклика с помощью защищенных полей ввода. Полученные в результате модели второго порядка адекватны в рамках изучаемого факторного пространства, выявляют существенные основные эффекты и эффекты взаимодействия и предсказывают рабочие периоды, которые были экспериментально подтверждены. В оптимизированных условиях удаление достигло 99,9% для Ca^{2+} и 99,8% для Mg^{2+}, в то время как содержание сульфата в продукте NaCl оставалось незначительным. Система позволяет воспроизводимо подбирать параметры и обеспечивает основу для интеграции процессов переработки побочных продуктов с практически нулевым уровнем отходов при последующем проектировании процесса.

	Ключевые слова: осаждение фосфатами, высокочистый хлорид натрия, моделирование и статистический анализ, технологическая схема, близкая к нулевому уровню отходов, удаление ионов Ca/Mg.
Уразкелдиева Дилбар Абдихамидовна	***Информация об авторах:*** *PhD докторант, Высшая школа химическая инженерия и биотехнология, Южно-Казахстанский исследовательский университет имени М. Ауезова, Шымкент, Казахстан. E-mail: urazkeldieva.97@list.ru; ORCID ID: https://orcid.org/0000-0001-7825-6995*
Кадирбаева Алмагул Аккопейкызы	*Кандидат технических наук, ассоцированный профессор, Высшая школа химическая инженерия и биотехнология, Южно-Казахстанский исследовательский университет имени М. Ауезова, Шымкент, Казахстан. E-mail: diac_2003@mail.ru; ORCID ID: https://orcid.org/0000-0003-0702-1114*

References

[1] Posokhov EV. Mineral wealth of the salt lakes of Kazakhstan. Alma-Ata. Kazakhstan. 2009.

[2] Assylkhankyzy A, Seitmagzimova G. An Innovative Environmentally Friendly Processing Method of Promising Carnallite Ores. Engineering. Technology & Applied Science Research. 2025; 15(4):24321-24327. https://doi.org/10.48084/etasr.11159

[3] Diarov MD, Diarova RA, Serikov FT. Boronicity and potassium content of rocks of the halogen formation of the Caspian basin. Almaty: Evero. 2006, 183.

[4] Myerson A, Erdemir D & Lee A. (Eds.). Handbook of Industrial Crystallization (3rd ed.). Cambridge: Cambridge University Press. 2019. http://dx.doi.org/10.1017/9781139026949

[5] Linnikov OD, Malinkina TI, & Zhuk NA. The Influence of Impurities on Crystallization Kinetics of Sodium Chloride. Crystal Research and Technology. 2006; 41(10):966–972. https://doi.org/10.1002/crat.200510653

[6] Penha F, Zago G, Seckler M. Strategies to control product characteristics in simultaneous crystallization of NaCl and KCl from aqueous solution: seeding with NaCl and KCl. CrystEngComm. 2020; 22:7950. https://doi.org/10.1039/D0CE01011A

[7] Shen Y, Linnow K, Steiger M. Crystallization behavior and damage potential of Na2SO4 –NaCl mixtures in porous building materials. Cryst. Growth Des. 2020; 20(9):5974–5985. https://doi.org/10.1021/acs.cgd.0c00671

[8] Abécassis B, Cottin-Bizonne C, Ybert C, & Bocquet L. How a Pinch of Salt Can Tune Chaotic Mixing of Colloids in Microchannels. 2014; 14(3):6390. https://doi.org/10.48550/arXiv.1403.6390

[9] Xingguo Luo, Xingbin Li, Chang Wei, Zhigan Deng, Ye Liu, Minting Li, Sanqiang Zheng, Xing Huang. Recovery of NaCl and Na2SO4 from high salinity brine by purification and evaporation. Desalination. 2022; 530:115631. https://doi.org/10.1016/j.desal.2022.115631

[10] Zhang X, Ren Y, Ping L, Ma H, Liu C, Wang Y, Kong L, Shen W. Solid-liquid equilibrium for the ternary systems (Na2SO4 + NaH2PO4 + H2O) and (Na2SO4 +NaCl + H2O) at 313.15 K and atmospheric pressure. J. Chem. Eng. 2014 ;59(12):3969-3974. https://doi.org/10.1021/je500854m

[11] Al Jibbouri S, & Ulrich J. The Influence of Impurities on the Crystallization Kinetics of Sodium Chloride. Crystal Research and Technology. 2001; 36(12):1365–1375. https://doi.org/10.1002/1521-4079(200112)36:12<1365::AID-CRAT1365>3.0.CO;2-H

[12] Cyran K, et al. The Influence of Impurities and Fabrics on Mechanical Properties of Rock Salt for Underground Storage in Salt Caverns. Archives of Mining Sciences. 2021; 66(2):155–179. https://doi.org/10.24425/ams.2021.13745

[13] Adnan Chakra, Christina Puijk, Goran T. Vladisavljević, Cécile Cottin-Bizonne, Christophe Pirat, Guido Bolognesi. Surface chemistry-based continuous separation of colloidal particles via diffusiophoresis and diffusioosmosis. Journal of Colloid and Interface Science. 2025; 693:137577. https://doi.org/10.48550/arXiv.2412.00246

[14] Sangwal K, & Zaniewska G. Influence of Impurities on the Etching of NaCl Crystals. Journal of Materials Science. 1984; 19:1131-1144. https://doi.org/10.1007/BF01120022

[15] Mi Z, Wang X, Zhang L, & Zhao Y. Characterization of calcium and magnesium salt removal in high-salinity brine treatment. Desalination. 2025; 569:117061. https://doi.org/10.1016/j.desal.2025.117061

[16] Bouaziz I, Hamzaoui A, & Ben Amor M. Sustainable brine management: Unlocking magnesium recovery from real RO brines. Desalination. 2024; 574:116534. https://doi.org/10.1016/j.desal.2024.116534

[17] Urazkeldiyeva D A, Kadirbayeva AA, Minakovsky AF, Sarybekova NK, Smailov BM. Methods for purifying table salt from the Bakhyt-Tany deposit. Kompleksnoe Ispolzovanie Mineralnogo Syra = Complex Use of Mineral Resources. 2025; 334(3):19-25. https://doi.org/10.31643/2025/6445.24

[18] Kadirbayeva A, Urazkeldiyeva D, Minakouski A, Seitmagzimova G, Koshkarbayeva S, Tukhtaev H. The Development of A Technology for the Purification of Sodium Chloride by Removing Impurities Using the Phosphate Method. Open Chem Eng J. 2025; 19:e18741231373719. http://dx.doi.org/10.2174/0118741231373719250430111944

[19] Pat. KG 1428. Metod ochistki solyanikx porod ot primestnyh ionov [Method for Purification of Salt Rock from Impurity Ions] Kochkorova ZB, Kalchaeva BSh, Murzubraimov BM, Satybaldiev AS. Opubl. 30.03.2012. (in Russ.).

[20] Pat. RU 2075440. Method for Producing Table Salt. Publ. 20.03.1997.

[21] Pat. RU 2495825. Fakeev AA, Polishchuk OM, Murskii GL. Method for Purifying Sodium Chloride. Publ. 20.10.2013.

[22] Li X, Zhang Y, Wang H, Liu J, & Chen Z. Review of the state of impurity occurrences and utilization of calcium sulfate. Minerals. 2023; 13(7):987. https://doi.org/10.3390/min13070987

[23] Xie Z, Liu X, Zhang Z, Wei C, Gu J. Application of the Industrial Byproduct Gypsum in Building Materials: A Review. Materials. 2024; 17(8):1837. https://doi.org/10.3390/ma17081837

Crossref
DOI: 10.31643/2027/6445.31
Mining & Mineral Processing

Activation of the mineralized mass of Central Kyzylkum using acidic wastewater from the oil and fat industry: Freundlich-based adsorption kinetics for fluorine release

[1*]Achilova S.S., [1]Saparbaeva N.K., [2] Matmuratov A.A., [3]Rustamova N.D., [4]Karimboyev O.Q.

[1]Urgench State University named after Abu Rayhon Biruni, Uzbekistan
[2]Mamun University, Khiva, Uzbekistan
[3]Urgench District General Secondary School No. 1, Uzbekistan
[4]Urgench State Pedagogical Institute, Uzbekistan

Corresponding author email: sanobar.a@urdu.uz

Received: *August 15, 2025*
Peer-reviewed: *October 16, 2025*
Accepted: *January 12, 2026*

ABSTRACT

This study investigates the simultaneous utilization of mineralized mass (MM) from Central Kyzylkum phosphorite waste and acidic wastewater (AWW) from the soapstock processing industry for efficient fluoride removal. The MM was chemically activated by AWW under controlled conditions, leading to surface modification, increased porosity, and enhanced active site heterogeneity. The chemical interaction between H^+ ions from AWW and fluorapatite in MM resulted in ion exchange, dissolution of phosphate groups, and the formation of volatile HF. Adsorption experiments were conducted at various MM: AWW ratios to determine the optimal operating parameters. Equilibrium data were fitted to the Freundlich isotherm model, confirming multilayer adsorption on heterogeneous surfaces. Kinetic analysis indicated that the pseudo-second-order (PSO) model provided the best fit, suggesting that chemisorption is the dominant rate-limiting mechanism. The Weber–Morris intra-particle diffusion model revealed that pore diffusion contributes to fluoride uptake but is not the sole controlling step. The synergy between isotherm and kinetic results supports a two-stage adsorption process involving rapid surface chemisorption followed by slower intraparticle diffusion. The developed method offers a dual environmental benefit by valorizing two industrial waste streams and reducing their ecological footprint. The produced sorbent showed high fluoride removal efficiency under simulated operational conditions. The process is simple, cost-effective, and compatible with existing industrial infrastructures. Large-scale application has the potential to reduce operational costs and promote circular economy principles. These findings provide a sustainable approach to water treatment in fluoride-affected regions while addressing industrial waste management challenges.

Keywords: fluoride removal, mineralized mass, acidic wastewater, Freundlich isotherm, adsorption kinetics, waste valorization.

Information about authors:

Achilova Sanobar Sobirovna — *Doctor of Philosophy in Technical Sciences, Associate Professor at the Faculty of Chemical Technology, Urgench State University named after Abu Rayhon Biruni, Urgench, H. Olimjon Street 14, 220100, Uzbekistan. Email: sanobar.a@urdu.uz; ORCID ID: https://orcid.org/0000-0003-4691-0248*

Saparbaeva Nasiba Kamilovna — *Candidate of Chemical Sciences, Associate Professor at the Faculty of Chemical Technology, Urgench State University named after Abu Rayhon Biruni, Urgench, H. Olimjon Street 14, 220100, Uzbekistan. Email: nasiba.s@urdu.uz; ORCID ID: https://orcid.org/0009-0002-1942-8958*

Matmuratov Azizbek Abdikarimovich — *Doctor of Philosophy in Pedagogical Sciences, Associate Professor at the Department of Pedagogical Sciences, Mamun University, 220900, Bol-Khovuz Street 2, Qibla Tozabog MCG, Khiva, Uzbekistan. Email: my_darling90@mail.ru; ORCID ID: https://orcid.org/0009-0007-4177-3738*

Rustamova Nodira Davronbekovna — *English teacher, Urgench District General Secondary School No. 1, 220500, 1 Navruz Street, Urgench district, Uzbekistan. Email: nodira.rustamova1007@gmail.com*

Karimboyev Ogabek Qadamboyevich — *Assistant in the Faculty of Natural and Applied Sciences, Urgench State Pedagogical Institute 220100, 1-A, Gurlan str, Urgench, Uzbekistan.*

Introduction

The Central Kyzylkum phosphorites constitute the largest portion of Uzbekistan's phosphorite raw material base, with deposits in this region being extensively enriched in phosphate-bearing rocks [1]. Studies indicate that the average P_2O_5 content of Central Kyzylkum phosphorites is 16–17%, a level that necessitates industrial-scale beneficiation [2]. During the beneficiation process, large quantities of waste, referred to as "mineralized mass" (MM), are generated, containing 12–15% P_2O_5, along with CaO,

MgO, F, and other components. According to statistical data, since the commencement of operations at the Central Kyzylkum phosphorite complex, millions of tons of MM waste have accumulated, with the total volume reaching 13–15 million tons [3]. These wastes are stored in open areas, posing a risk of environmental dispersion due to wind and rainfall [4].

Fluorine-containing compounds retained in the solid phase can be released into the atmosphere or water, posing ecological hazards, as elevated fluorine concentrations have adverse effects on human health and ecosystems [5]. The fluorapatite ($Ca_5(PO_4)_3F$) present in MM can decompose under acidic conditions, releasing fluoride ions [6]. Long-term open-air storage of such wastes can result in soil acidification and increased contamination with heavy metals and fluorine [7]. Therefore, the reduction or recycling of these wastes through environmentally safe methods is an urgent priority.

International practices employ various technologies for the processing of phosphorite wastes, including acid treatment, thermal activation, carbonate removal, and mechanochemical methods [8]. However, many of these technologies are not always economically viable due to high energy requirements or large acid consumption. Furthermore, the presence of fluorine in the wastes increases the technological complexity of many processing operations [6].

In the context of Uzbekistan, large-scale industrial practices for the effective utilization of MM wastes have not yet been implemented [4]. Recycling MM by integrating it with other industrial wastes represents a promising direction both ecologically and economically [3]. For example, the high acidity of acidic wastewater (AWW) from the fat-and-oil industry can partially decompose the fluorapatite in MM [5]. The mechanisms of fluorine removal in this process can be attributed to pH variation, ion exchange, and chemical decomposition [7]. Modeling the interaction between the two types of waste makes it possible to evaluate and optimize process efficiency [6]. The Freundlich adsorption model is among the effective approaches for describing fluorine removal in such systems. Studies have shown that fluorine removal during the acidification of phosphorite waste is sensitive to pH, temperature, mixing intensity, and mass ratios. Therefore, modeling fluorine removal from Central Kyzylkum MM by mixing it with AWW, using the Freundlich model, holds significant scientific and practical relevance for the fields of environmental protection, waste utilization, and industrial symbiosis [[6], [8]].

During the process of separating fatty acids from soapstock in the fat-and-oil industry, the resulting acidic wastewater—commonly referred to as “acidulated soapstock wastewater” (AWW)—is characterized by a high organic load (e.g., fats, glycerol, phospholipids, phosphatides, pigments, etc.) and low pH values, which significantly complicate both biological and chemical treatment systems [9]. The elevated chemical oxygen demand (COD) and biochemical oxygen demand (BOD) of these wastewaters slow down biological purification processes, thereby reducing overall treatment efficiency [10]. Extremely low pH values, such as those in the range of 0.7–1.2, have also been reported. Under such acidic conditions, both organic and mineral fractions remain in a free state, leading to corrosion and aggregation issues in treatment equipment [10]. Furthermore, the presence of surfactants (e.g., sulfates, lauryl sulfates, etc.) exerts a negative impact on microbial activity and destabilizes flocculation mechanisms during treatment processes [[11], [12]]. When such surfactants enter soil or groundwater, they may exert toxic effects on humans and animals—for instance, the activity of anionic surfactants can damage the gill tissues of aquatic organisms and disrupt microbial reproduction [12].

In addition, the high organic matter content can deplete oxygen in soils, create anaerobic conditions, and generate unfavorable environments in root zones [13]. When these wastewaters infiltrate soils, direct filtration and percolation processes are impaired, increasing the risk of groundwater contamination [[11], [13]]. Moreover, elevated concentrations of phosphates and nitrates in such effluents intensify the risk of eutrophication, leading to algal blooms and the formation of hypoxic “dead zones” in aquatic environments [[13], [14]]. These phenomena pose direct threats to ecological balance, aquatic biodiversity, and human health [14]. Consequently, the efficient treatment and utilization of acidic wastewaters from the fat-and-oil industry constitute a pressing and complex scientific–engineering challenge for ensuring environmental safety.

Fluorine is a widely distributed element in the environment, and its compounds are encountered in various industrial processes, particularly in phosphorite and aluminum production, as well as in certain chemical fertilizers. The introduction of fluoride ions into ecosystems via water, air, or soil directly affects their biological balance [15].

Numerous studies have reported that excessive fluoride concentrations in drinking water can cause dental fluorosis and, in severe cases, skeletal fluorosis in humans [[16], [17]]. Dental fluorosis is characterized by enamel brittleness, discoloration, and compromised aesthetics, while skeletal fluorosis leads to hardening of bone tissue and reduced joint mobility [18]. In animals, high fluoride doses slow growth rates and impair reproductive functions [15]. From an ecosystem perspective, excessive fluoride reduces photosynthetic activity in aquatic plants, decreases plankton and fish populations, and, in soils, diminishes microbial activity while limiting nutrient uptake in plants. Therefore, controlling fluoride removal during waste processing plays a crucial role in ensuring environmental sustainability. The reduction of fluoride in industrial wastes not only mitigates pollution sources but also helps preserve drinking water quality. Furthermore, managing the natural cycle of fluoride prevents its excessive accumulation in soil and water systems. From the standpoint of maintaining ecological balance and safeguarding public health, monitoring fluoride concentrations, reducing pollution sources, and implementing efficient utilization technologies remain urgent priorities [18].

The Freundlich isotherm expresses the equilibrium of adsorption from solution to solid phase in an empirical manner and, by accounting for surface energetic heterogeneity, is widely applicable to numerous real systems [[19], [20]]. Its general form is as follows:

$$q_e = K_F \cdot C_e^{\frac{1}{n}}$$

In the Freundlich isotherm, K_F represents the affinity between the adsorbent and the adsorbate, while $\frac{1}{n}$ expresses surface heterogeneity and adsorption favorability; when $\frac{1}{n} < 1$, the process is generally considered “favorable” [[19], [20], [21]].

Logarithmic linearization ($\log q_e = \log K_F + \frac{1}{n}\log C_e$) is often employed to estimate the parameters; however, modern guidelines recommend the use of non-linear fitting to minimize errors [[20], [21]]. The Freundlich model does not accurately describe saturation at high concentrations; therefore, extended isotherms such as Langmuir–Freundlich (Sips) or Redlich–Peterson are sometimes used [[19], [20]]. Nevertheless, in many systems, the Freundlich model provides reliable correlations within low-to-moderate concentration ranges due to its two-parameter simplicity and physically meaningful coefficients [[19], [20]].

In adsorption kinetics characterization, pseudo-first-order (PFO) and pseudo-second-order (PSO) models are most commonly applied; PSO often provides a better fit when chemical interactions—such as surface complexation or ion exchange—predominate [[22], [23]]. As demonstrated by Azizian, the origins of the PFO and PSO models can be interpreted as different limiting cases of the general Langmuir kinetic approach, thereby clarifying their respective domains of applicability [22]. To distinguish mass transfer limitations, the Weber–Morris intraparticle diffusion model ($q_t = k_i \cdot d \cdot t^{\frac{1}{2}} + C$) and the Boyd model are frequently used as diagAWWtic tools [24]. Recent analyses have highlighted cases of misinterpretation of the intraparticle diffusion model and provided guidelines for its correct application and solution methods (e.g., multi-stage linear plots, physical interpretation of the intercept) [24].

When selecting models and determining parameters, it is recommended to compare the results of linear and non-linear fitting using statistical indicators such as R^2, RMSE, X^2, and AIC, as linearization may distort weighting and lead to incorrect estimates of K_F and $\frac{1}{n}$ [[20], [24]].

Freundlich parameters can be temperature-sensitive; therefore, evaluating thermal effects via the van’t Hoff approach and repeating isotherm fitting at different temperatures is advisable [6]. In multicomponent mixtures or systems with strong competitive adsorption, the flexibility of the three-parameter Sips (Langmuir–Freundlich) model can be advantageous, although care must be taken to avoid improper linearization [[1], [8]]. From an experimental design perspective, it is recommended to first assess the time to equilibrium using PFO/PSO fitting, and then separately analyze intraparticle and film diffusion stages [23].

In our system (interaction of MM with AWW in the presence of fluoride-bearing species), the equilibrium sorption capacity is described using the Freundlich model, while the time dependence is characterized by the PSO model combined with intraparticle diffusion diagAWWtics. This approach allows separation of the initial rapid film transfer stage from the subsequent pore diffusion/reaction stages [22]. Ultimately, the correct interpretation of the physical meaning of parameters (e.g., $\frac{1}{n}$ as a measure of heterogeneity) and their role in design calculations (contact time, sorbent dosage) is essential for reliable modeling [24]. In conclusion,

the combined use of the Freundlich model and a kinetic framework (PFO/PSO with diffusion diagAWWtics) provides a robust methodological basis for both batch experiments and practical design applications [25].

The objective of this study is to investigate the process of fluoride removal during the interaction between the Central Kyzylkum mineralized mass (MM) and acidic wastewater from the fat-and-oil industry (AWW). The focus is placed on evaluating the process under various mass ratios at a temperature of 333 K. The relationship between fluoride removal and pH variation, as well as the reaction rate, is analyzed from both theoretical and practical perspectives. Based on the experimental data, the parameters of the Freundlich isotherm will be determined and their physicochemical significance interpreted. Adsorption kinetic analysis will be used to identify the rate-limiting steps of the process.

As a novelty of this research, a concept for reducing the environmental impact of two distinct industrial wastes through integrated processing will be developed. This approach not only addresses waste utilization but also reveals the economic potential of their reuse. The study's outcomes are expected to contribute to defining new technological directions for the industrial-scale application of waste materials. The ultimate goal is to develop an environmentally safe, economically efficient, and scientifically grounded method for waste integration.

Experimental part

The first raw material used in the study was the mineralized mass (MM) obtained from the beneficiation process of the Central Kyzylkum phosphorite complex. Its chemical composition is as follows: 15.09% P_2O_5, 43.17% CaO, 1.22% Al_2O_3, 1.34% Fe_2O_3, 1.21% MgO, 1.70% fluorine (F), 14.01% CO_2, 2.17% SO_3, and 13.23% residues of other inorganic substances (N.O.). The high percentages of P_2O_5 and CaO indicate the phosphate nature of the mineralized mass and its richness in calcium salts. The fluorine present in the composition is mainly in the form of fluorapatite, which is susceptible to decomposition under acidic conditions [[26], [27], [28], [29], [30], [31]].

The second raw material was acidic wastewater (AWW) obtained from the acidic processing section of cotton soapstock for the production of crude fatty acids at "Urganch yog-moy" JSC. The concentrations of cations and anions in its composition were as follows: H^+ (100 mg/L), Na^+ (43,158 mg/L), Ca^{2+} (300 mg/L), Mg^{2+} (1,824 mg/L), NH_4^+ (100 mg/L), and Fe^{2+} (30 mg/L). Anion concentrations included Cl^- (38,116 mg/L), SO_4^{2-} (48,145 mg/L), NO_3^- (840 mg/L), NO_2^- (20.01 mg/L), and HCO_3^- (3,446 mg/L). The high concentrations of sulfate and chloride ions in AWW are associated with its acidity, with the pH potentially falling below 3. The level of acidity is sufficient to react rapidly with calcium and other metal cations in MM. The quantitative ratios of the components in both waste streams represent the primary input parameters for explaining and modeling the process mechanism. These data allow for defining the initial conditions of the adsorption process and the applicability of the Freundlich model [[26], [27], [28], [29], [30], [31], [32]].

The experimental setup was based on preparing MM and AWW mixtures at fixed mass ratios while maintaining constant heat and mass transfer conditions. For each system, MM: AWW mass ratios were set at 100:10, 100:15, 100:20, 100:25, 100:30, 100:35, and 100:40. Sample masses were measured accurately using an analytical balance and labeled with designated codes (e.g., M100:10, M100:15, etc.). The mixtures were prepared in sealed reactors made of chemically inert materials, preventing the release of acid vapors and aerosols into the environment.

Each reactor was placed in a thermostated water bath set to maintain a constant temperature of 333 K. Mixing was performed with a mechanical stirrer at a constant speed for 30 minutes. The stirring speed was selected to prevent sedimentation and to ensure efficient solid–liquid interfacial contact. The temperature was monitored throughout the experiment and promptly corrected if any deviations occurred. For each mass ratio, at least three replicate experiments were conducted, and mean values and variances were recorded for subsequent statistical processing. Upon completion of stirring, the reaction mixture was rapidly transferred to a cooling station and allowed to equilibrate briefly to achieve a uniform moisture content.

Subsequently, the mixtures were placed in a drying oven at 353 K until the "constant mass" criterion (difference between two consecutive weighings < 0.001 g) was met. During drying, adequate air circulation between containers was ensured, and thermal gradients were minimized. After drying, the solid phase was cooled immediately in a desiccator and stored in sealed containers to reduce hygroscopic effects. The dried mass was used

for planned chemical–analytical analyses (e.g., pH extraction, fluorine determination, surface characterization). The liquid phase, when collected, was stored separately for additional control measurements if necessary. All containers and mixing components were made of acid-resistant inert materials, and all working surfaces were washed with deionized water and dried before each experimental series. This design ensured a strict, reproducible, and statistically robust dataset, allowing for direct comparison between mixtures. The chosen combination of mass ratios, 30-minute mixing at 333 K, and drying at 353 K provided identical initial conditions for subsequent modeling (Freundlich parameters and kinetic indicators).

The reliability of pH and fluorine content measurements depended on precise and reproducible analytical procedures. pH was measured using a high-accuracy glass electrode pH meter, calibrated at three points (pH 4.01, 7.00, 10.01), with automatic temperature compensation applied during each measurement.

Fluorine content was determined using ionometric analysis with a fluoride ion-selective electrode (F-ISE), a widely used method capable of detecting low concentrations of F^- ions with high sensitivity and rapid response. Before measurement, a Total Ionic Strength Adjustment Buffer (TISAB) was added to the sample. This reagent stabilizes the overall ionic strength, maintains pH within the optimal range, and releases bound fluorine by complexing with interfering metal ions such as Al^{3+} and Fe^{3+}. Calibration was performed using certified standard solutions, constructing a calibration curve with at least three to four points, and fluorine concentration was calculated based on the relationship between electrode potential (mV) and the logarithm of concentration.

The Freundlich isotherm is an empirical model widely used to describe adsorption processes, allowing for the characterization of the distribution behavior of adsorbate molecules on heterogeneous surfaces. According to this model, the equilibrium adsorption capacity (q_e, mg·g^{-1}) and the final solution concentration (C_e, mg·L^{-1}) are related as follows:

$$q_e = K_F \cdot C_e^{\frac{1}{n}}$$

Here, K_F is the Freundlich constant representing the adsorption capacity of the adsorbent, and nnn is an empirical parameter indicating the degree of heterogeneity of surface energies. For calculation purposes, this equation was transformed into a logarithmic form:

$$\log q_e = \log K_F + \frac{1}{n}\log C_e$$

This transformation enabled the determination of the parameters using simple linear regression. In the experimental procedure, q_e was defined as the mass of adsorbate retained per gram of adsorbent. When the equilibrium concentration (C_e) of the final solution was not directly measured, it was calculated using the mass balance equation:

$$q_e = \frac{(C_0 - C_e) \cdot V}{m}$$

where C_0 is the initial concentration (mg·L^{-1}), V is the volume of solution (L), and m is the adsorbent mass (g). The obtained data were plotted in coordinates $\log C_e$ versus $\log q_e$, and ordinary least squares (OLS) regression was applied to fit a straight line. The intercept of this line provided the value of $\log K_F$, while the slope corresponded to $\frac{1}{n}$.

The goodness-of-fit of the results to the model was evaluated using the determination coefficient (R^2) and the root mean square error (RMSE). High R^2 values indicated a strong agreement with the Freundlich isotherm, whereas lower values suggested the need for comparison with alternative isotherm models. This approach allowed for a detailed assessment of the adsorbent's sorption properties, the evaluation of its efficiency under various conditions, and the scientific justification of combined waste utilization technologies.

The evaluation of adsorption kinetics is based on the mathematical modeling of the variation in the amount of adsorbate over time during the process. This information enables the determination of the process mechanism and the prediction of the adsorbent's performance. Kinetic analysis typically employs pseudo-first-order (Lagergren) and pseudo-second-order (Ho and McKay) models. The pseudo-first-order model is expressed as:

$$\log(q_e - q_t) = \log q_e - \frac{k_1}{2.303} \cdot t$$

where q_e is the amount of substance adsorbed at equilibrium (mg·g^{-1}), q_t is the amount of substance adsorbed at time t (mg·g^{-1}), and k_1 is the pseudo-first-order kinetic rate constant (min^{-1}).

The pseudo-second-order model is expressed as:

$$\frac{1}{q_t} = \frac{1}{k_2 \cdot q_e^2} + \frac{1}{q_e}$$

where k_2 is the pseudo-second-order kinetic rate constant (g·mg^{-1}·min^{-1}). For both models, experimental q_t values are measured over time, plotted in the linearized form of the corresponding equations, and kinetic parameters are determined through regression analysis.

Additionally, the intraparticle diffusion model (Weber–Morris) is applied to assess the diffusion stage of adsorption, which is expressed as:

$$q_t = k_{id} \cdot t^{0.5} + C$$

where k_{id} is the intraparticle diffusion rate constant (mg·g^{-1}·min$^{-0.5}$), and C is a parameter describing the thickness of the boundary layer. The degree of fit for each kinetic model is evaluated using the coefficient of determination (R^2), root mean square error (RMSE), or other statistical indicators. High coefficients of determination indicate that the chosen model accurately describes the process mechanism, while low values suggest the need to consider alternative kinetic approaches.

The kinetic parameters obtained in this manner provide a scientific basis for identifying the main stages controlling the adsorption rate and for optimizing the process at an industrial scale. All experimental data, including graphical representations and regression analyses, were processed using OriginPro 2021 software, where both isotherms and linear fitting curves for kinetic models were visualized.

Results and Discussion

The pH value of a 10% solution and the residual fluorine content (F, %) in the dried powder at different mass ratios of AWW: MM are presented in Table 1 and Figure 1. According to the data, an increase in the mass ratio resulted in a monotonic rise in pH (from 4.10 to 7.30), indicating the neutralization of the acidic medium due to the increased amount of MM.

The residual fluorine content initially increased (from 1.07% to 1.42%, reaching a maximum at a 100:25 ratio) and then slightly decreased, stabilizing at approximately 1.38–1.40%. Based on the initial fluorine content in MM (1.70%), the calculated amount of fluorine removed (F lost = 1.70% – residual F) exhibited the opposite trend: initially high (0.63%), dropping to a minimum value (0.28%), and then slightly increasing and leveling off at about 0.30%.

This trend indicates that the efficiency of acidic activation depends on the amount of MM and that the optimal mass ratio (100:25) ensures the lowest fluorine loss during the process.

Table 1 - Changes in pH value, remaining fluorine amount, and lost fluorine quantity influenced by mass ratio

Mass ratio (AWW:MM)	pH indicator	Remaining fluorine (%)	Fluorine loss (%)
100:10	4.10	1.07	0.63
100:15	4.81	1.16	0.54
100:20	5.62	1.27	0.43
100:25	5.90	1.42	0.28
100:30	6.33	1.39	0.31
100:35	6.74	1.38	0.32
100:40	7.30	1.40	0.30

Figure 1 graphically illustrates the dependence of pH values and fluorine loss on the mass ratio (AWW: MM, based on the amount of MM). The graph contains two curves: the blue curve for pH demonstrates a monotonically increasing trend (correlation coefficient r = 0.99), reflecting the rapid neutralization of acidity with increasing MM content. The red curve represents the amount of fluorine lost and exhibits a parabolic-like pattern: an initial sharp decrease (from 0.63% to 0.28%), followed by a slight increase and stabilization at approximately 0.30%. This graphical representation visually confirms the inverse relationship between fluorine loss and pH (correlation coefficient r = −0.85): at lower pH values (higher acidity), fluorine loss is greater, highlighting the chemical dynamics of the process and aiding in the identification of the optimal mass ratio (100:25, pH ≈ 5.90).

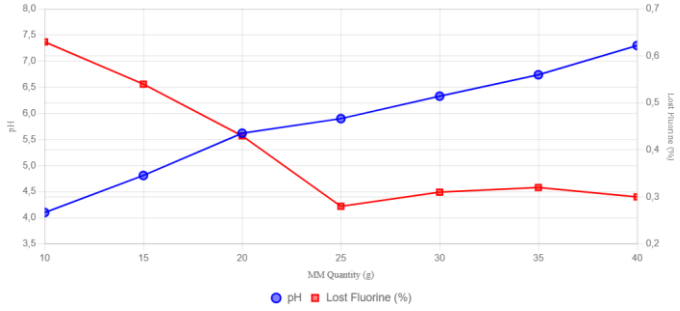

Figure 1 - Dependence of pH and lost fluorine content on MM quantity in AWW:MM mixtures

Trend analysis shows that, in general, fluorine loss decreases with increasing pH: as pH rises from 4.10 to 5.90, fluorine loss declines from 0.63% to 0.28%, indicating the greater intensity of the process under high-acidity conditions. Subsequently, when pH increases from 6.33 to 7.30, the amount of fluorine lost rises slightly (from 0.28% to 0.30%) and remains at a stable level. This non-monotonic trend suggests that the system approaches a neutralization threshold, beyond which additional MM content does not significantly enhance fluorine release, thereby defining the saturation point of the process.

The chemical basis lies in the interaction of H^+ ions from AWW with the fluorapatite structure *($Ca_5(PO_4)_3F$).* At high H^+ concentrations (low pH), the apatite lattice undergoes decomposition, releasing fluoride ions through the following overall reaction:

$$Ca_5(PO_4)_3F + 10H^+ \rightarrow 5Ca^{2+} + 3H_3PO_4 + HF$$

Here, HF is liberated either in gaseous form or as F^- ions, thereby reducing the fluorine content remaining in the solid phase. At low pH values (e.g., 4.10), the reaction rate is high, resulting in maximal fluorine loss. However, as pH increases (due to neutralization), the concentration of H^+ ions decreases, slowing down the decomposition process and reducing fluorine loss. This mechanism involves both adsorption and ion-exchange processes and conforms to the Freundlich model, as the process is empirically characterized by surface energy and heterogeneity effects. The experimental results were analyzed using the pH and fluorine content in the final powder (q_e, mg·g^{-1}) presented in Table 2 and Figure 2. The fluorine content values (F, wt.%) were converted to mg·g^{-1} (1% = 10 mg·g^{-1}), and the hydrogen ion activity was calculated as $a_{H^+} = 10^{-pH}$.

Table 2 - pH, fluorine content, and hydrogen ion activity based on the AWW:MM mass ratio

Mass ratio (AWW:MM)	pH	F (wt.%)	q_e (mg·g^{-1})	a_{H^+} (mol·L^{-1})
100:10	4.10	1.07	10.70	7.94×10^{-5}
100:15	4.81	1.16	11.60	1.55×10^{-5}
100:20	5.62	1.27	12.70	2.40×10^{-6}
100:25	5.90	1.42	14.20	1.26×10^{-6}
100:30	6.33	1.39	13.90	4.68×10^{-7}
100:35	6.74	1.38	13.80	1.82×10^{-7}
100:40	7.30	1.40	14.00	5.01×10^{-8}

From the table, it is evident that the q_e values are 10.70 mg·g^{-1} at a mass ratio of 100:10, increasing to a maximum of 14.20 mg·g^{-1} at a ratio of 100:25. Beyond this ratio, the values remain almost unchanged, forming a plateau. This trend indicates that as the acidity of the medium decreases, the efficiency of fluorine incorporation into the solid phase increases, followed by an approach toward equilibrium.

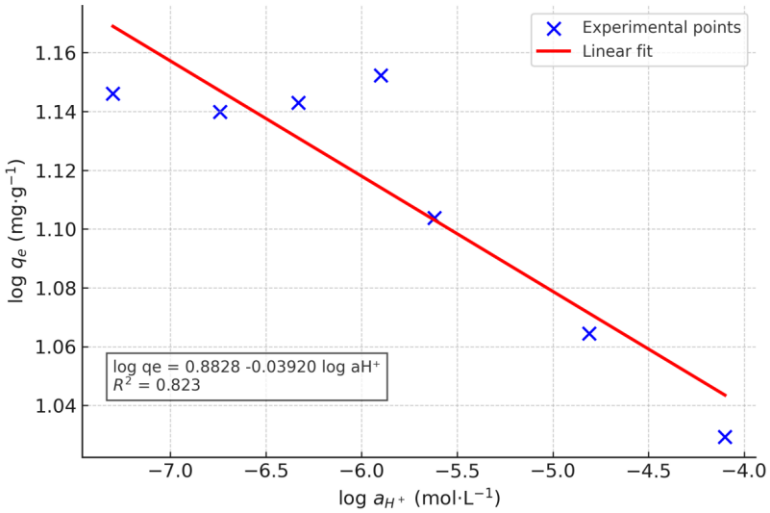

Figure 2 - Freundlich-type isotherm based on experimental data: log q_e versus log a_{H^+}. Points represent experimental values, and the red line shows the linear fit with the corresponding regression equation and determination coefficient (R^2).

The linear trend demonstrates that *log* q_e exhibits a negative slope with respect to *log* a_{H^+}: as pH increases (and a_{H^+} decreases), q_e rises. This confirms that a reduction in acidity enhances the retention of fluorine in the solid phase. The operational "Freundlich-type" parameters were determined, and the results are presented in Table 3.

Table 3 - Operational Freundlich-type parameters (*log* q_e - *log* a_{H^+} regression)

Parameter	Value
K_F (operatsion)	7.63
n (operatsion)	−25.51
R^2	0.823

The fact that R^2 = 0.823 indicates a high degree of model fit. The negative value of *n* mathematically expresses that q_e increases as a_{H^+} decreases, meaning the process becomes more active when acidity is reduced. When compared with trends observed in apatite-based minerals reported in the literature, our system also shows that an increase in pH reduces the concentrations of free *HF* and HF_2^- ions, which in turn promotes the fixation of fluorine in the solid phase.

It should be noted that, since the final fluorine concentration in the liquid phase C_e was not measured, these are not the classical Freundlich parameters derived from the $\log q_e - \log C_e$ relationship. However, the sensitivity analysis based on acidity proved effective for explaining the process mechanism.

The adsorption of fluoride from the mineralized mass (MM) activated by acidic wastewater (AWW) was investigated as a function of contact time to elucidate the mechanism and rate-controlling steps. The experimental (simulated) data of q_t versus time are presented in Figure 3. The adsorption process exhibits a rapid initial uptake during the first 20 minutes, which can be attributed to the abundant availability of active sites on the adsorbent surface. Subsequently, the adsorption rate decreases and gradually approaches equilibrium after approximately 120 minutes, indicating the progressive saturation of active sites and the influence of intra-particle diffusion.

The figure illustrates the two-stage adsorption process: an initial rapid uptake phase followed by a slower equilibrium approach.

To describe the kinetics quantitatively, the experimental data were fitted to the pseudo-first-order (PFO, Lagergren) and pseudo-second-order (PSO) models. The linearized form of the PFO model is given by:

$$\ln(q_e - q_t) = \ln(q_e) - k_1 t$$

where q_e and q_t are the adsorption capacities (mg/g) at equilibrium and at time t, respectively, and k_1 is the rate constant (1/min). The PSO model is expressed as:

$$\frac{t}{q_t} = \frac{1}{k_2 q_e^2} + \frac{t}{q_e}$$

Where, k_2 is the pseudo-second-order rate constant [g/(mg·min)].

The linear fits are shown in Figure 4 (PFO) and Figure 5 (PSO). The calculated kinetic parameters and determination coefficients (R^2) are summarized in Table 4**.**

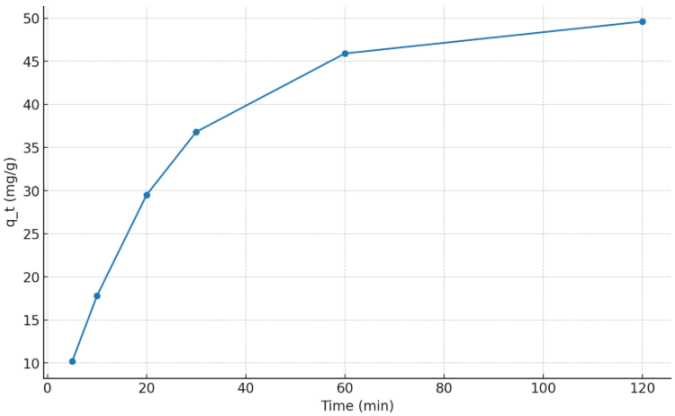

Figure 3 - Variation of adsorption capacity (q_t)with contact time (simulated data).

The results reveal that the PSO model provides an excellent fit (R^2 = 0.9957) compared to the PFO model (R^2 = 0.8634), suggesting that the adsorption process is more accurately described by the pseudo-second-order kinetic mechanism, which is typically associated with chemisorption involving valence forces through sharing or exchange of electrons between adsorbent and adsorbate.

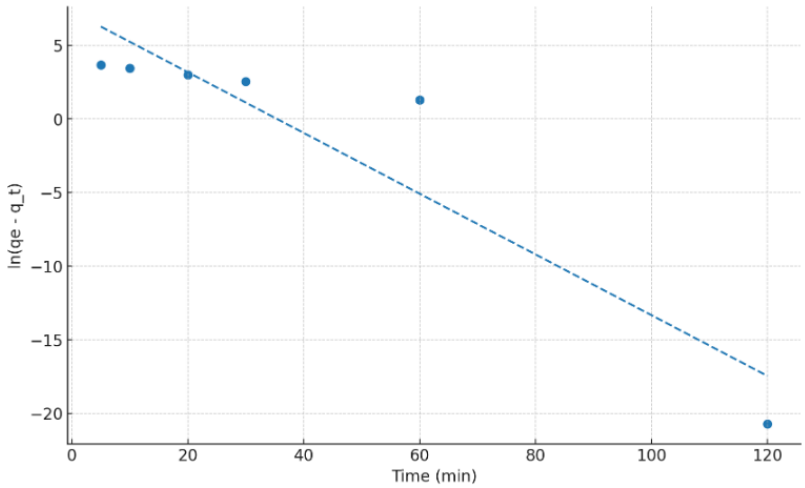

Figure 4 - Linear plot of the pseudo-first-order model: $\ln(q_e - q_t)$ versus t (simulated data). The slope represents $-k_1$ and the intercept corresponds to $\ln(q_e)$.

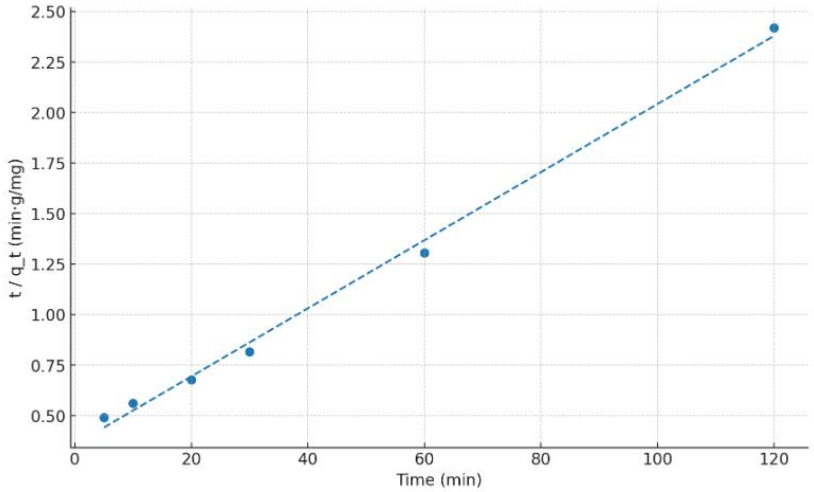

Figure 5 - Linear plot of the pseudo-second-order model: $\frac{t}{q_t}$ versus t (simulated data). The slope represents $\frac{1}{q_e}$ and the intercept represents $\frac{1}{k_2 q_e^2}$.

Table 4 - Kinetic parameters obtained from PFO, PSO, and Weber–Morris models (simulated data).

Model	Parameter 1	Parameter 2	R^2
Pseudo-first-order (Lagergren)	k_1=0.2063 1/min	q_e=1486.097 mg/g	0.8634
Pseudo-second-order	k_2=7.95×10^{-4} g/(mg·min)	q_e=59.346 mg/g	0.9957
Weber–Morris intraparticle diffusion model	k_{id}=4.5264 mg/(g·min$^{0.5}$)	C=5.947 mg/g	0.8781

Where, k_{id} is the intra-particle diffusion rate constant mg/(g·min$^{0.5}$), and C is the intercept related to the boundary layer effect. The plot of q_t versus $t^{0.5}$ (Figure 6) shows a linear relationship that does not pass through the origin, indicating that intra-particle diffusion is involved but is not the sole rate-controlling step. The positive intercept (C= 5.947 mg/g) suggests a significant contribution of surface adsorption during the initial stage, followed by intra-particle diffusion in the later stages.

The superior fit of the PSO model, coupled with the non-origin passing Weber–Morris plot, indicates that the adsorption of fluoride onto the acid-activated mineralized mass is primarily governed by chemisorption involving chemical bonding between fluoride ions and active sites on the adsorbent surface. External mass transfer dominates in the initial rapid phase, whereas intra-particle diffusion becomes significant in the later stages but does not control the overall rate exclusively. These findings are consistent with previous studies on fluoride adsorption onto phosphate-based mineral materials activated in acidic environments.

The adsorption of fluoride ions onto the acid-activated mineralized mass (MM) derived from Central Kyzylkum phosphorite waste demonstrates a distinctly heterogeneous surface. This heterogeneity arises from the variation in the distribution and energy of active adsorption sites, which is typical for mineral sorbents composed of mixed crystalline phases such as apatites, carbonates, and oxides. The surface complexity is further enhanced by microstructural defects and porosity created during acid activation with AWW. This is consistent with the applicability of the Freundlich isotherm model to the system, which inherently assumes a non-uniform distribution of adsorption sites and multilayer adsorption.

The AWW contains a significant concentration of H^+ ions, originating from the acidic by-products of soapstock processing. Upon contact with the mineralized mass, these protons promote the decomposition of fluorapatite ($Ca_5(PO_4)_3F$) according to the following reaction:

$$Ca_5(PO_4)_3F + 10H^+ \rightarrow 5Ca^{2+} + 3H3PO_4 + HF\uparrow$$

This reaction proceeds via an ion-exchange mechanism where Ca^{2+} ions are released into solution, while F^- ions are protonated to form volatile HF gas. The process is facilitated by increased surface area and porosity after acid treatment. Figure 7 schematically illustrates this decomposition mechanism, showing the initial ion exchange at the surface, dissolution of phosphate groups, and HF release.

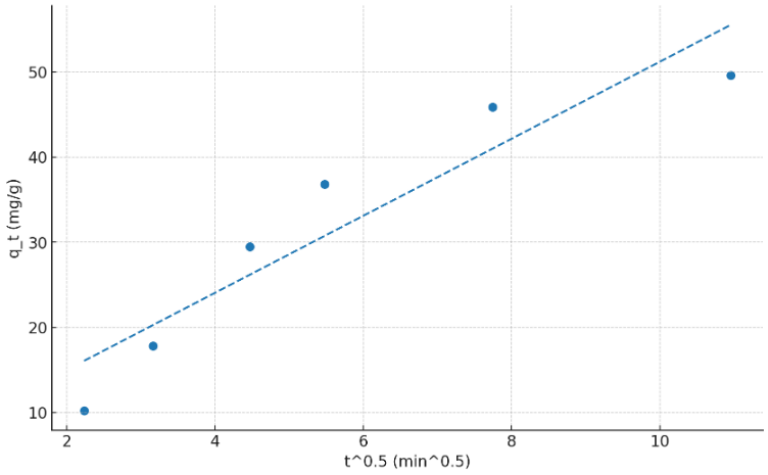

Figure 6 - Weber–Morris intra-particle diffusion plot (q_t versus $t^{0.5}$) for the adsorption process (simulated data). The slope (k_{id}) reflects the diffusion rate inside the pores of the adsorbent, while the intercept (C) represents the contribution of surface adsorption.

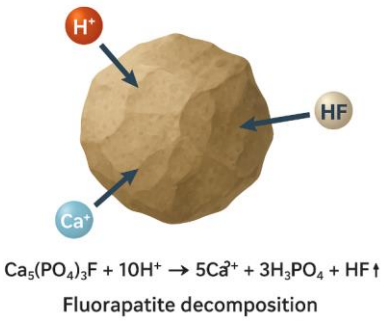

Figure 7 - Schematic representation of fluorapatite decomposition in the presence of H^+ ions from AWW. The diagram highlights ion exchange between H^+ and Ca^{2+}, dissolution of PO_4^{3-} groups, and HF volatilization from the solid surface.

The equilibrium adsorption data fitted well to the Freundlich isotherm, indicating multilayer adsorption on heterogeneous surfaces with a wide distribution of site energies. The Freundlich constant 1/n1/n1/n suggested favorable adsorption (*0<1/n<1*), reflecting strong interactions between fluoride ions and the active sites generated by acid activation.

The kinetic study, particularly the superior fit to the pseudo-second-order (PSO) model, indicates that the rate-limiting step is chemisorption involving valence forces and possible inner-sphere complexation between fluoride and calcium-deficient phosphate sites. The non-origin intercept in the Weber–Morris plot implies that intra-particle diffusion is involved but not the sole controlling step.

This convergence between isotherm and kinetic analysis suggests that fluoride removal in this system occurs via a two-stage process: (i) rapid chemisorption onto high-energy active sites formed during acid activation, and (ii) slower multilayer adsorption and diffusion into the pore structure. Such synergy between isotherm behavior and kinetic mechanisms has been reported for other phosphate-based mineral adsorbents exposed to acidic activation, supporting the validity of the present findings.

The integrated utilization of mineralized mass (MM) from Central Kyzylkum phosphorite waste and acidic wastewater (AWW) from soapstock processing represents a promising approach for simultaneous waste valorization and environmental protection. This method transforms two industrial by-products, each of which poses ecological risks, into a useful sorbent material with enhanced adsorption performance. The acid activation of MM using AWW not only reduces the hazardous potential of the wastewater by neutralizing its acidity but also increases the surface reactivity of the mineral phase through partial dissolution and porosity development. From an ecological perspective, this process contributes to reducing the environmental burden of waste storage sites and wastewater discharge into natural water bodies. Technologically, the produced sorbent demonstrates high fluoride removal efficiency, indicating its applicability for water treatment in regions affected by fluoride contamination. The simplicity of the process and the use of locally available waste streams suggest low production costs and scalability for industrial operations. Furthermore, integrating this method into existing phosphorite and oil-processing plants could reduce waste management costs and promote circular economy principles. Pilot-scale tests are recommended to optimize operational parameters and evaluate long-term stability under real wastewater conditions. Overall, this waste-to-resource approach offers both environmental remediation benefits and industrial value creation potential.

Conclusion

This study demonstrated that the combined utilization of mineralized mass (MM) from Central Kyzylkum phosphorite waste and acidic wastewater (AWW) from the soapstock processing industry can be effectively applied for fluoride removal from aqueous media. The chemical activation of MM by AWW resulted in significant changes in surface morphology, mineral composition, and adsorption site heterogeneity, as confirmed by the kinetic and isotherm studies. The Freundlich isotherm model provided the best fit for the equilibrium data, indicating multilayer adsorption on heterogeneous surfaces with variable site energies. Kinetic analysis revealed that the pseudo-second-order (PSO) model yielded the highest correlation coefficient (R^2 = 0.9957), implying chemisorption as the dominant mechanism. The Weber–Morris intraparticle diffusion model indicated that pore diffusion contributed to the process but was not the sole rate-controlling step, as evidenced by the positive intercept. The decomposition of fluorapatite under the influence of H^+ ions from AWW played a critical role, releasing Ca^{2+} and PO_4^{3-} ions while forming volatile HF. This reaction enhanced the number of active adsorption sites and improved fluoride removal efficiency. From an ecological perspective, the process provides a sustainable method for mitigating two major industrial waste streams simultaneously. Technologically, the method is simple, cost-effective, and adaptable to existing industrial facilities without requiring extensive infrastructure modification. The produced sorbent showed stable performance under simulated operational conditions, suggesting its viability for long-term application. The integration of waste activation and pollutant removal in a single step aligns with circular economy principles. Large-scale applications could reduce both operational and waste management costs in the phosphorite and oil-processing industries. Further optimization of process parameters such as temperature, contact time, and MM: AWW ratio can potentially improve efficiency even further. Future work should focus on evaluating the adsorbent's regeneration potential

and long-term stability under real wastewater conditions. Additionally, life cycle assessment (LCA) studies are recommended to quantify the environmental benefits of the proposed technology. The results of this research contribute valuable insights for developing eco-efficient fluoride removal strategies based on waste-derived sorbents.

Conflicts of interest. On behalf of all authors, the corresponding author states that there is no conflict of interest.

CRediT author statement: **S. Achilova, A. Matmuratov**: Conceptualization, Methodology, Software; **N. Rustamova**: Data curation, Writing draft preparation; **S. Achilova, A. Matmuratov**: Visualization, Investigation, Supervision, Reviewing and Editing; **N. Rustamova**: Software, Validation.

Formatting of funding sources. This research did not receive any specific grant from funding agencies in the public, commercial, or not-for-profit sectors.

Cite this article as: Achilova SS, Saparbaeva NK, Matmuratov AA, Rustamova ND, Karimboyev OQ. Activation of the mineralized mass of Central Kyzylkum using acidic wastewater from the oil and fat industry: Freundlich-based adsorption kinetics for fluorine release. Kompleksnoe Ispolzovanie Mineralnogo Syra = Complex Use of Mineral Resources. 2027; 342(3):65-79. https://doi.org/10.31643/2027/6445.31

Май-тоң май өнеркәсібінің қышқыл ағынды суларын пайдалана отырып Орталық Қызылқұмның минералданған массасын белсендіру: Фрейндлих моделіне негізделген фтордың бөлінуінің адсорбциялық кинетикасы

[1] Ачилова С.С., [1]Сапарбаева Н.К., [2] Матмуратов А.А., [3] Рустамова Н.Д., [4]Каримбоев О.К.

[1]Әбу Райхон Беруни атындағы Үргеніш мемлекеттік университеті, Өзбекстан
[2]Мамун университеті, Хива, Өзбекстан
[3] Үргеніш ауданы №1 жалпы орта мектебі, Өзбекстан
[4]Үргеніш мемлекеттік педагогикалық институты, Өзбекстан

Мақала келді: *15 тамыз 2025*
Сараптамадан өтті: *16 қазан 2025*
Қабылданды: *12 қаңтар 2026*

ТҮЙІНДЕМЕ

Бұл зерттеуде фторидті тиімді кетіру үшін Орталық Қызылқұм фосфат кенішінің қалдықтарынан алынған минералданған массаны (ММ) және сабын қалдықтарын өңдеуден алынған қышқылды ағынды суларды (ҚАС) бір мезгілде пайдалану қарастырылады. ММ қатаң бақыланған жағдайларда ҚАС көмегімен химиялық белсендірілді, нәтижесінде беткі қабаттың модификациясы, кеуектіліктің артуы және белсенді орталардың гетерогенділігінің күшеюі байқалды. ҚАС құрамындағы H^+ иондары мен ММ құрамындағы фторапатит арасындағы химиялық өзара әрекет ион алмасуға, фосфат топтарының еруіне және ұшқыш HF түзілуіне әкелді. Әртүрлі ММ:ҚАС қатынастарында адсорбция тәжірибелері жүргізіліп, оңтайлы жұмыс параметрлері анықталды. Теңгерімдік деректер Фрейндлих изотерма моделіне сәйкестендіріліп, гетерогенді беттерде көпқабатты адсорбция жүзеге асатыны расталды. Кинетикалық талдау псевдо-екінші ретті (PSO) модельдің ең жақсы сәйкестігін көрсетті, бұл химиялық адсорбцияның жылдамдықты шектейтін негізгі механизм екенін білдіреді. Вебер–Моррис бөлшекішілік диффузия моделі фтордың сіңірілуіне кеуектік диффузияның үлесінің бар екендігін көрсетті, бірақ бұл жалғыз шектейтін қадам емес екені анықталды. Изотерма мен кинетикалық нәтижелер арасындағы сәйкестік жылдам беттік хемосорбцияны және кейінгі баяу интрадиффузияны қамтитын екі сатылы адсорбция механизмін растайды. Дамытылған әдіс екі өнеркәсіптік қалдық ағындарын кәдеге жарату және олардың экологиялық ізін азайту арқылы қосарлы экологиялық пайда береді. Алынған сорбент модельдік жұмыс жағдайында фторды кетіруде жоғары тиімділік көрсетті. Процесс қарапайым, үнемді және қолданыстағы өнеркәсіп инфрақұрылымымен үйлесімді. Өндірістік ауқымда енгізу операциялық шығындарды азайтуға және тұйық экономикалық жүйе қағидаттарын ілгерілетуге мүмкіндік береді. Ұсынылған нәтижелер фтор әсеріне ұшыраған аудандарда суды тазартудың тұрақты тәсілін ұсынады, сонымен бірге өнеркәсіптік қалдықтарды басқару мәселелерін шешеді.

Түйін сөздер: фторидті кетіру, минералданған масса, қышқылдық ағынды су, Фрейндлих изотермасы, адсорбция кинетикасы, қалдықтарды қайта пайдалану.

Авторлар туралы ақпарат:

Ачилова Санобар Собировна

Техника ғылымдары бойынша философия докторы (PhD), Химиялық технология факультетінің доценті, Әбу Райхон Беруни атындағы Үргеніш мемлекеттік университеті, 220100, Х. Олимжон көшесі, 14-үй, Үргенч, Өзбекстан. Email: sanobar.a@urdu.uz; ORCID ID: https://orcid.org/0000-0003-4691-0248

Сапарбаева Насиба Камиловна	*Химия ғылымдарының кандидаты, Химиялық технология факультетінің доценті, Әбу Райхон Беруни атындағы Ургеніш мемлекеттік университеті, 220100, Х. Олимжон көшесі, 14-үй, Ургенч, Өзбекстан. Email: nasiba.s@urdu.uz; ORCID ID: https://orcid.org/0009-0002-1942-8958*
Маттмуратов Азизбек Абдикаримович	*Педагогика ғылымдары бойынша философия докторы (PhD), Педагогикалық ғылымдар кафедрасының доценті, Мамун университеті, 220900, Бол-Ховуз көшесі, 2-үй, Қыбла Тозабоғ МКӘ, Хива, Өзбекстан. Email: my_darling90@mail.ru; ORCID ID: https://orcid.org/0009-0007-4177-3738*
Рустамова Нодира Давронбековна	*Ағылшын тілі пәнінің мұғалімі, 220500, Ургеніш ауданы №1 жалпы орта мектебі, Наурыз көшесі, 1-үй, Ургеніш, Өзбекстан. Email: nodira.rustamova1007@gmail.com*
Каримбоев Огабек Кадамбоевич	*Ургеніш мемлекеттік педагогикалық институтының жаратылыстану және қолданбалы ғылымдар факультетінің ассистенті, 220100, Гүрлен көшесі, 1-А, Ургеніш, Өзбекстан.*

Активирование минерализованной массы Центрального Кызылкума с использованием кислых сточных вод масложировой промышленности: адсорбционная кинетика высвобождения фтора на основе модели Фрейндлиха

[1] Ачилова С.С., [1]Сапарбаева Н.К., [2] Матмуратов А.А., [3] Рустамова Н.Д., [4]Каримбоев О.К.

[1]Ургенчский государственный университет имени Абу Райхона Беруни, Узбекистан
[2]Университет Мамуна, Хива, Узбекистан.
[3] Ургенчская районная общеобразовательная школа №1, Узбекистан
[4]Ургенчский государственный педагогический институт, Узбекистан

Поступила: *15 августа 2025*
Рецензирование: *16 октября 2025*
Принята в печать: *12 января 2026*

АННОТАЦИЯ

В данном исследовании изучается одновременное использование минерализованной массы (ММ) из фосфоритовых отходов Центральных Кызылкумов и кислых сточных вод (КСВ) от промышленности по переработке соапстока для эффективного удаления фторида. ММ была химически активирована с применением КСВ в контролируемых условиях, что привело к модификации поверхности, увеличению пористости и возрастанию гетерогенности активных центров. Химическое взаимодействие ионов H^+ из КСВ с фторапатитом в составе ММ вызвало ионный обмен, растворение фосфатных групп и образование летучего HF. Эксперименты по адсорбции были проведены при различных соотношениях ММ:КСВ с целью определения оптимальных параметров процесса. Равновесные данные были аппроксимированы моделью изотермы Фрейндлиха, что подтвердило многоуровневую адсорбцию на гетерогенных поверхностях. Кинетический анализ показал, что модель псевдовторого порядка (PSO) обеспечивает наилучшее соответствие, что указывает на хемосорбцию как на доминирующий лимитирующий механизм. Модель внутридиффузии частиц Вебера–Морриса выявила, что поровая диффузия вносит вклад в поглощение фторида, но не является единственным определяющим этапом. Согласованность результатов изотерм и кинетики подтверждает двухстадийный механизм адсорбции, включающий быструю поверхностную хемосорбцию и последующую более медленную внутридиффузию. Разработанный метод обеспечивает двойной экологический эффект за счёт утилизации двух промышленных отходопотоков и снижения их экологического следа. Полученный сорбент показал высокую эффективность удаления фторида в модельных эксплуатационных условиях. Процесс является простым, экономичным и совместимым с существующей промышленной инфраструктурой. Промышленное внедрение способно снизить эксплуатационные затраты и способствует развитию принципов циркулярной экономики. Представленные результаты обеспечивают устойчивый подход к очистке воды в районах, затронутых фтором, одновременно решая задачи управления промышленными отходами.

Ключевые слова: удаление фтора, минерализованная масса, кислые сточные воды, изотерма Фрейндлиха, кинетика адсорбции, утилизация отходов.

Ачилова Санобар Собировна	***Информация об авторах:*** *Доктор философии (PhD) по технических наукам, доцент факультета химической технологии, Ургенчский государственный университет имени Абу Райхона Беруни, 220100, ул. Х. Олимжона, д. 14, Ургенч, Узбекистан. Email: sanobar.a@urdu.uz; ORCID ID: https://orcid.org/0000-0003-4691-0248*
Сапарбаева Насиба Камиловна	*Кандидат химических наук, доцент факультета химической технологии, Ургенчский государственный университет имени Абу Райхона Беруни, 220100, ул. Х. Олимжона, д. 14, Ургенч, Узбекистан. Email: Email: nasiba.s@urdu.uz; ORCID ID: https://orcid.org/0009-0002-1942-8958*

Маттуратов Азизбек Абдикаримович	*Доктор философии (PhD) по педагогическим наукам, доцент кафедры педагогики, Университет Мамуна, 220900, ул. Бол-Ховуз, д. 2, МСГ Кибла Тозабог, Хива, Узбекистан. Email: my_darling90@mail.ru; ORCID ID: https://orcid.org/0009-0007-4177-3738*
Рустамова Нодира Давронбековна	*Учитель английского языка, средняя общеобразовательная школа №1 Ургенчского района, ул. Наурыз, д. 1, Ургенчский район, 220500, Узбекистан. Email: nodira.rustamova1007@gmail.com*
Каримбоев Огабек Кадамбоевич	*Ассистент факультета естественных и прикладных наук Ургенчского государственного педагогического института 1-А, ул. Гурлана, Ургенч, 220100, Узбекистан.*

References

[1] Akhtamova M, Temirov U, Khurramov N, Shukurov A, & Karshiev B. Processing of phosphorites and additives with researching their thermodynamical properties. O. Tursunov, Ed., E3S Web of Conferences. EDP Sciences. 2023. https://doi.org/10.1051/e3sconf/202343403016

[2] Bekzod, Khoshimov, et al. Results of Physical and Chemical Research of Phosphorus Fertilizers and Problems in Certification. JournalNX. 2021; 7(10):96-100. https://doi.org/10.17605/OSF.IO/RZKE3

[3] Temirov U, Doniyarov N, Jurakulov B, Usanbaev N, Tagaev I, & Mamataliyev A. Obtaining complex fertilizers based on low-grade phosphorites. E3S Web of Conferences. 2021; 264:04009. https://doi.org/10.1051/e3sconf/202126404009

[4] Doniyarov N A, Tagaev I A, Muratova M N, & Andriyko L S. New organic-mineral fertilizer based on low-grade phosphorites and microflora of activated sludge. NaAWWystems: Physics, Chemistry, Mathematics. 2021; 19(2):391–405.

[5] Tagaev I A, Doniyarov N A, Andriyko L S, Murodov I N, & Asrorov A A. Acid treatment as a beneficiation method for phosphorite waste of Kyzylkum Phosphorite Plant. Voprosy Khimii i Khimicheskoi Tekhnologii. 2022; 4:75–83. https://doi.org/10.32434/0321-4095-2022-143-4-75-83

[6] Bazhirova K, Zhantasov K, Bazhirov T, Kolesnikov A, Toltebaeva Z, & Bazhirov N. Acid-Free Processing of Phosphorite Ore Fines into Composite Fertilizers Using the Mechanochemical Activation Method. Journal of Composites Science. 2024; 8(5):165. https://doi.org/10.3390/jcs8050165

[7] Paat A, Majak J, Karu V, & Hitch M. Fuzzy analytical hierarchy process based environmental, social and governance risks assessment for the future phosphorite mining in Estonia. Extractive Industries and Society. 2024; 17:101438. https://doi.org/10.1016/j.exis.2024.101438

[8] Muxammatova U, Ruxsora R, Durdona A, Jurabek S, & Temirov U. Production of Complex Fertilizers from Phosphorite Waste of the Central Kyzylkum. Excellencia: International Multi-Disciplinary Journal of Education. 2024; 2(9):569-573.

[9] Dhib R, Hamdaoui O, & Elaloui E. Problems of soapstock treatment of vegetable oil productions and their solutions. Journal of Oleo Science. 2016; 65(12):1001–1013. https://doi.org/10.5650/jos.ess16123

[10] Bensalah N, & Abdel-Wahab A. Study of refining wastewater pollution: Case of vegetable oil refining industry in Morocco. Journal of Environmental Chemical Engineering. 2016; 4(4):4153–4161. https://doi.org/10.1016/j.jece.2016.09.033

[11] Climate Policy Watcher. (n.d.). Impacts on wastewater treatment processes. Climate Policy Watcher. Retrieved August 12, 2025.

[12] Iris Publishers. (n.d.). Agricultural activity and chemical water pollution. Annals of Advanced Agricultural Sciences. 2025. https://irispublishers.com/aahds/fulltext/agricultural-activity-and-chemical-water-pollution.ID.000511.php

[13] Khalid S, Shahid M, Natasha Bibi I, Sarwar T, Shah A H, & Niazi N K. A Review of Environmental Contamination and Health Risk Assessment of Wastewater Use for Crop Irrigation with a Focus on Low and High-Income Countries. International Journal of Environmental Research and Public Health. 2018; 15(5):895. https://doi.org/10.3390/ijerph15050895

[14] Wikipedia. (n.d.). Nutrient pollution. In Wikipedia. Retrieved August 12, 2025. https://en.wikipedia.org/wiki/Nutrient_pollution

[15] Camargo J A. Fluoride toxicity to aquatic organisms: A review. Chemosphere. 2003; 50(3):251–264. https://doi.org/10.1016/S0045-6535(02)00498-8

[16] World Health Organization. Guidelines for drinking-water quality: Fourth edition incorporating the first addendum. Geneva: WHO. 2017. https://www.who.int/publications/i/item/9789241549950

[17] Jha S K, Mishra V K, Sharma D K, & Damodaran T. Fluoride in the environment and its metabolism in humans. In D. M. Whitacre (Ed.). Reviews of Environmental Contamination and Toxicology. Springer. 2011; 211:121–142. https://doi.org/10.1007/978-1-4419-8011-3_4

[18] Fawell J, Bailey K, Chilton J, Dahi E, Fewtrell L, & Magara Y. Fluoride in drinking-water. Geneva: World Health Organization. 2006. https://iris.who.int/handle/10665/43514

[19] Kalam S, Abu-Khamsin S A, Kamal M S, & Patil S. Surfactant adsorption isotherms: A review. ACS Omega. 2021; 6(48): 32342–32348. https://doi.org/10.1021/acsomega.1c04661

[20] Foo K Y, & Hameed B H. Insights into the modeling of adsorption isotherm systems. Chemical Engineering Journal. 2010; 156(1):2–10. https://doi.org/10.1016/j.cej.2009.09.013

[21] Murphy O P, Mayank V, Palanisamy P, & Kumar K V. Adsorption isotherms and design calculations for the optimization of adsorbent mass and contact time. ACS Omega. 2023; 8(20):17407–17430. https://doi.org/10.1021/acsomega.2c08155

[22] Azizian S. Kinetic models of sorption: A theoretical analysis. Journal of Colloid and Interface Science. 2004; 276(1):47–52. https://doi.org/10.1016/j.jcis.2004.03.048

[23] Ho Y S, & McKay G. Pseudo-second order model for sorption processes. Process Biochemistry. 1999; 34(5):451–465. https://doi.org/10.1016/S0032-9592(98)00112-5

[24] Chu K H, Hashim M A, Zawawi M H, & Bollinger J-C. The Weber–Morris model in water contaminant adsorption: Shattering long-standing misconceptions. Journal of Environmental Chemical Engineering. Elsevier BV. 2025. https://doi.org/10.1016/j.jece.2025.117266

[25] Weber WJ, & Morris JC. Kinetics of Adsorption on Carbon from Solution. Journal of the Sanitary Engineering Division. 1963; 89:31-59.

[26] Shamuratov Sanzharbek, Umid Baltaev, Umarbek Alimov, Namazov Shafoat, Sherzod Kurambaev, and Bazar Ibadullaev. Utilization Process Research of the Soap Industry Acid Waste Water with High Carbonate Phosphorite of Central Kyzylkum. E3S Web of Conferences. EDP Sciences. 2021. https://doi.org/10.1051/e3sconf/202126404079

[27] Shamuratov Sanjarbek, Umid Baltaev, Sanobar Achilova, Umarbek Alimov, Shafoat Namazov, and Najimuddin Usanbaev. Enhancement of Availability of High Calcareous Phosphorite by Neutralization of Acid Effluent and Composting of Cattle Manure. E3S Web of Conferences. EDP Sciences. 2023. https://doi.org/10.1051/e3sconf/202337703004

[28] Shamuratov Sanjarbek, Umid Baltaev, Olga Myachina, Umarbek Alimov, Elyor Atashev, and Tokhir Kuramboev. Agrochemical Efficiency of Slow Release Phosphate Fertilizers Derived on the Base of Phosphorite Activation. E3S Web of Conferences. EDP Sciences. 2023. https://doi.org/10.1051/e3sconf/202343403014

[29] Sotimboev Ilgizarbek, Umidbek Baltaev, Sanjarbek Shamuratov, Ruzimov Shamsiddin, Umarbek Alimov, and Mirzabek Saporboyev. Technical and Economic Efficiency of Processing Acidic Wastewater from the Oil and Fat Industry into Necessary Agricultural Products. E3S Web of Conferences. EDP Sciences. 2024. https://doi.org/10.1051/e3sconf/202456303072

[30] Turatbekova Aidai, Malokhat Abdukadirova, Sanjarbek Shamuratov, Bakhodir Latipov, Mirzabek Saporboyev, Jafar Shamshiyev, and Yusuf Makhmudov. Investigation of the Effect of Fertilizers on the Biochemical and Physical Characteristics of Carrots (Daucus Carota L.). E3S Web of Conferences. EDP Sciences. 2024. https://doi.org/10.1051/e3sconf/202456303074

[31] Yuldasheva A, Shamuratov S, Kurambayev S, & Radjabov M. Mathematical Analysis of CaO Content Variation in Acidic Wastewater and Mineralized Mass Mixture from Central Kyzylkum Phosphorite Based on Exponential Decay Model. Kompleksnoe Ispolzovanie Mineralnogo Syra = Complex Use of Mineral Resources. 2025; 339(4):79–86. https://doi.org/10.31643/2026/6445.42

[32] Atashev E. Decomposition of Magnesite-Sparing Waste in Sulfuric Acid with a High Concentration: Empirical Modeling and Determination of Optimal Conditions. Kompleksnoe Ispolzovanie Mineralnogo Syra = Complex Use of Mineral Resources. 2025; 339(4):71–78. https://doi.org/10.31643/2026/6445.41

Crossref
DOI: 10.31643/2027/6445.32
Mining & Mineral Processing

Sigmoid Neutralization Response of Acidic Soapstock Waste by Mineralized Phosphorite Residues: A 4-Parameter Logistic Approach

[1*] Shamuratov S.X., [1]Baltayev U.S., [2]Alimov U.K., [3]Jabbarov M.E., [4]Madaminov A.E.

[1]Urgench State University named after Abu Rayhon Biruni, Uzbekistan
[2]Institute of General and Inorganic Chemistry, Academy of Sciences of the Republic of Uzbekistan, Uzbekistan
[3]Mamun University, Khiva, Uzbekistan
[4]Urgench State Pedagogical Institute, Uzbekistan

** Corresponding author email: shamuratovsx@gmail.com*

Received: *December 9, 2025*
Peer-reviewed: *January 6, 2026*
Accepted: *January 16, 2026*

ABSTRACT

This study investigates the neutralization behavior of an acidic wastewater (AWW)–mineralized mass (MM) system at mass ratios ranging from 100:10 to 100:40, processed at 333 K for 30 min. The evolution of pH as a function of MM dosage and the corresponding CaO content (%) in the solid phase were quantitatively evaluated. The solution pH increased sigmoidally from 4.10 to 7.30, while the CaO content rose from 23.92% to 36.96%, approaching a saturation plateau at higher MM dosages. The pH–dose relationship was described using four-parameter logistic (4PL), Gompertz, and Weibull models, all showing a high goodness of fit ($R^2 \geq 0.97$). Model comparison based on AICc and BIC criteria indicated that the Gompertz model provided the best statistical performance, whereas the 4PL model ensured clearer physicochemical interpretability. A strong positive correlation between pH and CaO content was established (Pearson $r = 0.9649$, $n = 7$, $p < 0.001$), enabling estimation of CaO content from pH values. Numerical inversion of the 4PL model combined with a multi-model ensemble approach was used to determine optimal MM dosages for target pH levels. The recommended operating conditions were identified as 100:32 for pH 6.5, 100:36 for pH 6.8, and 100:38 for pH 7.0, with a stabilization zone observed at 100:37–100:40.

Keywords: neutralization, dose–response, 4-parameter logistic (4PL), pH–CaO correlation, operational optimization.

Information about authors:

Shamuratov Sanjarbek Xusinbay ugli — *Doctor of Philosophy in Technical Sciences, Associate Professor at the Faculty of Chemical Technology, Urgench State University named after Abu Rayhon Biruni, Urgench, H. Olimjon Street 14, 220100, Uzbekistan. Email: shamuratovsx@gmail.com; ORCID ID: https://orcid.org/0000-0002-1040-1807*

Baltaev Umidbek Sotimbayevich — *Candidate of Technical Sciences, doctoral student in the Faculty of Chemical Technologies, Urgench State University named after Abu Rayhon Biruni, Urgench, H. Olimjon Street 14, 220100, Uzbekistan. Email: umid.bo@urdu.uz; ORCID ID: https://orcid.org/0009-0004-5636-3318*

Alimov Umarbek Kadirbergenovich — *Doctor of Technical Sciences, leading scientific researcher at the Institute of General and Inorganic Chemistry, Academy of Sciences of the Republic of Uzbekistan, 77, Mirzo Ulugbek, Tashkent 100170, Uzbekistan. Email: umaralihonalimov@mail.ru; ORCID ID: https://orcid.org/0000-0001-5608-5304*

Jabbarov Majidbek Erzodovich — *Non-government Educational Institution Mamun University, Khiva, Uzbekistan. Email: jabbarovmajidbek2@gmail.com; ORCID ID: https://orcid.org/ 0009-0001-5987-0057*

Madaminov Azimbek Egamberganovich — *Doctor of Philosophy in Pedagogical Sciences, Associate Professor in the Faculty of Natural and Applied Sciences, Urgench State Pedagogical Institute 1-A, Gurlan str, Urgench city, 220100, Uzbekistan. Email: azimbekmadaminov66@gmail.com; ORCID ID: https://orcid.org/0000-0002-3482-8071*

Introduction

Acidic wastewater generated during the processing of soapstock in the fat-and-oil industry represents a significant environmental challenge due to its low pH, high salt content, and elevated concentrations of organic and inorganic contaminants [[1], [2], [3]]. Improper handling or disposal of such effluents may lead to soil acidification, groundwater contamination, and adverse effects on aquatic ecosystems. Therefore, the development of effective and resource-efficient neutralization strategies remains an important task for both environmental protection and industrial sustainability [[4], [5], [6], [7]].

In parallel, large volumes of mineralized phosphorite residues are accumulated during phosphate mining and beneficiation, particularly in

the Central Kyzylkum region [[8], [9], [10]]. These low-grade materials are typically characterized by high CaO content and limited direct industrial use, resulting in long-term storage and associated environmental risks. Recent studies have highlighted the potential of such calcium-rich mineral residues to serve as neutralizing agents for acidic waste streams, thereby enabling simultaneous wastewater treatment and waste valorization [[11], [12], [13], [14]].

Neutralization processes involving heterogeneous mineral systems often exhibit non-linear behavior due to buffering effects, phase transformations, and saturation phenomena [[15], [16], [17]]. However, many previous studies have relied on linear or simplified empirical approaches, which do not adequately describe the full pH response over a wide range of reagent dosages. In particular, the sigmoidal nature of pH variation during neutralization and its quantitative relationship with solid-phase CaO enrichment have received limited attention in the context of waste-derived mineral reagents [[18], [19]].

The objective of this study is to investigate the neutralization of acidic wastewater using mineralized phosphorite mass from the Central Kyzylkum region, with a focus on the sigmoidal pH–dose response and its mathematical description. By applying four-parameter logistic (4PL), Gompertz, and Weibull models, the work aims to identify optimal operating mass ratios and to establish a quantitative relationship between solution pH and CaO content in the solid phase. This approach provides a predictive basis for process optimization under experimentally defined conditions.

Experimental part

Materials. As feedstocks, the present study used AWW produced during the acid treatment of cottonseed soapstock at "Urganch Yog'-Moy" JSC and MM stored in the Central Kyzylkum region. According to the results of laboratory analyses, the AWW had pH 2.0 (strongly acidic), COD of 947.2 mg $O_2 \cdot L^{-1}$, BOD_5 of 380.2 mg $O_2 \cdot L^{-1}$, and total hardness of 140.5 mg-eq$\cdot L^{-1}$. Major cations were Na^+ (43,158 mg$\cdot L^{-1}$), Mg^{2+} (1,824 mg$\cdot L^{-1}$), Ca^{2+} (300 mg$\cdot L^{-1}$), and NH_4^+ (100 mg$\cdot L^{-1}$), while major anions were SO_4^{2-} (48,145 mg$\cdot L^{-1}$), Cl^- (38,116 mg$\cdot L^{-1}$), and HCO_3^- (3,446 mg$\cdot L^{-1}$). Besides, AWW contained 2.1 wt% total organics and 1.64 wt% total SO_3. The phosphorite residues of the Central Kyzylkum region represented low-grade mineralized mass of the following composition, wt%: P_2O_5 15.09, CaO 43.17, Al_2O_3 1.22, Fe_2O_3 1.34, MgO 1.21, F 1.7, CO_2 14.01, SO_3 2.17, and moisture 9.11. Due to the high CaO content, these residues can be used as the basic neutralizing agent for AWW treatment. The combined use of AWW and MM not only reduces ecological hazards but also opens up new sources of secondary raw materials for fertilizers and other products [[20], [21], [22], [23]].

In order to investigate neutralization, AWW and MM were mixed at different mass ratios from 100:10 to 100:40, enabling quantitative assessment of pH changes upon increasing phosphorite addition. Mixing was performed at 333 K (≈60 °C) to accelerate acid-base reactions and ensure a homogeneous medium. Each experiment was carried out under intense agitation for 30 min, during which the liquid phase reached quasi-equilibrium. Afterwards, the mixtures were dried at 353 K (≈80 °C) to eliminate moisture and accurately determine CaO in the final solid phase; such drying conditions also contribute to residual acid reactions being completed [[22], [23]]. In systematic variation through the mass ratios, the pH increased from 4.10 to 7.30, while the content of CaO in the solid phase increased from 23.92 wt% to 36.96 wt% (Table 1).

Methods. All experimental procedures reported in this study were carried out by the authors under laboratory conditions. Standard analytical methods cited from the literature were used solely as reference protocols for measurements, whereas sample preparation, neutralization experiments, data acquisition, and data processing were performed independently within the framework of this work.

This methodological approach offered the possibility to obtain a complete picture of the neutralization process, find the optimum mass ratio, and obtain reliable data for mathematical modeling. Moreover, experimental conditions were chosen considering realistic technological parameters in accordance with industrial reprocessing practice. pH and CaO content were selected as main performance indicators of the neutralization efficiency. pH was measured using a laboratory pH meter with an ion-selective electrode; the instrument was calibrated before each run with standard buffer solutions (pH 4.00, 7.00, and 9.18).

In order to avoid the effects of temperature, the measurements were performed after attaining equilibrium at 333 K for every mixture.

Table 1 - Composition of neutralization products derived from acidic wastewater (AWW) and the Central Kyzylkum mineralized phosphorite mass

Mass ratio (AWW:MM)	pH	CaO, %
100:10	4.1	23.92
100:15	4.81	27.95
100:20	5.62	28.66
100:25	5.9	32.68
100:30	6.33	35.48
100:35	6.74	36.74
100:40	7.3	36.96

The measurement of the content of CaO was done using the traditional method of complexometric titration using an EDTA solution to titrate calcium ions (Ca^{2+}), and murexide indicator. To maintain analytical accuracy, each assay was carried out in triplicate and mean values were provided as a result. Additionally, some of the samples were confirmed through the gravimetric method, where calcium was precipitated from solution as $CaCO_3$, and the mass correlation between that precipitation and the amount of CaO was determined mathematically via stoichiometry. The estimated overall analytical uncertainty was controlled to ±0.02 for pH and ±0.3% for CaO. The use of both complexometric and gravimetric methods enabled the researcher to collect a reliable dataset that is suitable for the mathematical modeling of neutralization reactions. For a mechanistic yet parsimonious description of the process, the four-parameter logistic (4PL) model was adopted, as it captures the sigmoidal pH–dose dependence effectively. The general form of the 4PL used in this work is:

$$\boldsymbol{y(x) = A1 + \frac{A2 - A1}{1 + (\frac{x}{x_0})^{-n}}}$$

Here, *A1* denotes the initial lower asymptote (acid-region pH), *A2* the upper asymptote (neutral/alkaline region), *x* the half-response mass (dose at which *pH≈(A1+A2)/2*), and *n* the transition steepness, which reflects buffer capacity and the sharpness of the reaction front [24].

Parameter estimation was performed by nonlinear least squares; starting values were anchored to the observed minimum and maximum pH, and 95% confidence intervals were obtained by bootstrap resampling (≥1000 replicates) [25]. Model selection relied on AICc [26] and BIC [27], with the lowest scores indicating the preferred specification. As alternatives to 4PL, Weibull and Gompertz functions were also evaluated. Weibull model (four-parameter, CDF form):

$$y\,(x) = A2 - (A2 - A1)e^{-(\frac{x}{\lambda})^{\beta}}$$

Here, λ is the scale parameter, and β is the shape parameter; in practice, the Weibull specification captures the gradual, decelerating approach to the plateau as the dose increases.

Gompertz model.

$$y\,(r) = A1 + (A2 - A1)\,e^{-exp[-k(x-x_0)]}$$

This model describes an initial lag phase, a period of accelerating growth, and a final brief saturation stage; it is thus better suited to asymmetric response curves [28]. All models were validated by residual diagnostics (residuals vs. fitted values, Q–Q plots, and Cook's distance) and weighted regression was applied when heteroscedasticity was detected. The key benefit of the 4PL formulation derives from the physicochemical interpretability of the parameters: A1 corresponds to the starting acidic baseline, A2 to the final neutral/alkaline plateau, x0 to the half-response dose (i.e., operational mass ratio at the midpoint of the process), and n describes the transition steepness (i.e., process sensitivity), thereby elevating the analysis of neutralization from simple empirical observation to a predictive, parametric basis. In this regard, numerical inversion of the 4PL model was also implemented to calculate the required mass ratio for a given target pH, which allows for actionable decisions in industrial practice. In all, the 4PL constitutes a rigorous mathematical representation of full sigmoidal neutralization behavior and returns results that are at once reliable and practically useful, while Weibull and Gompertz provide supporting checks and further insight when asymmetry in the process response is present.

Although standard analytical approaches reported in the literature were used as methodological references, all experimental work and data presented in this article were generated by the authors.

Results and Discussion

The results presented below were obtained exclusively from experiments conducted in this study. All data points correspond to independently performed neutralization tests at defined AWW:MM mass ratios, and no secondary or literature-derived datasets were used in the analysis.

The AWW:MM ratios tested in this research ranged from 100:10 to 100:40, all trials carried out on day 333 K; all agitation times lasted 30 minutes and were performed according to protocols described in the 'Materials and Methods' section. The solution's pH was monitored after each experiment, and the mass fraction of CaO contained within the solid portion of the solution was computed and expressed as a percentage of that solution mass. Solutions were two-point calibrated with buffers, one at pH 4.00 and the other at pH 7.00, before obtaining the pH measurements of each solution; all solutions were corrected for temperature variations by using ATC. The electrodes utilized for pH measurements were cleaned before each use, and electrode drift was accounted for. The results of CaO determinations were obtained through STN methods; sample treatments and measurements of ions using the ion-selective electrode were consistently performed in the same manner from run to run. The major contributors to uncertainty associated with analysing the data were identified as, but are not limited to, electrode drift, the effects of ionic strength, and the potential for heterogeneity in the samples being analysed; therefore, the responses obtained from calibrating and controlling test solutions were completed before each measurement series began. The resulting raw dataset covered AWW:MM points 100:10, 100:15, 100:20, 100:25, 100:30, 100:35, and 100:40. The corresponding pH values were 4.10, 4.81, 5.62, 5.90, 6.33, 6.74, and 7.30, and CaO contents were 23.92%, 27.95%, 28.66%, 32.68%, 35.48%, 36.74%, and 36.96%, respectively (Table 1). Descriptive statistics confirmed data stability and controlled dispersion. For pH, N = 7, min = 4.10, max = 7.30, mean = 5.829, SD = 1.105, and CV = 18.95% (Table 2).

Table 2 - Descriptive statistics for pH and CaO (%): N, Min, Max, Mean, SD, CV (%)

Metric	N	Min	Max	Mean	SD*	CV, %
pH	7	4.10	7.30	5.829	1.105	18.95
CaO, %	7	23.92	36.96	31.770	5.035	15.85

*SD — sample standard deviation; CV (%) = SD / Mean × 100.

For CaO, N=7, a minimum of 23.92% to a maximum of 36.96%. The mean CaO content was 31.770% with SD=5.035 and CV=15.85%. This data preliminarily indicates that there is a sigmoidal increase with respect to the pH levels and near-saturation of CaO. The dataset is sufficiently informative for future stages of modelling. The increase of the AWW:MM ratio caused an increase in the pH of the solutions. An initial monotonic increase and a distinct sigmoidal response was seen as the AWW:MM ratio was increased from 100:10 to 100:40. The growth rate of the pH-response increased between the AWW:MM ratios of 100:20 - 100:30, followed by a plateau from 100:35 - 100:40. This response demonstrated that the Neutralisation process occurred stepwise during Buffering and Carbonation. Four-parameter Logistic, Gompertz, and Weibull Models were fitted to the pH-dose data according to the procedures and constraints set forth in Materials and Methods; these three models all fitted the data adequately with minor differences in goodness of fit. The Gompertz model yielded the lowest AICc and BIC and thus emerged as the preferred specification; its $R^2 = 0.989$ indicates a high explanatory power. The Weibull model achieved $R^2 = 0.987$ with competitive AICc/BIC values. Although the 4PL model also produced $R^2 \approx 0.989$, it was penalized more strongly by AICc and therefore ranked slightly lower. Figure 1 presents the observed points and the three fitted curves on a single plot, clearly illustrating the sigmoidal trajectory.

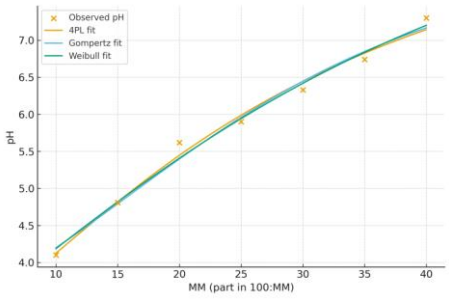

Figure 1 - pH vs. MM: observed data points with fitted 4PL, Gompertz, and Weibull curves

Figure 2 residual distribution for the best-fitting model, confirming the absence of systematic patterns.

Random dispersion of the residuals around zero indicates that the model is correctly specified. The physical interpretation of the 4PL parameters is convenient: the lower asymptote is $A_1 \approx 3.03$ and the upper asymptote is $A_2 \approx 9.50$. For 4PL, the half-response dose EC_{50} (x_0) ≈ 27.93, meaning that the response reaches its midpoint at this dose, and the slope parameter n ≈ 1.55 reflects a moderately sharp transition. In the Gompertz model, the upper asymptote is a ≈ 8.82, while the shape parameter c ≈ 0.043 indicates a gradually advancing neutralization front; the half-response occurs at x_{50} ≈ 11.87, i.e., at a lower dose. For the Weibull model,

the upper asymptote is a ≈ 9.50 and the shape parameter c ≈ 0.659, capturing dynamics that accelerate initially and then decelerate; the corresponding half-response is x_{50} ≈ 14.18, which marks the dose yielding the median response. Table 3 reports the goodness-of-fit indicators—R^2, AICc, and BIC—enabling direct comparison among the models.

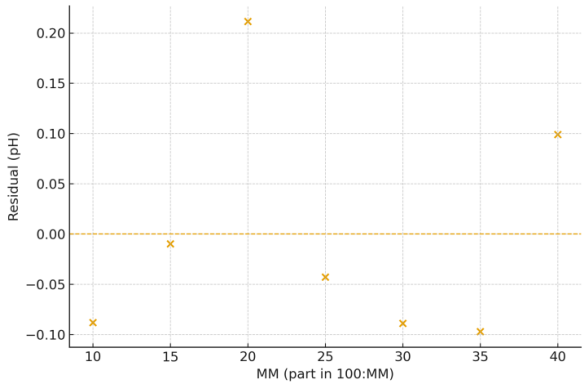

Figure 2 - Residuals for the best-fitting model (Weibull).

Random dispersion of the residuals around zero indicates that the model is correctly specified. The physical interpretation of the 4PL parameters is convenient: the lower asymptote is $A_1 \approx 3.03$, and the upper asymptote is $A_2 \approx 9.50$. For 4PL, the half-response dose EC_{50} (x_0) ≈ 27.93, meaning that the response reaches its midpoint at this dose, and the slope parameter n ≈ 1.55 reflects a moderately sharp transition. In the Gompertz model, the upper asymptote is a ≈ 8.82, while the shape parameter c ≈ 0.043 indicates a gradually advancing neutralization front; the half-response occurs at x_{50} ≈ 11.87, i.e., at a lower dose. For the Weibull model, the upper asymptote is a ≈ 9.50 and the shape parameter c ≈ 0.659, capturing dynamics that accelerate initially and then decelerate; the corresponding half-response is x_{50} ≈ 14.18, which marks the dose yielding the median response. Table 3 reports the goodness-of-fit indicators—R^2, AICc, and BIC—enabling direct comparison among the models.

The table also includes an interpretation of the EC_{50} (x_0) and n parameters to guide practical dose selection. While the Gompertz model attains the lowest AICc/BIC, indicating the statistically preferred specification, the 4PL parameters remain the most operationally intuitive.

Table 3 - Parameter estimates and goodness-of-fit statistics for pH models (4PL, Gompertz, Weibull)

Model	4PL	Gompertz	Weibull
Lower asymptote (y↓)	3.03	~0.00	~0.00
Upper asymptote (y↑)	9.50	8.82	9.50
EC50, x_{50}	27.93	11.87	14.18
n (slope/shape)	1.55	0.043	0.659
R^2	0.989	0.989	0.987
AICc	−2.998	−17.255	−15.903
BIC	−23.214	−25.417	−24.066

Accordingly, we recommend balancing statistical optimality with physicochemical interpretability. For example, in production terms, the 4PL x_0 points to the transition region around pH = 6.2–6.3. By contrast, Gompertz and Weibull emphasize the early-transition segment more strongly and are useful for assessing reagent economy. Residual diagnostics confirmed adequacy across the main domain, with minor edge deviations that may arise from buffer phases and solid-phase formation. Overall, the pH–dose response corroborates the multistage nature of neutralization. In the next step, the CaO–dose results are integrated to recommend a clear optimal dose window. In the AWW–MM system, the association between pH and CaO (%) is strongly positive: Pearson r = 0.96490, n = 7, p = 0.000435 (Table 4).

Table 4 - Pearson correlation (pH vs. CaO), significance, sample size, 95% confidence interval for r, and linear regression summary (slope, intercept, R^2).

Metric	Value
Pearson r	0.96490
p-value	0.000435
n (observations)	7
95% CI (r, lower)	0.77494
95% CI (r, upper)	0.99498
Linear slope, dCaO/dpH	4.39823
Slope 95% CI (lower)	3.02215
Slope 95% CI (upper)	5.77431
Intercept (CaO % at pH = 0)	6.13460
R^2	0.93104

This implies that as pH increases, the CaO fraction in the solid phase also increases monotonically; the 95% confidence interval for the Pearson correlation is [0.77494, 0.99498]. A simple linear regression (CaO = 6.13460 + 4.39823·pH) yielded R^2 = 0.93104, indicating that ≈93% of the variance in CaO is explained by pH (Figure 3). In the scatter plot of Figure 3 (markers = observations), the least-squares regression line shows that a one-unit increase in pH raises CaO by ~4.40% (95% CI for the slope: [3.02215, 5.77431]).

These quantitative results are mechanistically consistent with: (a) consumption of free acidity during neutralization, leading to a pH rise; (b) increasing buffering strength (phosphate–calcium and carbonate buffers) as pH grows; (c) formation of carbonate and Ca–phosphate phases (e.g., brushite/apatite), which transfers Ca species to the solid phase and increases CaO (%); and (d) emergence of a plateau at high pH due to solubility constraints and slower phase-growth kinetics.

As a result, CaO can be practically predicted from on-line pH control; for example, at pH ≈ 6.8, CaO≈6.13460+4.39823×6.8≈36.0%. The strong, monotonic pH–CaO association, together with the plateau observed in the upper segment of the pH–dose curve (zone of sharply diminishing marginal gains) forming around 100:37–100:40, informed the dose selection for target pH. Accordingly, the required doses were obtained by numerical inversion of the 4-parameter logistic (4PL) model (the primary specification described in Materials and Methods) and stabilized via triangulation with Gompertz, Weibull, and local linear interpolation (see Table 5).

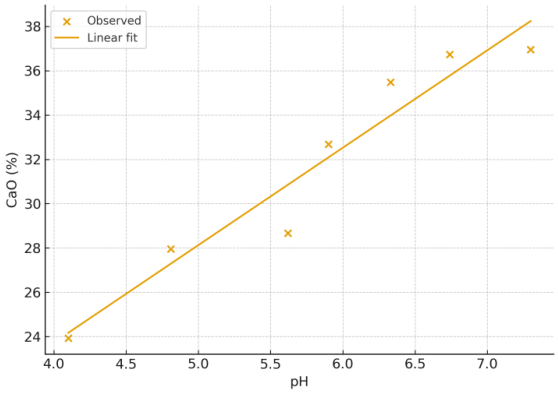

Figure 3 - Relationship between pH and CaO (%) in the AWW–MM system (n = 7).
Markers indicate observations; line shows the least-squares linear fit (CaO = 6.13460 + 4.39823·pH; R^2 = 0.93104; p < 0.001).

All computations were interpreted strictly within the observed range (MM = 10–40). For each target pH, the ensemble median across the four approaches was adopted as the recommended dose, whereas the model min–max defined the operational control window.

Table 5 - Target pH → recommended dose (100:MM), based on 4PL inversion with multi-model triangulation (Gompertz, Weibull, and local linear interpolation)

Target pH	6,5	6,8	7.0
4PL (MM)	30.67	34.63	37.63
Gompertz (MM)	32.55	36.38	38.74
Weibull (MM)	32.00	35.52	37.57
Linear interp. (MM)	32.07	35.54	37.32
Ensemble median (MM)	32.07	35.98	37.60
Recommended (100:MM)	100:32	100:36	100:38*
Operational window	100:31–100:33	100:35–100:37	100:37–100:40

Accordingly, the most suitable settings are pH 6.5 → ~100:32, pH 6.8 → ~100:36, and pH 7.0 → ~100:38. Because the last setting lies very close to the onset of the plateau, a cost-aware operating policy is to start at 100:37 and, under on-line pH control, adjust 37 → 38 only if required.

Conclusions

The neutralization of acidic wastewater by the Central Kyzylkum mineralized mass exhibited a clear sigmoidal pH response within the investigated mass ratio range of 100:10–100:40. Under the applied conditions (333 K, 30 min), the solution pH increased from 4.10 to 7.30, while the CaO content in the solid phase rose from 23.92% to 36.96%, indicating progressive incorporation of calcium-bearing components during neutralization.

Mathematical description of the pH–dose relationship using four-parameter logistic (4PL), Gompertz, and Weibull models demonstrated a high goodness of fit ($R^2 \geq 0.97$). Although the Gompertz model showed the most favorable statistical criteria (AICc/BIC), the 4PL model provided parameters with clearer physicochemical interpretation, enabling identification of the transition region and the onset of saturation. Based on model inversion and multi-model comparison, the optimal operating mass ratios were determined as 100:32 for pH 6.5, 100:36 for pH 6.8, and 100:38 for pH 7.0, with a stabilization (plateau) zone observed at 100:37–100:40.

A strong positive correlation between pH and CaO content was established (Pearson $r = 0.9649$, $p < 0.001$), demonstrating that pH can serve as a reliable operational indicator for estimating CaO enrichment in the solid phase under the investigated conditions. This relationship provides a quantitative basis for process control and dose selection during neutralization.

The conclusions of this study are limited to experimentally measured pH and CaO parameters and their mathematical interpretation. Potential effects related to corrosion behavior, environmental impact, carbonation processes, and the agronomic suitability of the solid product were not evaluated and therefore remain outside the scope of the present work. These aspects should be addressed in future investigations.

Conflicts of interest. On behalf of all authors, the corresponding author states that there is no conflict of interest.

CRediT author statement: **S. Shamuratov**: Conceptualization, Methodology, Software, Data curation, Writing draft preparation, Supervision, Software, Validation, Reviewing and Editing; **U. Baltaev, U. Alimov, M. Jabbarov, A. Madaminov**: Visualization, Investigation.

Formatting of funding sources. This research did not receive any specific grant from funding agencies in the public, commercial, or not-for-profit sectors.

Cite this article as: Shamuratov SX, Baltaev US, Alimov UK, Jabbarov ME, Madaminov AE. Sigmoid Neutralization Response of Acidic Soapstock Waste by Mineralized Phosphorite Residues: A 4-Parameter Logistic Approach. Kompleksnoe Ispolzovanie Mineralnogo Syra = Complex Use of Mineral Resources. 2027; 342(3):80-89. https://doi.org/10.31643/2027/6445.32

Қышқыл сабын қалдықтарының сигмоидты бейтараптандыру реакциясында минералданған фосфорит қалдықтарын пайдалану: 4 параметрлі логистикалық тәсіл

[1*]Шамуратов С.Х., [1]Балтаев У.С., [2]Алимов У.К., [3]Жаббаров М.Э., [4]Мадаминов А.Э.

[1]Абу Райхон Беруни атындағы Ургенч мемлекеттік университеті, Өзбекстан
[2]Өзбекстан Республикасы Ғылым академиясының Жалпы және бейорганикалық химия институты, Өзбекстан
[3]Мамун университеті, Хива, Өзбекстан
[4]Ургенч мемлекеттік педагогикалық институты, Өзбекстан

Мақала келді: *9 желтоқсан 2025*
Сараптамадан өтті: *6 қаңтар 2026*
Қабылданды: *16 қаңтар 2026*

ТҮЙІНДЕМЕ

Бұл зерттеуде 333 К температурада және 30 минут өңдеу уақытында 100:10–100:40 массалық қатынастарда «қышқылды ағынды су (AWW) – минералданған масса (ММ)» жүйесінің бейтараптану процесінің жүрісі зерттелді. ММ дозасына байланысты pH өзгерісі және қатты фазадағы CaO мөлшері (%) сандық түрде бағаланды. Ерітінді pH мәні 4,10-нан 7,30-ға дейін сигмоидалы түрде артты, ал CaO мөлшері 23,92%-дан 36,96%-ға дейін өсіп, ММ-нің жоғары дозаларында қанығу платосына жақындады. «pH–доза» тәуелділігі төртпараметрлі логистикалық (4PL), Гомпертц және Вейбулл модельдері арқылы сипатталды, олардың барлығы жоғары сәйкестік дәрежесін көрсетті ($R^2 \geq 0,97$). AICc және BIC критерийлері негізінде жүргізілген модельдерді салыстыру нәтижесінде Гомпертц моделі ең жақсы статистикалық көрсеткіштерге ие екені анықталды, ал 4PL моделі физика-химиялық тұрғыдан неғұрлым айқын интерпретацияланатын параметрлерді қамтамасыз етті. pH пен

	CaO мөлшері арасында күшті оң корреляция орнатылды (Пирсон коэффициенті r = 0,9649, n = 7, p < 0,001), бұл CaO мөлшерін pH мәндері арқылы бағалауға мүмкіндік береді. 4PL моделін сандық кері есептеу мультимодельді ансамбльдік тәсілмен біріктіріліп, берілген pH деңгейлері үшін ММ-нің оңтайлы дозаларын анықтау мақсатында қолданылды. Ұсынылған жұмыс режимдері pH 6,5 үшін 100:32, pH 6,8 үшін 100:36 және pH 7,0 үшін 100:38 болып анықталды, ал тұрақтану аймағы 100:37–100:40 аралығында байқалды.
	Түйін сөздер: бейтараптандыру, доза–реакция тәуелділігі, төрт параметрлі логистикалық модель (4PL), pH–CaO корреляциясы, технологиялық процесті оңтайландыру.
Шамұратов Санжарбек Хусинбай ұлы	***Авторлар туралы ақпарат:*** *Техника ғылымдарының философия докторы, Әбу Райхан Беруни атындағы Үргеніш мемлекеттік университетінің химия-технология факультетінің доценті, Үргеніш қаласы, Х.Олимжон көшесі 14, 220100, Өзбекстан. Email: shamuratovsx@gmail.com; ORCID ID: https://orcid.org/0000-0002-1040-1807*
Балтаев Үмітбек Сотымбайұлы	*Техника ғылымдарының кандидаты, Әбу Райхан Беруни атындағы Үргеніш мемлекеттік университетінің химиялық технологиялар факультетінің докторанты, 220100, Х.Олимжон көшесі 14, Үргеніш, Өзбекстан. Email: umid.bo@urdu.uz; ORCID ID: https://orcid.org/0009-0004-5636-3318*
Алимов Умарбек Кадирбергенович	*Техника ғылымдарының докторы, Өзбекстан Республикасы Ғылым академиясының Жалпы және бейорганикалық химия институтының жетекші ғылыми қызметкері, 100170, Мирзо Улугбек, 77, Ташкент, Өзбекстан. Email: umaralihonalimov@mail.ru; ORCID ID: https://orcid.org/0000-0001-5608-5304*
Жаббаров Мажидбек Ерзодович	*Мамун университеті мемлекеттік емес білім беру мекемесі, Хиуа, Өзбекстан. Email: jabbarovmajidbek2@gmail.com; ORCID ID: https://orcid.org/ 0009-0001-5987-0057*
Мадаминов Азимбек Эгамберганович	*Педагогика ғылымдарының философия докторы, Үргеніш мемлекеттік педагогикалық институтының жаратылыстану және қолданбалы ғылымдар факультетінің доценті, Гүрлен көшесі, 1-А, Үргеніш, 220100, Өзбекстан. Email: azimbekmadaminov66@gmail.com; ORCID ID: https://orcid.org/0000-0002-3482-8071*

Сигмоидная нейтрализационная реакция кислых отходов соапстока с использованием минерализованных остатков фосфоритов: 4-параметрический логистический подход

[1*]Шамуратов С.Х., [1]Балтаев У.С., [2]Алимов У.К., [3]Жаббаров М.Э., [4]Мадаминов А.Э.

[1]Ургенчский государственный университет имени Абу Райхона Беруни, Узбекистан
[2]Институт общей и неорганической химии Академии наук Республики Узбекистан, Ташкент
[3]Университет Мамун, Хива, Узбекистан
[4]Ургенчский государственный педагогический институт, Узбекистан

Поступила: *9 декабря 2025*
Рецензирование: *6 января 2026*
Принята в печать: *16 января 2026*

АННОТАЦИЯ

В настоящем исследовании изучается поведение процесса нейтрализации системы «кислотные сточные воды (AWW) – минерализованная масса (ММ)» при массовых соотношениях от 100:10 до 100:40 при температуре 333 K и продолжительности обработки 30 мин. Количественно оценена зависимость изменения pH от дозировки ММ, а также соответствующее содержание CaO (%) в твердой фазе. Значение pH раствора возрастало по сигмоидальной зависимости от 4,10 до 7,30, в то время как содержание CaO увеличивалось с 23,92% до 36,96%, приближаясь к плато насыщения при более высоких дозировках ММ. Зависимость «pH–доза» была описана с использованием четырехпараметрической логистической (4PL), моделей Гомпертца и Вейбулла, которые показали высокую степень аппроксимации ($R^2 \geq 0,97$). Сравнение моделей на основе критериев AICc и BIC показало, что модель Гомпертца обеспечивает наилучшие статистические показатели, тогда как модель 4PL обладает более четкой физико-химической интерпретируемостью. Установлена сильная положительная корреляция между pH и содержанием CaO (коэффициент Пирсона r = 0,9649, n = 7, p < 0,001), что позволяет оценивать содержание CaO по значениям pH. Численное обращение модели 4PL в сочетании с мультимодельным ансамблевым подходом было использовано для определения оптимальных доз ММ при заданных значениях pH. Рекомендуемые рабочие условия составили 100:32 для pH 6,5, 100:36 для pH 6,8 и 100:38 для pH 7,0, при этом зона стабилизации наблюдалась в диапазоне 100:37–100:40.

Ключевые слова: нейтрализация, зависимость доза–отклик, четырёхпараметрическая логистическая модель (4PL), корреляция pH–CaO, оптимизация технологического процесса.

Шамуратов Санжарбек Хусинбай угли

Информация об авторах:
Доктор философии по техническим наукам, доцент химико-технологического факультета Ургенчского государственного университета имени Абу Райхана Беруни, 220100, улица Х. Олимджона, 14, Ургенч, Узбекистан. Email: shamuratovsx@gmail.com; ORCID ID: https://orcid.org/0000-0002-1040-1807

Балтаев Умидбек Сотимбаевич	*Кандидат технических наук, докторант факультета химических технологий Ургенчского государственного университета имени Абу Райхана Беруни, 220100, улица Х. Олимджона, 14, Ургенч, Узбекистан. Email: umid.bo@urdu.uz; ORCID ID: https://orcid.org/0009-0004-5636-3318*
Алимов Умарбек Кадирбергенович	*Доктор технических наук, ведущий научный сотрудник Института общей и неорганической химии Академии наук Республики Узбекистан, 100170, Мирзо Улугбек, 77, Ташкент Узбекистан. Email: umaralihonalimov@mail.ru; ORCID ID: https://orcid.org/0000-0001-5608-5304*
Жаббаров Мажидбек Ерзодович	*Негосударственное образовательное учреждение Мамунский университет, Хива, Узбекистан. Email: jabbarovmajidbek2@gmail.com; ORCID ID: https://orcid.org/0009-0001-5987-0057*
Мадаминов Азимбек Эгамберганович	*Доктор философии по педагогическим наукам, доцент факультета естественных и прикладных наук Ургенчского государственного педагогического института, 220100, ул. Гурлана, 1-А, Ургенч, Узбекистан. Email: azimbekmadaminov66@gmail.com; ORCID ID: https://orcid.org/0000-0002-3482-8071*

References

[1] Ahmed A, & Geed SR. Sustainable refinery waste management through biotechnological interventions: Health impacts, historical successes, and emerging solutions. Environmental Research. Elsevier BV. 2025. https://doi.org/10.1016/j.envres.2025.120967

[2] Sattar S, Hussain R, Shah SM, Bibi S, Ahmad SR, Shahzad A, Zamir A, Rauf Z, Noshad A, & Ahmad L. Composition, impacts, and removal of liquid petroleum waste through bioremediation as an alternative clean-up technology: A review. Heliyon. 2022; 8(10): e11101. https://doi.org/10.1016/j.heliyon.2022.e11101

[3] Burks SL. Review of pollutants in petroleum refinery wastewaters and effect upon aquatic organisms. Environment International. Elsevier BV. 1982. https://doi.org/10.1016/0160-4120(82)90117-9

[4] ISCC System GmbH. ISCC Guidance Waste and Residues From Food … ISCC. 2025.

[5] Casali B, Brenna E, Parmeggiani F, Tessaro D, Tentori F. Sustain. Chem. 2021; 2:74–91. https://doi.org/10.3390/suschem2010006

[6] United Nations Environment Programme (UNEP), & International Fertilizer Industry Association (IFA). Environmental aspects of phosphate and potash mining. Paris: UNEP & IFA. 2001. ISBN 92-807-2052-X

[7] Orris GJ, Dunlap P, & Wallis JC. Phosphate occurrence and potential in the region of Afghanistan, including parts of China, Iran, Pakistan, Tajikistan, Turkmenistan, and Uzbekistan (with a section on geophysics by Jeff Wynn) (Open-File Report 2015–1121). U.S. Geological Survey. 2015. https://doi.org/10.3133/ofr20151121

[8] Safirova E. The mineral industry of Uzbekistan in 2022. In U.S. Geological Survey, 2022 Minerals Yearbook (Advance Release). U.S. Department of the Interior, U.S. Geological Survey. 2025. https://www.usgs.gov/centers/nmic/minerals-yearbook

[9] Levine RM, & Wallace GJ. The mineral industries of the Commonwealth of Independent States in 2001. In U.S. Geological Survey, 2001 Minerals Yearbook (Vol. III, Area Reports: International, Europe and Central Eurasia. U.S. Department of the Interior, U.S. Geological Survey. 2003, 6.1–6.32. https://doi.org/10.3133/myb2001v3

[10] Xudoyberdiev J, Reymov A, Kurbaniyazov R, Namazov Sh, Badalova O, & Seytnazarov A. Mineral composition of nodular phosphorite of Karakalpakstan and its processing into simple superphosphate. E3S Web of Conferences. 2023; 449:06005. https://doi.org/10.1051/e3sconf/202344906005

[11] Ruan Y, Han H, & Li L. Review on beneficiation techniques and reagents used for phosphate ores. Minerals. 2019; 9(4):253. https://doi.org/10.3390/min9040253

[12] Bazhirova K, Zhantasov K, & Kolesnikov A. Acid-free processing of phosphorite ore fines into composite fertilizers using the mechanochemical activation method. Journal of Composites Science. 2024; 8(5):165. https://doi.org/10.3390/jcs8050165

[13] Jurayev RS, Eshkulov BR, & Kakhkhorov NT. Production of Complex and Mixed Fertilizers by Acidic Processing of Phosphorites. Engineering Proceedings. 2024; 67(1): 59. https://doi.org/10.3390/engproc2024067059

[14] Jasinski SM. Phosphate rock. In U.S. Geological Survey, Mineral commodity summaries U.S. Department of the Interior, U.S. Geological Survey. 2025, 134-135. https://doi.org/10.3133/mcs2025

[15] Gessner PK, & Hasan MM. Freundlich and Langmuir isotherms as models for the adsorption of toxicants on activated charcoal. Journal of pharmaceutical sciences. 1987; 76(4):319–327. https://doi.org/10.1002/jps.2600760412

[16] Jarnerud T, Karasev AV, & Jönsson PG. Neutralization of Acidic Wastewater from a Steel Plant by Using CaO-Containing Waste Materials from Pulp and Paper Industries. Materials (Basel, Switzerland). 2021; 14(10):2653. https://doi.org/10.3390/ma14102653

[17] Jeppu GP, & Clement TP. A modified Langmuir-Freundlich isotherm model for simulating pH-dependent adsorption effects. Journal of contaminant hydrology. 2012; 129-130:46–53. https://doi.org/10.1016/j.jconhyd.2011.12.001

[18] Dasgupta A, Chandel MK. Enhancement of biogas production from organic fraction of municipal solid waste using acid pretreatment. SN Appl. Sci. 2020; 2:1437. https://doi.org/10.1007/s42452-020-03213-z

[19] Balarak D, Mostafapour FK, Azarpira H, & Joghataei A. Langmuir, Freundlich, Temkin and Dubinin–radushkevich Isotherms Studies of Equilibrium Sorption of Ampicilin unto Montmorillonite Nanoparticles. Journal of Pharmaceutical Research International. 2017; 20(2):1-9. https://doi.org/10.9734/JPRI/2017/38056

[20] Sotimboev Ilgizarbek, Umidbek Baltaev, Sanjarbek Shamuratov, Ruzimov Shamsiddin, Umarbek Alimov, and Mirzabek Saporboyev. Technical and Economic Efficiency of Processing Acidic Wastewater from the Oil and Fat Industry into Necessary Agricultural Products. E3S Web of Conferences. EDP Sciences. 2024. https://doi.org/10.1051/e3sconf/202456303072

[21] Turatbekova, Aidai, Malokhat Abdukadirova, Sanjarbek Shamuratov, Bakhodir Latipov, Mirzabek Saporboyev, Jafar Shamshiyev, and Yusuf Makhmudov. “Investigation of the Effect of Fertilizers on the Biochemical and Physical Characteristics of Carrots (Daucus Carota L.). E3S Web of Conferences. EDP Sciences, 2024. https://doi.org/10.1051/e3sconf/202456303074

[22] Yuldasheva A, Shamuratov S, Kurambayev S, & Radjabov M. Mathematical Analysis of CaO Content Variation in Acidic Wastewater and Mineralized Mass Mixture from Central Kyzylkum Phosphorite Based on Exponential Decay Model. Kompleksnoe Ispolzovanie Mineralnogo Syra = Complex Use of Mineral Resources. 2025; 339(4):79–86. https://doi.org/10.31643/2026/6445.42

[23] Shamuratov Sanjarbek, Umid Baltaev, Sanobar Achilova, Umarbek Alimov, Shafoat Namazov, and Najimuddin Usanbaev. Enhancement of Availability of High Calcareous Phosphorite by Neutralization of Acid Effluent and Composting of Cattle Manure. E3S Web of Conferences. EDP Sciences. 2023. https://doi.org/10.1051/e3sconf/202337703004

[24] MyAssays. (n.d.). Four-parameter logistic regression. Retrieved from https://www.myassays.com/four-parameter-logistic-regression.html

[25] Efron B. Bootstrap methods: Another look at the jackknife. Annals of Statistics. 1979; 7(1):1–26. https://doi.org/10.1214/aos/1176344552

[26] Hurvich CM, & Tsai C-L. Regression and time series model selection in small samples. Biometrika. 1989; 76(2):297–307. https://doi.org/10.1093/biomet/76.2.297

[27] Schwarz G. Estimating the dimension of a model. Annals of Statistics. 1978; 6(2):461–464. https://doi.org/10.1214/aos/1176344136

[28] Ritz C, Baty F, Streibig JC, & Gerhard D. Dose-response analysis using R. PLOS ONE. 2015; 10(12):e0146021. https://doi.org/10.1371/journal.pone.0146021

Crossref
DOI: 10.31643/2027/6445.33
Mining & Mineral Processing

Mathematical analysis of the linear increase in SiO_2 content during the activation of Navbakhor alkaline bentonite with hydrochloric acid

[1*]Boyjanov N.I., [1]Rakhimov U.B., [2]Ataullaev Z.M., [3]Boltayev M.A., [3]Serkayev Q.P., [3]Khamidova M.O.

[1]Urgench State University named after Abu Rayhon Beruni, Urgench, Uzbekistan
[2]Urganch State Pedagogical Institute, Urgench, Uzbekistan
[3]Tashkent Chemical-Technological Institute, Tashkent, Uzbekistan

**Corresponding author email: b.nodirbek@urdu.uz*

Received: *December 11, 2025*
Peer-reviewed: *December 26, 2025*
Accepted: *January 19, 2026*

ABSTRACT

In this study, the acid activation process of the bentonite clay, which was conducted for producing a bleaching sorbent for the oil and fat industry, was mathematically analyzed. Increase in SiO_2 content under different concentrations of HCl was analyzed using the different mathematical models. During acid activation, increasing the acid concentration from 5% to 20% resulted in an increase in the SiO_2 content from 61.94% to 65.12%. During the activation process, a moderate increase in HCl concentration caused the improvement of the sorption properties of the clay by dissolving some components and restructuring the active sites. An excessive increase in the concentration of HCl leads to degradation of the mineral structure and partial breakdown of the silica framework, which negatively influences sorption performance. Analysis of the obtained results using the different mathematical approaches showed that an increase in SiO_2 content during activation corresponds fully to a linear model. According to this, a linear model was described by the equation $y = 60.785 + 0.2088 \cdot X$. Accuracy of the results obtained from the linear equation was confirmed by a coefficient of determination, $R^2 = 0.9845$, indicating a high accordance with the experimental data. This model mathematically predicts the increase in SiO_2 content and proves that the activation process proceeds as a linear function. A mathematical approach to the activation process enables one to calculate in advance the properties of sorption of the clay, to reduce the consumption of acid and water, and to calculate the eventual demands of other reagents.

Keywords: bentonite clay, activation, sorption properties, mathematical modeling, linear model.

Information about authors:

Boyjanov Nodirbek Ilxomovich — *Doctor of Philosophy in Technical Sciences, Associate Professor at the Faculty of Chemical Technology, Urgench State University named after Abu Rayhon Beruni, 220100, H. Olimjon Street 14, Urgench, Uzbekistan. Email: b.nodirbek@urdu.uz; ORCID ID: https://orcid.org/0009-0002-1454-9478*

Rakhimov Umarbek Beknazarovich — *Assistant, food technology, Urgench State University named after Abu Rayhan Biruni, 220100, Khamid Alimjan Street, 14, Urgench, Khorezm Region, Uzbekistan. Email: umarbek.raximov.88@gmail.com; ORCID ID: https://orcid.org/0000-0002-8704-6612*

Ataullaev Zokir Makhsudovich — *Doctor of Philosophy (PhD) in Pedagogical Sciences, Associate Professor at the Department of Natural Sciences, Urgench State Pedagogical Institute, Uzbekistan. Email: zokirjon16081987@gmail.com; ORCID ID: https://orcid.org/0000-0002-6517-8163*

Boltayev Mirjalol Allayarovich — *Doctoral candidate at the Tashkent Institute of Chemical Technology, Navoi Street, 32, Tashkent, Uzbekistan. email: mirjalolboltayev@mail.ru; ORCID ID: https://orcid.org/0000-0002-3172-658X*

Serkayev Qamar Pardayevich — *Professor at the Tashkent Institute of Chemical Technology, Navoi Street, 32, Tashkent, Uzbekistan. Email: serkayev@mail.ru, ORCID ID: https://orcid.org/0009-0009-8316-4994*

Khamidova Madina Olimjonovna — *Associate Professor at the Tashkent Institute of Chemical Technology, Navoi Street, 32, Tashkent, Uzbekistan. Email: m.khamidova@mail.ru; ORCID ID: https://orcid.org/0000-0002-7299-0395*

Introduction

Natural mineralized clays (including both raw and activated forms) were characterized with high sorption capacity, among which are bentonite, kaolin, palygorskite, opoka-type clays, and others.

The structure of bentonite clays is based on the mineral montmorillonite, which represents the group of aluminosilicates. Their physicochemical properties depend on the structure of the crystal lattice of this mineral. The availability of ion-exchangeable components in bentonite clays provides possibilities to improve the sorption properties in the course of activation [1].

Depending on the mineralogical composition, structural characteristics, chemical properties, and intended field of application, natural clays' activation methods are carried out under different

conditions.

As a chemical modification process, acid activation replaces exchangeable metal cations, such as Na^+, Ca^{2+}, and Mg^{2+}, with H^+ ions. After the removal of the interlayer metal ions, a silica-rich framework is formed. In addition, new kinds of active sites within the clay structure will be generated in this process [1].

The specific surface area varies depending on the type of acid, its concentration, temperature, duration of treatment, and the hydromodule. A moderate acid concentration leads to an increase in

Due to acid activation, there is an increase in the specific surface area of the clay, its pore size, and pore volume [2].

The specific surface area depends on the kind of acid, the acid concentration, temperature, time of treatment, and the hydromodule. An increase in specific surface area due to a moderate acid concentration is accompanied by an increase in the SiO_2 content. A further increase in acid concentration reduces the ion-exchange capacity and provokes the degradation of the crystal structure of the mineral. As a result, the sorption properties of the clay decrease [3].

Of the different parameters, specific surface area and pH have been mainly considered in activated bleaching clays used for refining vegetable oils. The activation results in a manyfold increase of the specific surface area of the clay compared to its natural state, which increases its sorption capacity [[4], [5]].

However, at acid concentrations beyond the moderate values, deformation and blockage of pores occur; this would further reduce sorption performance. Controlling the type of acid and conditions of activation can yield selective sorbents suitable for different kinds of molecules, besides making a structure with varying proportions of micro, meso, and microporosity possible to obtain [[6], [7]].

Adsorption processes occurring between the sorbent and the sorbate generally proceed through physical and chemical mechanisms. Maximum sorption of dye compounds, oxidation products, cations, anions, and other components present in the sorbate is achieved when the pore size, pore volume, and pH of the adsorbent are optimal. In particular, harmful anionic substances can be effectively removed from industrial wastewater with polar sorbents [[8], [9], [10]].

Various compositions developed through different approaches in adsorbent development have been studied, which showed that the process is kinetically described by the pseudo-second-order model. This indicates that, aside from physical adsorption, chemical bonding-i.e., chemisorption-adds to the active role of the sorption process. Thus, the mechanism of adsorption is not just a physical interaction of the molecules with the material but also involves chemical interactions.

The Langmuir and the Freundlich models are two of the most frequent models used in the study of the equilibrium state of adsorption processes. According to the assumptions of the Langmuir model, adsorption on the surface occurs as a monolayer-that is, as a single layer of adsorbate molecules. The Freundlich model characterizes sorption on a heterogeneous solid that is composed of sites with different energies and affinities [8].

As a result of acid treatment, the dissolution of soluble components in the octahedral layer increases or redistributes active sites surrounding the Si-O bonds. In this way, it increases the energetic activity of these sites and strengthens their interactions with organic compounds, pigments, peroxides, and other oxidation products. In bleaching clays applied in the oil and fat industry, activation with moderate acid concentrations is effective. High acid concentrations destroy the crystal structure of the mineral and subsequently its sorption properties. Washing the suspension in water after the process should be conducted at pH = 4-5, because, under such conditions, ion-forming substances present in oil bind effectively [4].

The pH of the sorbent, therefore, plays an important role in the efficient removal of contaminants in industrial wastewater. Its surface charge is one of the most important parameters for treating a variety of sorbates with differing pHs. Control of the surface charge of the sorbent properly orients the adsorption process and makes it highly feasible to achieve maximum efficiency in wastewater treatment applications [5].

Bentonite clays are considered to be abundant, low-cost materials that can be easily activated. At the same time, they offer the possibility to produce environmentally safe sorbents. They find wide application both as bleaching earths in the food industry and as sorbents for the removal of contaminants from industrial wastewater. Specific application of bleaching earths depends on their pore structure: mesopores effectively adsorb larger molecules such as phospholipids, while micropores are more suitable for the adsorption of smaller and more polar molecules. In the process of vegetable oils bleaching, the sorption properties and pH value of the sorbent directly influence the final result of

the process. The linear relationship between these parameters facilitates optimization of practical applications. Moreover, in the analysis of adsorption processes, it is recommended to evaluate the compatibility of kinetic and isotherm models, verify relative errors and statistical criteria, and assess the stability of the selected model [[4], [11], [12], [13], [14], [15], [16]].

Activated clays, due to their high specific surface area, tunable particle size distribution, and adjustable pH values, can be used as selective adsorbents that preferentially remove contaminants from multicomponent mixtures. In addition, in the study of physical and chemical properties of adsorbents obtained by activation of natural clays, adsorption isotherms and the kinetic characteristics of the adsorption processes have been described in detail [17].

In the detailed analysis of adsorbents, the study of adsorption–desorption isotherms is of great importance, as these curves characterize the equilibrium established between the sorbent and the sorbate. In this context, the Langmuir model is considered a classical approach, assuming that all active sites on the surface possess identical energies. Accordingly, molecules occupy the surface in a monolayer fashion. This model of monolayer adsorption applies to homogeneous surfaces with similar structural active sites and is based on assumptions of a finite number of adsorption sites. In contrast, the Freundlich model assumes that sorbent surfaces are inherently heterogeneous, possessing adsorption sites with dissimilar energetic characteristics. The arrangement of the molecules on such heterogeneous surfaces, according to this model, is not restricted to a monolayer; the adsorption may be a polylayer, reflecting a more complex nature of adsorption [18].

In the adsorption of different organic compounds using various modified bentonite clays, kinetic and isotherm properties of the process have been evaluated according to the pseudo-second-order kinetic model. This model is considered one of the most valuable mathematical models that describes the basic mechanisms of the adsorption rate. Usually, the use of a pseudo-second-order model indicates that the adsorption rate proceeds via a chemical mechanism, so that the active sites on the surface of the adsorbent interact with sorbate molecules through a direct covalent or strong chemical bonding. Therefore, the pseudo-second-order kinetic model can provide a theoretical basis for the study of the extent and rate at which the sorbate molecules are bound by the adsorbent [19].

The chemical mechanisms of adsorption are described by the pseudo–second-order kinetic model (1).

$$\frac{t}{q_t} = \frac{1}{k_2 \cdot q_e^2} + \frac{t}{q_e} \qquad (1)$$

here:

q_t - amount of substance adsorbed at time *t*, *mg/g;*

q_e - amount of substance adsorbed at equilibrium, *mg/g;*

k_2 - rate constant, *g* mg^{-1} min^{-1}*;*

t - time, *min.*

According to the volumetric distribution of their pores, bentonite clays can serve as selective adsorbents, catalysts, or raw materials in the production of pharmaceutical preparations [20].

In scientific studies on the purification of wastewater from pharmaceutical manufacturing facilities, the sorption efficiency of natural bentonite clay and acid-activated samples has been comparatively evaluated for the removal of harmful antibiotics. The results indicate that the adsorption of antibiotic compounds from wastewater follows the pseudo-second-order kinetic model. Among the isotherm analyses based on the Langmuir and the Freundlich models, the Langmuir model yielded the highest coefficient of determination (R^2) [21].

Mathematical modeling of production processes enables the preliminary analysis of technological systems and the optimization of operational costs [[22], [23]]. A mathematical approach to industrial operations allows technological processes to be expressed in a digital framework and facilitates the examination of the relationship between theoretical predictions and practical outcomes. Such an approach significantly enhances production efficiency by reducing the consumption of raw materials and energy resources.

Although numerous studies have been devoted to the acid activation of bentonite clays, the majority of these works primarily focus on changes in adsorption properties and increases in specific surface area. In contrast, the quantitative relationship between hydrochloric acid concentration and the increase in silicon dioxide (SiO_2) content has not been systematically investigated. In particular, for alkali-earth bentonite

from the Navbahor deposit, the dependence of SiO_2 content on hydrochloric acid concentration has not yet been consistently described using a deterministic mathematical approach.

The scientific novelty of the present study lies in the fact that, for the first time, a statistically reliable and clearly defined linear relationship between hydrochloric acid concentration and the increase in SiO_2 content during the acid activation of Navbahor bentonite has been established. Unlike previous studies that relied mainly on empirical observations, this work proposes a simple yet highly reliable mathematical model that quantitatively characterizes the structural transformation of the silica framework during acid treatment.

The mathematical modeling of the HCl activation process of natural bentonite clay allows for an examination of the effect that increasing SiO_2 content has on the behavior of the specific surface area, as well as to predict the surface area that can be obtained. This makes it possible to maximize the quality parameters of the resulting adsorbent, control the process of activation digitally, and optimize the consumption of reagents.

Based on the experimental data, an empirical and deterministic mathematical model is developed to describe the relationship between SiO_2 content and hydrochloric acid concentration. An analysis of the proposed model was then made using a linear regression equation, as well as an evaluation of its reliability based on statistical indicators (R^2).

Materials and Methods

The material of the research is alkaline (calcium) bentonite of the Navbahor deposit, which is located in the Navoi region. The main component, according to the chemical composition of natural bentonite clay, is SiO_2-61.54%. That very fact testifies to the presence of a silica-based structural framework of this mineral. A high proportion of SiO_2 in its composition ensures stability of the mineral layers, and it acts as a non-degradable structural carcass during acid activation.

In addition, the bentonite clay contains 12.60% aluminum oxide (Al_2O_3), 6.23% iron oxide (Fe_2O_3), as well as other oxides, the respective amounts of which are presented in Table 1. This chemical composition was taken as the initial parameter for modeling the kinetics of SiO_2 increase during the activation of bentonite with hydrochloric acid.

Bentonite clay samples weighing 100 g each were activated in HCl solutions of varying concentrations (5, 10, 15, and 20%) at a hydromodule of 1:2.5 and a temperature of 373 K for 2 hours under continuous stirring in a water bath. The activated suspension was washed with distilled water until reaching pH 4, followed by drying at 473 K, grinding, and sieving through a 56 µm mesh. The SiO_2 content in the clay was determined using the colorimetric method [7].

Three parallel experiments were conducted simultaneously, and their average values were used for analysis. Based on the obtained experimental results, the relationship between the increase in hydrochloric acid concentration and the change in SiO_2 content was examined. Accordingly, a mathematical model was developed that describes this process. The analytical results were processed by mathematical-statistical methods, and the reliability of the data was checked.

Accordingly, it has been determined that the increase in SiO_2 content as a function of hydrochloric acid concentration can be given by the linear regression Equation (2), from which the mathematical treatment clearly shows the level of accuracy of the experimental results.

$$y = a + b \cdot X \quad (2)$$

here:
y - *SiO_2* content, %
a - Value of *y* when *X = 0*
b – Regression coefficient, %
X – hydrochloric acid concentration, %

In the model, hydrochloric acid concentration was an independent variable, while SiO_2 content was the dependent variable. The value of the coefficient of determination (R^2) was used to determine the exactitude of the results from the model. Mathematically, R^2 is given by expression 3.

$$R^2 = 1 - \frac{SST}{SSE} \quad (3)$$

here:
R^2 - coefficient of determination
SST - deviation of experimental values from the mean
SSE - difference between the model and experimental values.

Table 1 - Chemical composition of natural Navbahor alkali-earth bentonite

Sample	Content, %							
	SiO_2	Al_2O_3	Fe_2O_3	TiO_2	CaO	MgO	Na_2O	K_2O
Natural bentonitic clay	61.54	12.60	6.23	0.56	0.75	3.98	0.82	2.11

A high value of the coefficient obtained, R^2, means that the increase in the concentration of hydrochloric acid translates into a rise in the rate of disruption of the silicon-oxygen bonds within the silica framework; that is, it reflects structural changes corresponding to increasing the acid concentration. For example, usually, when $R^2 \geq 0.95$, the model is considered highly accurate; however, with $R^2 < 0.80$, the model has failed to effectively describe the process at hand. In this context, the results of the correlation analysis also support the findings above. The value of r = 0.992 further confirms the linear relationship between acid concentration and SiO_2 content. That is to say, it demonstrates the stability of the model and its physical soundness 4.

$$r = \frac{(u_i - \hat{u}) \cdot (y_i - \acute{y}}{\sqrt{(u_i - \hat{u})^2 \cdot (y_i - \acute{y})^2}} \quad (4)$$

here:
r - correlation coefficient
u_i - independent variable
y_i - dependent variable
û ȳ - mean value of the variables

A larger value of the correlation implies that the model is strongly accurate and that random scattering in the experimental data is practically absent. The closeness of the r value to 1 indicates that with an increase in SiO_2 content, this proceeds in a well-defined and deterministic linear pattern.

$$\mathrm{MRE} = \frac{1}{n} \sum_{i=1}^{n} \left[\frac{y_i - \acute{y}_i}{y_i}\right] \cdot 100 \quad (5)$$

here:
y_i - experimental value
$\acute{y}_i$ - model value
n - number of experiments
$(y_i - \acute{y}_i)$ - relative error for each experiment

MRE gives the estimation of the average deviation of the model results from the experimental values. The standard deviation (SD) and the root mean square error (RMS) are used to further judge the reliability of the model results. These kinds of analyses confirm the accuracy and stability of the empirical model describing the dependence of SiO_2 content in the clay on the acid concentration.

The coefficient of determination obtained from the modeling was $R^2 = 0.9845$, which reveals an excellent fit of the model to the experimental data. Origin 2021 Pro software was used to build the graphical analyses shown in Figure 1 below. These plots are a visual representation of the agreement between the model predictions and the experimental values.

Results and Discussions

The results of experiments carried out in this research demonstrate the processes of structure transformations during the hydrochloric acid activation of Navbahor alkaline earth bentonites. In contrast with previous observations made on certain qualitative criteria, in this research, the linear relationship between hydrochloric acid concentration and content of SiO_2 has been revealed.

Table 2 shows the variations in SiO_2 content in samples activated with HCl solutions of different concentrations (5%, 10%, 15%, and 20%) at hydromodule 1:2.5.

Table 2 – SiO_2 content (%) for the clay samples activated at different concentrations of hydrochloric acid

HCL concentration, %	SiO_2 content, %
5	61.95
10	62.79
15	63.72
20	65.12

Experimental results indicated that whereas the specific surface area for the natural clay was 43.52 m^2/g, that of the sample activated with 15% HCl had a specific surface area of 134.43 m^2/g as obtained by BET analysis. This value reduced to 95.34 m^2/g at an HCl concentration of 20%. In other words, with increasing acid concentration beyond 20%, the specific surface area of the clay decreased. Such findings suggest that when the acid concentration exceeds the optimum, both

exchangeable ions are removed from the clay structure, and structural degradation of the mineral occurs.

As observed from the table, SiO_2 content in the bentonite increases steadily with an increase in the hydrochloric acid concentration. While the value of SiO_2 content for the natural clay was 61.54%, this reached up to 65.12%, increasing the acid concentration to 20%.

The SiO_2 increase caused by acid activation can be explained by the forced leaching of alkaline and alkaline-earth metals, magnesium, aluminum, and iron from the clay structure. In this procedure, the removal of a large proportion of bonded hydroxyl ions from the silicate lattice, together with the release of Ca^{2+}, Mg^{2+}, Na^{+}, K^{+}, and other cations, formed unsatisfied valences with a net increase in surface area. This implies that structural rearrangement occurred in the montmorillonite crystal lattice during the process of acid activation. Thus, more extensive voids were created, and atoms or ions located in these areas were transformed into an unsaturated state, increasing their potential to bind other atoms or ions; in other words, enhancing adsorption capacity.

Furthermore, sorption properties depend not only on the specific surface area but also on the pH of the medium. Thus, the increase in the specific surface area of the clay during the activation process can be predicted based on changes in SiO_2 content and by mathematical modeling. This, in turn, helps reduce the number of expensive analyses such as BET measurements.

The model yielded a coefficient of determination $R^2 = 0.9845$, indicating a high degree of accuracy and strong agreement with the experimental data.

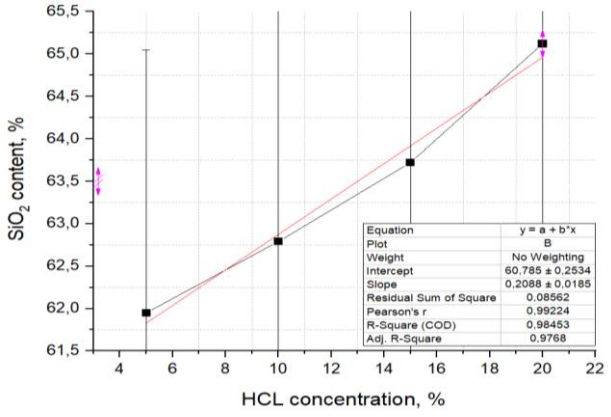

Figure 1 - Linear increase in SiO_2 content as a function of hydrochloric acid concentration

Based on the results obtained during the activation process, the dependence of SiO_2 content on hydrochloric acid concentration was established and graphically illustrated (Figure 1).

According to the graph, the linear increase in SiO_2 content is confirmed by the model, and the value $R^2 = 0.9845$ indicates an excellent agreement between the model and the experimental data. This relationship is expressed by the following equation:

$$SiO_2 = 60.785 + 0.2088 \cdot X$$

According to the above equation, each 1% increase in hydrochloric acid concentration results in a 0.2088% increase in SiO_2 content.

During the activation process, H^{+} ions leach out the exchangeable cations Ca^{2+}, Mg^{2+}, Na^{+}, K^{+}, Al^{3+} , and Fe^{3+} from the interlayer spaces of the bentonite clay. At the same time, when the acid concentration reaches 20% and above, it leads to degradation of the mineral structure, as illustrated in the figure (Figure 2).

As shown in the figure, the ion-exchange process leads to the expansion of interlayer spaces in the clay structure, resulting in an increase in specific surface area and an improvement in adsorption properties.

The experimental results and the model-calculated values were compared.

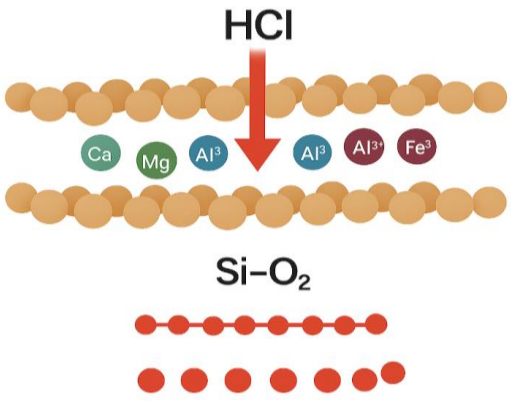

Figure 2 - Ion-exchange mechanism during acid activation

The differences between these values, along with evaluation parameters such as relative error (RE), standard deviation (SD), and root mean square error (RMSE), are presented in Table 3.

Table 3 - Experimental and modeled values of SiO_2 content increase in the clay

HCl, %	SiO_2 (Experimental), %	SiO_2 (model), %	Difference ($\Delta = y-\hat{y}$)	Relative error, (RE), %	Standard deviation (SD), %	Root mean square error (RMSE)
5	61.95	62.36	-0.41	0.65	0.289914	62.155
10	62.79	63.29	-0.50	0.80	0.353553	63.04
15	63.72	64.23	-0.51	0.79	0.360624	63.97
20	65.12	65.16	-0.04	0.06	0.028284	65.14

The table presents the absolute difference and relative error between the experimental and model-derived SiO_2 values for each trial. Relative error values below 5% indicate a high degree of accuracy of the model.

Conclusion

The results of the study indicate that the SiO_2 content increases consistently with rising hydrochloric acid concentration. This relationship is given by the equation $SiO_2 = 60.78 + 0.187 \cdot X$, and the coefficient $R^2 = 0.9845$ testifies to an excellent fit of the model to the experimental data. The rate of the SiO_2 increase in the silica framework rises linearly with acid concentration, confirming that the process proceeds according to a linear mechanism.

The destructive change in the structure during acid activation with HCl results in fragmentation of montmorillonite particles. This way, the dispersity of the clay increases. During the first stage of activation, the exchangeable cations Ca^{2+}, Mg^{2+}, Na^{+}, and K^{+} are leached out and replaced by H^{+} and Al^{3+} ions acting as active sites afterward. In the second stage, each particle was further divided into thinner units-down to a single elementary layer-while each fragment retains the internal structure of the original crystal packet.

Based on the above findings, it can be concluded that treating Navbahor alkaline-earth bentonite with HCl solutions up to 15% increases the adsorption properties of the clay, while treatment at 20% or higher concentrations results in degradation of the mineral crystal structure and a reduction in specific surface area.

The importance of this approach is that, based on the increase in SiO_2 content, one might predict increases in the specific surface area of the clay during activation and through mathematical modeling. This reduces the number of analyses involving such expensive analytical techniques as BET measurements.

This mathematical model of the acid activation process allows for a digital approach to enhance the specific surface area of bentonite, optimizes the concentration of hydrochloric acid, and minimizes the consumption of water during the neutralization of acidic effluents.

Conflicts of interest. On behalf of all authors, the corresponding author states that there is no conflict of interest.

CRediT author statement: **N. Boyjanov**: Conceptualization, Methodology, Software, Data curation, Writing draft preparation; **U. Rakhimov and Z. Ataullayev**: Visualization, Investigation; **M. Boltayev**: Supervision; **M. Khamidova**: Software, Validation; **Q. Serkayev**: Reviewing and Editing.

Formatting of funding sources. This research did not receive any specific grant from funding agencies in the public, commercial, or not-for-profit sectors.

Cite this article as: Boyjanov NI, Rakhimov UB, Ataullaev ZM, Boltayev MA, Serkayev QP, Khamidova MO. Mathematical analysis of the linear increase in SIO_2 content during the activation of Navbakhor alkaline bentonite with hydrochloric acid. Kompleksnoe Ispolzovanie Mineralnogo Syra = Complex Use of Mineral Resources. 2027; 342(3):90-99. https://doi.org/10.31643/2027/6445.33

Навабахор сілтілі бентонитін тұз қышқылымен белсендендіру кезінде SiO_2 мөлшерінің сызықтық артуын математикалық талдау

[1]Бойжанов Н.И., [1]Рахимов У.Б., [2]Атауллаев З.М., [3]Болтаев М.А., [3]Серкаев Қ.П., [3]Хамидова М.О.

[1] Әбу Райхан Беруни атындағы Ургенч мемлекеттік университеті, Ургенч, Өзбекстан
[2] Ургенч мемлекеттік педагогикалық институты, Ургенч, Өзбекстан
[3] Ташкент химия-технология институты, Ташкент, Өзбекстан

Мақала келді: *11 желтоқсан 2025*
Сараптамадан өтті: *26 желтоқсан 2025*
Қабылданды: *19 қаңтар 2026*

ТҮЙІНДЕМЕ

Бұл зерттеуде май-тоң май өнеркәсібіне арналған ағартқыш сорбент алу мақсатында жүргізілген бентонит сазын қышқылдық активация процесіне математикалық талдау жүргізілді Әртүрлі концентрациядағы HCl әсерінде SiO_2 мөлшерінің артуы түрлі математикалық модельдер қолдану арқылы талданды. Қышқылдық активтендіру барысында қышқыл концентрациясының 5%-дан 20%-ға дейін жоғарылауы SiO_2 құрамының 61,94%-дан 65,12%-ға дейін өсуіне алып келді. Активтендіру кезінде HCl концентрациясының орташа деңгейде артуы кейбір компоненттердің еруі және белсенді орталықтардың қайта құрылуы есебінен саздың сорбциялық қасиеттерін жақсартады. HCl концентрациясының шамадан тыс жоғарылауы минералдық құрылымның бұзылуына және кремнезем қаңқасының ішінара ыдырауына алып келеді, бұл сорбциялық сипаттамаларға теріс әсер етеді. Әртүрлі математикалық әдістерді қолдану арқылы алынған мәліметтерді талдау белсендіру процесі кезіндегі SiO_2 құрамының жоғарылауы сызықтық модельге толық сәйкес келетінін көрсетті. Осыған сәйкес, сызықтық модель мына теңдеумен сипатталады: $y = 60.785 + 0.2088 \cdot X$. Сызықтық теңдеу арқылы алынған нәтижелердің дәлдігі детерминация коэффициенті $R^2 = 0.9845$ мәнімен расталды, бұл эксперименттік мәліметтермен жоғары сәйкестігін көрсетеді. Ұсынылған модель SiO_2 құрамының артуын математикалық түрде болжайды және активтендіру процесі сызықтық функция ретінде жүретінін дәлелдейді. Активтендіру процесін математикалық тәсілмен сипаттау саздың сорбциялық қасиеттерін алдын ала болжауға, қышқыл мен судың шығынын азайтуға, сонымен қатар басқа реагенттерге деген қажеттілікті есептеуге мүмкіндік береді.

Түйін сөздер: бентонит сазы, ативация, сорбциялық қасиеттер, математикалық модельдеу, сызықтық модель.

Авторлар туралы ақпарат:

Бойжанов Нодирбек Илхомович — *Техника ғылымдары бойынша философия докторы, Әбу Райхан Беруни атындағы Үргеніш мемлекеттік университетінің химиялық технология факультетінің қауымдастырылған профессоры, 220100, Х. Әлімжан көшесі, 14, Үргеніш, Өзбекстан. Email: b.nodirbek@urdu.uz; ORCID ID: https://orcid.org/0009-0002-1454-9478*

Рахимов Умарбек Бекназарович — *Әбу Райхан Бируни атындағы Үргеніш мемлекеттік университетінің тамақ технологиясы бойынша ассистенті, 220100, Хамид Әлімжан көшесі, 14, Хорезм облысы, Үргеніш, Өзбекстан. Email: umarbek.raximov.88@gmail.com; ORCID ID: https://orcid.org/0000-0002-8704-6612*

Атауллаев Зокир Махсудович — *Педагогика ғылымдарының философия докторы (PhD), Үргеніш мемлекеттік педагогикалық институтының жаратылыстану ғылымдары кафедрасының доценті, Үргеніш, Өзбекстан. Email: zokirjon16081987@gmail.com; ORCID ID: https://orcid.org/0000-0002-6517-8163*

Болтаев Миржалол Аллаярович — *Ташкент химиялық технология институтының докторанты, Навои көшесі, 32, Ташкент, Өзбекстан. Email: mirjalolboltayev@mail.ru; ORCID ID:https://orcid.org/0000-0002-3172-658X*

Серкаев Камар Пардаевич — *Ташкент химиялық технология институтының профессоры, Навои көшесі, 32, Ташкент, Өзбекстан. Email: serkayev@mail.ru; ORCID ID: https://orcid.org/0009-0009-8316-4994*

Хамидова Мадина Олимжоновна — *Ташкент химиялық технология институтының доценті, Навои көшесі, 32, Ташкент, Өзбекстан. Email: m.khamidova@mail.ru; ORCID ID: https://orcid.org/0000-0002-7299-0395*

Математический анализ линейного увеличения содержания SiO_2 при активации навбахорского щелочного бентонита соляной кислотой

[1]Бойжанов Н.И., [1]Рахимов У.Б., [2]Атауллаев З.М., [3]Болтаев М.А.,[3]Серкаев К.П., [3]Хамидова М.О.

[1]Ургенчский государственный университет имени Абу Райхона Беруни, Ургенч, Узбекистан
[2]Ургенчский государственный педагогический институт, Ургенч, Узбекистан
[3]Ташкентский химико-технологический институт, Ташкент, Узбекистан

Поступила: *11 декабря 2025*
Рецензирование: *26 декабря 2025*
Принята в печать: *19 января 2026*

АННОТАЦИЯ

В данном исследовании был проведён математический анализ процесса кислотной активации бентонитовой глины, осуществляемой для получения отбеливающего сорбента для масложировой промышленности. Повышение содержания SiO_2 при различных концентрациях HCl было проанализировано с использованием разных математических моделей. В ходе кислотной активации увеличение концентрации кислоты с 5% до 20% привело к росту содержания SiO_2 с 61,94% до 65,12%. При активации умеренное повышение концентрации HCl улучшает сорбционные свойства глины за счёт растворения отдельных компонентов и перестройки активных центров. Чрезмерное увеличение концентрации HCl вызывает деградацию минеральной структуры и частичное разрушение кремнезёмного каркаса, что отрицательно сказывается на сорбционных характеристиках. Анализ полученных данных различными математическими методами показал, что повышение содержания SiO_2 в процессе активации полностью соответствует линейной модели. Согласно этому, линейная зависимость описывается уравнением: $y = 60.785 + 0.2088 \cdot X$. Точность результатов, полученных по линейному уравнению, подтверждена коэффициентом детерминации $R^2 = 0.9845$, что указывает на высокую согласованность с экспериментальными данными. Данная модель математически предсказывает увеличение содержания SiO_2 и доказывает, что процесс активации протекает как линейная функция. Математический подход к описанию процесса активации позволяет заранее рассчитывать сорбционные свойства глины, снижать расход кислоты и воды, а также определять потребность в других реагентах.

Ключевые слова: бентонитовая глина, активация, сорбционные свойства, математическое моделирование, линейная модель.

Информация об авторах:

Бойжанов Нодирбек Илхомович — *Доктор технических наук, доцент факультета химической технологии Ургенчского государственного университета имени Абу Райхана Бируни, 220100, ул. Х. Олимжон, 14, Ургенч, Узбекистан. Email: nodirbek@urdu.uz; ORCID ID: https://orcid.org/0009-0002-1454-9478*

Рахимов Умарбек Бекназарович — *Ассистент, пищевая технология, Ургенчский государственный университет имени Абу Райхана Бируни, 220100, ул. Хамида Алимжана, 14, Хорезмская область, Ургенч, Узбекистан. Email: umarbek.raximov.88@gmail.com; ORCID ID: https://orcid.org/0000-0002-8704-6612*

Атауллаев Зокир Махсудович — *Доктор педагогических наук, доцент кафедры естественных наук Ургенчского государственного педагогического института, Ургенч, Узбекистан. Email: zokirjon16081987@gmail.com; ORCID ID: https://orcid.org/0000-0002-6517-8163*

Болтаев Миржалол Аллаярович — *Аспирант Ташкентского института химической технологии, Улица Навои, 32, Ташкент, Узбекистан. Email: mirjalolboltayev@mail.ru; ORCID ID: https://orcid.org/0000-0002-3172-658X*

Серкаев Камар Пардаевич — *Профессор Ташкентского института химической технологии. Улица Навои, 32, Ташкент, Узбекистан. Email: serkayev@mail.ru; ORCID ID: https://orcid.org/0009-0009-8316-4994*

Хамидова Мадина Олимжоновна — *Доцент Ташкентского института химической технологии. Улица Навои, 32, Ташкент, Узбекистан. Email: m.khamidova@mail.ru; ORCID ID: https://orcid.org/0000-0002-7299-0395*

References

[1] Komadel P, & Madejová J. Chapter 7.1: Acid Activation of Clay Minerals. In Handbook of Clay Science. Developments in Clay Science. 2006; 1:263–287. https://doi.org/10.1016/S1572-4352(05)01008-1

[2] Hussin F, Aroua MK, & Daud WMAW. Textural characteristics, surface chemistry and activation of bleaching earth: A review. Chemical Engineering Journal. 2011; 170(1):90-106. https://doi.org/10.1016/j.cej.2011.03.065

[3] Christidis GE, Scott PW, & Dunham AC. Acid activation and bleaching capacity of bentonites from the islands of Milos and Chios, Aegean, Greece. Applied Clay Science. 1997; 12(4):329-347. https://doi.org/10.1016/S0169-1317(97)00017-3

[4] Falaras P, Kovanis I, Lezou F, & Seiragakis G. Cottonseed oil bleaching by acid-activated montmorillonite. Clay Minerals. 1999; 34(2):221-232. https://doi.org/10.1180/000985599546181

[5] Maged A, Kharbish S, Ismael IS, & Bhatnagar A. Characterization of activated bentonite clay mineral and the mechanisms underlying its sorption for ciprofloxacin from aqueous solution. Environmental Science and Pollution Research. 2020; 27(26):32980-32997. https://doi.org/10.1007/s11356-020-09267-1

[6] Noyan H, Önal M, & Sarıkaya Y. The effect of sulphuric acid activation on the crystallinity, surface area, porosity, surface acidity and bleaching power of a bentonite. Food Chemistry. 2007; 105(1):156-163. https://doi.org/10.1016/j.foodchem.2007.03.060

[7] Boyjanov N, Radjabov M, Serkayev Q, Boyjanov I, & Yaxshimuradov N. Activation and comparison of indicators of bentonite clay of the Navbakhor deposit. E3S Web of Conferences. 2024; 563:02018. https://doi.org/10.1051/e3sconf/202456302018

[8] Özcan AS, & Özcan A. Adsorption of acid dyes from aqueous solutions onto acid-activated bentonite. Journal of Colloid and Interface Science. 2004; 276(1):39-46. https://doi.org/10.1016/j.jcis.2004.03.043

[9] Ogbu AI, Ovuoraye PE, Ajemba RO, & Dehghani MH. Functionality and mechanistic parametric study of the potential of waste plantain peels and commercial bentonite for soybean oil refining. Scientific Reports. 2023; 13:19569. https://doi.org/10.1038/s41598-023-46842-1

[10] Haidar Abbas, Sarmad Jaafar Mohammed Alrubaye, Ali Fawzi Al-Hussainy, Basim Mohammed Saadi, Mohannad Abdulrazzaq Gati, Talib Kh. Hussein, Boyjanov Nodirbek Ilxomovich, Nafaa Farhan Muften. Role of Carrageenan and Health Approach for Adsorption of Safranin-T Dye from Aqueous Solution by Using Polymer/CNT Surface. Journal Nanostruct. 2025; 15(4): 1798-1807. https://doi.org/10.22052/JNS.2025.04.027

[11] Tyagi B, Chudasama CD, & Jasra RV. Determination of structural modification in acid activated montmorillonite clay by FT-IR spectroscopy. Spectrochimica Acta Part A: Molecular and Biomolecular Spectroscopy. 2006; 64(2):273–278. https://doi.org/10.1016/j.saa.2005.07.018

[12] Woumfo ED, Kamga R, Figueras F, & Njopwouo D. Acid activation and bleaching capacity of some Cameroonian smectite soil clays. Applied Clay Science. 2007; 37(1-2):149-156. https://doi.org/10.1016/j.clay.2006.12.008

[13] Shattar SFA, et al. One-step acid activation of bentonite derived adsorbent for effective removal of contaminants. Scientific Reports. 2020; 10:20053. https://doi.org/10.1038/s41598-020-76723-w

[14] Berhe MT, et al. Characterization of acid activation of bentonite clay using factorial experimental design. Advances in Materials Science and Engineering. 2024, 6413786. https://doi.org/10.1155/2024/6413786

[15] Al-Dunem K, Al-Ani R, & Al-Rawi A. Activation of Jordanian bentonite by hydrochloric acid and its use as bleaching clay. Advances in Materials Science and Engineering. 2018, 8385692. https://doi.org/10.1155/2018/8385692

[16] Al-Degs YS, Sweileh JA, Awawdeh M, & El-Barghouthi MI. Adsorption from aqueous solution onto natural and acid activated bentonite. American Journal of Environmental Sciences. 2012; 8(5):510–522. https://thescipub.com/pdf/ajessp.2012.510.522.pdf

[17] Ghouti MA, & Hussein F. Guidelines for the use and interpretation of adsorption isotherm models: A review. Journal of Hazardous Materials. 2020; 385:121621. https://doi.org/10.1016/j.jhazmat.2019.121621

[18] Ahmed HR, Kayani KF, Ealias AM, et al. A Comprehensive Review of Forty Adsorption Isotherm Models: An In-depth Analysis of Ten Statistical Error Measures. Water Air Soil Pollut. 2025; 236:346. https://doi.org/10.1007/s11270-025-07982-4

[19] Zaghouane-Boudiaf H, Ouederni A, Ksibi M, & Jessel N. Adsorption characteristics, isotherm, kinetics, and diffusion of 2,4,5-trichlorophenol onto organo-bentonites. Applied Clay Science. 2014; 101:131–139. https://doi.org/10.1016/j.clay.2014.01.00

[20] Babaki H. Kinetic model for the isothermal activation of bentonite by sulfuric acid. Applied Surface Science. 2008; 254(2):637–644. https://doi.org/10.1016/j.matchemphys.2007.09.034

[21] Maged A, Kharbish S, Ismael IS, & Bhatnagar A. Characterization of activated bentonite clay mineral and the mechanisms underlying its sorption for ciprofloxacin from aqueous solution. Environmental Science and Pollution Research. 2020; 27:32980-32997. https://doi.org/10.1007/s11356-020-09267-1

[22] Yuldasheva A, Shamuratov S, Kurambayev Sh, & Radjabov M. Mathematical analysis of CaO content variation in acidic wastewater and mineralized mass mixture from Central Kyzylkum phosphorite based on exponential decay model. Kompleksnoe Ispolzovanie Mineralnogo Syra = Complex Use of Mineral Resources. 2025; 339(4):79-86. https://doi.org/10.31643/2026/6445.42

[23] Sotimboev Ilgizarbek, Umidbek Baltaev, Sanjarbek Shamuratov, Ruzimov Shamsiddin, Umarbek Alimov, and Mirzabek Saporboyev. Technical and Economic Efficiency of Processing Acidic Wastewater from the Oil and Fat Industry into Necessary Agricultural Products. E3S Web of Conferences. EDP Sciences. 2024. https://doi.org/10.1051/e3sconf/202456303072

Crossref
DOI: 10.31643/2027/6445.34
Mining & Mineral Processing

Evaluation of the Effect of Additives on the Workability of Concrete Mix as Part of a Study of a Modified Wall Block

[1,2]Lukpanov R.E., [1,2]Dyussembinov D.S., [1,2*]Altynbekova A.D., [3]Kaklauskas G., [1,2]Zhumagulova A.A.

[1]Solid Research Group LLP, Astana, Kazakhstan
[2]L.N. Gumilyov Eurasian National University, Astana, Kazakhstan
[3]Gediminas Technical University of Vilnius, Vilnius, Lithuania

**Correspondence: kleo-14@mail.ru*

Received: *November 23, 2025*
Peer-reviewed: *December 3, 2025*
Accepted: *January 20, 2026*

Abstract

The article presents the results of an experimental investigation into the effect of modifying additives on the workability and setting times of a concrete mix used in the production of a two-component wall block. The block structure consists of an external façade layer and an internal structural–thermal insulation layer, which requires precise control of the rheological and technological parameters of the concrete mix during sequential casting. Lignin and soapstock, which are by-products of the wood-processing and fat-processing industries, were used as modifying components. The experimental program included the determination of concrete mix flowability and cement paste setting times at various additive dosages. The results showed that the incorporation of lignin and soapstock increased the workability of the concrete mix compared to the reference composition: the maximum increase in flowability reached up to 6.4% for lignin and up to 9.5% for soapstock. Their combined application produced a pronounced synergistic effect, resulting in an increase in workability of up to 16% in linear terms and up to 35% in terms of spread area, as well as a reduction in data dispersion. The setting time tests revealed opposite effects of the additives: lignin contributed to a reduction in both initial and final setting times, whereas soapstock, due to its hydrophobic properties, led to their extension. The obtained results can be used to optimize the technological regulations for manufacturing two-component wall blocks and to improve the quality and stability of the final products.

Keywords: wall block, additive, workability, setting time, lignin, soapstock.

Information about authors:

Lukpanov Rauan Ermagambetovich — *Senior Researcher, Solid Research Group LLP; PhD, Professor, Department of Industrial and Civil Engineering, L.N. Gumilyov Eurasian National University, 2 Satpayeva Street, 010009, Astana, Kazakhstan. Email: rauan_82@mail.ru; ORCID ID: https://orcid.org/0000-0003-0085-9934*

Dyussembinov Duman Serikovich — *Scientific Supervisor, Solid Research Group LLP; C.t.s., Associate Professor, Department of Industrial and Civil Engineering, L.N. Gumilyov Eurasian National University, 2 Satpayeva Street, 010009, Astana, Kazakhstan. Email: dusembinov@mail.ru; ORCID ID: https://orcid.org/0000-0001-6118-5238*

Altynbekova Aliya Doszhankyzy — *Researcher, Solid Research Group LLP; PhD, Department of Technology of Industrial and Civil Construction, L.N. Gumilyov Eurasian National University, Astana, Kazakhstan. Email: kleo-14@mail.ru; ORCID ID: https://orcid.org/0000-0003-1010-9328*

Kaklauskas Gintaris — *Professor of Structural Engineering, Gediminas Technical University of Vilnius, Vilnius, Lithuania. Email: Gintaris.Kaklauskas@vgtu.lt*

Zhumagulova Adiya Askarovna — *Researcher, Solid Research Group LLP; Candidate of Technical Sciences, Associate Professor, Department of Industrial and Civil Engineering, L.N. Gumilyov Eurasian National University, 2 Satpayeva Street, 010009, Astana, Kazakhstan. Email: zaaskarovna@gmail.com; ORCID ID: https://orcid.org/0000-0002-6310-2501*

Introduction

The relevance of wall enclosing structures and products is beyond doubt, as the majority of existing and ongoing construction projects are, in one way or another, carried out using artificial stone.

Traditionally, heavy wall structures include brick masonry and concrete walls made from high-density concretes [[1], [2], [3], [4]]. In contrast, lightweight wall systems are formed using aerated concrete and foam concrete [5]. The key distinction between these two groups of materials lies in their intended purpose and structural role: heavy, high-strength concrete is primarily used for load-bearing elements such as columns, foundations, and walls (including panel walls) of multi-storey buildings [6]. The drawbacks of using heavy wall structures include low economic efficiency due to high production costs,

the complexity of the construction process (in the case of brick walls), and the need for additional insulation measures (for heavy concrete) [[7], [8], [9]].

Lightweight concretes, on the other hand, are primarily intended for external enclosures and internal partitions [[10], [11], [12]]. Their porous structure provides enhanced thermal and sound insulation properties, while reduced density decreases the load on the foundation, which is a significant structural advantage. The disadvantages of using lightweight wall structures include their relatively low performance compared to heavy ones, which is associated with lower load-bearing capacity, higher hygroscopicity (in the case of aerated concrete), low frost resistance, high brittleness, and so on [[13], [14], [15], [16], [17], [18], [19]].

The construction product proposed in this project—a two-component multi-purpose wall block—offers novelty both in the technological solution of the wall structure and in its composition and production technology. The novelty also includes the development of a modifying additive derived from industrial waste, whose use is aimed at targeted improvements of the operational characteristics of the wall block composite material (water repellency, frost resistance, and strength). The proposed product differs in composition from existing analogues, and the proposed technological solution is distinct from previously known production technologies (analogues are presented below).

This article presents research on the workability of the concrete mixture used to manufacture the wall block. Studying the workability of the mixture provides essential information for the production process of the wall block. This is particularly relevant because the block consists of two parts: the external façade part and the internal structural-thermal insulation part (Figure 1).

Both parts of the block constitute a monolithic, unified structure; however, they differ in their technological composition as well as their functional purpose. Therefore, the workability of the concrete mixture, as well as the setting time, plays an important role in the production process, since manufacturing involves the sequential pouring into molds—first the heavy façade part, followed by the internal lightweight part of the block. The workability (workability) of the concrete mixture is also particularly important during the production of the façade part, as decorative elements (e.g., imitating brickwork or patterns) may be incorporated into the mold.

Based on the above, the research objectives were defined as follows:

1) To determine the effect of additives on the workability of the concrete mix.
2) To determine the effect of additives on the setting times of the concrete mix.

These indicators will be key for adjusting the placement time of each block layer to ensure a high-quality building product.

Experimental part

Figures 2 and 3 show the technological schemes for the production of the external and internal parts of the blocks. The production of the wall block involves the use of the following components: cement (C), sand (S), lignin (Lg), soapstock (Sp), basalt waste (Bs), aluminum powder (Al), caustic soda (N), and the remainder being water (W).

Lignin in concrete mixtures is used predominantly in the form of lignosulfonates, which are by-products of the sulfite pulping of wood. These compounds act as industrial chemical additives, the performance of which is determined by their interactions with cement particles at the molecular level. Due to their negative charge, lignosulfonate molecules are adsorbed onto the surface of cement grains, imparting a negative charge to the particles themselves. Hydrated shells are formed on their surfaces, which reduce the tendency of particles to coagulate and form aggregates. This effect improves cement dispersion and increases the workability of the concrete mixture [[20], [21]].

Soapstock, which represents a complex of fatty acids, exhibits activity in cement systems mainly due to its surface-active and ion-exchange properties. Its action is associated with a number of characteristic chemical processes. Soapstock components with an amphiphilic structure contain both hydrophilic groups that interact with the aqueous phase and hydrophobic hydrocarbon chains that orient toward air voids or outward from the system. Such molecular orientation contributes to a reduction in surface tension, improves the wetting of cement grains, and ensures the formation of a stable dispersed system [[22], [23]].

To improve the durability of the façade layer against environmental exposure, lignin (a by-product of the wood industry) and soapstock (a waste product of the fat-processing industry) are incorporated into the mixture. The hydrophobicity of soapstock, as well as its resistance to certain acids

and alkalis, enhances the durability of the façade layer exposed to the environment. Additional hydrophobization is achieved through lignin, which promotes polymerization within the façade layer structure.

Because both lignin and soapstock affect mix workability, quantitative evaluation was necessary for developing a technological regulation for two-component block production.

Tests were conducted on series with varying contents of modifying components, compared to reference samples (RS).

For the outer layer, the mass fraction of lignin relative to cement was 0.015; 0.020; 0.025; 0.030; 0.035%. The soapstock fractions were identical— 0.015; 0.020; 0.025; 0.030; 0.035%.

For the inner layer, lignin contents were 0.02; 0.025; 0.03; 0.035; 0.04%, and the basalt filler content varied from 0.5 to 0.9% of sand mass.

Table 1 presents the mix proportions, indicating the masses of the components required to prepare 1 cubic meter of concrete. Sample preparation and testing were carried out under laboratory conditions at an air temperature of 21–23 °C and a relative humidity of 60–65%.

The following laboratory methods were used:

1) Concrete mix workability — GOST 7473-2010 [24].
2) Setting times — GOST 310.3-76 [25].

Table 1 – Proportions of components for concrete preparation

Additives, %	Cement (C)	Lingin (Lg),	Soapstock (Sp),	Sand (S)	Water (W)
RS: Reference sample	950.000	0.000	0	950.0	427.5
Lg=0.015	949.858	0.143	0	950.0	427.5
Lg=0.020	949.810	0.190	0	950.0	427.5
Lg=0.025	949.763	0.238	0	950.0	427.5
Lg=0.030	949.715	0.285	0	950.0	427.5
Lg=0.035	949.668	0.333	0	950.0	427.5
Sp=0.015	950.000		0.045	950.0	427.5
Sp =0.020	949.810		0.190	950.0	427.5
Sp =0.025	949.763		0.238	950.0	427.5
Sp =0.030	949.715		0.285	950.0	427.5
Sp =0.035	949.668		0.333	950.0	427.5

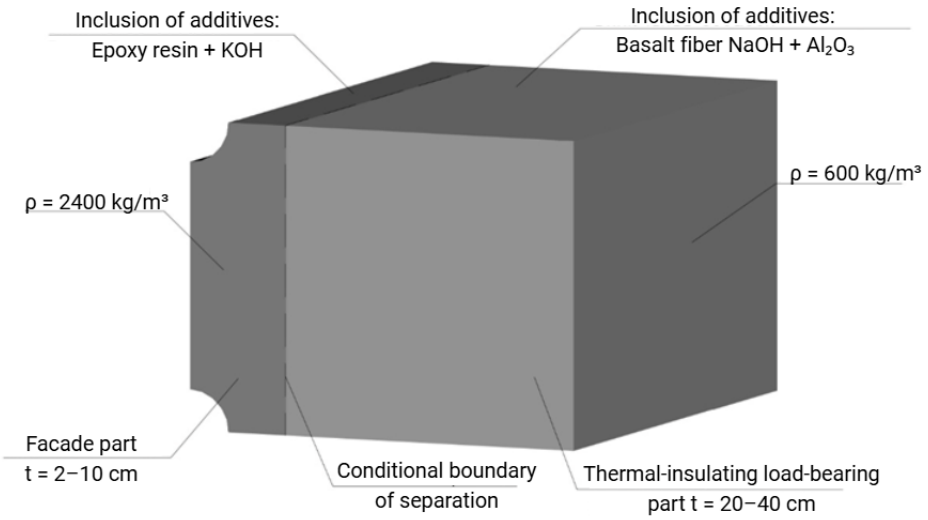

Figure 1 - Structure of the wall block

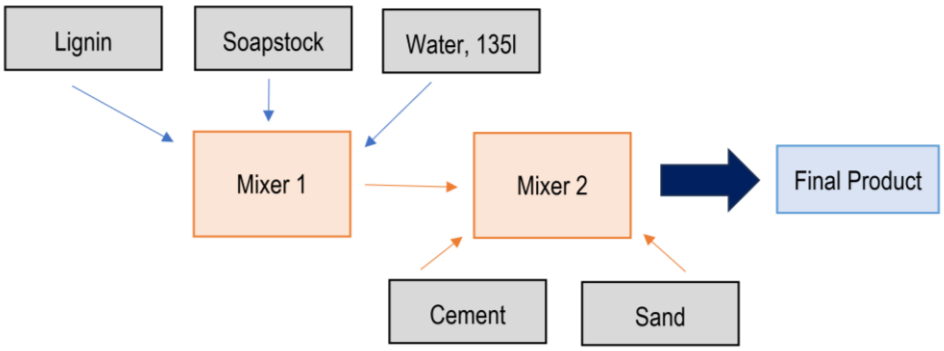

Figure 2 - Production technology of the outdoor part of the unit

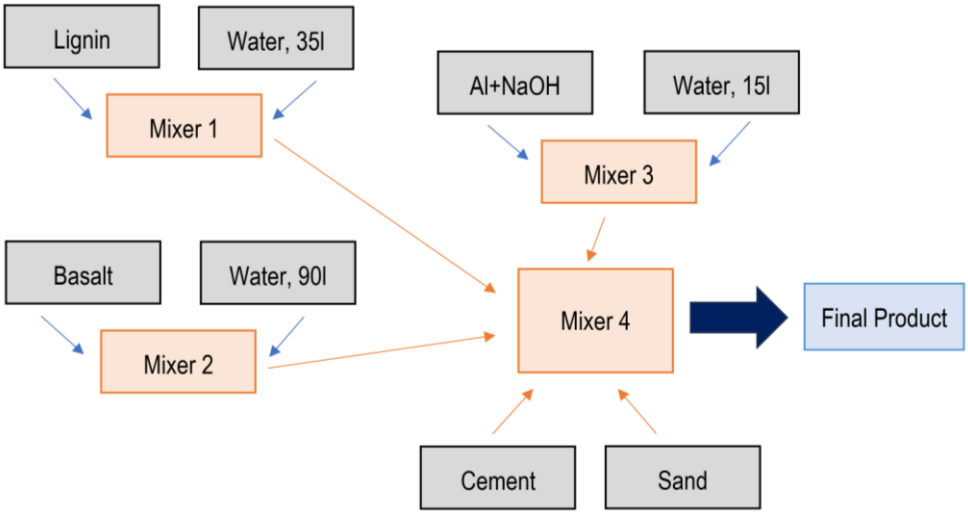

Figure 3 - Production technology of the inner layer

Results and Discussion

1. Workability of Concrete Mix

Figure 4 shows the results of the workability of the concrete mixture with varying composition. Specifically, Figure 1 presents the flow results of the mixture at different lignin (Lg) contents. Figure 5 shows the flow results of the mixture with varying soapstock (Sg) content. Figure 6 presents the flow results of the mixture at the maximum contents of both Lg and Sg.

According to preliminary tests, the water–cement ratio at which a flow spread of 150 cm was achieved is 0.55. Therefore, all workability tests were conducted at this water–cement ratio. The W/C ratio was intentionally kept constant (0.55) to isolate the effect of additives on rheology. Although plasticizers may allow water reduction in conventional concrete technology, varying w/c conditions would introduce additional uncertainty and make it difficult to attribute rheological changes solely to the additives being investigated. Therefore, a fixed w/c ratio was selected to ensure accurate interpretation and comparability of the results. As can be seen from the curve in Figure 4, lignin (Lg) has a pronounced effect on the workability of the mixture: with each increase in Lg concentration, the spread diameter increases. It is also noticeable that the dynamics of the spread change are proportional to the change in concentration.

However, upon the initial introduction of the additive at a concentration of 0.015, a sharp increase in spread is observed (indicating the maximum intensity of the additive's effect), whereas with further increases, the effect decreases, although it remains consistent. Overall, the increment in spread diameter averages 1–2 cm, indicating the stability of Lg's influence on the workability parameter of the concrete mixture.

Analysis of the coefficients of variation further confirms the stability of this positive effect, as the

data dispersion for samples with the additive sharply decreased to 1.5–1.9%, whereas for the reference sample this value was 3.2%. It cannot be concluded that the stability of results increases with higher additive content (despite the apparent decreasing trend in the coefficient of variation with increasing additive), since the fluctuations in variation values are minor and fall within the statistical error, which has a minimum threshold of 1.5%.

According to the curve in Figure 5, the positive effect of the Sp component is also clearly observed. However, the dynamics of change are not consistent. The maximum effect occurs upon the initial introduction of the component. With subsequent additions, the rate of increase decreases but remains noticeable relative to further concentration increases. When the maximum concentration is applied, the increase in spread diameter compared to the previous value is only 1 cm, whereas the initial introduction produced an increase of 4 cm. This indicates that the maximum concentration of Sp = 0.035% approaches the peak effect of the component on enhancing workability. Despite the decreased intensity of the increase, the influence of Sp remains stable.

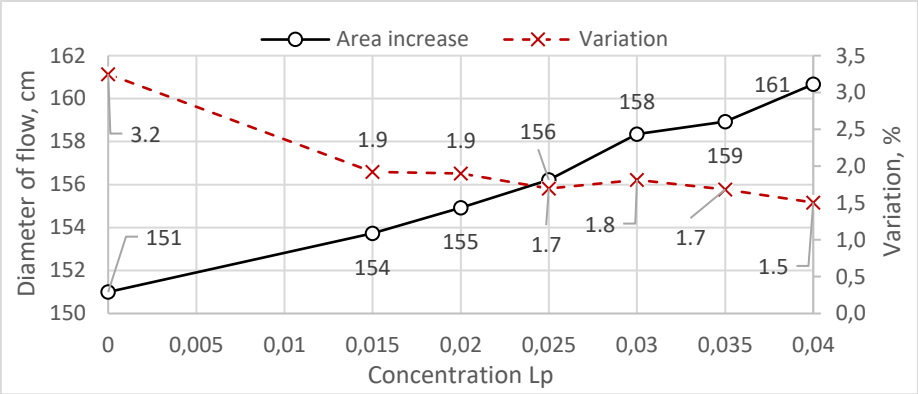

Figure 4 - Change in mix workability with Lg

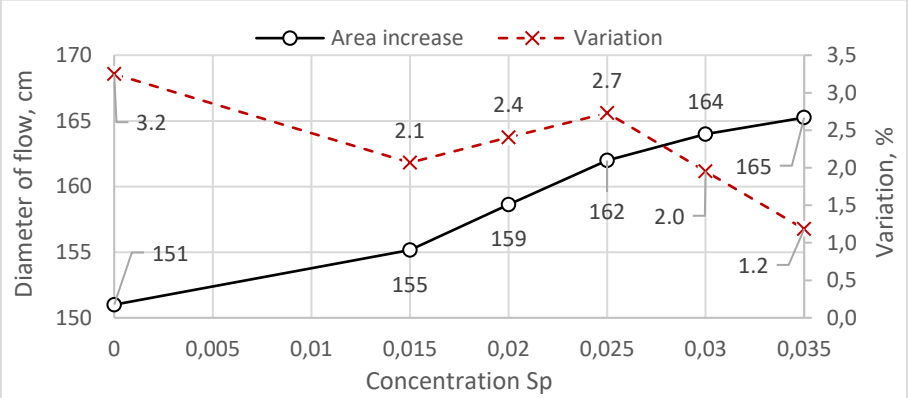

Figure 5 - Change in mix workability with Sp

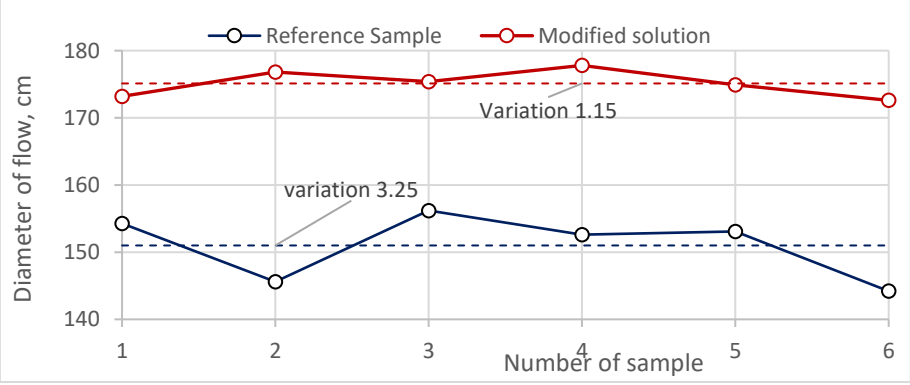

Figure 6 - Workability at maximum Lg and Sp

Moreover, although the intensity of workability improvement decreases with higher concentrations, the stability of the data points increases, as indicated by the coefficients of variation. The dynamics of the coefficients' changes are evident: they decrease proportionally to the increase in concentration, and minor fluctuations (observed in the range of 0.015–0.030%) fall within the statistical error.

According to the curve in Figure 6, which shows the change in spread at the maximum concentrations of Lg and Sp, a presumptive synergistic effect of the components is observed. If the average spread diameter of the reference sample is 151 cm, it reaches 161 cm at the maximum concentration of Lg = 0.04 and 165 cm at the maximum concentration of Sp = 0.035. Under the combined action of Lg and Sp, the increase reaches 175 cm.

In percentage terms, the increase in workability is 15.9% when evaluated based on the increase in diameter as a linear dimension $\left(15.9\% = 100 \times \frac{(175-151)}{151}\right)$, while considering the radial proportional increase in spread area, the gain reaches 34.5% $\left(34.5\% = 100 \times \frac{3.14\times(^{175}/_{2})^{2}-3.14\times(^{151}/_{2})^{2}}{3.14\times(^{151}/_{2})^{2}}\right)$. The coefficients of variation also indicate a synergistic effect of the combined influence of the components.

2. Setting Time of Concrete Mix

Figures 7 and 8 show the results of cement setting time tests. In Figure 7A, the initial setting time, setting duration, and final setting time are presented, while Figure 7B illustrates the dynamics of their changes depending on the Lg concentration. Figures 8A and 8B show the same results for varying concentrations of Sp.

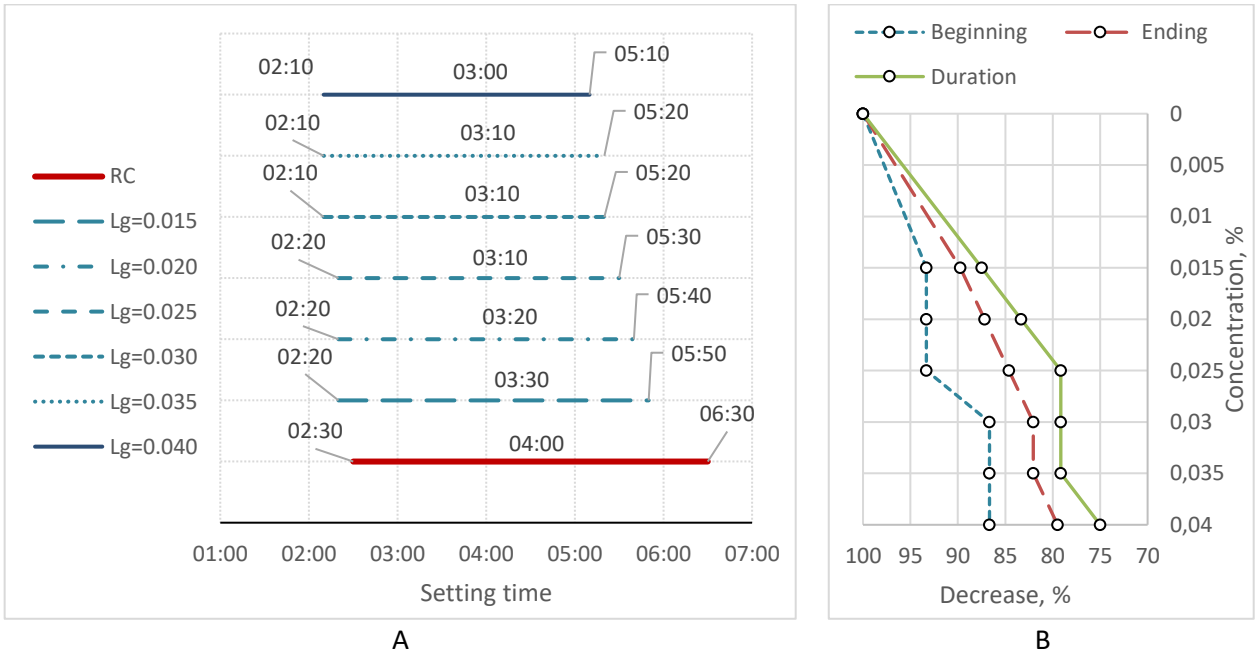

Figure 7 - Setting times at varying Lg content

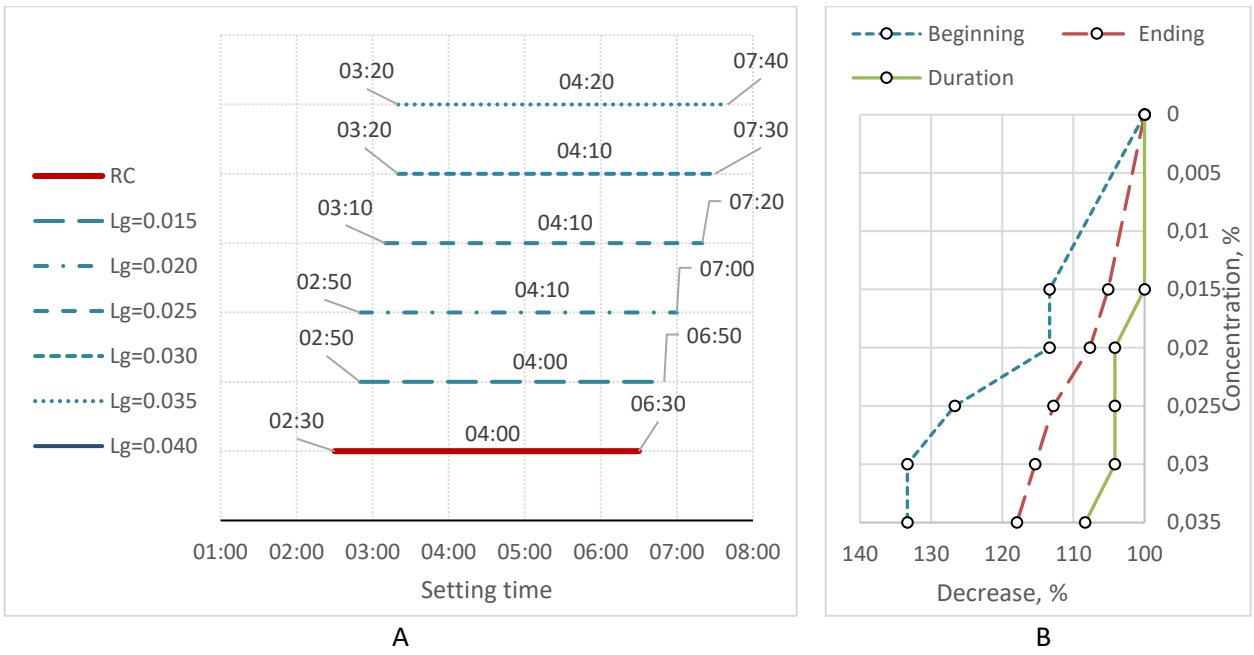

Figure 8 - Setting times at varying Sp content

According to the tests, for samples without admixtures (RS – reference samples), the setting of the paste began 150 minutes after mixing, while full hardening occurred after 420 minutes, with a duration of 240 minutes.

With the addition of Lg, a trend toward a reduction in all setting times is observed, and the higher the admixture concentration, the greater the reduction: at the initial dosage, the initial setting time decreases by 7%, the duration by 10%, and the final setting time by 12%; at the maximum concentration, the same parameters decrease (relative to RS) by 13%, 21%, and 25%, respectively. This trend is of minor significance for the outer layer, as it only requires adjustments in the production process. However, for the inner layer made of lightweight concrete, this trend is more advantageous, as the reduction in setting times contributes to the formation of a more stable pore structure. Therefore, a higher concentration of Lg for the inner layer can be considered justified in terms of reducing setting times, due to the higher alkalinity of the mix compared to the outer layer. Lignosulfonate-based lignin acts primarily as a plasticizing agent, improving cement grain dispersion and reducing the effective w/c ratio. Therefore, lignin leads to a moderate reduction in both initial and final setting times (18–34%), which is consistent with hydration acceleration.

In contrast, the addition of Sp exhibits the opposite pattern. This behavior is expected because soapstock contains vegetable fats with water-repellent properties, which slow the hardening process: at the initial dosage, the initial setting time increases by 13%, the duration by 5%, and the final setting time remains unchanged; at the maximum concentration, the same parameters increase (relative to RS) by 33%, 18%, and 8%, respectively.

Soapstock contains fatty acids, glycerides, and small amounts of alkaline residues. These amphiphilic molecules adsorb onto cement grain surfaces and form thin hydrophobic films which reduce water penetration and slow ionic transport to clinker phases, thereby delaying the dissolution of alite and the nucleation and growth of early C–S–H. The hydrophobic films and altered air-entrainment behavior also change pore-formation and capillary connectivity, which jointly modify hydration kinetics and early age microstructure [[22], [26], [27], [28]].

The coefficients of variation in all tests (six samples per series) did not exceed 5.0%; thus, the observed trends in setting times can be considered significant, as the percentage changes exceed the statistical measurement error. Since the effects of these components partially offset each other, and the setting time primarily influences adjustments in the production process rather than operational performance, the resulting indicators for selecting the optimal concentration should be the concrete's compressive strength (which is expected to increase due to plasticizing and water-reducing effects) and water absorption (which is expected to decrease due to hydrophobization).

Conclusions

1. A comprehensive set of laboratory tests was conducted to evaluate the workability of concrete, including workability and setting time tests. The studies were carried out to facilitate the subsequent adjustment of the technological process for manufacturing the wall block, which is composed of a two-component concrete mix. Tests were performed on samples with varying contents of lignin (Lg) and soapstock (Sp).

2. Workability tests confirmed the influence of Lg and Sp on the workability of the concrete mixture. Each component significantly affects the dynamics of the spread diameter. The higher the concentration of each component, the more pronounced the change in workability. The maximum increase in spread diameter with the addition of Lg, relative to the reference sample, was 6.4%. For Sp, this increase was 9.5%. When both components were added to the concrete mixture, a synergistic effect was observed, with workability increasing by 16% relative to the linear diameter, and by 35% in terms of the radial area. The increase in workability due to Lg is primarily attributed to its plasticizing effect, whereas the increase observed with Sp is due to the presence of vegetable fats in its composition. It should also be noted that the inclusion of these components stabilizes the results, reducing deviations in individual measurements, which positively affects the material quality.

3. Setting time tests produced contrasting results. The addition of Lg to the mixture resulted in a relatively linear decrease in all setting times, whereas the addition of Sp caused an increase in all setting times. The increase in setting times with Sp is explained by the water-repellent effect of the vegetable fats in its composition, while the reduction in setting times with Lg is associated with a decreased w/c ratio due to its plasticizing effect. The trend of increased setting times has little significance for the external part, as it only requires adjustments in the production process. However, for the internal part made of lightweight concrete, the trend is more beneficial, as the reduction in setting time contributes to the formation of a more stable pore structure. In any case, the final adjustment of setting times will be carried out after a control assessment of the basic operational parameters of the wall block (such as strength, frost resistance, water absorption, etc.).

1. Vehicle types were divided into five categories: A1 – bicycles; A2 – motorcycles (mopeds); A3 – passenger cars; A4 – light trucks and buses with very low capacity; A5 – trucks and buses. For each category, voltage ranges were calculated depending on the type of vehicle, the standard load capacity, and tire pressure.

2. For each category of motor vehicles, calculations of normal stresses on the road surface have been performed: for category A1, the stress range is from 48.7 kN/m^2 (0.50 kg/cm^2) to 229.8 kN/m^2 (2.34 kg/cm^2); for A2, from 111.4 kN/m^2 (1.13 kg/cm^2) to 346.2 kN/m^2 (3.53 kg/cm^2); for A3, from 168.8 kN/m^2 (1.72 kg/cm^2) to 316.2 kN/m^2 (3.22 kg/cm^2); for A4 from 259.0 kN/m^2 (2.62 kg/cm^2) to 546.6 kN/m^2 (5.57 kg/cm^2); for A5 from 349.4 kN/m^2 (3.56 kg/cm^2) to 1216.7 kN/m^2 (12.41 kg/cm^2).

Conflicts of interest. The corresponding author declares that there is no conflict of interest.

CRediT author statement: **R. Lukpanov:** concept, methodology; **D. Duyssembinov**: analysis, modeling; **A. Altynbekova**: data collection, editing; **G. Kaklauskas**: editing; **A. Zhumagulova**: analysis, interpretation, visualization.

Acknowledgements. This research has been/was/is funded by the Science Committee of the Ministry of Science and Higher Education of the Republic of Kazakhstan (Grant No. AP26197589 « Development of production technology and composition of composite material for wall blocks using modifying additives from industrial waste»).

Cite this article as: Lukpanov RE, Dyussembinov DS, Altynbekova AD, Kaklauskas G, Zhumagulova AA. Evaluation of the Effect of Additives on the Workability of Concrete Mix as Part of a Study of a Modified Wall Block. Kompleksnoe Ispolzovanie Mineralnogo Syra = Complex Use of Mineral Resources. 2027; 342(3):100-110. https://doi.org/10.31643/2027/6445.34

Модификацияланған қабырға блогын зерттеу аясында бетон қоспасының қозғалғыштығына қоспалардың әсерін бағалау

[1,2]Лукпанов Р.Е., [1,2]Дюсембинов Д.С., [1,2*]Алтынбекова А.Д., [3]Kaklauskas G., [1,2]Жумагулова А.А.

[1]Solid Research Group ЖШС, Астана, Қазақстан
[2]Л.Н. Гумилёв атындағы Еуразия ұлттық университеті, Астана, Қазақстан
[3]Гедиминас техникалық университеті, Вильнюс, Литва

Мақала келді: *23 қараша 2025*
Сараптамадан өтті: *3 желтоқсан 2025*
Қабылданды: *20 қаңтар 2026*

ТҮЙІНДЕМЕ

Мақалада екі компонентті қабырға блокттарын өндіруде қолданылатын бетон қоспасының қозғалғыштығы мен қату уақытына модификациялық қоспалардың әсерін эксперименттік зерттеу нәтижелері ұсынылған. Блок құрылымы сыртқы қасбет қабатын және құрылымдық және жылу оқшаулағыш қабатын қамтиды, бұл бетон қоспасының реологиялық және технологиялық параметрлерін тізбекті қалыптау кезінде дәл реттеуді талап етеді. Модификациялық компоненттер ретінде ағаш және май өңдеу өнеркәсібінің қосалқы өнімдері болып табылатын лигнин және соапсток пайдаланылды. Тәжірибелік бағдарлама бетон қоспасының ағындылығын және қоспалардың әртүрлі концентрацияларында цемент қамырының қату уақытын анықтауды қамтыды. Лигнин мен сабын қоспасын енгізу бақылау құрамымен салыстырғанда бетон қоспасының қозғалғыштығына оң әсер ететіні анықталды: ағып кетудің максималды өсуі лигнин енгізілгенде 6,4%-ға дейін, ал сабын қоспасын енгізген кезде 9,5%-ға дейін жетті. Қоспаларды бірге қолдану айқын синергетикалық әсер берді, бұл қозғалғыштықтың сызықтық тұрғыдан 16%-ға дейін және таралу аймағында 35%-ға дейін артуымен сондай-ақ эксперименттік деректердің шашырауын азайтуды қамтамасыз етті. Қату уақытын зерттеу компоненттердің көп бағытты әсерін көрсетті: лигнин бастапқы және соңғы қату уақытын азайтуға көмектеседі, ал соапсток гидрофобты қасиеттерге ие болғандықтан, олардың артуына әкеледі. Алынған нәтижелер қоспалардың оңтайлы мөлшерін негіздеуге және оларды қасиеттерінің тұрақтылығы мен дайын өнім сапасын арттыратын екі компонентті қабырға блоктарын өндірудің технологиялық регламенттерін түзету үшін пайдалануға мүмкіндік береді.

Түйін сөздер: қабырға блогы, қоспа, қозғалғыштық,, қатаю уақыты, лигнин, соапсток.

Авторлар туралы ақпарат:

Лукпанов Рауан Ермагамбетович — *Аға ғылыми қызметкер, Solid Research Group ЖШС; PhD, профессор, Өнеркәсіптік және азаматтық құрылыс кафедрасы, Л.Н. Гумилёв атындағы Еуразия ұлттық университеті, Сәтпаева көшесі 2, 010009, Астана, Қазақстан. Email: rauan_82@mail.ru; ORCID ID: https://orcid.org/0000-0003-0085-9934*

Дюсембинов Думан Серикович — *Ғылыми жетекші, Solid Research Group ЖШС; Қ.т.ғ.к., доцент, Өнеркәсіптік және азаматтық құрылыс кафедрасы, Л.Н. Гумилёв атындағы Еуразия ұлттық университеті, Сәтпаева көшесі 2, 010009, Астана, Қазақстан. Email: dusembinov@mail.ru; ORCID ID: https://orcid.org/0000-0001-6118-5238*

Алтынбекова Алия Дожанкызы — *Ғылыми қызметкер, Solid Research Group ЖШС; PhD, Өнеркәсіптік және азаматтық құрылыс технологиясы кафедрасы, Л.Н. Гумилёв атындағы Еуразия ұлттық университеті, Астана, Қазақстан. Email: kleo-14@mail.ru; ORCID ID: https://orcid.org/0000-0003-1010-9328*

Kaklauskas Gintaris — *Құрылыс конструкциялары кафедрасының профессоры, Гедиминас атындағы Вильнюс техникалық университеті, Вильнюс, Литва. Email: Gintaris.Kaklauskas@vgtu.lt*

Жумагулова Адия Аскаровна — *Ғылыми қызметкер, Solid Research Group LLP; Техника ғылымдарының кандидаты, Л.Н. Гумилёв атындағы Еуразия ұлттық университетінің Өнеркәсіптік және азаматтық құрылыс кафедрасының доценті, Сәтбаев көш., 2, 010009, Астана, Қазақстан. Email: zaaskarovna@gmail.com; ORCID ID: https://orcid.org/0000-0002-6310-2501*

Оценка влияния добавок на подвижность бетонной смеси в рамках исследования модифицированного стенового блока

[1,2]Лукпанов Р.Е., [1,2]Дюсембинов Д.С., [1,2*]Алтынбекова А.Д., [3]Kaklauskas G., [1,2]Жумагулова А.А.

[1]ТОО Solid Research Group, Астана, Казахстан
[2]Евразийский национальный университет имени Л.Н. Гумилёва, Астана, Казахстан
[3]Технический университет Гедиминаса, Вильнюс, Литва

Поступила: *23 ноября 2025*
Рецензирование: *3 декабря 2025*
Принята в печать: *20 января 2026*

АННОТАЦИЯ

В статье представлены результаты экспериментального исследования влияния модифицирующих добавок на подвижность и сроки схватывания бетонной смеси, применяемой при производстве двухкомпонентного стенового блока. Конструкция блока включает наружный фасадный слой и внутренний конструкционно-теплоизоляционный слой, что требует точного регулирования реологических и технологических параметров бетонной смеси при последовательном формовании. В качестве модифицирующих компонентов использованы лигнин и соапсток — побочные продукты деревообрабатывающей и жировой промышленности. Экспериментальная программа включала определение показателей растекаемости бетонной смеси и сроков схватывания цементного теста при различных концентрациях добавок. Установлено, что введение лигнина и соапстока оказывает положительное влияние на подвижность бетонной смеси по сравнению с контрольным составом: максимальный прирост растекаемости составил до 6,4% при введении лигнина и до 9,5% при введении соапстока. Совместное применение добавок обеспечило выраженный синергетический эффект, сопровождающийся увеличением подвижности до 16% по линейному показателю и до 35% по площади растекания, а также снижением разброса экспериментальных данных. Исследование сроков схватывания показало разнонаправленное влияние компонентов: лигнин способствует сокращению начальных и конечных сроков схватывания, тогда как соапсток, обладая гидрофобными свойствами, приводит к их увеличению. Полученные результаты позволяют обосновать оптимальные дозировки добавок и использовать их для корректировки технологического регламента производства двухкомпонентных стеновых блоков с повышенной стабильностью свойств и качеством готовой продукции.

Ключевые слова: стеновой блок, добавка, подвижность, сроки схватывания, лигнин, соапсток.

Информация об авторах:

Лукпанов Рауан Ермагамбетович — *Старший научный сотрудник, ТОО Solid Research Group; PhD, профессор, кафедра промышленного и гражданского строительства, Евразийский национальный университет имени Л.Н. Гумилёва, ул. Сатпаева 2, 010009, Астана, Казахстан. Email: rauan_82@mail.ru; ORCID ID: https://orcid.org/0000-0003-0085-9934*

Дюсембинов Думан Серикович — *Научный руководитель, ТОО Solid Research Group; К.т.н., доцент, кафедра промышленного и гражданского строительства, Евразийский национальный университет имени Л.Н. Гумилёва, ул. Сатпаева 2, 010009, Астана, Казахстан. Email: dusembinov@mail.ru; ORCID ID: https://orcid.org/0000-0001-6118-5238*

Алтынбекова Алия Дожанкызы — *Научный сотрудник, ТОО Solid Research Group; PhD, кафедра технологии промышленного и гражданского строительства, Евразийский национальный университет имени Л.Н. Гумилёва, Астана, Казахстан. Email: kleo-14@mail.ru; ORCID ID: https://orcid.org/0000-0003-1010-9328*

Kaklauskas Gintaris — *Профессор кафедры строительных конструкций, Вильнюсский технический университет имени Гедиминаса, Вильнюс, Литва. Email: Gintaris.Kaklauskas@vgtu.lt*

Жумагулова Адия Аскаровна — *Научный сотрудник, ТОО Solid Research Group; Кандидат технических наук, доцент кафедры промышленного и гражданского строительства, Евразийский национальный университет имени Л.Н. Гумилёва, ул. Сатпаева 2, 010009, Астана, Казахстан. Email: zaaskarovna@gmail.com; ORCID ID: https://orcid.org/0000-0002-6310-2501*

References

[1] Peceño B, Alonso-Fariñas B, Vega G, Carrizo D, Leiva C. Sustainable Fire-Resistant Materials: Thermal, Physical, Mechanical, and Environmental Behavior of Walls with Waste from the Aquaculture Industry. Materials. 2024; 18(22):5086. https://doi.org/10.3390/ma18225086

[2] Tamošaitienė J, Parham S, Sarvari H, Chan D W, Edwards D J. A review of the application of synthetic and natural polymers as construction and building materials for achieving sustainable construction. Buildings. 2024; 14(8):2569. https://doi.org/10.3390/buildings14082569

[3] Roy A, Shaik S. Investigation of the potential of repurposing waste disposals into concretes: mechanical properties, reduction in cooling/heating energy costs, and carbon exudation mitigation prospective. Environ Sci Pollut Res. 2025; 32: 21495–21521. https://doi.org/10.1007/s11356-025-36897-0

[4] Sau-Soto N, Lucero-Álvarez J, Borbón-Almada AC, Nájera-Trejo M, Rodríguez-Muñoz NA. Structural analysis for a slab-on-grade cellular concrete foundation to reduce heat losses in temperate climate residential buildings. Journal of Building Engineering. 2024; 91:109740. https://doi.org/10.1016/j.jobe.2024.109740

[5] AlSuwaidi N, Alfalasi S, Al Tayyari R, Al Buraimi K, AlQassimi M, Aidan A, Al-Asheh S. Silica Enrichment and Aerated Light Concrete for Sustainable Construction from Multiple Geographic Locations Within the UAE and UK. Buildings. 2025; 15(21):3869. https://doi.org/10.3390/buildings15213869

[6] Zhang J, Guo X, Tang X. Experimental and numerical simulation of seismic behavior of reinforced concrete frames infilled with refractory straw blocks. In Structures. 2024; 69:107475. https://doi.org/10.1016/j.istruc.2024.107475

[7] Celik A, Mercimek Ö, Akkaya ST, Bıçakçıoğlu K, Anıl Ö. A novel bond-slip model between TRM strips and different types of masonry walls: Experimental approach. Construction and Building Materials. 2025; 458:139595. https://doi.org/10.1016/j.conbuildmat.2024.139595

[8] Lisowski P, Glinicki MA. Promising biomass waste–derived insulation materials for application in construction and buildings. Biomass Conv. Bioref. 2025; 15:57–74. https://doi.org/10.1007/s13399-023-05192-8

[9] Hassan A, Alomayri T, Noaman MF. 3D Printed Concrete for Sustainable Construction: A Review of Mechanical Properties and Environmental Impact. Arch Computat Methods Eng. 2025; 32:2713–2743. https://doi.org/10.1007/s11831-024-10220-5

[10] Thienel K-C, Haller T, Beuntner N. Lightweight Concrete—From Basics to Innovations. Materials. 2020; 13(5):1120. https://doi.org/10.3390/ma13051120

[11] Bertino G, Kisser J, Zeilinger J, Langergraber G, Fischer T, Österreicher D. Fundamentals of Building Deconstruction as a Circular Economy Strategy for the Reuse of Construction Materials. Applied Sciences. 2021; 11(3):939. https://doi.org/10.3390/app11030939

[12] Qadir G, Rashid Y, Hassan A, Vall E, Saleh S, Salim K. Development and Mechanical Testing of Porous-Lightweight Geopolymer Mortar. Buildings. 2021; 11(1):1. https://doi.org/10.3390/buildings11010001

[13] Zajac M, Kuzniar K, Tatara T. Effect of Load-Bearing Wall Material on Building Dynamic Properties. Materials. 2024; 17(24): 6101. https://doi.org/10.3390/ma17246101

[14] Hassan HZ, Saeed NM. Advancements and applications of lightweight structures: a comprehensive review. Discov Civ Eng. 2024; 1:47. https://doi.org/10.1007/s44290-024-00049-z

[15] Yeo S J, Oh M J, Yoo P J. Structurally controlled cellular architectures for high-performance ultra-lightweight materials. Advanced Materials. 2019; 31(34):1803670. https://doi.org/10.1002/adma.201803670

[16] Tao L, Shi C, Ding P. A study on bearing characteristic and failure mechanism of thin-walled structure of a prefabricated subway station. Front. Struct. Civ. Eng. 2022; 16:359-377. https://doi.org/10.1007/s11709-022-0816-2

[17] Costantino C, Bigiotti S, Marucci A, Gulli R. Long-Term Comparative Life Cycle Assessment, Cost, and Comfort Analysis of Heavyweight vs. Lightweight Construction Systems in a Mediterranean Climate. Sustainability. 2024; 16(20):8959. https://doi.org/10.3390/su16208959

[18] Jelčić Rukavina M, Skejić D, Kralj A, Ščapec T, Milovanović B. Development of Lightweight Steel Framed Construction Systems for Nearly-Zero Energy Buildings. Buildings. 2022; 12(7):929. https://doi.org/10.3390/buildings12070929

[19] Santos P, Lopes P, Abrantes D. Thermal Performance of Load-Bearing, Lightweight, Steel-Framed Partition Walls Using Thermal Break Strips: A Parametric Study. Energies. 2022; 15(24):9271. https://doi.org/10.3390/en15249271

[20] Wei R, Sakai Y. Improving the properties of botanical concrete based on waste concrete, wood, and kraft lignin powder. Powder Technology. 2022; 397:117024. https://doi.org/10.1016/j.powtec.2021.11.068

[21] Wang L, Wang Y, Zhang J, Wang F, Liu Z, Jiang J. Investigation on self-healing polyurethane coating doped with lignin composites for protecting cementitious materials. Construction and Building Materials. 2024; 411:134368. https://doi.org/10.1016/j.conbuildmat.2023.134368

[22] Dyussembinov D, Lukpanov R, Altynbekova A, Zhantlesova Z, Awwad T. Effect of soapstock in the composition of modified additive for improving strength characteristics of concrete structures. Kompleksnoe Ispolzovanie Mineralnogo Syra= Complex use of mineral resources. 2025; 334(3):37-50. https://doi.org/10.31643/2025/6445.26

[23] Kozhas A, Kozhasov S. Fine-grained concrete for repair and restoration based on complex modifiers. Technobius. 2023; 3(2):0038. https://doi.org/10.54355/tbus/3.2.2023.0038

[24] GOST 310.4–2012 Cements. Methods for determining consistency, setting time and soundness. Moscow: Standartinform. 2013.

[25] GOST 56587–2015 Concrete mixtures. Methods for determining workability. Moscow: Standartinform. 2016.

[26] Lukpanov R, Dyussembinov D, Altynbekova A, Yenkebayev S, Zhumagulova A. Investigation of Effect of proposed two-stage foam injection method and modified additive on workability of Foam concrete. Materials. 2024; 17(9):024. https://doi.org/10.3390/ma17092024

[27] Sartaev DT, Orynbekov YS, Baisarieva AM, Uxikbayeva DA. Influence of additives and temperature regime on the setting kinetics and strength of foamed concrete. Kompleksnoe Ispolzovanie Mineralnogo Syra= Complex use of mineral resources. 2027; 340(1):5-16. https://doi.org/10.31643/2027/6445.01

[28] Abdyrov A, Niyazbekova P, Serekbayev H, Ibrayeva Ж, Shansharova Л, Ospanova H, Aldabergenova C. The effect of ash and slag waste on the setting time of cement dough and paste. Bulletin of L.N. Gumilyov Eurasian National University Technical Science and Technology Series. 2023; 145(4):98–110. https://doi.org/10.32523/2616-7263-2023-145-4-98-110

Crossref
DOI: 10.31643/2027/6445.35
Mining & Mineral Processing

Flowsheet Design and Modelling for High Purity Praseodymium and Neodymium by Solvent Extraction

[1] Zulkifli N., [1*] Shoparwe N., [1] Yusoff A.H., [2]Abdullah A.Z., [3] Ahmad M. N.

[1] Gold, Rare Earth and Materials Technopreneurship Centre (GREAT) at Universiti Malaysia Kelantan, Jeli, Malaysia
[2] Universiti Sains Malaysia, Pulau Pinang, Malaysia
[3] Universiti Islam Antarabangsa Malaysia, Kuantan, Pahang, Malaysia

** Corresponding author email: fazliani.s@umk.edu.my*

Received: *November 28, 2025*
Peer-reviewed: *November 30, 2025*
Accepted: *January 20, 2026*

ABSTRACT

Purifying rare earth elements (REEs) from ion-adsorbed clay (IAC) deposits demands complex solvent extraction (SX) setups to achieve commercial-grade purity. This study presents the design and validation of a four-train counter-current SX flowsheet for processing a pre-treated REE chloride liquor sourced from Malaysia's Jeli deposit. Using an iterative steady-state mass-balance simulation in Microsoft Excel, the research determines the operational parameters needed to achieve a 4N (99.99%) terminal purity target for each REE stream. The methodology involved pinpointing critical A/B separation cuts and optimising the organic-to-aqueous (O/A) ratios across the cascade. The results show that the flowsheet effectively fractionates the feedstock, starting with a bulk LREE/HREE separation (Train 1) and culminating in the challenging separation of praseodymium (Pr) and neodymium (Nd) (Train 4). The simulation identified Pr/Nd separation as the primary technical bottleneck, requiring 62 equilibrium stages (NE) due to a low separation factor (β) of 1.70. In contrast, simpler bulk splits needed as few as 16 stages. These findings confirm the theoretical minimum stage requirements (N_{min}) and provide a detailed stage-wise concentration profile for each train. The study concludes that the Pr/Nd circuit dictates the overall plant footprint and capital intensity. The developed flowsheet offers a solid technical blueprint for commercialising Malaysian IAC resources, ensuring high-purity REE recovery through optimised metallurgical design.

Keywords: REE separation, solvent extraction, P507, equilibrium curve, extraction stages.

Information about authors:

Norazihan Zulkifli — *PhD candidate at Gold, Rare Earth and Material Technopreneurship Centre (GREAT), Faculty of Bioengineering and Technology, Universiti Malaysia Kelantan, Jeli 17600 Kelantan, Malaysia. Email: norazihan.zulkifli@gmail.com; ORCID ID: https://orcid.org/0009-0009-4772-0578*

Noor Fazliani Shoparwe — *Associate Professor at Gold, Rare Earth and Material Technopreneurship Centre (GREAT), Faculty of Bioengineering and Technology, Universiti Malaysia Kelantan, Jeli 17600 Kelantan, Malaysia. Email: fazliana.s@umk.edu.my; ORCID ID: https://orcid.org/0000-0002-4329-2459*

Abdul Hafidz Yusoff — *Associate Professor at Gold, Rare Earth and Material Technopreneurship Centre (GREAT), Faculty of Bioengineering and Technology, Universiti Malaysia Kelantan, Jeli 17600 Kelantan, Malaysia. Email: hafidz.y@umk.edu.my; ORCID ID: https://orcid.org/0000-0003-0229-886X*

Abdullah A.Z. — *Professor at School of Chemical Engineering, Engineering Campus, Universiti Sains Malaysia, 14300 Nibong Tebal, Pulau Pinang, Malaysia. Email: chzuhairi@usm.my*

Mohammad Norazmi Ahmad — *Associate Professor at Sustainable Nanotechnology and Computational Chemistry (SuNCoM) Research Group, Department of Chemistry, Kulliyyah of Science, Universiti Islam Antarabangsa Malaysia, 25200 Kuantan, Pahang, Malaysia. Email: mnorazmi@iium.edu.my; ORCID ID: https://orcid.org/0000-0001-5742-0346*

Introduction

Rare Earth Elements (REEs), including the 15 lanthanides, scandium, and yttrium, are vital to high-tech sectors such as defense, renewable energy, and electronics [1]. Ensuring a stable and sustainable supply has become a global priority, prompting intensive research into new primary ore sources and innovative recovery methods for secondary materials [[2], [3], [4], [5]]. Robust processing techniques are essential in the global supply chain for handling complex raw materials such as hydrometallurgical recovery of rare earth elements (REEs) from secondary sources, including neodymium-iron-boron (NdFeB) permanent magnet scrap [6]. Recovering from primary REE sources remains essential, especially as the world shifts its focus to unconventional resources [[7], [8], [9]]. The ion-adsorbed clay (IAC), the raw material for this study, is a complex feed material sourced from the

Jeli deposit in Malaysia. It is an ionic resource extracted by in situ leaching (ISL). This feedstock poses significant challenges owing to its heterogeneity and the complex mixture of light and heavy rare-earth elements (LREEs and HREEs) [10]. Developing a specialised, sophisticated processing method capable of efficiently recovering all valuable REE from ISL liquors, particularly Pr and Nd, is crucial to the successful exploitation of the Jeli resource.

The core technological challenge in the REE industry is the separation of individual elements, which share remarkably similar chemical properties [11]. Historically, solvent extraction (SX) has been the industry standard for commercial-scale, continuous separation [12], with the Lynas Advanced Materials Plant (LAMP) serving as a contemporary benchmark [13]. However, even within world-class facilities, separating the entire REE series presents significant operational hurdles. These challenges highlight gaps in current industrial SX practice, particularly in the number of stages required for the separation of adjacent elements at high purity.

The stringent purity requirements of downstream applications, such as optics and photonics, further complicate process design. For example, the separation of praseodymium (Pr) from neodymium (Nd) is particularly demanding due to its extremely low separation factor (b) [14]. Achieving a 99.99% (4N) purity target for these elements is crucial for commercial viability, necessitating complex systems with high stage counts [15]. Research has shown that even trace contaminants can significantly reduce luminescence efficiency in optical materials, as demonstrated by studies comparing Nd, Ho, Er, and Sm oxides in glass matrices [[16], [17], [18], [19], [20], [21], [22]]. Consequently, this application-driven standard mandates that the entire flowsheet reliably produce individual rare-earth oxides at 4N purity.

Ion-exchange (IX) chromatography and crystallisation are typically reserved for laboratory applications or the final purification of high-purity materials. Nevertheless, they are neither scalable nor cost-effective for continuous, large-volume REE separation. For example, even in specific applications such as ion exchange of lanthanum chloride with advanced resins, the process remains inherently batch-oriented, presenting significant scaling challenges compared with continuous SX [23]. The key decision in high-volume REE processing, therefore, lies between IX and SX, as other methods, such as fractional crystallisation, cannot separate the entire REE series [[24], [25], [26]]. Figure 1 provides a comparative overview illustrating the fundamental differences in mechanism and operation between IX and SX.

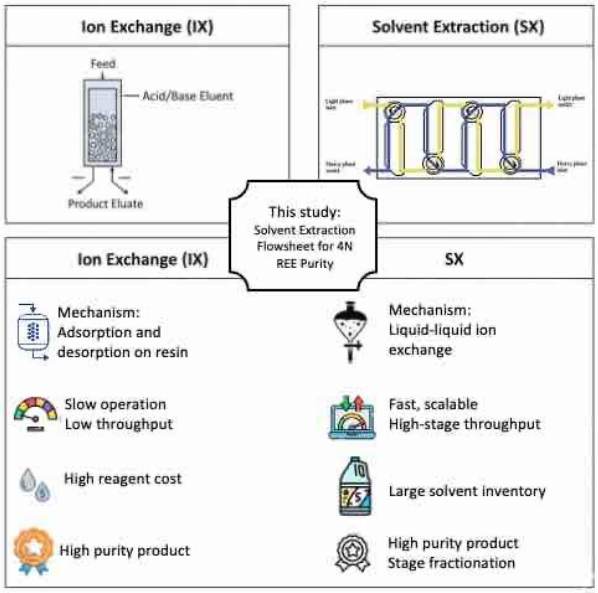

Figure 1 - Comparative Analysis and Process Principle of Ion Exchange (IX) versus Solvent Extraction (SX) for Rare Earth Element Separation

SX is overwhelmingly preferred for primary industrial separation due to its ability to handle large, continuous throughput. It employs counter-current flow through mixer-settlers or columns relying on subtle differences in distribution coefficients ($) between adjacent elements. The choice of the organic extractant is the single most critical chemical decision in an SX flowsheet. The acidic extractant bis(2-ethylhexyl) phosphoric acid (P507) was selected for the flowsheet based on its established industrial use and capacity for controllable selectivity via pH adjustments, which is essential for LREE fractionation, particularly the challenging Pr/Nd split [[27], [28]].

Complex mixed-extractant systems are effective for the bulk separation of HREEs; their performance is typically suboptimal for LREE fractionation. For example, the combination of P507 with bis(2,4,4-trimethylpentyl) phosphinic acid (Cyanex 272) [29] or its equivalent, Cyanex 572 [[30], [31], [32]], is known to enhance the extraction of HREEs from chloride solutions. However, in such systems, the resulting enhanced selectivity for HREEs conversely leads to poorer separation performance among the LREE group [33], which constitutes the majority of the Jeli feedstock. Therefore, the use of P507 alone is justified to provide the necessary selectivity

control for the difficult LREE-focused splits required to achieve the 4N purity target.

The highly efficient separation required by SX is achieved physically through a series of interconnected mixer-settler units operating in a counter-current flow configuration, as shown in Figure 2, where Figure 2(a) explains the working principle of a single mixer settler and Figure 2(b) illustrates the separation principle in a series circuit.

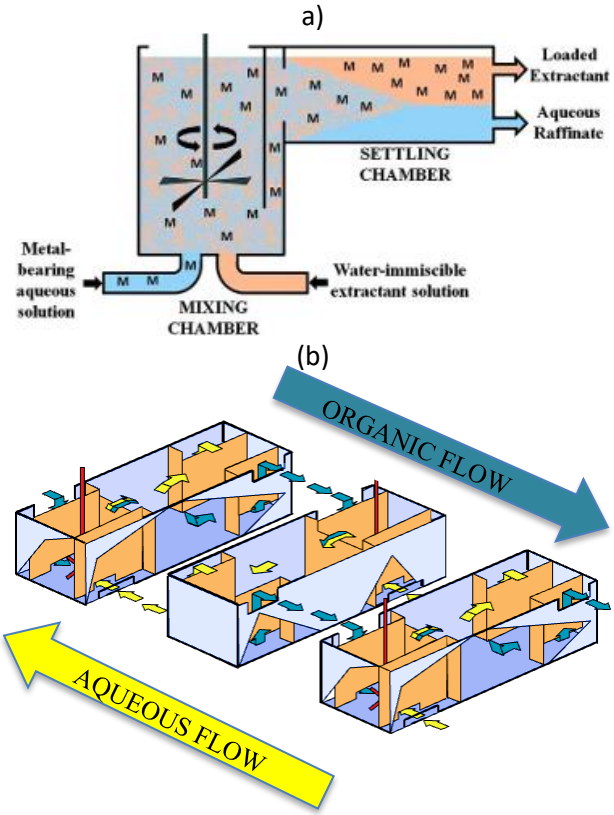

Figure 2 - Working principle of mixer settler

In the mixing chamber, a motor drives a mixing and pumping turbine. This turbine draws two liquids from adjacent settler stages, mixes them and transfers the resulting emulsion to the corresponding settler. Efficient mixing creates a large interfacial area, maximising solute mass transfer. The emulsion then overflows into the settling chamber, where gravity separates the liquids. The heavier aqueous liquid settles at the bottom, while the lighter organic liquid rises to the top and overflows a fixed-height weir. This gravity-driven discharge transports the liquid to the next mixing chamber or downstream equipment.

Rare earth extraction (REEP) is typically a sequential cascade process involving three main stages: extraction, scrubbing, and stripping. Industrial facilities such as LAMP employ a six-stage process comprising saponification, loading, extraction, scrubbing, stripping, and washing. Figure 3 illustrates this cascade operating under counter-current flow: the organic phase enters at one end, and the aqueous feed enters at an internal stage, moving in the opposite direction.

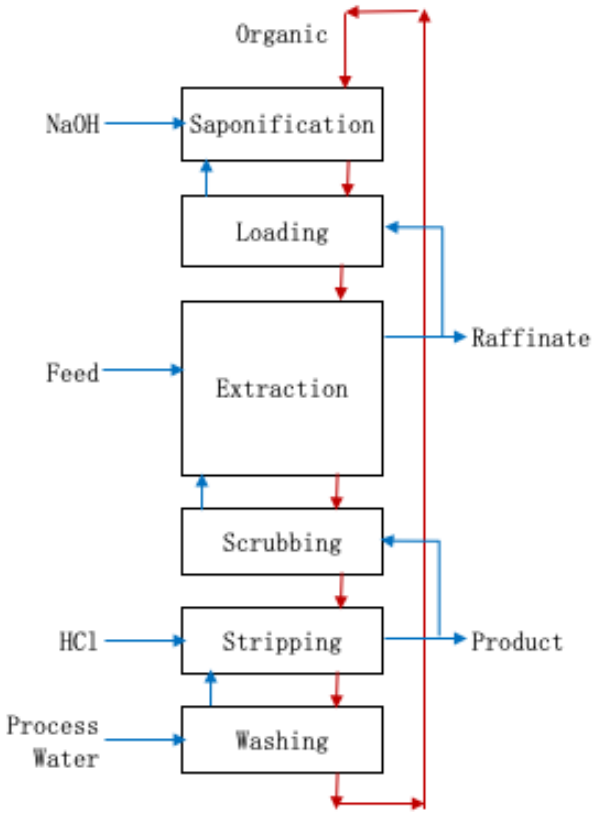

Figure 3 - Schematic Diagram of a Six-Block Counter-Current Solvent Extraction Cascade (Saponification, Loading, Extraction, Scrubbing, Stripping, and Washing).

This inherent counter-current arrangement maximises mass-transfer efficiency, thereby enabling the use of a rigorous mass-balance model. The main challenge in SX design is accurately determining the optimal flow ratios (O/A) and the minimum number of equilibrium stages (N_{min}). These parameters are crucial for converting the slight chemical differences provided by P507 into commercial purity.

This study addresses a technological gap by presenting a rigorously designed and validated four-train SX flowsheet for separating a complex mixture of LREE and HREE from the Jeli resource. The primary objective is to rigorously justify the flowsheet's design parameters, particularly the high stage counts required for adjacent-element separation. Using an iterative mass-balance model, the paper systematically derives the overall-to-actual flow ratios. It calculates the necessary

equilibrium stages (N_E) to ensure the flowsheet can produce individual rare-earth oxide products to the stringent 4N purity standard.

Experimental part

Materials and Feedstock Preparation. The feed material for the SX flowsheet design was a pre-treated REE chloride solution from the Jeli deposit in Malaysia. The original Jeli IAC resource was initially processed via the ISL hydrometallurgical route to produce a bulk REE liquor. To ensure high-purity separation, the liquor underwent upstream purification, including selective precipitation and redissolution, to concentrate REEs and remove non-metallic contaminants and gross impurities such as silica and carbonates. The resulting clarified REE chloride solution was the primary input for iterative mass-balance modelling. The elemental composition is detailed in Table 1, with concentrations expressed in both parts per million (ppm) and as a mass percentage of the total REE content.

Theoretical Framework of Solvent Extraction. The SX process using P507 operates via an ion-exchange mechanism. In the organic phase, P507 (usually represented as HL) predominantly exists as a dimer $(HL)_2$. During extraction, the trivalent REE ion (REE^{3+}) from the aqueous phase replaces the protons (H^+) in the extractant dimer, forming an organometallic complex that then partitions into the organic phase. The balanced chemical equation for this extraction is given by Equation 1.

$$REE^{3+}_{(aq)} + 3(HL)_{2(org)} \rightleftharpoons REE(HL_2)_{3(org)} + 3H^+_{(aq)} \quad (1)$$

In practice, the extraction complex can be solvated and the number of extractant molecules per metal ion may vary. The distribution coefficient (*D*) is strongly inversely related to aqueous pH (or H^+ concentration) as shown in the equilibrium relationship of Equation 2.

$$D = \frac{[REE]org}{[REE]aq} = K_{ex}\frac{[(HL)_2]^3_{org}}{[H^+]^3_{aq}} \quad (2)$$

This relationship demonstrates that aqueous-phase acidity and extractant concentration govern the extent of extraction. These dynamics are typically visualised through extraction isotherms, which illustrate how pH adjustments are leveraged to control extraction and stripping across the various flowsheet trains [34].

Table 1 - Jeli mix REE chloride composition

Element	Concentration (ppm)	Normalised Concentration (%)
REE		
La	1245.431	38%
Ce	161.159	5%
Pr	211.278	6%
Nd	596.106	18%
Sm	88.268	3%
Eu	11.463	0%
Gd	115.513	4%
Tb	18.351	1%
Dy	94.645	3%
Ho	17.166	1%
Er	83.993	3%
Tm	12.583	0%
Yb	52.871	2%
Lu	5.359	0%
Y	578.472	18%
Sc	0.104	0%
Total	3292.762	100%
Non-REE		
Al	0.950	-
Pb	0.381	-
Cu	0.259	-
Ga	0.227	-
Ca	0.141	-
Al	0.056	-
Pb	0.048	-
Na	0.047	-
Mo	0.040	-
Sr	0.017	-
Co	0.015	-
Ag	0.005	-
Mg	0.001	-
Total	2.187	-

The required N_E for a counter-current SX circuit is fundamentally governed by β of the critical adjacent pair and the stringency of the purity requirement. β is defined as the ratio of D of the two elements being separated (A and B), where β is the most extracted element, and A is the least attracted component. This is expressed in Equation 3.

$$\beta_{B/A} = \frac{D_B}{D_A} \quad (3)$$

The theoretical β values used were sourced from the literature, primarily the work of Krishnamurthy Gupta (1990) [35] for the P507-HCl REE extraction system [36]. A high β facilitates an efficient separation, whereas a low β necessitates an increased number of mixer-settler contacts to achieve the same purity [37]. N_{min}, is approximated using the relationship derived from the Fenske equation, as shown in Equation 4.

$$N_{min} = \frac{\log\left(\frac{Purity\ Ratio}{Recovery\ Ratio}\right)}{\log(\beta)} \quad (4)$$

In this context, the purity ratio is the ratio of the key component B to the impurity A in the final product stream. The recovery ratio is the ratio of B recovered in the product stream to the amount of A lost to the raffinate.

This requirement justifies the complex design and detailed mass-balance analysis in the following sections.

Flowsheet Design and Mass Balance Methodology. The practical number of equilibrium stages (N_E) and the required organic-to-aqueous ratio (O/A; R) were determined using a process simulation developed in Microsoft Excel. The schematic representation of the counter-current mixer-settler stage configuration used as the basis for this mass-balance calculation is presented in Figure 4.

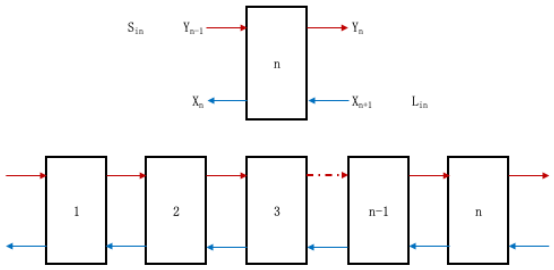

Figure 4 - Input and output flow variables for a mixer-settler stage configuration

This iterative approach is essential for accurately modelling the complex requirements of ultra-high-purity targets (4N), where conventional graphical methods often lack the precision required to resolve concentrations at the 0.01% threshold. The 4N target purity necessitates a high stage count throughout the flowsheet. To achieve this, the impurity concentration in each product stream must be rigorously reduced, thereby approaching near-total theoretical recovery in the respective raffinate and extractant streams. This design philosophy is most critical for separating the Pr/Nd pair, the most capital-intensive step in the process.

The initialisation of the solvent flow was based on a fractional extraction approach. A base flow parameter (W) was established as a function of β and a fractional extraction parameter (K).

$$W = \frac{1}{\beta^K - 1} \quad (5)$$

For the Jeli flowsheet, K was optimized at 0.75. This value was selected to bias the extraction intensity toward the organic phase, thereby shifting the concentration crossover point toward the extract terminal. This design strategy aims to provide an expanded scrubbing section within the calculated cascade, ensuring that the aqueous raffinate meets 4N requirements by effectively "washing" entrained impurities from the organic phase. To account for the mass flux required to satisfy terminal purity targets (P) and feed fractions (f), the final Total Organic-to-Aqueous Ratio (R) was calculated as equation 6.

$$R = W + \left(\frac{f_A \cdot P_B}{P_A}\right) \quad (6)$$

A key feature of this flowsheet design is the requirement for 4N purity in intermediate product fractions. While a lower intermediate target (e.g., 2N or 3N) would reduce the stage requirements of the preceding separation cascades, it would introduce an "impurity carryover" effect. By enforcing a 4N target at these intermediate steps, the flowsheet acts as a metallurgical firewall, ensuring that downstream circuits are not burdened with residual light or heavy impurities from prior splits. This isolation prevents a "snowball effect," in which downstream-stage requirements would otherwise increase significantly to accommodate cross-contamination. This strategic approach ensures that each separation battery operates only on its intended adjacent pairs, maintaining the integrity of the final high-purity oxides.

After defining the cut, the simulation iteratively calculated concentration profiles across all stages until terminal concentration requirements were satisfied. At stage n, the total mass balance for component A is given by Equation 5, where L and S represent the aqueous and organic flow rates, respectively.

$$(L.X_{n-1}) + (S.Y_{n+1}) = (L.X_n) + (S.Y_n) \quad (5)$$

By substituting D_A with Y_n / X_n and the flow ratio A/O as represented with R equivalent to S/L, the balance solved in the iterative form shown in Equation 6.

$$X_{n-1} + R.D_A.X_{n+1} = (L + R.D_A).X_n \quad (6)$$

This modelling relies on the assumption of ideal equilibrium behaviour at each stage and constant flow rates throughout the cascade. The simulation explicitly examines the separation of adjacent elements within each train, aiming for near-total recovery driven by strict 4N terminal purity requirements. Table 2 outlines the key inputs for the iterative mass-balance model, including the derived β and the resulting N_{min} needed to achieve the 4N purity target for each critical separation train.

Results and Discussion

The complex composition of the Jeli feedstock necessitates a sequential, four-train SX flowsheet to achieve the stringent 4N purity target for rare-earth oxides. This flowsheet prioritises broader bulk splits before addressing more chemically similar cuts, exploiting differences in β values between adjacent elements. The Pr/Nd separation primarily dictates the overall flowsheet scale and capital intensity, as its low β of 1.70 necessitates the highest number of stages. After calculating N_{min}, an iterative mass-balance simulation was used to determine the necessary operational parameters, specifically the optimal O/A ratio and the N_E required to achieve the 4N purity target for each split. Figure 5 presents the block diagram for the four-train sequential SX flowsheet, summarising the proposed processing route. It details the mass distribution and specific fractional cuts for the Jeli REE chloride feedstock, progressing from the initial bulk LREE/HREE split to the final high-purity products.

Table 2 – Summary of **b**, target purities, and N_{min} for the Jeli REE separation aims

Train	Separation Cut	β	Component		Fraction In Feed		Target Purity		*K*
			A	***B***	f_A	***B***	***PA***	***PB***	
1	LaCePrNd/Sm-Lu	8	LaCePrNd	Sm-Lu	0.65	0.35	99.99%	99.99%	0.75
2	LaCe/PrNd	2.25	LaCe	PrNd	0.64	0.36	99.99%	99.99%	0.75
3	La/Ce	6	La	Ce	0.88	0.12	99.99%	99.99%	0.75
4	Pr/Nd	1.70	Nd	Pr	0.25	0.75	99.99%	99.99%	0.75

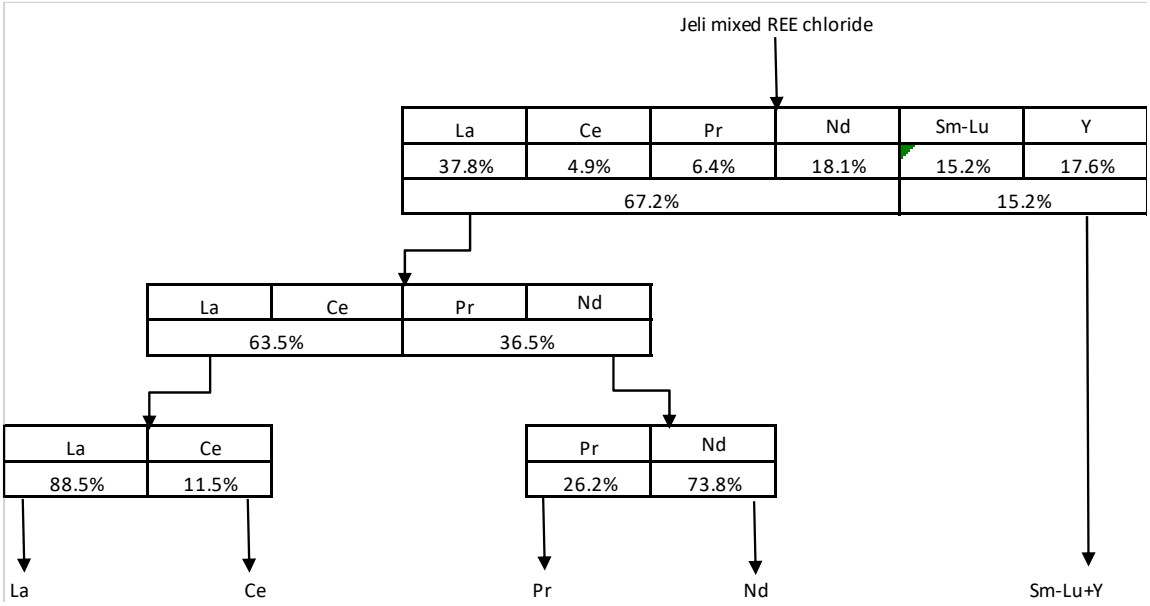

Figure 5 - Block diagram of the proposed four-train sequential solvent extraction flowsheet for Jeli REE chloride feedstock

Figure 6 illustrates the concentration profiles of components A and B across the extraction stages. Stage 1 (leftmost terminal) is the raffinate outlet, highly enriched in the least-extracted element (A). Stage 2 (rightmost terminal) is the extract outlet, enriched in the most-extracted element (B). The crossover point, where A and B concentrations intersect, shifts with different separation factors. Figure 6 (a) (LREE/HREE, β = 8.0) shows a sharp crossover, indicating efficient separation with fewer stages. Figure 6 (d) (Pr/Nd, β = 1.70) shows a shallower gradient, indicating greater difficulty in separation and requiring more stages to reduce impurity levels to 0.01%. Figure 7 presents the separation flowsheet matching the stage numbers for each train.

The final operational deliverables, determined by the iterative mass-balance model, are shown in Table 3. The data confirm that the 4N purity target for both the raffinate (PA) and extract (PB) streams was achieved in all four separation trains. A comparison between N_{min} and N_E reveals a consistent scaling factor of 1.8. Table 3 also compares the total stage count required for each train, highlighting the disparity in separation difficulty. Notably, Train 4 (Pr/Nd) requires the most intensive configuration, with an N_E of 62 stages to overcome the pair's low separation factor. This is nearly four times the stage count required for the bulk LREE/HREE split (Train 1), highlighting the significant impact of adjacent-element chemistry on total plant footprint.

The findings confirm the industrial principle that the Pr/Nd separation is the main bottleneck, limiting the maximum CAPEX and OPEX of the entire LREE purification facility. The 62-stage cascade requires a large physical footprint and complex process control for flow rates and pH stability. However, the simulation shows that the optimised O/A ratios in Table 3 can reliably achieve high recovery and purity without significant material loss.

Conclusions

This study developed and validated a four-train counter-current solvent extraction flowsheet for processing a pre-treated REE chloride solution from the Jeli IAC deposit. An iterative steady-state mass-balance simulation determined operational parameters for a stringent 4N purity target for five product streams.

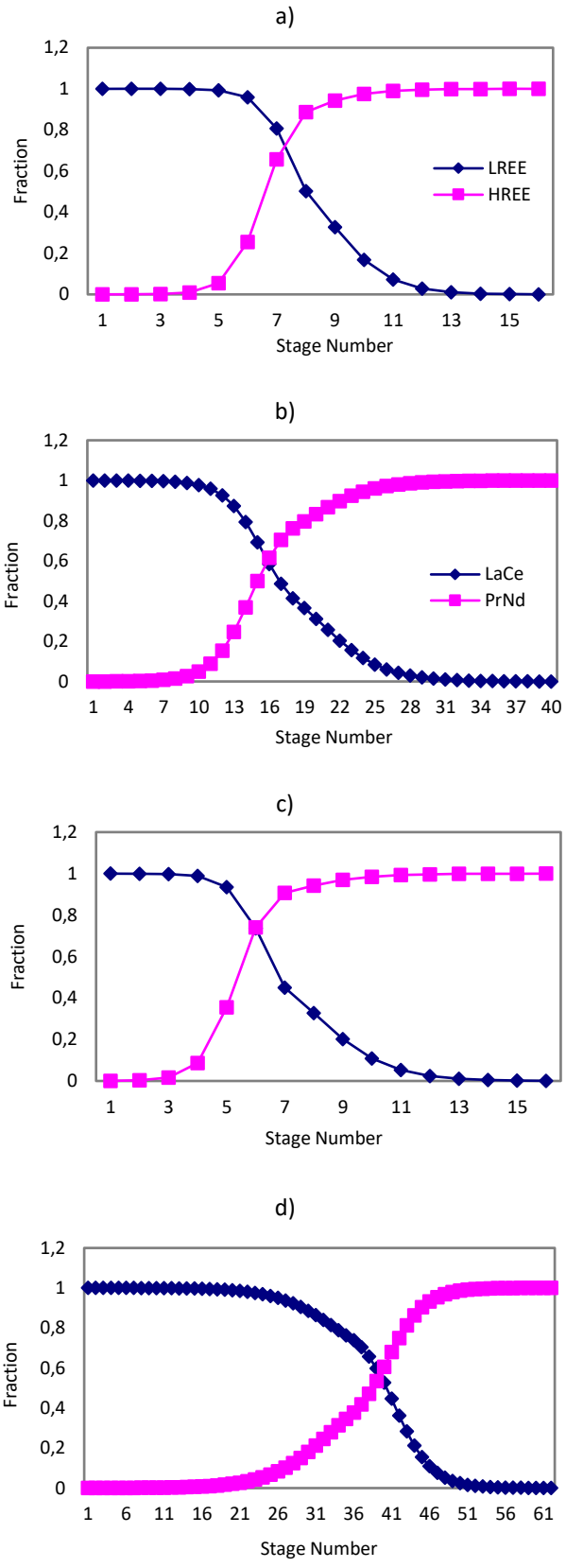

Figure 6 – Extraction battery concentration profile a) LREE/HREE (67:15, β=8), b) LaCe/PrNd (64:36, β=4.57), c) La/Ce (88:12, β=6), and Pr/Nd (76:24, β=1.7)

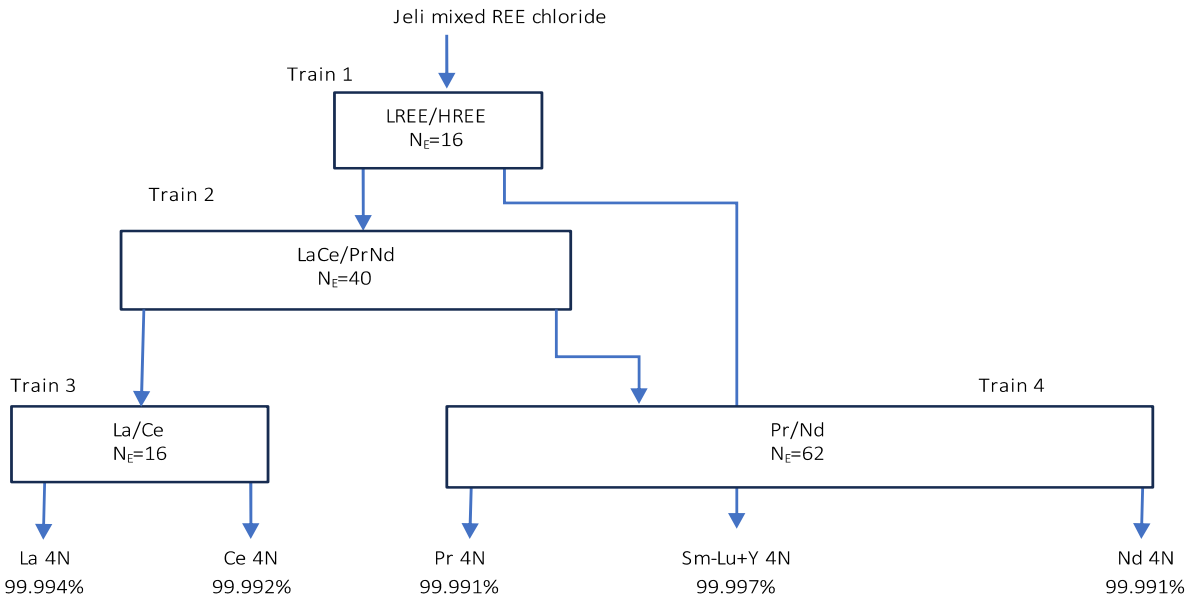

Figure 6 – LREE separation process flowsheet with P507-HCl

Table 3 – Input to equilibrium state calculation

Train	Separation Split (A/B)	Theoretical Minimum Stages (N_{min})	Actual Equilibrium Stages (N_E)	Optimized O/A Ratio	Purity A (P_A)	Purity B (P_B)
1	LaCePrNd/Sm-Lu	8.86	16	0.27	99.99%	99.99%
2	LaCe/PrNd	22.72	40	1.20	99.99%	99.99%
3	La/Ce	10.28	16	0.35	99.99%	99.99%
4	Pr/Nd	34.72	62	2.32	99.99%	99.99%

The Pr/Nd separation (Train 4) is the critical design bottleneck due to its low separation factor (β = 1.70), requiring 62 equilibrium stages, a nearly four-fold increase compared to the 16 stages required for initial LREE/HREE bulk split.

This high stage count affects the primary capital expenditure (CAPEX) and operational complexity (OPEX), requiring precise control over O/A ratios and pH stability to prevent material loss. Simulation results in Table 3 show that N_E aligns with N_{min}, providing a foundation for future pilot-scale testing. The successful separation of La, Ce, and the PrNd group from the Jeli feedstock demonstrates the technical feasibility of producing high-value individual rare earth oxides from Malaysian ion-adsorbed clay resources. This flowchart offers a scalable plan for processing IAC ores, which helps create a local and sustainable rare earth supply chain.

Conflicts of interest. On behalf of all authors, the corresponding author states that there is no conflict of interest.

CRediT author statement: **N. Zulkifli**: Conceptualization, Methodology; **N. Shoparwe**: Supervision; **A. H. Yusoff**: Co-supervision; **A. Z. Abdullah:** Co-supervision; **M. N. Ahmad**: Co-supervision.

Acknowledgements. This work was supported by the GREAT Universiti Malaysia Kelantan Research Fund grant number R/FRGS/A1300/01702A/007/2023/01193.

Cite this article as: Zulkifli N, Shoparwe N, Yusoff AH, Abdullah AZ, Ahmad MN. Flowsheet Design and Modelling for High Purity Praseodymium and Neodymium by Solvent Extraction. Kompleksnoe Ispolzovanie Mineralnogo Syra = Complex Use of Mineral Resources. 2027; 342(3):111-122. https://doi.org/10.31643/2027/6445.35

Еріткішпен экстракциялау арқылы жоғары тазалықтағы празеодим мен неодимді алудың технологиялық схемасын әзірлеу және модельдеу

[1] Zulkifli N., [1*] Shoparwe N., [1] Yusoff A.H., [2]Abdullah A.Z., [3] Ahmad M. N.

[1] Малайзия университеті Келантан, Джели, Малайзия
[2] Малайзия ғылым университеті, Пенанг, Малайзия
[3] Малайзия Халықаралық Ислам Университеті, Куантан, Паханг, Малайзия

Мақала келді: *28 қараша 2025*
Сараптамадан өтті: *30 қараша 2025*
Қабылданды: *20 қаңтар 2026*

ТҮЙІНДЕМЕ

Сирек жер элементтерін (СЖЭ) иондық адсорбцияланған саздардан (ИАЖ) тазартып, коммерциялық тазалыққа қол жеткізу үшін күрделі еріткіш экстракция (SX) жүйелері қажет. Бұл зерттеуде Малайзиядағы Джели кенішінен алынған алдын ала өңделген REE хлоридін өңдеуге арналған төрт тізбекті қарсы ток SX ағындық сұлбасының дизайны мен валидациясы ұсынылады. Microsoft Excel бағдарламасындағы итеративті тұрақты күйдегі массалық балансты модельдеуді қолдана отырып жүргізілген зерттеу әрбір сирек кездесетін жер элементтері ағындарында 4N тазалық мақсатына (99,99%) жету үшін қажетті жұмыс параметрлерін анықтады. Әдістеме маңызды A/B бөлу кесінділерін дәл анықтауды және каскадтағы органикалық пен су (O/A) қатынастарын оңтайландыруды қамтыды. Нәтижелер сұлба шикізатты тиімді түрде фракциялайтынын көрсетеді, ол LREE/HREE (1-ші желі) көлемдік бөлуден бастап, празеодим (Pr) мен неодимді (Nd) кешенді бөлумен аяқталады (4-ші желі). Модельдеу Pr/Nd бөлінуін негізгі техникалық кедергі ретінде анықтады, ол 1,70 төмен бөліну коэффициентіне (β) байланысты 62 тепе-теңдік сатысын (NE) қажет етті. Ал қарапайым масса бөлінулері тек 16 сатыны қажет етеді. Бұл нәтижелер теориялық минималды сатылы талаптарды (Nmin) растайды және әрбір пойыз үшін сатылы концентрацияның егжей-тегжейлі профилін ұсынады. Зерттеу нәтижесінде Pr/Nd қатынасы жалпы зауыт ауданын және оның күрделі қаржы сыйымдылығын анықтайды деген қорытынды жасалды. Әзірленген хаттама Малайзияның IAC ресурстарын коммерцияландырудың сенімді техникалық жол картасын ұсынады, оңтайландырылған металлургиялық жобалау арқылы жоғары тазалықтағы СЖЭ алуды қамтамасыз етеді.

Түйін сөздер: СЖЭ бөлінуі, еріткішпен экстракциялау, P507, тепе-теңдік қисығы, экстракция кезеңдері.

Авторлар туралы ақпарат:

Norazihan Zulkifli
PhD докторант, Малайзия университеті Келантан, Джели 17600 Келантан, Малайзиядағы Биоинженерия және технология факультетінің Алтын, сирек жер және материалдар технокәсіпкерлік орталығы (GREAT). Email: norazihan.zulkifli@gmail.com; ORCID ID: https://orcid.org/0009-0009-4772-0578

Noor Fazliani Shoparwe
Қауымдастырылған профессор, Алтын, сирек жер және материалдар технологиялары орталығы (GREAT), биоинженерия және технология факультеті, Малайзия университеті Келантан, Джели 17600 Келантан, Малайзия. Email: fazliana.s@umk.edu.my; ORCID ID: https://orcid.org/0000-0002-4329-2459

Abdul hafidz Yusoff
Қауымдастырылған профессор, Малайзия университеті Келантан, Джели 17600 Биоинженерия және технология факультетінің Алтын, сирек жер және материалдық технокәсіпкерлік орталығы (GREAT). Email: hafidz.y@umk.edu.my; ORCID ID: https://orcid.org/0000-0003-0229-886X

Abdullah A.Z.
Малайзия ғылым университеті, Химиялық инженерия мектебінің профессоры, 14300 Нибонг Тебал, Пулау Пинанг, Малайзия. Email: chzuhairi@usm.my

Mohammad Norazmi Ahmad
Тұрақты нанотехнология және есептеу химиясы (SuNCoM) зерттеу тобының қауымдастырылған профессоры, Малайзия Халықаралық Ислам Университеті, 25200, Куантан, Паханг, Малайзия. Email: mnorazmi@iium.edu.my; ORCID ID: https://orcid.org/0000-0001-5742-0346

Разработка и моделирование технологической схемы получения высокочистого празеодима и неодима методом экстракции растворителем

[1] Zulkifli N., [1*] Shoparwe N., [1] Yusoff A.H., [2]Abdullah A.Z., [3] Ahmad M. N.

[1] Университет Малайзии Келантан, Джели, Келантан, Малайзия
[2] Университет науки Малайзии, Пенанг, Малайзия
[3] Международный исламский университет Малайзии, Куантан, Паханг, Малайзия

Поступила: *28 ноября 2025*
Рецензирование: *30 ноября 2025*
Принята в печать: *20 января 2026*

АННОТАЦИЯ

Очистка редкоземельных элементов (REE) для достижения коммерческой чистоты из ионно-адсорбированных глин (IAC) требует сложных систем экстракции растворителями (SX). В данном исследовании представлены проектирование и валидация четырёхпоездного противотокового SX расходного листа для переработки предварительно обработанного хлорида REE, полученного из месторождения Jeli в Малайзии. В исследовании, проведенном с использованием итеративного моделирования баланса массы в стационарном режиме в Microsoft Excel, определены рабочие параметры, необходимые для достижения целевого показателя чистоты 4N (99,99%) для каждого потока редкоземельных элементов. Методология включала точное определение критических разрезов между A/B и оптимизацию соотношения органического к водному (O/A) по всему каскаду. Результаты показывают, что схема эффективно фракционирует сырьё, начиная с массового разделения LREE/HREE (поезд 1) и заканчивая сложным разделением празеодима (Pr) и неодима (Nd) (Поезд 4). Симуляция определила разделение Pr/Nd как основное техническое узкое место, требующее 62 равновесных стадий (NE) из-за низкого коэффициента разделения (β) 1,70. В отличие от этого, более простые массовые сплиты требовали всего 16 этапов. Эти результаты подтверждают теоретические минимальные требования к этапам (Nmin) и предоставляют подробный профиль концентрации по этапам для каждого поезда. Исследование пришло к выводу, что контур Pr/Nd определяет общую площадь завода и его капиталоёмкость. Разработанный протокол предлагает надёжный технический план коммерциализации ресурсов малайзийских IAC, обеспечивая высокочистое извлечение РЗЭ благодаря оптимизированному металлургическому проектированию.

Ключевые слова: разделение РЗЭ, экстракция растворителем, P507, кривая равновесия, этапы экстракции.

Информация об авторах:

Norazihan Zulkifli *PhD докторант, Центр технопредпринимательства в области золота, редкоземельных элементов и материалов (GREAT), факультет биоинженерии и технологий, Университет Малайзии Келантан, Jeli 17600, Келантан, Малайзия. Email: norazihan.zulkifli@gmail.com; ORCID ID: https://orcid.org/0009-0009-4772-0578*

Noor Fazliani Shoparwe *Ассоциированный профессор, Центр технопредпринимательства в области золота, редкоземельных элементов и материалов (GREAT), факультет биоинженерии и технологий, Университет Малайзии Келантан, Jeli 17600, Келантан, Малайзия. Email: fazliana.s@umk.edu.my; ORCID ID: https://orcid.org/0000-0002-4329-2459*

Abdul hafidz Yusoff *Ассоциированный профессор, Центр технопредпринимательства в области золота, редкоземельных элементов и материалов (GREAT), факультет биоинженерии и технологий, Университет Малайзии Келантан, Jeli 17600, Келантан, Малайзия. Email: hafidz.y@umk.edu.my; ORCID ID: https://orcid.org/0000-0003-0229-886X*

Abdullah A.Z. *Профессор Школы химической инженерии, инженерный кампус, Университет науки Малайзии, 14300 Нибонг Тебал, Пулау Пинанг, Малайзия. Email: chzuhairi@usm.my*

Mohammad Norazmi Ahmad *Ассоциированный профессор исследовательской группы по устойчивым нанотехнологиям и вычислительной химии (SuNCoM), кафедра химии, Международный исламский университет Малайзии, 25200 Куантан, Паханг, Малайзия. Email: mnorazmi@iium.edu.my; ORCID ID: https://orcid.org/0000-0001-5742-0346*

References

[1] Balaram V. Rare earth elements, resources, applications, extraction technologies, chemical characterization, and global trade – A comprehensive review. 2024. https://doi.org/10.1016/B978-0-323-99762-1.00041-3

[2] Chang CS, Yusoff AH, Mohamed CAR, Liu SF, Shoparwe NF, Husain NA, & Azlan MN. Geochemistry of rare earth elements in Pahang river sediment, Malaysia. Kompleksnoe Ispolzovanie Mineralnogo Syra = Complex Use of Mineral Resources. 2024; 331(4):42–50. https://doi.org/10.31643/2024/6445.37

[3] Salehi H, Maroufi S, Mofarah SS, Nekouei RK, & Sahajwalla V. Recovery of rare earth metals from Ni-MH batteries: A comprehensive review. Renewable and Sustainable Energy Reviews. 2023; 178:113248. https://doi.org/10.1016/j.rser.2023.113248

[4] Balaram V. Sustainable recovery of rare earth elements by recycling of E-waste for a circular economy. 2024, 499–544. https://doi.org/10.1016/B978-0-443-22069-2.00023-1

[5] Hua H, Yasuda K, Norikawa Y, & Nohira T. Highly efficient and precise rare-earth elements separation and recycling process in molten salt. Engineering. 2025; 45:165–173. https://doi.org/10.1016/j.eng.2022.12.013

[6] Zhang Y, Gu F, Su Z, Liu S, Anderson C, & Jiang T. Hydrometallurgical recovery of rare earth elements from NdFeB permanent magnet scrap: a review. Metals. 2020; 10(6):841. https://doi.org/10.3390/met10060841

[7] Hermassi M, Granados M, Valderrama C, Ayora C, & Cortina JL. Recovery of rare earth elements from acidic mine waters: An unknown secondary resource. The Science of the Total Environment. 2022; 810:152258. https://doi.org/10.1016/j.scitotenv.2021.152258

[8] Wu M, Yu M, Cheng Q, Yuan Q, Mei G, Liang Q, & Wang L. Flotation recovery of Y2O3 from waste phosphors using ionic liquids as collectors. Chemical Physics Letters. 2023; 825:140608. https://doi.org/10.1016/j.cplett.2023.140608

[9] Gkika DA, Chalaris M, & Kyzas GZ. Review of methods for obtaining rare earth elements from recycling and their impact on the environment and human health. Processes. 2024; 12(6). https://doi.org/10.3390/pr12061235

[10] Shafiee NS, Achmad Bahar AM, & Ali Khan MM. Potential of rare earth elements (REEs) in Gua Musang granites, Gua Musang, Kelantan. IOP Conference Series: Earth and Environmental Science. 2020; 549(1):012027. https://doi.org/10.1088/1755-1315/549/1/012027

[11] Liu T, & Chen J. Extraction and separation of heavy rare earth elements: A review. Separation and Purification Technology. 2021; 276:119263. https://doi.org/10.1016/j.seppur.2021.119263

[12] Dewulf B, Riaño S, & Binnemans K. Separation of heavy rare-earth elements by non-aqueous solvent extraction: Flowsheet development and mixer-settler tests. Separation and Purification Technology. 2022; 290:120882. https://doi.org/10.1016/j.seppur.2022.120882

[13] Zulkifli N, Shoparwe NF, Yusof AH, Abdullah AZ, & Ahmad MN. From light to heavy: addressing gaps in rare earth element extraction at the lynas advanced materials plant. Malaysian Journal of Bioengineering and Technology (MJBeT). 2024; 1(2):113–120. https://doi.org/10.31643/2024/6445.32

[14] Salehi H, Khani S, Adeli M, & Aboutalebi MR. Multistage hydrometallurgical process for enhanced recovery and individual separation of Nd and Pr from NdFeB magnet scrap. Mineral Processing and Extractive Metallurgy. 2024; 133(1-2):33-41. https://doi.org/10.1177/25726641241233219

[15] Ahmad I, Jamal MA, Iftikhar M, Ahmad A, Hussain S, Asghar H, Saeed M, Yousaf AB, Karri RR, Al-Kadhi NS, Ouladsmane M, Ghfar A, & Khan S. Lanthanum-Zinc Binary Oxide Nanocomposite with Promising Heterogeneous Catalysis Performance for the Active Conversion of 4-Nitrophenol into 4-Aminophenol. Coatings. 2021; 11(5). https://doi.org/10.3390/coatings11050537

[16] Azlina Y, Azlan MN, Halimah MK, Umar SA, El-Mallawany R, & Najmi G. Optical performance of neodymium nanoparticles doped tellurite glasses. Physica B: Condensed Matter. 2022; 577:411784. https://doi.org/10.1016/j.physb.2019.411784

[17] Nazrin SN, Halimah MK, Muhammad FD, Latif AA, Iskandar SM, & Asyikin AS. Experimental and theoretical models of elastic properties of erbium-doped zinc tellurite glass system for potential fiber optic application. Materials Chemistry and Physics. 2021; 259:123992. https://doi.org/10.1016/j.matchemphys.2020.123992

[18] Vani P, Vinitha G, Praveena R, Durairaj M, Sabari Girisun TC, & Manikandan N. Influence of holmium ions on the structural and optical properties of barium tellurite glasses. Optical Materials. 2023; 136:113438. https://doi.org/10.1016/j.optmat.2023.113438

[19] Yusof NN, Abd Azis MN, & Mohammad Yusoff N. Exploring the impact of plasmonic nanoparticles on photoluminescence of Er^{3+}—doped sodium zinc tellurite glass for solid-state laser applications. Kompleksnoe Ispolzovanie Mineralnogo Syra = Complex Use of Mineral Resources. 2024; 330(3):85-91. https://doi.org/10.31643/2024/6445.32

[20] Azlina Y, Azlan MN, Suriani AB, Shaari HR, Al-Hada NM, Umar SA, Kenzhaliyev BK, Zaid MHM, Hisam R, Iskandar SM, Yusof NN, & Yusoff AH. Incorporation of neodymium, holmium, erbium, and samarium (oxides) in zinc-borotellurite glass: Physical and optical comparative analysis. Kompleksnoe Ispolzovanie Mineralnogo Syra = Complex Use of Mineral Resources. 2025; 332(1):32–48. https://doi.org/10.31643/2025/6445.03

[21] Kumari H, Ansari GF, Mahajan SK, Rezaul K, & Bairagi S. Study of visible upconversion luminescence in Er3+ and Er3+/Yb3+ doped tungsten tellurite glasses. Materials Today: Proceedings. 2023. https://doi.org/10.1016/j.matpr.2023.06.294

[22] Wu Y, Niu C, Wang L, Yang M, & Zhang S. Structural, luminescence, and temperature sensing properties of the Er3+-doped germanate-tellurite glass by excitation at different wavelengths. Journal of Luminescence. 2024; 266:120323. https://doi.org/10.1016/j.jlumin.2023.120323

[23] Zulkifli N, Shoparwe N, Yusof AH, Abdullah, AZ, & Ahmad MN. Ion exchange of lanthanum chloride and Lewatit Monoplus S 108 H resin. Malaysian Journal of Bioengineering and Technology (MJBeT). 2025; 2(3):115-128. https://doi.org/10.70464/mjbet.v2i3.1710

[24] Talan D & Huang. QA review of environmental aspect of rare earth element extraction processes and solution purification techniques. Minerals Engineering. 2022; 179:107430. https://doi.org/10.1016/j.mineng.2022.107430

[25] Traore M, Gong A, Wang Y, Qiu L, Bai Y, Zhao W, Liu Y, Chen Y, Liu Y, Wu H, Li S, & You Y. Research progress of rare earth separation methods and technologies. Journal of Rare Earths. 2023; 41(2):182-189. https://doi.org/10.1016/j.jre.2022.04.009

[26] Pathapati SVSH, Free ML, Sarswat PK. A comparative study on recent developments for individual rare earth elements separation. Processes. 2023; 11(7). https://doi.org/10.3390/pr11072070

[27] Dorozhko, VA, & Afonin MA. Nonstationary separation of Nd and Pr by P507 extractant. E3S Web of Conferences. 2021; 266:02005. https://doi.org/10.1051/e3sconf/202126602005

[28] Pan J, Zhao X, Zhou C, Yang F, & Ji W. Study on solvent extraction of rare earth elements from leaching solution of coal fly ash by P204. Minerals. 2022; 12(12):1547. https://doi.org/10.3390/min12121547

[29] Afonin MA, Nechaev AV, Yakimenko IA, & Belova VV. Extraction of rare earth elements from chloride solutions using mixtures of P507 and Cyanex 272. Compounds. 2024; 4(1):172-181. https://doi.org/10.3390/compounds4010008

[30] Belova VV, Tsareva YuV, & Kostanyan AE. Extraction of rare-earth elements from chloride solutions in multicomponent systems using CYANEX 572. Theoretical Foundations of Chemical Engineering. 2022; 56(5):915-919. https://doi.org/10.1134/S0040579522050025

[31] Belova V, Petyaeva M, & Kostanyan A. Extraction of lanthanides from chloride solutions in hexane–isopropanol–water systems using Cyanex 572. Theoretical Foundations of Chemical Engineering. 2022; 56:595–599. https://doi.org/10.1134/S0040579522040078

[32] Dashti S, Shakibania S, Rashchi F, & Ghahreman A. Synergistic effects of Ionquest 801 and Cyanex 572 on the solvent extraction of rare earth elements (Pr, Nd, Sm, Eu, Tb, and Er) from a chloride medium. Separation and Purification Technology. 2021; 279:119797. https://doi.org/10.1016/j.seppur.2021.119797

[33] Salehi H, Maroufi S, Khayyam Nekouei R & Sahajwalla V. Solvent extraction systems for selective isolation of light rare earth elements with high selectivity for Sm and La. Rare Metals. 2025; 44(3):2071–2084. https://doi.org/10.1007/s12598-024-03019-7

[34] Srivastava V, Werner J, & Honaker R. Design of multi-stage solvent extraction process for separation of rare earth elements. Mining. 2023; 3(3):552–578. https://doi.org/10.3390/mining3030031

[35] Krishnamurthy N, & Gupta CK. Extractive metallurgy of rare earths (0 ed.). CRC Press. 2015. https://doi.org/10.1201/b19055

[36] Merroune A, Ait Brahim J, Berrada M, Essakhraoui M, Achiou B, Mazouz H, & Beniazza R. A comprehensive review on solvent extraction technologies of rare earth elements from different acidic media: Current challenges and future perspectives. Journal of Industrial and Engineering Chemistry. 2024; 139:1–17: https://doi.org/10.1016/j.jiec.2024.04.042

[37] Turgeon K, Boulanger JF, Bazin, C Turgeon K, Boulanger JF, & Bazin C. Simulation of solvent extraction circuits for the separation of rare earth elements. Minerals. 2023; 13(6). https://doi.org/10.3390/min13060714

МАЗМҰНЫ
СОДЕРЖАНИЕ
CONTENTS

METALLURGY AND METALLURGICAL ENGINEERING

EARTH AND PLANETARY SCIENCES: EARTH-SURFACE PROCESSES

MINING & MINERAL PROCESSING

Техникалық редакторлар:
Г.К. Қасымова, Н.М.Айтжанова, Т.И. Қожахметов

Компьютердегі макет:
Г.К. Қасымова

Дизайнер:
Г.К. Қасымова, Н.М.Айтжанова

“Металлургия және кен байыту институты” АҚ
050010, Қазақстан Республикасы, Алматы қаласы, Шевченко к-сі, 29/133

Жариялауға 21.01.2026 жылы қол қойылды

Технические редакторы:
Г.К. Касымова, Н.М. Айтжанова, Т.И. Кожахметов

Верстка на компьютере:
Г.К. Касымова

Дизайнер:
Г.К. Касымова, Н.М.Айтжанова

АО “Институт металлургии и обогащения”
050010, г. Алматы, Республика Казахстан. ул. Шевченко, 29/133

Подписано в печать 21.01.2026 г.

Technical editors:
G.K. Kassymova, N.M. Aitzhanova, T.I. Kozhakhmetov

The layout on a computer:
G.K. Kassymova

Designer:
G.K. Kassymova, N.M. Aitzhanova

“Institute of Metallurgy and Ore Beneficiation” JSC
050010, Almaty city, the Republic of Kazakhstan. Shevchenko str., 29/133

Signed for publication on 21.01.2026